OPTIMIZED DESIGN OF STATICALLY EQUIVALENT MOORING AND CATENARY RYSER SYSTEMS

A Dissertation

by

IVAN FELIX GONZALEZ

Submitted to the Office of Graduate and Professional Studies of
Texas A&M University
in partial fulfillment of the requirements for the degree of

DOCTOR OF PHILOSOPHY

Chair of Committee,	Richard Mercier
Committee Members,	Jun Zhang
	Moo-Hyun Kim
	Daniel McAdams
Head of Department,	Robin Autenrieth

May 2015

Major Subject: Ocean Engineering

ABSTRACT

Due to size limitations of wave basins worldwide it is necessary to employ statically equivalent truncated mooring and riser systems to test floating systems to be deployed in deep and ultra-deep waters. A procedure for the optimized design of the statically equivalent truncated mooring and riser system was developed using a Genetic Algorithm, considering that the equivalent mooring/system needs to reproduce the net static forces and moments exerted by the prototype mooring/riser system on the floater in its six rigid body degrees of freedom (surge, sway, heave, roll, pitch and yaw).

A fit-for-purpose program was developed to evaluate the three-dimensional static equilibrium of floating structures, considering the attached mooring and steel catenary riser systems. The static response is calculated for a set of offsets in the surge direction from the calm water equilibrium position up to a maximum user defined offset.

Four study cases were considered to demonstrate the effectiveness and robustness of a Genetic Algorithm procedure developed for the optimize design of the statically equivalent mooring and riser system. The four study cases were a semisubmersible with a symmetric polyester mooring system, a semisubmersible with a symmetric steel wire mooring system, a semisubmersible with a non-symmetric polyester mooring and steel catenary riser system attached, and a spar with a non-symmetric polyester mooring and a steel catenary riser system attached.

To gain insight on the distortion of the dynamic mooring forces exerted on the floater when dynamic effects are ignored in the design, a procedure to assess the mooring

system inertia and damping force contributions to the floater was developed. The application of the procedure was demonstrated using two study cases corresponding to deepwater polyester and steel mooring systems.

DEDICATION

I dedicate my dissertation work to Almighty God for all His blessings and to allow me to successfully conclude this research work and get the PhD degree. To my lovely wife, *Alicia*, for her kindly love and support each day; and for sharing her life with me for the last 17 years and counting. She also encourage me to walk that extra mile each day of my life. To my son, *Ian*, who gives us those precious moments in life, he shows us that we can learn new things each day and if something is not easy to do, we need to try and try again until we can reach that goal.

I also dedicate this work to my parents, *Ofelia* and *Nazario*, for their lovely support, teaching and guidance. To my brothers and sisters: *Victor*, *Nazario*, *Monica* and *Cynthia*. To my grandparents: *Pomposa* and *Manuel* (R.I.P.).

ACKNOWLEDGEMENTS

I would like to thank my committee chair, Dr. Richard Mercier, first of all for giving me the opportunity to work with him developing this research project, and also for his continuous guidance, advice, recommendations and support throughout the course of this research. I would also like to thank my committee members, Dr. Zhang, Dr. Kim and Dr. McAdams, for their advice and recommendations to enrich this research work.

My thanks also go to Eng. Oscar Valle Molina and Dr. Federico Barranco Cicilia at the Mexican Petroleum Institute ("*Instituto Mexicano del Petróleo, IMP*") for their guidance and support since the beginning and throughout the course of my doctoral studies. I would like to thank Eng. Rafael Ramos Palmeros for his support and addressing in a fast and easy way any inquiry related with the financial support from the SENER-CONACYT-Hidrocarburos scholarship.

I would also like to thank the Mexican Petroleum Institute, SENER-CONACYT-Hidrocarburos fund and Texas A&M University which provide the financial resources for developing this research work.

Thanks also go to Shell International Exploration and Production, Inc. to allow me use of information from one of its semisubmersible models as a study case for this research work which allow me to assess the effectiveness and robustness of the procedures developed in this research.

TABLE OF CONTENTS

Page

LIST OF FIGURES

Page

LIST OF TABLES

Page

1 INTRODUCTION

1.1 Background and Motivation

The increasing worldwide oil demand has created the need to develop oil fields in deeper water; these new fields are a technological challenge for all infrastructure required to be installed. One of those technological challenges is to design the floating systems required to accommodate the equipment for processing the oil produced and for controlling all the subsea equipment.

A station keeping system is required for any floating offshore structure to maintain its position over a specified location with certain allowable offset limits, so that the floating structure can perform its intended functions in a safe way. The station keeping system is selected based on the floating structure's service requirements and characteristics, including the water depth where the system is to be deployed. The main categories of station keeping systems commonly used are:

a) Passive mooring systems

i. *Spread mooring.* This station keeping system is used mainly in floating production systems like Spars and Semisubmersibles. There are some applications in FPSOs (Floating, Production, Storage and Offloading systems) for mild and directional prevailing environmental conditions (Brazil and West Africa). Those systems can be mooring lines in catenary configuration, taut configuration or semi-taut configuration.

ii. *Vertical mooring*. This station keeping system is used in TLPs (Tension Leg Platforms) where tendons are used to keep the floating system in the specified location with specified offset limits. The restoring force developed by this station keeping system, as the vessel offsets from its vertical tendon, calm water equilibrium position, is the horizontal component of the tendons' top tension.

iii. *Single point mooring*. This station keeping system is widely used for FPSO applications where all the mooring lines are attached to a turret which allows the vessel to weathervane due to the environmental conditions. The turret can be internal or external to the vessel.

iv. *Catenary Anchor Leg Mooring (CALM)* This system is used for FPSO applications in shallow waters. It is based on a buoy maintained on location with a catenary mooring line system. The upper part of the buoy can rotate allowing the FPSO to weathervane due to the environmental conditions.

v. *Single Anchor Leg Mooring (SALM)*. This station keeping system is used for FPSO applications similar to the CALM station keeping system, where the catenary mooring lines in the buoy are replaced by a single vertical leg connected to an anchoring point base.

b) **Dynamic positioning systems**. This station keeping system uses thrusters to maintain the floater in a specific location with reasonable offset limits. This system is widely used for offshore drilling units, which are deployed in a

specific location for a relatively short period of time. This application is too expensive for a floating structure which has to be on location for several years and has to withstand severe weather conditions, like an offshore production facility.

c) **Thruster assisted mooring (TAM)** This station keeping system is based on mooring lines and thrusters to reduce the floater's offset and the mooring line forces. This station keeping system is too expensive for offshore production facilities which have to be on location for several years and have to withstand severe weather conditions.

Apart from vertical mooring systems which are inherently taut, passive mooring systems can be categorized as either catenary, taut or semi-taut, the main difference being the degree to which weight or axial stiffness play an important role in the mooring system restoring force. In the catenary mooring system the restoring force is mainly due to the submerged weight (w) of the mooring line components. In the taut mooring system the restoring force is mainly contributed by the axial stiffness (AE) of the mooring line, while in the semi-taut mooring system both mooring line component properties, submerged weight and axial stiffness, play an important role in developing the restoring force.

The selection of the type of riser to be used for a specific floating offshore structure is based on the intended service for the facility. There are four main categories for the riser type:

a) *Marine drilling riser*. This riser type is used in Mobil Offshore Drilling Units (MODUs) for drilling or work over purposes.

b) *Top-tensioned riser (TTR)* This riser type is used for drilling and/or production. The advantages of this riser are the use of dry trees and direct vertical access to the well.

c) *Compliant risers*. These can be Steel Catenary Risers (SCRs) or flexible risers. Compliant Risers are used to transport oil from distributed subsea systems to the floating production system or to export oil and gas from the floating system.

d) *Hybrid risers*. This type of riser is a combination of a TTR and flexible risers. Examples are riser towers, single leg risers, etc.

As previously mentioned, a floating deepwater drilling or production system requires a mooring system to keep it in position. The mooring system is made of sets of single mooring lines. Commonly each line is composed of three segments: chain at the bottom segment, steel wire or polyester rope for the middle segment and chain at the upper segment. It is also important to mention that the risers (TTR or SCR) also provide restoring forces that assist in keeping the FPS on location.

Numerical simulations and model testing are used to design a floating system to assess its behavior in operational conditions and in extreme weather conditions, always looking to preserve the safety and functionality of all the components involved.

The adequacy of a concept design is verified through model testing of a prototype to evaluate its behavior (Fryer *et al*, 2001). There are critical parameters that are verified from model testing, including floating system motions, maximum tensions in mooring lines and in risers, collision between mooring lines, risers and/or hull, airgap, global wave

loads, local wave loads, wave run up, wave deck slamming, etc. (Stansberg *et al*, 2002). Model tests of floating systems have been used to study and verify the design for many years.

For water depths less than about 500 m it is feasible with existing deepwater wave basins to test a model with a directly scaled, full depth mooring and riser system at reasonable model scales (commonly model test scales between 1:50 to 1:70). However testing the response of a floating system in deep and ultra-deep water is a challenge, because the basin dimensions required to accommodate the scaled full depth mooring and riser system are beyond the capabilities of available facilities worldwide, both now and for the foreseeable future. Figure 1.1 illustrates the truncation requirement for model testing in a basin; it shows a typical full depth mooring system with the outline of a wave basin at a typical test scale ratio. Since further reducing the size of the floater relative to the basin dimensions would lead to measurement issues it is necessary to truncate the scaled full depth mooring/riser system so that it fits within the basin dimensions.

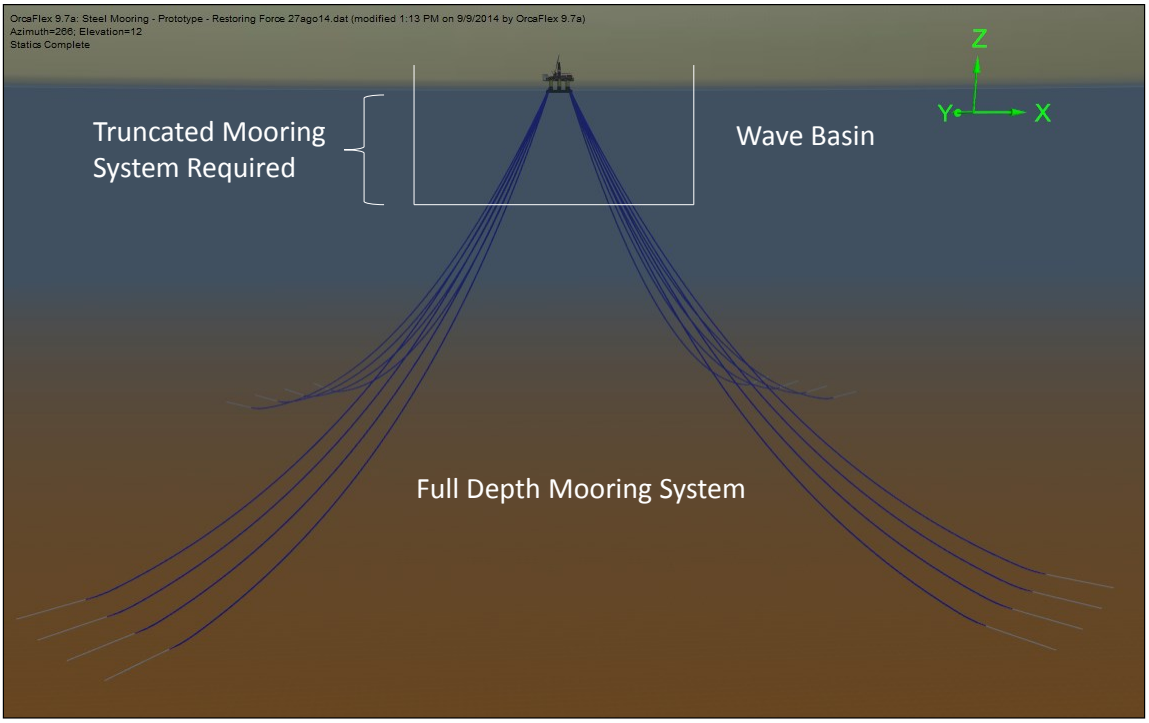

Figure 1.1. Scaled mooring system truncation required for model testing in a wave basin.

Due to basin dimension limitations it is necessary to establish a truncated mooring and riser system that is somehow equivalent to the prototype mooring system. Stansberg *et al* (2000), Stansberg *et al* (2002) and the ITTC (2008) proposed that the equivalent truncated mooring reproduce, as close as possible, the total horizontal restoring force, the quasi-static coupling between vessel responses (i.e. coupling between surge, heave and pitch for semisubmersibles and spars), a representative level of mooring and riser system damping and current force and the individual line tension force.

The truncation of the mooring and riser system implies that the departure and declination angles for the mooring lines and risers change faster than in the full depth

mooring and riser system. To compensate for these geometric differences between the full depth and the truncated mooring system, the submerged weight and/or axial stiffness of the mooring line and riser components must be adjusted to reproduce as closely as possible the full depth mooring system static response. However those changes in submerged weight (mass or diameter) and/or axial stiffness will change the dynamic behavior of the mooring lines and risers. The level of complexity required to match the static and dynamic responses of the prototype with an equivalent truncated mooring and riser system is currently beyond reach.

The truncated mooring and riser system combined with the scale selected for the model testing introduce uncertainties in the test results. In order to reduce the uncertainties related to the extrapolation of the test results from a truncated mooring and riser system to a full depth mooring and riser system it is required to design the equivalent mooring and riser system so that it results in the same motion responses of the floater as would result if the floater was attached to the full depth mooring and riser system.

Stansberg *et al* (2004) established that for designing an equivalent truncated mooring system it is necessary to model correctly a prioritized set of parameters. The parameters to be considered are: floating system mass, total horizontal stiffness, quasi-static coupling between important vessel responses, total horizontal and vertical mooring and riser restoring forces, adequate level of mooring and riser system damping in waves and currents, and adequate tension characteristics for each mooring line and riser.

The offshore industry, through proprietary model tests of a wide array of floating systems, has investigated various strategies for design of equivalent mooring and riser

systems. Two different philosophies for designing an equivalent mooring system involve the use of a passive or an active equivalent truncated mooring system. In the passive truncated mooring system, the equivalency to the full depth mooring system is reached by passive mooring line components (i.e. masses, springs, buoys, etc.). In the active truncated mooring system, the equivalency to the full depth mooring system is reached by using actuators and controllers to reproduce the full depth response at the truncation point (Cao, 2013). With either approach the goal is to design the equivalent system so that the net forces and moments imparted by the truncated mooring/riser system to the floater in its 6 rigid body degrees of freedom are as closely reproduced as practically possible.

There have been some efforts to develop active truncated mooring systems reported in the literature. Buchner *et al* (1999) at MARIN developed a study for an active equivalent mooring system using arm robots at the end of the truncated mooring lines on the basin floor; they refer to this concept as the ATLAS system (Active Truncated Line Anchoring Simulator). The idea is that this system simulates in real time the behavior of virtual mooring lines and risers below the depth of the wave basin. This will require heavy computational work to reproduce the behavior of the virtual mooring lines and risers and to send the signal to the arm robots in real time. The authors also mentioned that there could be interactions between the robot arms and the mooring lines and risers, due to hydrodynamic effects induced by the robot arms. They don't provide any additional information about the required real time inputs in the numerical simulations of the virtual mooring lines and how they will be solving the problems related with time lags in the response of the actuators.

Cao (2013) mentioned that Marintek has been working on a theoretical and numerical study to assess the feasibility of an active hybrid decomposed mooring system (Hydemoor) which uses actuators and controllers at the truncation point in the mooring lines. The actuator responds based on numerical simulations of the truncated mooring line segments not included in the physical model, so the force expected at the truncation point due the numerical simulation is applied to the model mooring line segment at this point.

Due to a) the expensive cost to implement an active equivalent mooring system which requires actuators and controllers, b) heavy computational requirements to simulate the virtual mooring lines in real time and respond also in real time, c) the uncertainties introduced by the simulation response of the mooring and riser system cut-off part and the lag in the response related with the virtual mooring lines and risers simulations, it doesn't look feasible or practical to use actively-controlled equivalent mooring and riser systems.

It is currently the common practice to focus the design effort entirely on reproducing the net *static* restoring forces and moments that the mooring and risers impart on the floater over some pre-defined range of offsets. Because of the highly nonlinear behavior of mooring and riser systems over large offset ranges, achieving the design objective typically involves significant effort and challenges the skill of the designer.

There are different design approaches related to the passive equivalent truncated mooring systems. Elgamiel *et al* (2006) present three different design techniques for the truncation problem. For the first technique they modified a previous design philosophy for truncated mooring systems called SMART (Simple Mooring and Risers Truncation) where the mooring and riser restoring force is provided by a hanging weight connected on

one side to a fairlead on the floater and on the other side to a fixed anchoring point. There are five design parameters per mooring line: three anchoring point coordinates, and the weight and the length of one cable. The second cable length is dependent on the required geometry to match the line downward angle at the fairlead. The technique was modified by introducing an additional degree of freedom in their design, in particular by inserting a frictionless pulley at the anchoring position and controlling the exit vertical angle at this pulley with a second weight.

The second approach presented by Elgamiel *et al* (2006) is that, for each mooring line in the model, the anchoring points are sliders which move in horizontal pipes. The fairlead is connected to this slider anchoring point with a stiff spring, and the slider anchoring points are connected with a spring to a fixed anchoring point, the latter spring providing the horizontal stiffness. The third proposed design approach uses pulleys at the fairlead locations on the model and single spring lines through these pulleys connected to two fixed anchoring points, one downwind and the other upwind. They concluded that these three systems yield good agreement with the target horizontal and vertical restoring force curves.

The primary contribution of the research documented herein is the development of an automated procedure for optimized design of statically equivalent mooring and riser systems considering, for a set of offsets, six static response characteristics for the floater: horizontal restoring force in surge, sway displacement, heave (set-down), pitch, roll and yaw rotations. In the literature it is commonly mentioned that the design of the equivalent truncated mooring system is focused on the static response characteristic for restoring

force in surge and heave and on the static tension in individual mooring lines (Kim *et al*, 2005; Udoh, 2008; Zhang *et al*, 2009; Zhang *et al*, 2012) . Here the design strategy used by the Offshore Technology Research Center will be adopted, which focuses exclusively on reproducing the net six degree of freedom restoring forces and moments exerted on the floater with a statically equivalent system whose individual lines are not constrained to bear any resemblance to individual lines of the prototype system but rather are as simple as possible so that they can be robustly represented in a numerical model.

As previously mentioned, for practical reasons it is a common practice to design the truncated mooring system based on an approach that seeks equivalency in *static* floater responses over defined ranges of offsets. However model testing is employed to assess the floater's dynamic behavior, so it is important to have knowledge of the dynamic response of the mooring system and its contributions to the floater. The equivalent truncated mooring system contributions to the dynamics of the floater can be directly compared with those of the full depth prototype mooring system. In order to evaluate the *dynamic* behavior of the forces imparted by the mooring system, a procedure to assess the mooring system inertia and damping contributions to the vessel is developed. The procedure is applied to analyze and compare the dynamic contributions of the equivalent truncated mooring system with the full depth prototype system. The procedure developed consists of decomposing in orthogonal components (in phase and ninety degrees out of phase with the vessel acceleration) the dynamic horizontal force exerted by the mooring system to the vessel that remains after the elastic restoring force has been removed, and comparing the results for the equivalent mooring system with the prototype mooring system.

1.2 Review of Optimized Design Approaches for Equivalent Mooring Systems

In the literature there are a few works focused on developing an automatic procedure for the optimized design of the statically equivalent truncated mooring system. Mainly those works consider just one degree of freedom for the static response of the floating system. Some of the efforts to develop a procedure for the design of the statically equivalent truncated mooring system are reviewed in this section.

The challenges for model testing of floating systems in deep waters were investigated by Stansberg *et al* (2002), who concluded that due to dimension limitations in available laboratory basins it is necessary to consider truncated moorings systems for model testing of floating systems that will be deployed in deep and ultra-deep waters. To test such systems using a reasonable scale factor, the hybrid approach "*is then likely to be the most relevant tool*". The hybrid approach (Stansberg *et al*, 2000) is a combination of model testing with a truncated mooring system and computer simulations to rationalize the systematic differences between the scale model and the prototype system.

Stansberg *et al* (2002) mention that the uncertainties in results related with physical modeling and testing are larger when large scale factors are used (small models), and the uncertainties in results related with truncation and numerical extrapolation are larger when small scale factors are used (larger truncation factors), so it is necessary to select an optimum scale factor where the total uncertainties on results are smallest. Figure 1.2 (from Stansberg *et al*, 2002) notionally shows the effect of the scale factor on the uncertainties in results related with the physical modelling and testing, and with the truncation and

numerical extrapolation. The scale factor must be selected to balance the uncertainties, in order to minimize the total uncertainty in the results.

The truncation factor γ can be defined as the ratio between the full scale water depth wd_{full} and the truncated water depth in the basin (reported in full scale units) wd_{trunc},

$$\gamma = \frac{wd_{full}}{wd_{trunc}} \tag{1.1}$$

So, the water depth for the truncated mooring system can be calculated from equation (1.1) as:

$$wd_{trunc} = \frac{wd_{full}}{\gamma} \tag{1.2}$$

It is important to note that the maximum anchoring radius may also be limited by the basin dimensions, in which case the truncated mooring system has to be designed considering both constraints (the basin horizontal dimensions as well as the water depth).

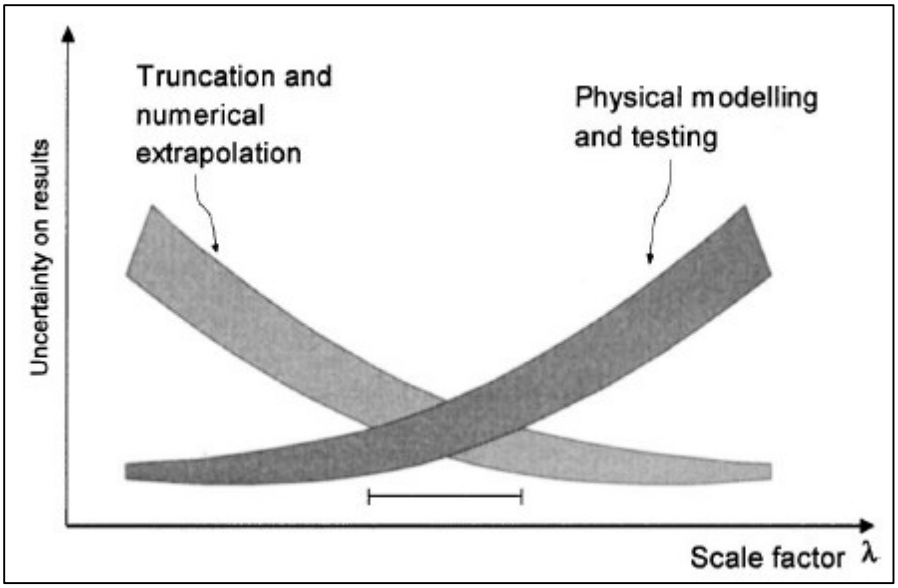

Figure 1.2. Scale factor effect in uncertainties for truncation and numerical extrapolation and for physical modelling and testing (Source: Stansberg *et al*, 2002).

Stansberg *et al* (2004) reviewed the procedures for model testing of floating systems deployed in ultra-deep water. They concluded that model test results using a truncated mooring system have to be interpreted in combination with advanced computer models. Their procedure establishes that model test results from floating systems with truncated mooring lines and risers are used to validate and calibrate a numerical model of the truncated mooring/riser system, and this validation and calibration is taken into account in the numerical simulations of the full depth prototype system that will be used as a final verification.

An iterative procedure for the optimized design of equivalent mooring systems is presented by Waals and Van Dijk (2004). Two separate optimization processes are

proposed. The first process is for matching the static response of the truncated mooring system with that of the full depth mooring, by adjusting the length, submerged weight and axial stiffness of the truncated lines. The second optimization process is focused on matching the dynamic behavior of individual mooring lines for the truncated mooring system with that of the full depth mooring system. For this second process they proposed to develop forced oscillation simulations of the floater for various frequencies, and the individual mooring line responses are compared between the truncated mooring system and the full scale mooring system. The values of the unit mass and diameter for the truncated mooring lines are adjusted iteratively to achieve approximate dynamic equivalency. Waals and Van Dijk applied their procedure on a semisubmersible case, also considering to optimize the design of the truncated mooring system taking into account the heave and pitch responses of the floater. They obtained good agreement with the prototype for the floater's static responses.

Kim *et al* (2005) compared the results of a numerical dynamic analysis for a FPSO with an experiment held at OTRC where a truncated equivalent mooring system was used. The equivalent mooring system was designed to match as closely as possible the static surge stiffness of the prototype mooring system. They obtained good agreement between the numerical simulations and the experimental results for the system's stiffness, line tensions, natural periods and damping as measured by static offset and free decay tests. They also concluded that the dynamic mooring tension can be underestimated when the mooring dynamic effects are significant and the mooring line damping can be

underestimated depending on the level of mooring line truncation, and those differences will be larger with additional risers and riser truncation.

A spreadsheet tool for the design of a statically equivalent mooring system involving the solution of the mooring system restoring force, and the mooring stiffness in the longitudinal and transverse directions, was developed by Udoh (2008). That tool can be used by the designer to optimize the design of the statically equivalent truncated mooring system in a manual iterative process. The process involves changing the characteristics of the mooring lines (submerged weight, length and axial stiffness of line elements, anchor position) and examining the effect of the changes on the horizontal restoring force, and the longitudinal and transverse stiffness of the mooring system. In this tool only the surge degree of freedom is considered, associated with the horizontal offsets of the given floating system.

The optimized design of the equivalent truncated mooring system using a simulated annealing algorithm and a complex algorithm was investigated by Zhang *et al* (2009). For that research they used an objective function with weighting factors for the similarity of overall system restoring force and for forces in individual mooring lines. They do not specify the degrees of freedom considered in the floating system motion response, but it can be assumed that they consider just one degree of freedom (surge response) for the floating system static response.

Zhang *et al* (2012) used a non-dominated sorting genetic algorithm to optimize the design of an equivalent truncated mooring system for a FPSO (Floating Production, Storage and Offloading system). They used a multi-objective fitness function focused on

the static characteristics related with the restoring forces in the horizontal and vertical direction and the tension in a single mooring line for a set of offsets. Their results showed that they had a similar static response between the truncated and the full scale mooring system, for the variables selected in their fitness functions.

Furthermore, a procedure for designing equivalent mooring systems considering the static and damping characteristics of the full depth mooring system was developed by Fan *et al* (2013). The characteristics considered in the optimization design process are: horizontal restoring force, vertical restoring force, mooring line top tension and mooring induced damping coefficient at low frequencies. A Genetic Algorithm is used in their optimization process based on a fitness function that minimizes the root mean square error of the static and damping characteristics between the truncated and the full depth mooring systems. They used a quasi-static method to calculate the mooring system damping contribution, assuming that the line profile is well described by the quasi-static catenary equations at any time of the harmonic oscillation and that the inertia forces on the mooring lines can be neglected.

1.3 Review of Previous Work on Dynamics of Mooring Systems

The slow drift motion of a moored floating vessel is a resonant response associated with its large mass and small horizontal mooring stiffness, leading to motions with period of hundreds of seconds. This resonant response is mainly controlled by the different sources of damping (Triantafyllou and Yue, 1994) which are: wave drift damping, wind damping, current and viscous flow damping and mooring system damping. Commonly,

the moored vessel's total damping is below the critical damping, which leads to large amplitude motions at the resonant frequency. The mooring system damping contribution could be of the same order of magnitude as the wave drift damping contribution (Triantafyllou and Yue, 1994), so it is important to assess the mooring system damping contribution to the total damping of the system.

Huse and Matsumoto (1988) presented a procedure for practical estimation of mooring line damping contributions and they also presented experimental results to verify their calculation procedure. They concluded that, based on their experimental results, the mooring line drag forces can be the main damping contribution in the surge direction for the low frequency resonant response of a moored vessel. As they noticed, through nonlinear mechanisms the superposition of the first order motions of the vessel at wave frequencies can dramatically increase the mooring system damping contribution to the low frequency surge motion.

Furthermore, Huse and Matsumoto (1989) presented the theory and a numerical method for calculating the mooring system damping contributions in the surge direction and compared their analytical results with some tests for a catenary moored ship. They stated that the moored vessel resonant response amplitude at low frequencies is completely related with the total system damping of the surge motion, the main damping contributions being due to wave drift, viscous drag and skin friction forces on the main structure, and the mooring line drag forces. Based on their test results they concluded that the mooring system damping contribution can be up to 80% of the total damping of the slow drift motion in irregular waves, the remaining 20% of total damping being due to wave drift

and viscous damping of the floater. They further concluded that in the case of single sinusoidal excitation of the resonant response at low frequency, the mooring system damping contribution can be calculated theoretically.

In 1990 Wichers *et al* investigated the mooring chain damping contributions to the total damping for a turret moored tanker, considering first only the surge motion at low frequency and secondly the coupled effect of the surge motion at low frequency with the heave motions at wave frequency. They presented the theory to calculate the mooring chain damping contribution of the low frequency motion and the influence of the high frequency motions on the chain damping contributions. They developed some numerical simulations and tests to evaluate the theory. Based on their results they concluded that simulations of low frequency motions cannot be decoupled from the high frequency motions due to the increased damping occurring in chain mooring systems. Additionally, they also concluded that the chain mooring system viscous damping contribution of the low frequency motion of a turret moored tanker in deepwater exposed to current and irregular waves can be of the same order of magnitude as the viscous damping for the tanker. The chain mooring system damping contribution to the floater's total damping can be increased considerably due to the superposition of the low frequency motion in surge and the high frequency motions in heave.

1.4 Heuristic Optimization Methods for Structural Design

Different heuristic optimization methods focused on structural optimization problems were compared by Manoharan *et al* (1999). Tabu Search, Simulated Annealing, Genetic Algorithm and Branch and Bound Method were the heuristic optimization methods compared. They applied those optimization methods for three design examples of different structures, concluding that Tabu Search, Simulated Annealing and Genetic Algorithm work well with an acceptable solution in a reasonable time.

In the literature there are many references to the use of Genetic Algorithm approaches to solve problems in different fields of study. One of these that use Genetic Algorithms to solve problems of optimized design in the field of engineering is a work by Carbono *et al* (2005). They developed a Genetic Algorithm (GA) to optimize the design of mooring patterns for floating units used in the offshore oil industry. The procedure was focused on optimizing the mooring pattern to minimize the floater's offset in anticipated environmental conditions (waves, currents and winds). They also used the catenary equation solution to calculate the forces exerted by the mooring system on the floater in order to obtain the static equilibrium position of the floater under the influence of the environmental forces. A representative example was used to test the optimization procedure and illustrate its capabilities.

1.5 Research Objectives

Due to size limitations of wave basins worldwide it is necessary to employ statically equivalent truncated mooring and riser systems to test floating systems to be deployed in deep and ultra-deep waters. The equivalent truncated mooring system is designed iteratively, with a trial and error approach. Obtaining an acceptable design for the mooring system using a manual iterative approach is challenging and could take from some days to some weeks of work. In order to facilitate this task, this research is developed with the main objectives to:

1. develop an automated procedure for the optimized design of statically equivalent truncated mooring and catenary riser systems (in particular, steel catenary risers or SCRs);
2. develop a procedure to assess the equivalency of the inertia and damping contributions from the designed statically equivalent mooring/SCR system to the dynamic motion of the floater;
3. develop 4 study cases to demonstrate the effectiveness and robustness of the automated procedure for the design of a statically equivalent truncated mooring and riser system;
4. develop 2 study cases to demonstrate the procedure for assessment of inertia and damping contributions by the equivalent mooring system compared to that contributed by the prototype system.

1.6 Assumptions and Constraints for the Design of the Equivalent Truncated Mooring and Riser Systems

The design of the equivalent mooring/riser system should be such that it is as simple as possible, so that it can be readily fabricated as well as readily modeled using standard numerical tools. Following the practice at the Offshore Technology Research Center, some assumptions and constraints for the design of the statically equivalent mooring and riser systems were established and considered during all the phases of this research. For design purposes, the equivalent mooring and riser systems will be decoupled and designed independently; however the effect of the full depth prototype risers will be taken into account when designing the equivalent mooring system. The assumptions and constraints considered are:

1. Each equivalent mooring line consists of (from the fairlead to the anchoring position):
    a. load cell segment
    b. cable segment
    c. spring segment
    d. cable segment
2. Each equivalent steel catenary riser (SCR) consists of (from the fairlead point to the anchoring point):
    a. load cell segment
    b. short length cable segment
    c. long, soft spring segment

d. short length cable segment

3. It is required to match the static response in all 6 rigid body degrees of freedom of the floating structure, but each degree of freedom will have a different acceptance criterion on the extent to which the prototype static response is matched.
4. The procedure should be valid and applicable for any prototype mooring and catenary riser configuration in water depths exceeding 500 m.
5. A catalog of commercially-available spring properties is used for the model mooring lines and risers, which means that the springs will be constrained to discrete values of submerged weight (w) and stiffness (EA).
6. At any offset, the mooring line/riser is contained in a vertical plane which also includes the fairlead and anchoring points. The seabed friction is neglected for any mooring/riser segment laying on the seabed, so even if there is any portion of the mooring line/riser laying on the seabed, at any offset, it is kept in the vertical plane which contains the mooring line/riser, fairlead/porch and anchoring point.

1.7 Methodology

There is a series of tasks required as a part of the optimization process for the design of the statically equivalent truncated mooring and riser system. Those tasks are focused on reproducing the floating system static response over a range of vessel offsets in 6 degrees of freedom with a specific mooring and riser system attached. The main tasks required to determine the static response of the floating system are:

1. Using the catenary equation, calculate the tensile forces at the fairlead position, for all individual mooring lines and risers.
2. Calculate the calm water equilibrium position of the complete floating system, where all the static forces and moments acting on the vessel are in equilibrium, in particular where the forces and moments induced by the mooring and riser system, in combination with user defined forces and moments, are in equilibrium with the net buoyancy of the floater, as affected by its hydrostatic stiffness in heave, roll and pitch.
3. Relative to the calm water equilibrium position for the floating structure, a set of equally spaced horizontal offsets in the surge direction are considered and at any offset the full static equilibrium solution of the system is calculated, generally resulting in incremental sway, heave (setdown), roll, pitch and yaw of the floater.

For design purposes, the equivalent riser system design is decoupled from the equivalent mooring system design, which means that in the presence of SCRs the design of the equivalent mooring system is taking into account the full depth prototype riser

system behavior. Once, the equivalent mooring system is designed, the equivalent riser system is designed taking into account the equivalent mooring system designed previously.

A fit-for-purpose program was developed to obtain the six degrees of freedom static behavior of a floating system considering a specific mooring and catenary riser system attached. For each degree of freedom the static behavior is tracked for a prescribed set of offsets in a given horizontal direction from the calm water equilibrium position up to a maximum offset in that direction equal to some user-specified value as a percentage of the full water depth (typically about 8%).

The floating system hydrostatic stiffness in heave, pitch and roll are considered as input values. For the prototype, the solution developed can consider as many mooring lines and risers attached to the floating system as is required, and each mooring line and riser can be composed of as many segments as needed. For the design of the truncated equivalent mooring and riser systems, the solution considers as many equivalent mooring lines and risers attached as needed, but only four segments for each equivalent mooring line and riser. Typically these equivalent mooring lines and risers include a load cell, an upper cable or chain segment, a spring segment and a lower cable or chain segment.

A Genetic Algorithm (GA) is used for the optimized design of statically equivalent truncated mooring and riser systems focusing on trying to match the full depth prototype floater's six static response characteristics (horizontal restoring force, heave and sway displacements, and pitch, roll and yaw rotations). Four different solution scenarios are considered for the GA. The first scenario considers a symmetric equivalent mooring

system where all mooring lines are identical. The second solution scenario is a non-symmetric mooring system; this scenario considers different design parameters between the upwind and downwind mooring lines. The third solution scenario considers six design parameters per each mooring line in the equivalent mooring system (i.e. each equivalent mooring line may be unique). The fourth and last solution scenario considers the design of the equivalent truncated riser system where there are six design parameters per each steel catenary riser (SCR) in the equivalent system.

A procedure is developed to assess the mooring system inertia and damping contributions to the vessel motion and to compare those contributions between the equivalent mooring system and the full depth prototype mooring system. The procedure developed consists of decomposing in orthogonal components (ninety degrees out of phase) the dynamic horizontal force exerted by the mooring system to the vessel.

In the remainder of this dissertation the statically equivalent truncated mooring/riser system will be referred to simply as the equivalent mooring/riser system, it being understood that the model system will involve truncated mooring lines and risers, and that the system will be designed for static equivalence only.

2 STATIC RESPONSE SOLUTION

The optimized design of the static equivalent mooring and risers relies on a computationally efficient capability to solve for the static response of the system. Such a fit-for-purpose program was developed in Matlab (Mathworks Inc.), which can evaluate the static response of a floating structure considering the attached mooring and riser system, taking into account the floating structure hydrostatic stiffness characteristics. This fit-for-purpose program evaluates the six degree of freedom static response for a set of pre-defined offsets in a specified direction, from the calm water equilibrium position up to some specified percentage of the water depth (typically 8%). For simplicity the right-handed, global and local (body-fixed) coordinate systems are aligned with positive x-direction in the direction of static offset, so that the offset direction may be referred to as the surge direction. Figure 2.1 shows the six degrees of freedom considered for the static response of the floating structure. Positive rotations in roll, pitch and yaw follow the right-handed rule.

There are two coordinate systems defined for the procedure to calculate the static equilibrium for the calm water condition and for each one of the offsets considered, as is shown in Figure 2.2. The first coordinate system is defined as a global coordinate system (X, Y and Z). The global coordinate system origin must be located at the still water plane and will be used to define the anchor coordinates (x'_b, y'_b, and z'_b) for the mooring lines and the steel catenary risers (SCRs), and the initial position of the vessel's tracking point (body-fixed local coordinate system). This coordinate system will also be used to calculate

the static equilibrium solution for the calm water condition and for each offset position of the floating structure.

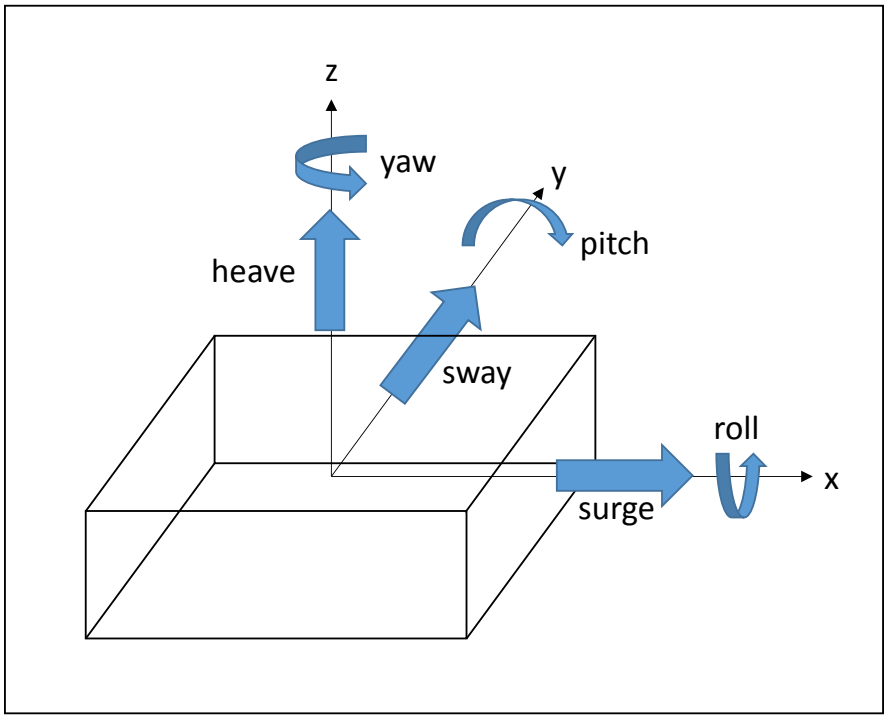

Figure 2.1. Degrees of freedom for a floating structure.

The second coordinate system defined is a local (body-fixed) coordinate system for the floating structure (*X'*, *Y'* and *Z'*) with its origin at the vessel's tracking point, that can be the floating system center of gravity (CG). The vessel local coordinate system will be used to define the hydrostatic stiffness characteristics in heave, pitch and roll. It is also used to define the local system coordinates (x_a, y_a, and z_a) for the mooring line fairlead and riser porch locations. In the initial calm water equilibrium position the horizontal axis for the global and local coordinate systems overlap each other when viewed from above.

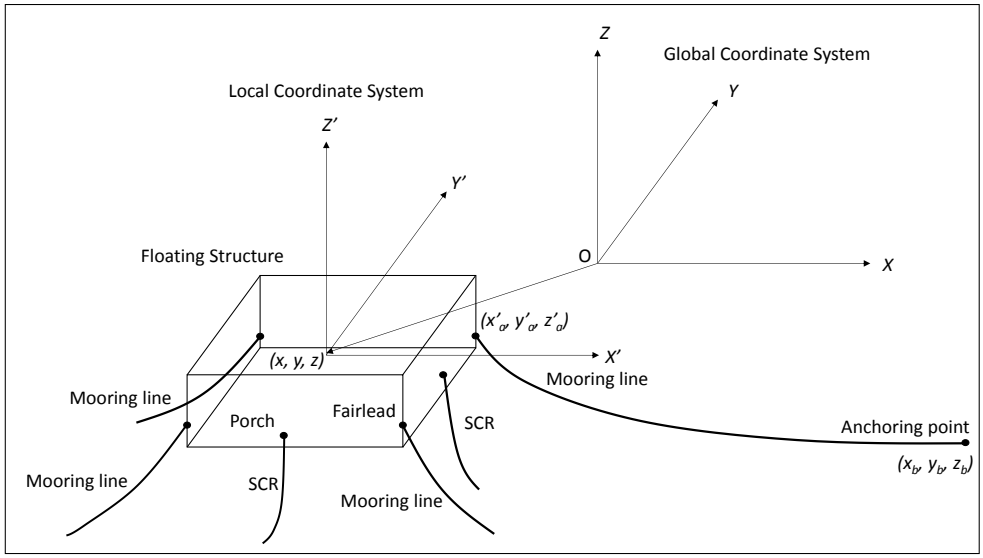

Figure 2.2. Global and local coordinate systems.

2.1 Catenary Solution

The first step to calculate the static response curves for the floater is to obtain the mooring line and riser forces at the fairlead and porch locations, respectively. To calculate the forces exerted by the mooring lines and risers to the floater at the fairlead and porch locations, it is necessary to solve the catenary equation for each one of the mooring lines and risers attached to the floater. Figure 2.3 shows the free body diagram for a mooring line segment of length s and submerged weight per unit length w. At the lower segment end (a) the horizontal and vertical force components, H_a and V_a respectively, of the tension T_a at this point are shown, and similarly at the upper segment end (b) the horizontal and vertical force components, H_b and V_b respectively, of the tension T_b at this point are shown.

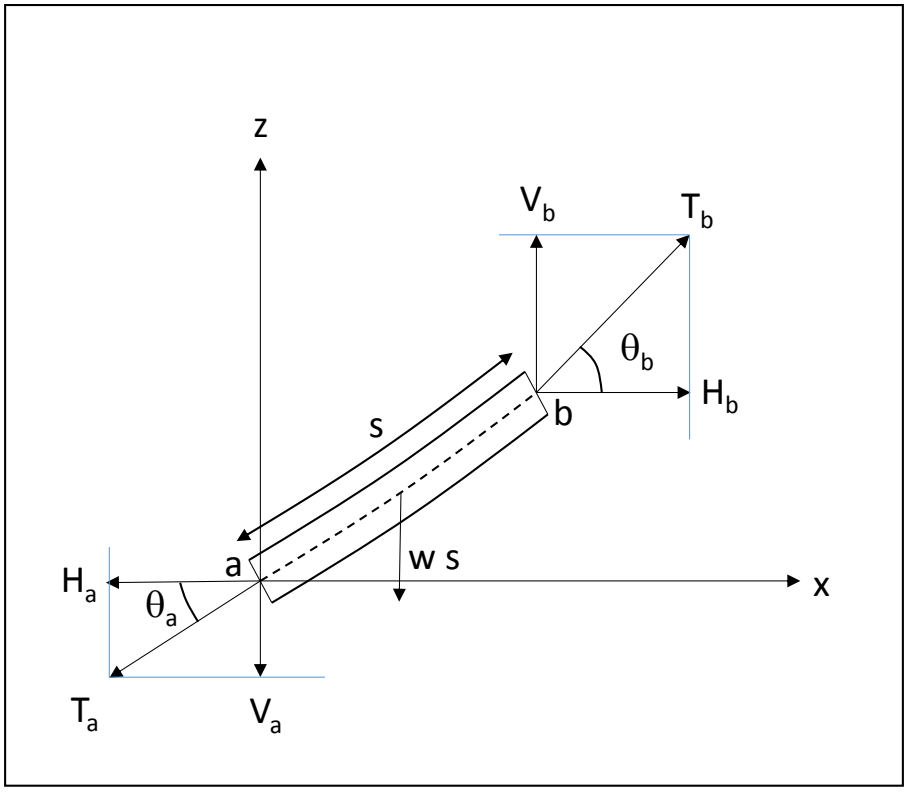

Figure 2.3. Free body diagram for a mooring line segment.

The local coordinate system for the mooring line catenary solution has the origin at the anchor point, the *x* axis defined in the horizontal direction of the fairlead and the *z* axis oriented vertically upward. Considering the mooring segment in Figure 2.3 to be in static equilibrium and summing forces in the horizontal direction, we have

$$H_b = H_a \tag{2.1}$$

Equation (2.1) shows that in a free span of the mooring line the horizontal force component remains constant. This will be the case from the seabed touchdown point all the way up to the fairlead. If the seabed friction is neglected then the horizontal force will

remain constant all the way to the anchor point and the entire mooring line will be contained in the same vertical plane.

Summing forces in the vertical direction, it is evident that

$$V_b = V_a + \text{ws} \tag{2.2}$$

The tension at the segment lower end (point a) is

$$T_a = \sqrt{{H_a}^2 + {V_a}^2} \tag{2.3}$$

while that at the segment upper end (point b) is

$$T_b = \sqrt{{H_b}^2 + {V_b}^2} \tag{2.4}$$

Substituting Equations (2.1) and (2.2) in (2.4), and recognizing that $V_a = H_a tan\,\theta_a$, the upper tension can be written as

$$T_b = H_a \sqrt{1 + \left(tan\,\theta_a + \frac{\text{ws}}{H_a}\right)^2} \tag{2.5}$$

Equations (2.1), (2.2) and (2.5), may be used to calculate the tension and the horizontal and vertical components at the segment upper end taking into account the forces acting at the segment lower end. Furthermore, it is also necessary to calculate the catenary configuration. Figure 2.4 shows the free body diagram of a mooring line segment, including the deformation caused by the tension and self-weight. Following the approach developed by Irvine (1981) and also presented by Udoh (2008), let the point S be the Lagrangian coordinate of the non-deformed end of the mooring line segment and let the point P be the Lagrangian coordinate of the new position of the deformed end under the

acting forces (segment end forces and submerged self-weight) . The Cartesian coordinates of point P are *x* and *y* and its Lagrangian coordinate is *p*. Figure 2.5 shows a differential element of the non-deformed mooring line and the corresponding differential strain under the forces acting on it.

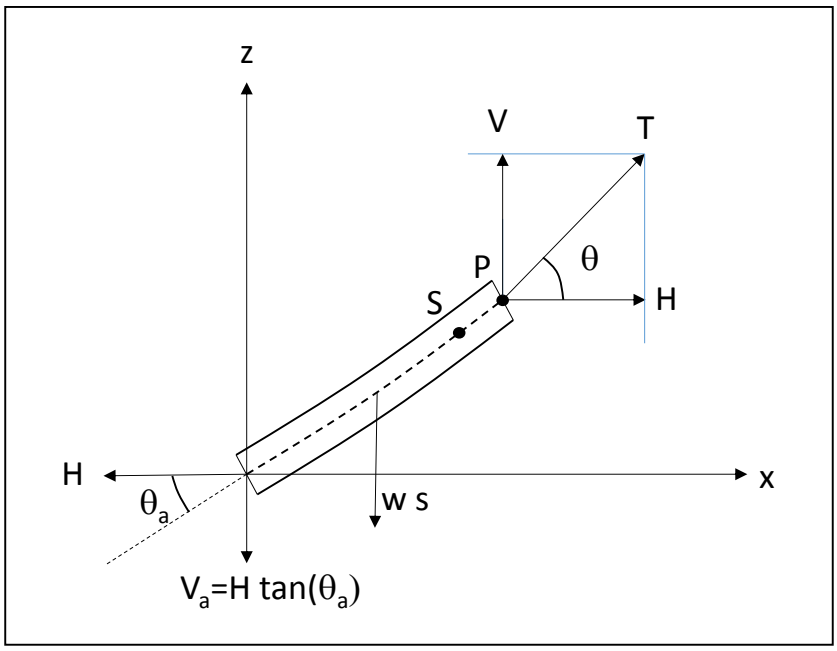

Figure 2.4. Free body diagram for a mooring line segment, including the mooring line strain.

The unit strain can be written in terms of tension *T*, Young's Modulus *E* and effective cross section area A_0 of the mooring line segment as

$$\epsilon = \frac{\sigma}{E} = \frac{T/A_o}{E} = \frac{T}{EA_o} \tag{2.6}$$

As illustrated in Figure 2.5, the unit strain can be also written in terms of Lagrangian coordinates *dp* and *ds* as

$$\epsilon = \frac{\Delta L}{L_o} = \frac{dp - ds}{ds} = \frac{dp}{ds} - \frac{ds}{ds} = \frac{dp}{ds} - 1 \tag{2.7}$$

So we can write Equation (2.6) and (2.7) as

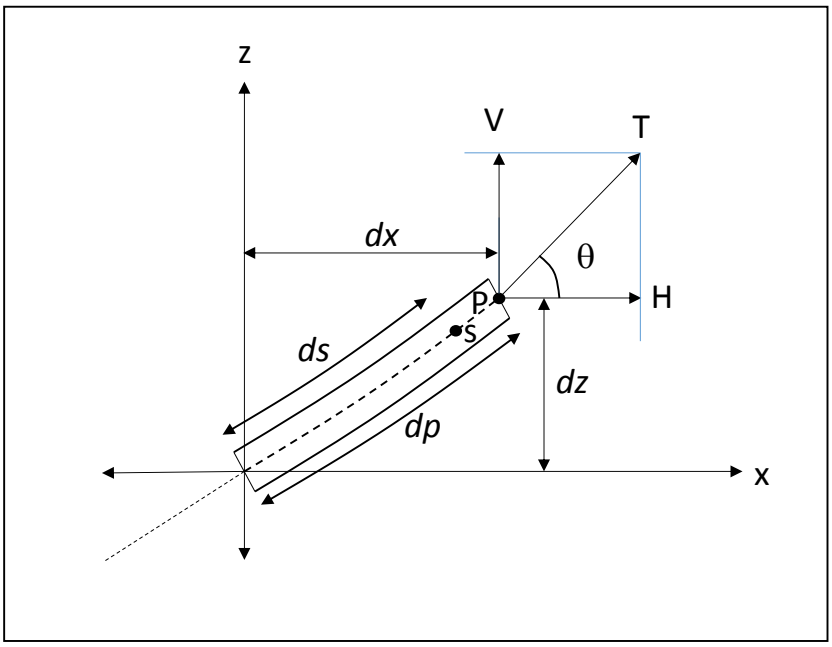

Figure 2.5. Configuration for a mooring line differential element, including its strain.

$$\frac{\Delta L}{L_o} = \frac{T}{EA_o} \tag{2.8}$$

$$\frac{dp}{ds} = \frac{T}{EA_o} + 1 \tag{2.9}$$

From Figure 2.5 is shown that

$$tan\,\theta = \frac{V}{H} = \frac{dz}{dx} \tag{2.10}$$

and

$$cos\,\theta = \frac{H}{T} = \frac{dx}{dp} \tag{2.11}$$

$$sin\,\theta = \frac{V}{T} = \frac{dz}{dp} \tag{2.12}$$

The *x* coordinate change of point S with respect to its Lagrangian coordinate can be written as

$$\frac{dx}{ds} = \frac{dx}{dp}\,\frac{dp}{ds} \tag{2.13}$$

Substituting Equations (2.9) and (2.11) in (2.13),

$$\frac{dx}{ds} = \frac{H}{T}\left(\frac{T}{EA_o} + 1\right) = \left(\frac{H}{EA_o} + \frac{H}{T}\right)$$

Since $T = \sqrt{H^2 + (V_a + ws)^2}$, then

$$dx = \frac{H}{EA_o}ds + \frac{1}{\sqrt{1 + \left(\frac{V_a + ws}{H}\right)^2}}ds \tag{2.14}$$

Integrating Equation (2.14), we obtain

$$x(s) = \frac{Hs}{EA_o} + \frac{H}{w}sinh^{-1}\left(\frac{V_a + ws}{H}\right) + C \tag{2.15}$$

At $s = 0, X(s) = 0$, so

$$C = -\frac{H}{w} sinh^{-1}\left(\frac{V_a}{H}\right)$$

Substituting the value of this integration constant in equation (2.15), the *x* coordinate of the mooring segment as a function of *s* can be written as

$$x(s) = \frac{Hs}{EA_o} + \frac{H}{w} sinh^{-1}\left(\frac{V_a + ws}{H}\right) - \frac{H}{w} sinh^{-1}\left(\frac{V_a}{H}\right) \tag{2.16}$$

In a similar way the *z* coordinate change of point *S* with respect to its Lagrangian coordinate can be defined as

$$\frac{dz}{ds} = \frac{dz}{dp}\,\frac{dp}{ds} \tag{2.17}$$

Substituting Equations (2.9) and (2.12) in (2.17),

$$\frac{dz}{ds} = \frac{V}{T}\left(\frac{T}{EA_o} + 1\right) = \frac{V}{EA_o} + \frac{V}{T}$$

Since $V = ws + H\ tan(\theta_a)$ and $T = \sqrt{H^2 + (V_a + ws)^2}$, then

$$dz = \frac{ws}{EA_o} ds + \frac{H\ tan(\theta_a)}{EA_o} ds + \frac{\left(\frac{ws}{H} + tan(\theta_a)\right)}{\sqrt{1 + \left(\frac{ws}{H} + tan(\theta_a)\right)^2}} ds \tag{2.18}$$

Integrating Equation (2.18), we obtain

$$z(s) = \frac{ws^2}{2EA_o} + \frac{Hs\ tan(\theta_a)}{EA_o} + \frac{H}{w}\sqrt{1 + \left(\frac{ws}{H} + tan(\theta_a)\right)^2} + C \tag{2.19}$$

At $s = 0, Z(s) = 0$, so

$$C = -\frac{H}{w}(1 + tan^2\,\theta_a)^{\frac{1}{2}} = -\frac{H}{w} sec\ (\theta_a)$$

Substituting the value of this integration constant in equation (2.19) will result in equation (2.20) which defines the z coordinate of the mooring segment as a function of length s.

$$z(s) = \frac{ws^2}{2EA_o} + \frac{Hs\ tan(\theta_a)}{EA_o} + \frac{H}{w}\sqrt{1 + \left(\frac{ws}{H} + tan(\theta_a)\right)^2} - \frac{H}{w}sec\ (\theta_a) \qquad (2.20)$$

Table 2.1 summarizes the key catenary equations for a free span and how they are applied.

As it was mentioned previously in this section that the friction between the mooring line and the seabed is neglected, this means that there is no change in the horizontal force (H) at any mooring line segment laying on the seabed and those segments also will remain in the vertical plane which includes the anchor and fairlead points. For any segment laying on the seabed the elongation can be calculated considering equation (2.8) as

$$\Delta L = \frac{TL_o}{EA_o}$$

Since $T = H$ and $L_o = s$, then

$$\Delta L = \frac{Hs}{EA_o}$$

So the horizontal coordinate of the segment laying on the seabed as a function of the segment length s can be written as the length s plus the elongation of the segment,

$$x(s) = s + \frac{Hs}{EA_o} \qquad (2.21)$$

Table 2.1. Summary of useful catenary equations

Equation	Purpose
$H_b = H_a$	Horizontal force component at mooring line segment upper end considering the horizontal force component at the mooring line segment lower end. The horizontal force component is equal at any location of the mooring line.
$V_b = V_a + \text{ws}$	Vertical force component at mooring line segment upper end considering the vertical force component at the mooring line segment lower end and the submerged weight per unit length and segment length.
$T_b = \sqrt{{H_a}^2 + (V_a + \text{ws})^2}$	Tension force at the segment upper end based in the horizontal and vertical force components at the segment lower end and the submerged segment weight per unit length (w) and segment length (s).
$x(s) = \frac{Hs}{EA_o} + \frac{H}{w} sinh^{-1}\left(\frac{V_a + ws}{H}\right) - \frac{H}{w} sinh^{-1}\left(\frac{V_a}{H}\right)$	Calculate the horizontal coordinate of the segment upper end based on the horizontal and vertical force components at the segment lower end and segment properties: Young's modulus E, effective cross section area (A_0), submerged weight per unit length (w) and length (s).
$z(s) = \frac{ws^2}{2EA_o} + \frac{Hs\ tan(\theta_a)}{EA_o} + \frac{H}{w}\sqrt{1 + \left(\frac{ws}{H} + tan(\theta_a)\right)^2} - \frac{H}{w} sec\ (\theta_a)$	Calculate the vertical coordinate of the segment upper end based on the horizontal and vertical force components at the segment lower end and segment properties: Young's modulus E, effective cross section area (A_0), submerged weight per unit length (w) and length (s).

In order to calculate the horizontal and vertical force components of the tension at the fairlead position it is necessary to solve iteratively the boundary value problem for the catenary equations. For this boundary value problem the known quantities are the anchor

position (x_a,z_a) and fairlead position (x_b,z_b), the number of segments in the mooring line, and the properties of each segment: length (L), unit submerged weight (w) and unit stiffness (EA_0). The unknown quantities are the horizontal and vertical force components at the anchor point and at the fairlead position.

Table 2.2. Summary of useful equations for segments laying on the seabed.

Equation	Purpose
$H_b = H$	Horizontal force component along the mooring line segment from the anchoring point up to the fairlead point.
$V_b = 0$	Vertical force component equal to zero along the mooring line segment laying on the seabed, all the weight is directly transmitted to the seabed, up to the touch down point.
$T_b = H$	Tension at any location of the mooring line segment laying on the seabed up to the touch down point
$x(s) = s + \frac{Hs}{EA_o}$	Calculate the horizontal coordinate as function of s for segments laying on the seabed, considering the horizontal force component and segment properties: Young's modulus E, effective cross section area (A_0) and length (s).
$z(s) = z_a$	The vertical coordinate as function of s for segments laying on the seabed is equal to the vertical coordinate of the anchoring point (there is no change in z coordinate position).

The iterative procedure consists of defining initial values for the horizontal and vertical force components at the anchor point and calculating the mooring line end position at the fairlead using the equations shown in Table 2.1 and Table 2.2. The calculated end

position is compared with the actual fairlead position and if the positions are close enough (less than a specified tolerance) then the associated forces at the fairlead position are used in the vessel equilibrium calculation, otherwise new values for the horizontal and vertical force component at the anchor point are selected. This process is repeated until the specified tolerance or the given maximum number of iterations is achieved.

Based on the actual fairlead position, three different ranges are defined to apply a specific procedure to obtain the horizontal and vertical force components at the fairlead position. The limits for those ranges are defined as follows.

The first limit corresponds to the situation where the value of the horizontal force component in the line is equal to zero, so the tension at the fairlead will be just the weight of the mooring line length hanging from the fairlead down to the touch down point, as illustrated in Figure 2.6. The mooring line hanging length is calculated iteratively seeking to match the vertical coordinate of the mooring line end at the fairlead position with the actual fairlead vertical coordinate (z_b). Thus, the horizontal coordinate (x_1) of the mooring line end at the fairlead position is equal to the length of the mooring line laying on the seabed as shown in Figure 2.6. The equations provided in Table 2.3 are used to calculate the vertical force and the upper position for any segment hanging vertically. So, at this position the horizontal force component is $H_1=0$, the vertical force component is V_1, the horizontal coordinate is x_1 and the vertical coordinate is $z_1=z_b$.

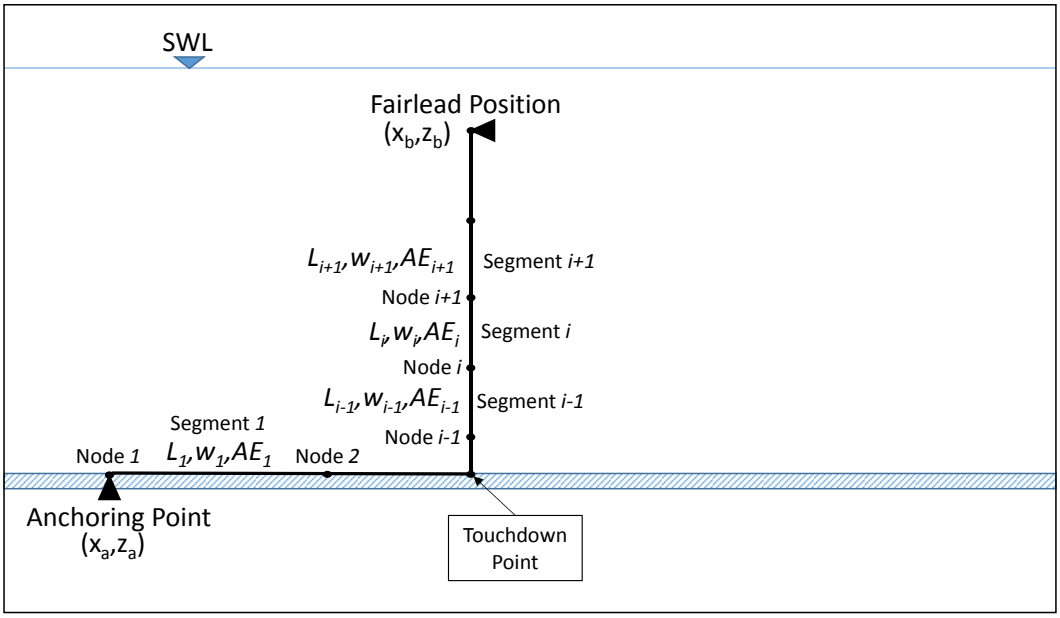

Figure 2.6. Fairlead position limit considering the horizontal force equal to zero.

Table 2.3. Summary of useful equations for segments hanging completely vertical

Equation	Purpose
$H_{i+1} = 0$	Horizontal force component at any node.
$V_{i+1} = V_i + w_i s_i$	Vertical force component at node *i*+1 as a function of the vertical force component at node *i* and the length *s* and submerged weight per unit length *w* of segment *i*.
$T_{i+1} = V_{i+1}$	Tension at node *i*+1 as a function of the vertical force component at the same node.
$x_{i+1} = x_i$	Horizontal coordinate of node *i*+1 as a function of the horizontal coordinate at node *i*
$z_{i+1} = z_i + \frac{V_i s_i}{AE_i} + \frac{w_i {s_i}^2}{2AE_i}$	Vertical coordinate of node *i*+1 as a function of the vertical coordinate at node *i* and segment *i* properties: length *s*, submerged weight per unit length *w* and unit stiffness *AE*.

The second limit corresponds to the situation where the value of the vertical force at the anchor point is equal to zero (the mooring line angle at the anchor point is equal to zero), so the vertical force at the fairlead position is equal to the total mooring line submerged weight, as illustrated in Figure 2.7. For this case the horizontal force (H) is calculated iteratively using the equations provided in Table 2.1, until the vertical coordinate at the mooring line end is close enough to the actual fairlead vertical coordinate (z_b). Once this horizontal force is defined, the horizontal coordinate (x_2) is calculated for the mooring line end at the fairlead position. At the fairlead the horizontal force component is denoted as H_2, the vertical force component is denoted as V_2, the horizontal coordinate as x_2 and the vertical coordinate as $z_2=z_b$.

Considering those two limits, three different ranges are defined where different procedures are used to calculate the horizontal and vertical force components at the actual fairlead position. The first range corresponds to the situation where the line is completely slack, in which case the actual fairlead horizontal coordinate (x_b) is less than or equal to the first range limit (x_1). In this range the horizontal (H_f) and vertical (V_f) force components at the fairlead position are the same as the forces calculated for this first range limit, namely for $x_b \leq x_1$, $H_f=H_1=0$ and $V_f=V_1$.

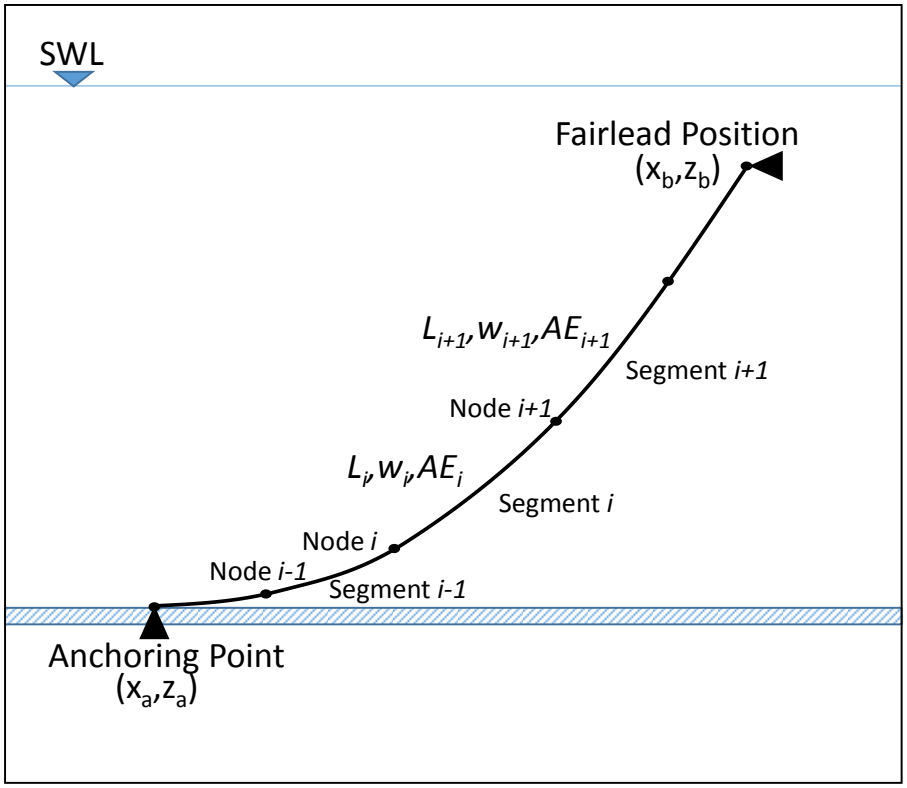

Figure 2.7. Fairlead position limit setting to zero the vertical force at the anchor point.

The second range corresponds to the situation where the actual fairlead horizontal coordinate (x_b) lies between the first range limit (x_1) and the second range limit (x_2). As shown in Figure 2.8, there is a part of the mooring line lying on the seabed. If the touchdown point is between two initially defined nodes, the initially defined segment is divided in two segments using a third node that will be defining the touchdown point.

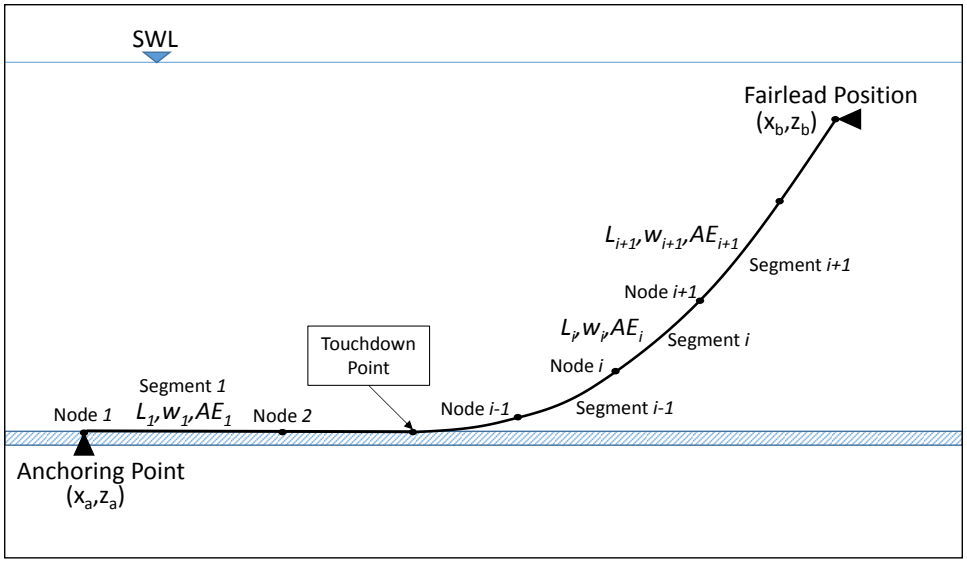

Figure 2.8. Conditions considered to calculate forces at fairlead position for the second range.

The iterative procedure developed for this range to calculate the horizontal (H_f) and vertical (V_f) force components at the actual fairlead position is as follows:

1. Define the values calculated for the first range limit as lower limit values for the horizontal and vertical force components and for the horizontal and vertical coordinates ($H_l = H_1$, $V_l = V_1$, $x_l = x_1$ and $z_l = z_1 = z_b$). Calculate the total mooring line length laying on the seabed, and define this as the initial upper limit for the mooring line length laying on the seabed (L_{sbu}).
2. Define the values calculated for the second range limit as upper limit values for the horizontal and vertical force components and for the horizontal and vertical coordinates ($H_u = H_2$, $V_u = V_2$, $x_u = x_2$ and $z_u = z_2 = z_b$). In this case there is

not any segment of the mooring line laying on the seabed; this will be the initial lower limit for the mooring line length laying on the seabed (L_{sbl}=0).

3. Calculate the bisecting mooring line length laying on the seabed considering the lower and upper limits defined (L_{sb}=0.5[L_{sbl}+ L_{sbu}]).
4. Calculate the new horizontal (x) and vertical (z) coordinates for the upper end of the mooring line using equations included in Table 2.2 (for the segments lying on the seabed from the anchor point to the touchdown point) and Table 2.1 (for the segments included from the touchdown point up to the mooring line end at the fairlead position).
5. Iteratively modify the horizontal force component in order to match the vertical (z) coordinate of the upper end of the mooring line end with the actual fairlead vertical (z_b) coordinate.
6. Compare the resulting horizontal (x) coordinate for the mooring line end with the actual fairlead horizontal coordinate (x_b). If $x \leq x_b$ then the lower limit is defined as H_l= H, V_l=V, x_l=x, z_l=z=z_b and the upper limit as L_{sbu}=L_{sb}; If $x_b \leq x$, then the upper limit is defined as H_u= H, V_u=V, x_u=x and z_u=z=z_b and the lower limit as L_{sbl}=L_{sb}. Repeat from point 3 until the difference between the horizontal (x) coordinate for the upper mooring line end and the actual fairlead horizontal coordinate (x_b) is equal to or less than the specified tolerance or the maximum number of iterations is reached.
7. Upon reaching convergence, the horizontal and vertical force components are defined as H_f=H and V_f=V.

The third range corresponds to the situation where the actual fairlead horizontal coordinate (x_b) is greater than or equal to the horizontal coordinate for the upper end of the mooring line (x_2) calculated for the second range limit. The iterative procedure to calculate the horizontal (H_f) and vertical (V_f) force components at the actual fairlead position is as follows:

1. Define the values calculated for the second range limit as lower limit values for the horizontal and vertical force components and for the horizontal and vertical coordinates ($H_l = H_2$, $V_l = V_2$, $x_l = x_2$ and $z_l = z_2 = z_b$).
2. Set the horizontal force component at the anchor point as $H_a = 2H_l$.
3. Calculate the new horizontal (x) and vertical (z) coordinates for the upper end of the mooring line using equations included in Table 2.1.
4. Iteratively modify the vertical force component in order to match the vertical (z) coordinate for the upper end of the mooring line to the actual fairlead vertical (z_b) coordinate.
5. Compare the resulting horizontal (x) coordinate for the mooring line end with the actual fairlead horizontal coordinate (x_b). If $x \leq x_b$ then set $H_l = H$, $V_l = V$, $x_l = x$ and $z_l = z = z_b$ and repeat from point 2. If $x_b \leq x$ then the upper limit is defined as $H_u = H$, $V_u = V$, $x_u = x$ and $z_u = z = z_b$ and continue at point 6.
6. Set the horizontal force at the anchoring point as bisecting the upper and lower limits ($H_a = 0.5\,[H_u + H_l]$).
7. Calculate the new horizontal (x) and vertical (z) coordinates for the upper mooring line end using equations included in Table 2.1.

8. Iteratively modify the vertical force component in order to match the vertical (z) coordinate for the upper mooring line end to the actual fairlead vertical (z_b) coordinate. Compare the resulting horizontal (x) coordinate for the mooring line end with the actual fairlead horizontal coordinate (x_b). If $x \leq x_b$, then set $H_l = H$, $V_l = V$, $x_l = x$ and $z_l = z = z_b$ and repeat from point 6. If $x_b \leq x$, then set $H_u = H$, $V_u = V$, $x_u = x$ and $z_u = z = z_b$ and repeat from point 6. If the difference between the horizontal (x) coordinate for the upper end of the mooring line and the actual fairlead horizontal coordinate (x_b) is equal to or less than the specified tolerance or the maximum number of iterations is reached then set the horizontal and vertical force components as $H_f = H$ and $V_f = V$.

The values calculated for the horizontal (H_f) and vertical (V_f) force components based on the procedures described above are used to calculate the static equilibrium position of the floating structure as described in the following section.

2.2 Vessel Static Equilibrium Position

The second step to calculate the static response curves is to obtain the calm water equilibrium position of the vessel considering its hydrostatic stiffness characteristics, the attached mooring and riser system and any user defined force and moment applied to the vessel. In Figure 2.9 are shown the forces and moments acting on the floater at the calm water equilibrium position. The sum of all forces and moments exerted by all mooring lines and risers on the floater, in combination with hydrostatic restoring forces and moments in heave roll and pitch (Fz_{hs}, Mx_{hs}, My_{hs}, respectively) of the floater, must be in

equilibrium with any number of user-defined forces and moments (Fx_j, Fy_j, Fz_j, Mx_j, My_j, Mz_j) applied at user-defined points with coordinates (x_j', y_j', z_j') with respect to the vessel local coordinate system.

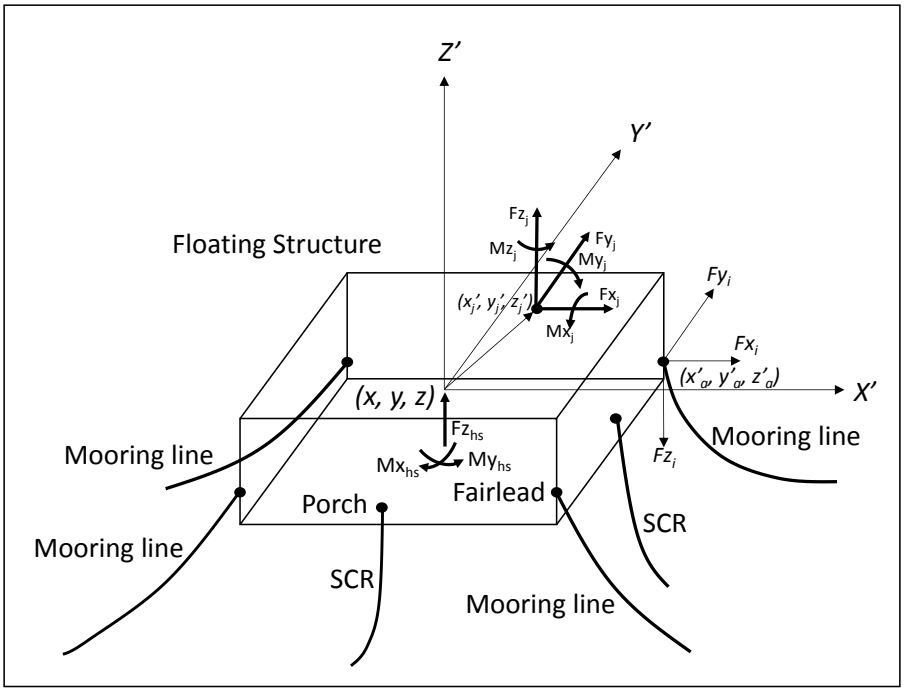

Figure 2.9. Forces and moments acting on the vessel at calm water equilibrium position.

The steps followed to calculate the force components in the global coordinate system for each one of the mooring lines and steel catenary risers attached to the floater are as described below.

The fairlead or porch coordinates must be transformed from the local coordinate system into the global coordinate system, as shown in Figure 2.10. The rigid body floater

rotations (local coordinate system) around the global coordinate axis are θ_x, θ_y and θ_z, respectively; and the fairlead position in local coordinates are x'_a, y'_a and z'_a. The fairlead coordinates in the global system (x_a, y_a and z_a) are calculated using the following transformation functions:

i. Transformation function of coordinates considering the rotation around the X axis can be written as

$$[T_x] = \begin{bmatrix} 1 & 0 & 0 \\ 0 & \cos\theta_x & -\sin\theta_x \\ 0 & \sin\theta_x & \cos\theta_x \end{bmatrix} \quad (2.22)$$

ii. In a similar way the transformation function of coordinates considering the rotation around the Y axis can be written as

$$[T_y] = \begin{bmatrix} \cos\theta_y & 0 & \sin\theta_y \\ 0 & 1 & 0 \\ -\sin\theta_y & 0 & \cos\theta_y \end{bmatrix} \quad (2.23)$$

iii. And finally the transformation function of coordinates considering the rotation around the Z axis can be written as

$$[T_z] = \begin{bmatrix} \cos\theta_z & -\sin\theta_z & 0 \\ \sin\theta_z & \cos\theta_z & 0 \\ 0 & 0 & 1 \end{bmatrix} \quad (2.24)$$

iv. The transformation of coordinates from the local coordinate system into the global coordinate system considering the three angles of rotation shown in Figure 2.10 is calculated using equations (2.22), (2.23) and (2.24) as

$$[T] = [T_z]\,[T_y][\,T_x]$$

$$[T] = \begin{bmatrix} \cos\theta_z & -\sin\theta_z & 0 \\ \sin\theta_z & \cos\theta_z & 0 \\ 0 & 0 & 1 \end{bmatrix} \begin{bmatrix} \cos\theta_y & 0 & \sin\theta_y \\ 0 & 1 & 0 \\ -\sin\theta_y & 0 & \cos\theta_y \end{bmatrix} \begin{bmatrix} 1 & 0 & 0 \\ 0 & \cos\theta_x & -\sin\theta_x \\ 0 & \sin\theta_x & \cos\theta_x \end{bmatrix}$$

So, the fairlead coordinates in the global coordinate system relative to the floater's local coordinate system origin can be calculated as

$$\begin{Bmatrix} x_a \\ y_a \\ z_a \end{Bmatrix} = \begin{bmatrix} \cos\theta_z & \sin\theta_z & 0 \\ -\sin\theta_z & \cos\theta_z & 0 \\ 0 & 0 & 1 \end{bmatrix} \begin{bmatrix} \cos\theta_y & 0 & -\sin\theta_y \\ 0 & 1 & 0 \\ \sin\theta_y & 0 & \cos\theta_y \end{bmatrix} \begin{bmatrix} 1 & 0 & 0 \\ 0 & \cos\theta_x & \sin\theta_x \\ 0 & -\sin\theta_x & \cos\theta_x \end{bmatrix} \begin{Bmatrix} x'_a \\ y'_a \\ z'_a \end{Bmatrix} \qquad (2.25)$$

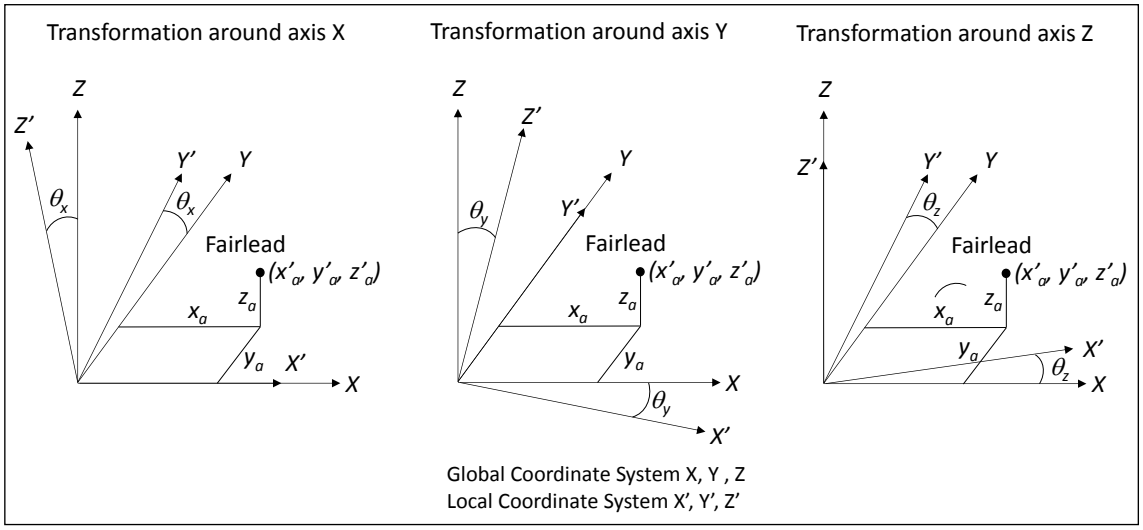

Figure 2.10. Coordinate transformation from local to global coordinate system.

In order to calculate the forces at the fairlead locations exerted by the mooring lines it is necessary to know the relative position between the fairleads and the anchor points. To know the relative position between those points for each mooring line, and remembering that the fairlead coordinates are in the vessel's local coordinate system and the anchor location is in the global coordinate system, the fairlead coordinates must be

transformed to the global coordinate system including the vessel's position and rotations. So, the fairlead coordinates in the vessel's coordinate system must be rotated to the global coordinate system considering the vessel's local coordinate system origin (rotation reference point for the vessel). With the vessel position in the global coordinate system the fairlead location in the global coordinate system can be obtained as

$$\begin{Bmatrix} x_{a\prime} \\ y_{a\prime} \\ z_{a\prime} \end{Bmatrix} = \begin{Bmatrix} x_a \\ y_a \\ z_a \end{Bmatrix} + \begin{Bmatrix} x \\ y \\ z \end{Bmatrix} \tag{2.26}$$

Once the coordinates of the fairleads and porches are transformed to the global coordinate system using Equation (2.26), the vertical plane of each individual mooring line and riser is defined which includes the fairlead or porch and the anchor point. In this vertical plane will be calculated the horizontal and vertical force components at the fairlead or porch positions for each mooring line and riser with the procedure described in section 2.1. Figure 2.11 shows the floater with the mooring lines and risers attached, and the coordinates in the global system for the fairlead and anchor point for a mooring line to define the vertical plane which includes the fairlead and anchor point. In this vertical plane are calculated the horizontal (H) and vertical (V) force components for the mooring line. The horizontal force at the fairlead, calculated with the procedure described in section 2.1, is decomposed into its global coordinate system components (Fx_i and Fy_i) taking into account the angle (ϕ) that is formed by the vertical plane containing the mooring line and the global system axis X, as shown in Figure 2.11. The length of the horizontal projection of the mooring line between the fairlead and the anchor point is calculated as

$$L_h = \sqrt{(x_b - x_{a\prime})^2 + (y_b - y_{a\prime})^2} \tag{2.27}$$

So, the *cos(ϕ)* and *sin(ϕ)* can be written, respectively, as

$$\cos(\emptyset) = \frac{(x_b - x_{a\prime})}{\sqrt{(x_b - x_{a\prime})^2 + (y_b - y_{a\prime})^2}} \tag{2.28}$$

$$\sin(\emptyset) = \frac{(y_b - y_{a\prime})}{\sqrt{(x_b - x_{a\prime})^2 + (y_b - y_{a\prime})^2}} \tag{2.29}$$

and the angle ϕ (in degrees) can be calculated as

$$\emptyset = \left(\frac{180}{\pi}\right) \tan^{-1}\left(\frac{(y_b - y_{a\prime})}{(x_b - x_{a\prime})}\right)$$

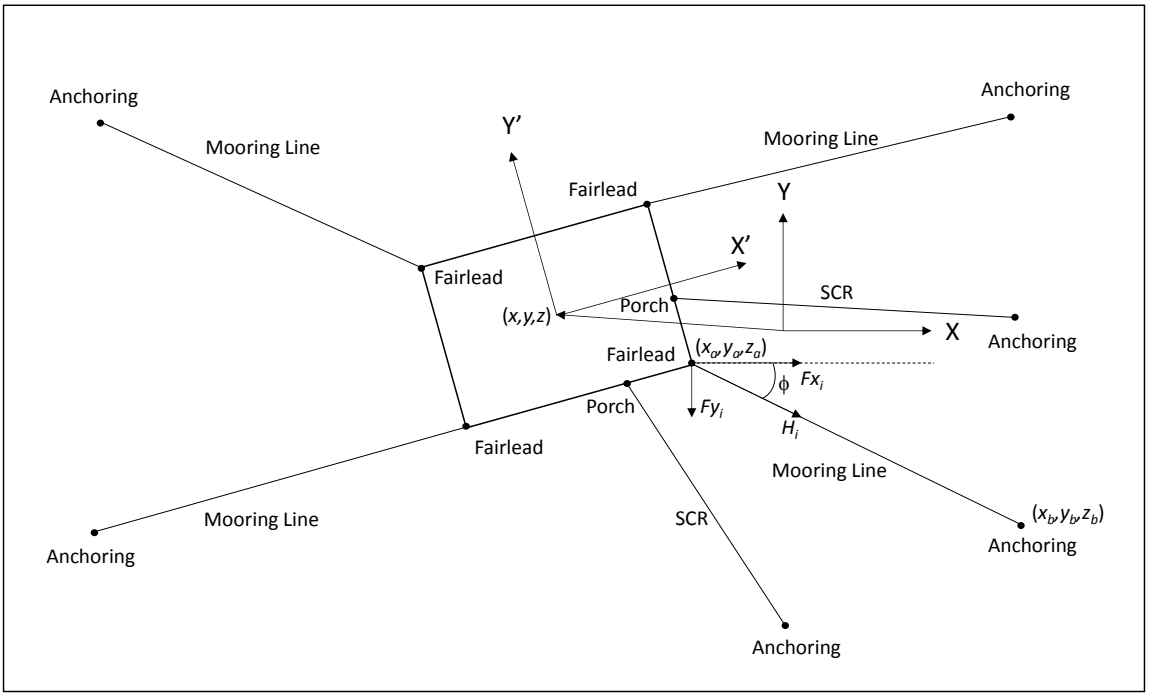

Figure 2.11. Mooring line vertical plane definition and force components at fairlead.

The local coordinate system for each mooring line and riser, to be used in the procedure for the catenary solution described in section 2.1, is defined with its *x* axis in the horizontal direction from the anchor point to the fairlead and its *z* axis in the vertical direction from the anchor point upward, so that the origin is at the anchor point (0, 0) and the fairlead coordinates in this local coordinate system (vertical plane in global coordinate system, containing the anchor and fairlead points) is defined as (L_h, z_a-z_b) where L_h is calculated with equation (2.27).

The mooring line horizontal (*H*) and vertical (*V*) force components are calculated with the procedure described in section 2.1. The vertical (*V*) force component is parallel to the vertical Z axis in the global coordinate system, so it can be applied directly at the fairlead position in the global coordinate system (Fz_i=*V*). The horizontal (*H*) force component, which is contained in the vertical plane of the mooring line, must be decomposed into its global coordinate system components (Fx_i and Fy_i), as shown in Figure 2.11, using the equations (2.28) and (2.29), respectively, as

$$Fx_i = H\cos(\emptyset) = \frac{H\ (x_b - x_{a'})}{\sqrt{(x_b - x_{a'})^2 + (y_b - y_{a'})^2}} \tag{2.30}$$

and

$$Fy_i = H\ \sin(\emptyset) = \frac{H\ (y_b - y_{a'})}{\sqrt{(x_b - x_{a'})^2 + (y_b - y_{a'})^2}} \tag{2.31}$$

The moments around the floater's local coordinate system origin exerted by the mooring line and riser forces at the fairlead/porch position can be calculated using their force components (Fx_i, Fy_i, Fz_i) in the global coordinate system and the fairlead/porch coordinates (x_a,y_a,z_a) in the global system. The moments exerted by each mooring line and

riser are calculated as the cross product of the force vector ($\vec{F}$) and the position vector ($\vec{r}$) between the point where the force vector is applied and the floater's origin:

$$\vec{M} = \vec{r}\mathrm{x}\vec{F} = \begin{vmatrix} \hat{\imath} & \hat{\jmath} & \hat{k} \\ x_a & y_a & z_a \\ Fx_i & Fy_i & Fz_i \end{vmatrix} = \begin{pmatrix} +(Fz_i y_a - Fy_i z_a)\hat{\imath} \\ -(Fz_i x_a - Fx_i z_a)\hat{\jmath} \\ +(Fy_i x_a - Fx_i y_a)\hat{k} \end{pmatrix} = \begin{pmatrix} (-Fy_i z_a + Fz_i y_a)\hat{\imath} \\ (Fx_i z_a - Fz_i x_a)\hat{\jmath} \\ (-Fx_i y_a + Fy_i x_a)\hat{k} \end{pmatrix}$$

So, the total moment components around each axis in the global coordinate frame at the floater's local coordinate system origin can be written as the sum of the moment component exerted by each one of the mooring lines and risers (where *n* is the total number of mooring lines and risers) according to

$$Mx_m = \sum_{i=1}^{n} (-Fy_i\,(z_a)_i + Fz_i\,(y_a)_i) \tag{2.32}$$

$$My_m = \sum_{i=1}^{n} (Fx_i\,(z_a)_i - Fz_i\,(x_a)_i) \tag{2.33}$$

$$Mz_m = \sum_{i=1}^{n} (-Fx_i\,(y_a)_i + Fy_i\,(x_a)_i) \tag{2.34}$$

To calculate the moments exerted by the user-defined forces applied to the vessel, Equation (2.25) is used for transforming the application point coordinates from the local coordinate system to the global coordinate system:

$$\begin{Bmatrix} x_j \\ y_j \\ z_j \end{Bmatrix} = \begin{bmatrix} \cos\theta_y & 0 & -\sin\theta_y \\ 0 & 1 & 0 \\ \sin\theta_y & 0 & \cos\theta_y \end{bmatrix} \begin{bmatrix} 1 & 0 & 0 \\ 0 & \cos\theta_x & \sin\theta_x \\ 0 & -\sin\theta_x & \cos\theta_x \end{bmatrix} \begin{bmatrix} 1 & 0 & 0 \\ 0 & \cos\theta_x & \sin\theta_x \\ 0 & -\sin\theta_x & \cos\theta_x \end{bmatrix} \begin{Bmatrix} x_j{}' \\ y_j{}' \\ z_j{}' \end{Bmatrix} \tag{2.35}$$

The moments due to the user-defined forces can be calculated with the following equations (where *m* is the total number of user-defined forces) as

$$Mx_f = \sum_{j=1}^{m} \left(-Fy_j\, z_j + Fz_j\, y_j\right) \tag{2.36}$$

$$My_f = \sum_{j=1}^{m} \left(Fx_j\, z_j - Fz_j\, x_j\right) \tag{2.37}$$

$$Mz_f = \sum_{j=1}^{m} \left(-Fx_j\, y_j + Fy_j\, x_j\right) \tag{2.38}$$

The force and moments due the hydrostatic stiffness in heave, roll and pitch (Fx_{hs}, Mx_{hs}, My_{hs}, respectively) are calculated based on the floater response in heave (z), roll (θx) and pitch (θy).

The restoring force in heave can be written as

$$Fx_{hs} = -z\, K_z \tag{2.39}$$

where K_z is the hydrostatic stiffness in the heave direction.

The restoring moment in roll (around X axis) can be written as

$$Mx_{hs} = -\theta_x\, K_r \tag{2.40}$$

where θ_x is the rotation of the vessel around the X axis and K_r is the roll hydrostatic stiffness.

And finally, the restoring moment in pitch (around Y axis) can be written as

$$My_{hs} = -\theta_y\, K_p \tag{2.41}$$

where θ_y is the rotation of the vessel around the Y axis and K_p is the pitch hydrostatic stiffness.

At each offset considered in the surge direction there will be a net horizontal restoring force from the mooring and riser system that is acting in the opposite direction

to that of the given offset. This restoring force is the floater's static response to environmental loads acting on the floater (wind and currents) so it is considered that the total applied horizontal force, which is equal in magnitude to the static horizontal restoring force exerted by the mooring and riser system, is acting at a defined elevation Z_{EF}. This applied force produces an additional moment (*My*) around the Y axis that must be considered in the static equilibrium solution for each offset considered. The elevation (Z_{EF}) is defined in the global coordinate system relative to the vessel's local coordinate system and it is considered constant at any offset. The moment around the Y axis due this force can be written as

$$My_{EF} = Fx_{EF}\, z_{EF} \tag{2.42}$$

where:

My_{EF} = moment induced by the environmental applied force in the surge direction on the floater

Fx_{EF}= environmental applied force on the floater that produces its offset in surge direction, equal in magnitude to the total mooring and riser system restoring force, but in the opposite direction

z_{EF}= elevation of the environmental applied force on the floater with respect to the local coordinate system.

At the calm water static equilibrium position of the floating structure, and for any one of the horizontal offsets which are considered to obtain the static response

characteristics, the following static force and moment equilibrium equations must be satisfied:

$$\sum Fx = 0\,;\ \sum Fy = 0\,;\ \sum Fz = 0$$

$$\sum Mx = 0\,;\ \sum My = 0\,;\ \sum Mz = 0$$

As mentioned above, the first step is to calculate the calm water equilibrium position in the absence of applied environmental loads. The procedure developed to calculate the equilibrium position of the vessel is an iterative process, due to the nonlinear behavior of the mooring and riser system.

The initial position and rotation vector of the floating structure is defined as

$$\{D_{init}\} = \begin{Bmatrix} x \\ y \\ z \\ \theta_x \\ \theta_y \\ \theta_z \end{Bmatrix} \tag{2.43}$$

At the initial position the unbalanced forces and moments are calculated as (where *n* is the total number of mooring lines and risers, and *m* is the total number of user-defined forces and moments applied to the vessel)

$$Fx_u = \sum_{i=1}^{n} Fx_i + \sum_{j=1}^{m} Fx_j \tag{2.44}$$

$$Fy_u = \sum_{i=1}^{n} Fy_i + \sum_{j=1}^{m} Fy_j \tag{2.45}$$

$$Fz_u = \sum_{i=1}^{n} Fz_i + \sum_{j=1}^{m} Fz_j + \mathrm{Fz_{hs}} \tag{2.46}$$

$$Mx_u = Mx_m + \sum_{j=1}^{m} Mx_j + \mathrm{Mx_{hs}} + Mx_f \tag{2.47}$$

$$My_u = My_m + \sum_{j=1}^{m} My_j + \mathrm{My_{hs}} + My_f \tag{2.48}$$

$$Mz_u = Mz_m + \sum_{j=1}^{m} Mz_j + Mz_f \tag{2.49}$$

These can be accumulated in an unbalanced force and moment vector $\{F_u\}$ as

$$\{F_u\} = \begin{Bmatrix} Fx_u \\ Fy_u \\ Fz_u \\ Mx_u \\ My_u \\ Mz_u \end{Bmatrix} \tag{2.50}$$

The stiffness matrix for this position is calculated assuming small displacements (∂x, ∂y, ∂z) and small rotations ($\partial\theta_x$, $\partial\theta_y$, $\partial\theta_z$) of the floater with respect to the origin of the body-fixed coordinate system. The linearized stiffness matrix at this position can be written as

$$[K] = \begin{bmatrix} \frac{\partial F_x}{\partial x} & \frac{\partial F_x}{\partial y} & \frac{\partial F_x}{\partial z} & \frac{\partial F_x}{\partial \theta_x} & \frac{\partial F_x}{\partial \theta_y} & \frac{\partial F_x}{\partial \theta_z} \\ \frac{\partial F_y}{\partial x} & \frac{\partial F_y}{\partial y} & \frac{\partial F_y}{\partial z} & \frac{\partial F_y}{\partial \theta_x} & \frac{\partial F_y}{\partial \theta_y} & \frac{\partial F_y}{\partial \theta_z} \\ \frac{\partial F_z}{\partial x} & \frac{\partial F_z}{\partial y} & \frac{\partial F_z}{\partial z} + K_z & \frac{\partial F_z}{\partial \theta_x} & \frac{\partial F_z}{\partial \theta_y} & \frac{\partial F_z}{\partial \theta_z} \\ \frac{\partial M_x}{\partial x} & \frac{\partial M_x}{\partial y} & \frac{\partial M_x}{\partial z} & \frac{\partial M_x}{\partial \theta_x} + K_r & \frac{\partial M_x}{\partial \theta_y} & \frac{\partial M_x}{\partial \theta_z} \\ \frac{\partial M_y}{\partial x} & \frac{\partial M_y}{\partial y} & \frac{\partial M_y}{\partial z} & \frac{\partial M_y}{\partial \theta_x} & \frac{\partial M_y}{\partial \theta_y} + K_p & \frac{\partial M_y}{\partial \theta_z} \\ \frac{\partial M_z}{\partial x} & \frac{\partial M_z}{\partial y} & \frac{\partial M_z}{\partial z} & \frac{\partial M_z}{\partial \theta_x} & \frac{\partial M_z}{\partial \theta_y} & \frac{\partial M_z}{\partial \theta_z} \end{bmatrix} \tag{2.51}$$

where K_z, K_r and K_p are the linearized hydrostatic stiffness components in heave, roll and pitch, respectively.

Considering the unbalanced force vector shown in equation (2.50) and the stiffness matrix shown in equation (2.51) applied to the Hooke's Law equation shown in equation (2.52), an incremental displacement and rotation vector $\{\delta D\}$ can be calculated in the following way

$$[K]\{\delta D\} = \{F_u\} \tag{2.52}$$

$$\{\delta D\} = \begin{bmatrix} \delta x \\ \delta y \\ \delta z \\ \delta \theta_x \\ \delta \theta_y \\ \delta \theta_z \end{bmatrix} = [K]^{-1}\{F_u\} \tag{2.53}$$

So, the final position and rotation vector for the vessel can be calculated as

$$\{D_{final}\} = \{D_{init}\} + \{\delta D\} = \begin{Bmatrix} x \\ y \\ z \\ \theta_x \\ \theta_y \\ \theta_z \end{Bmatrix} + \begin{Bmatrix} \delta x \\ \delta y \\ \delta z \\ \delta\theta_x \\ \delta\theta_y \\ \delta\theta_z \end{Bmatrix} = \begin{Bmatrix} x + \delta x \\ y + \delta y \\ z + \delta z \\ \theta_x + \delta\theta_x \\ \theta_y + \delta\theta_y \\ \theta_z + \delta\theta_z \end{Bmatrix} \quad (2.54)$$

At this final position are calculated the unbalanced force and moment vector $\{F_u\}$, and if each one of the elements in this vector are equal to zero or less than the pre-defined tolerance, or the specified maximum number of iterations is reached, the calm water equilibrium position of the floating structure is defined as the position and rotations calculated in this last step. If one or more of the elements in the unbalanced force and moment vector is greater than the defined tolerance, the process described above is repeated with an updated stiffness matrix calculated at the last "final position".

If convergence is reached, the origin of the global coordinate system is translated to the *x* and *y* position calculated for the calm water equilibrium condition, but it is kept at the still water plane. Due to this translation the coordinates of the mooring line and riser anchor points are updated with respect to the new global coordinate system origin.

Once the calm water equilibrium position is defined, the static equilibrium position and the restoring force for each one of the horizontal offsets considered for the static response curves are calculated. The procedure developed to calculate the static equilibrium position for each one of the offsets considered is similar to that for the calm water equilibrium position, with the modifications described below.

At each specified horizontal offset position the *x* coordinate is fixed and equal to the offset in that direction (global *X* axis), the unbalanced force in the *x* direction Fx_u is equal to the restoring force at that offset position and it is also equal to the applied force in the

opposite direction. Equation (2.48) for the unbalanced moment My_u is modified to take into account the moment due the applied force,

$$My_u = My_m + \sum_{j=1}^{m} My_j + My_f + \mathrm{My_{hs}} + My_{EF} \tag{2.55}$$

The other modification in the procedure to calculate the static equilibrium position for each specified offset is to remove the displacements and forces in the *x* direction from equations (2.50) thru (2.54). Removing the force in the *x* direction from equation (2.50) leads to

$$\{F_u\} = \begin{Bmatrix} Fy_u \\ Fz_u \\ Mx_u \\ My_u \\ Mz_u \end{Bmatrix} \tag{2.56}$$

and removing the displacement in the *x* direction from equation (2.51) leads to the 5 x 5 stiffness matrix

$$[K] = \begin{bmatrix} \frac{\partial F_y}{\partial y} & \frac{\partial F_y}{\partial z} & \frac{\partial F_y}{\partial \theta_x} & \frac{\partial F_y}{\partial \theta_y} & \frac{\partial F_y}{\partial \theta_z} \\ \frac{\partial F_z}{\partial y} & \frac{\partial F_z}{\partial z} + K_z & \frac{\partial F_z}{\partial \theta_x} & \frac{\partial F_z}{\partial \theta_y} & \frac{\partial F_z}{\partial \theta_z} \\ \frac{\partial M_x}{\partial y} & \frac{\partial M_x}{\partial z} & \frac{\partial M_x}{\partial \theta_x} + K_r & \frac{\partial M_x}{\partial \theta_y} & \frac{\partial M_x}{\partial \theta_z} \\ \frac{\partial M_y}{\partial y} & \frac{\partial M_y}{\partial z} & \frac{\partial M_y}{\partial \theta_x} & \frac{\partial M_y}{\partial \theta_y} + K_p & \frac{\partial M_y}{\partial \theta_z} \\ \frac{\partial M_z}{\partial y} & \frac{\partial M_z}{\partial z} & \frac{\partial M_z}{\partial \theta_x} & \frac{\partial M_z}{\partial \theta_y} & \frac{\partial M_z}{\partial \theta_z} \end{bmatrix} \tag{2.57}$$

Equation (2.53) for the incremental displacement becomes

$$\{\delta D\} = \begin{Bmatrix} \delta y \\ \delta z \\ \delta\theta_x \\ \delta\theta_y \\ \delta\theta_z \end{Bmatrix} = [K]^{-1}\{F_u\} \tag{2.58}$$

The final position and rotation vector for the vessel at the prescribed offset position (x) is

$$\{D_{final}\} = \{D_{init}\} + \{\delta D\} = \begin{Bmatrix} y \\ z \\ \theta_x \\ \theta_y \\ \theta_z \end{Bmatrix} + \begin{Bmatrix} \delta y \\ \delta z \\ \delta\theta_x \\ \delta\theta_y \\ \delta\theta_z \end{Bmatrix} = \begin{Bmatrix} y + \delta y \\ z + \delta z \\ \theta_x + \delta\theta_x \\ \theta_y + \delta\theta_y \\ \theta_z + \delta\theta_z \end{Bmatrix} \tag{2.59}$$

As before, at this final position the unbalanced force and moment vector $\{F_u\}$ is calculated and tested for convergence. If convergence is achieved then the vessel's static equilibrium position for the specified offset is defined as the position and rotations calculated in this last step, and the restoring force can be calculated as the unbalanced force (Fx_u) at this offset. If one or more of the elements in the unbalanced force and moment vector is greater than the defined tolerance, and the specified maximum number of iterations has not been reached, then the stiffness matrix is updated and the process described above is repeated until the tolerance or the defined maximum number of iterations is reached. This procedure is repeated for each one of the horizontal offsets specified to define the static response curves.

2.3 Results

A commercial program, Orcaflex (Orcina Ltd), was used to validate the fit-for-purpose program to calculate the static response curves for the six degrees of freedom of a floating structure. Orcaflex is a well-recognized program to calculate static and/or dynamic responses of floating structures considering the attached mooring and riser systems. Two cases are considered to validate the Matlab fit-for-purpose program capabilities, comparing the results for those two cases with the results obtained by Orcaflex.

2.3.1 Single Mooring Line

The first validation case considered is a single mooring line composed of three segments with the properties provided in Table 2.4. For the analysis in Orcaflex a Poisson's ratio (v) of 0.5 valid for incompressible materials is applied, indicating that there is no effect on the strains of the mooring line due to the hydrostatic pressure acting on it. This is the same condition considered in the fit-for-purpose program.

The horizontal restoring force, vertical force and tension at the top end of the line were calculated for a set of offsets from -8% up to 8% of the water depth. A total of 31 offset positions equally spaced from -108 m up to 108 m were considered.

Figure 2.12, 2.13 and 2.14 compare the horizontal restoring force, the vertical force and the tension at the top end, respectively, calculated by Orcaflex and the fit-for-purpose program. The correlation between the two solutions is excellent, with maximum differences of 0.10% or less.

Table 2.4. Single mooring line characteristics.

Property	Value			
Water Depth (m)	1,350			
Coordinates	*X (m)*	*Y(m)*	*Z(m)*	
Fairlead Position	50	0	-25	
Anchoring Position	2,100	0	-1,350	
Number of segments	3			
Segment Properties	*L* (m)	*w* (N/m)	*EA* (N)	*Elements*
Platform Chain	160	3,327	1.69e9	16
Polyester	2,010	132.8	2.40e8	201
Anchor Chain	255	3,075	1.54e9	26

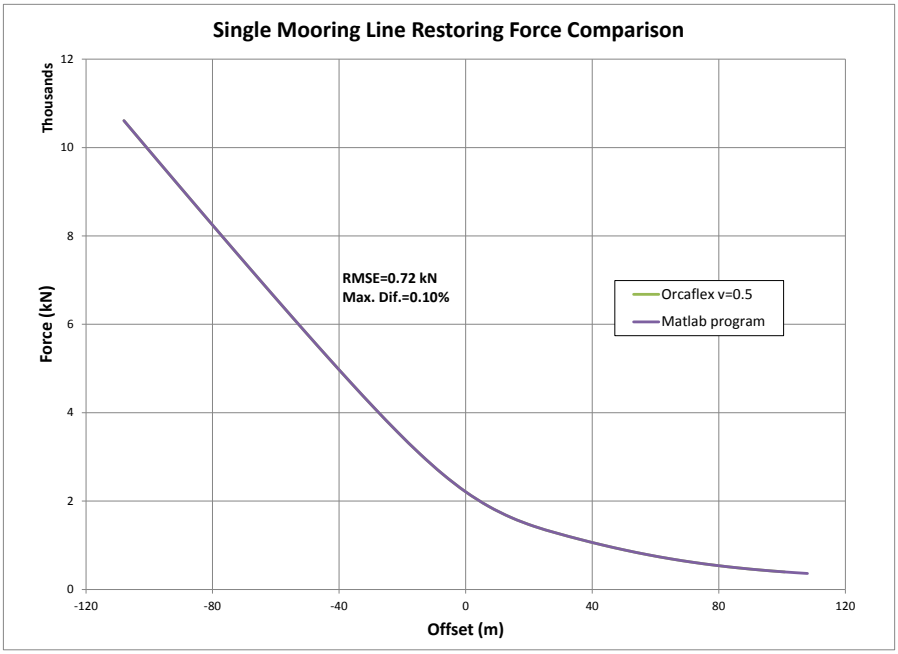

Figure 2.12. Single mooring line, restoring force comparison.

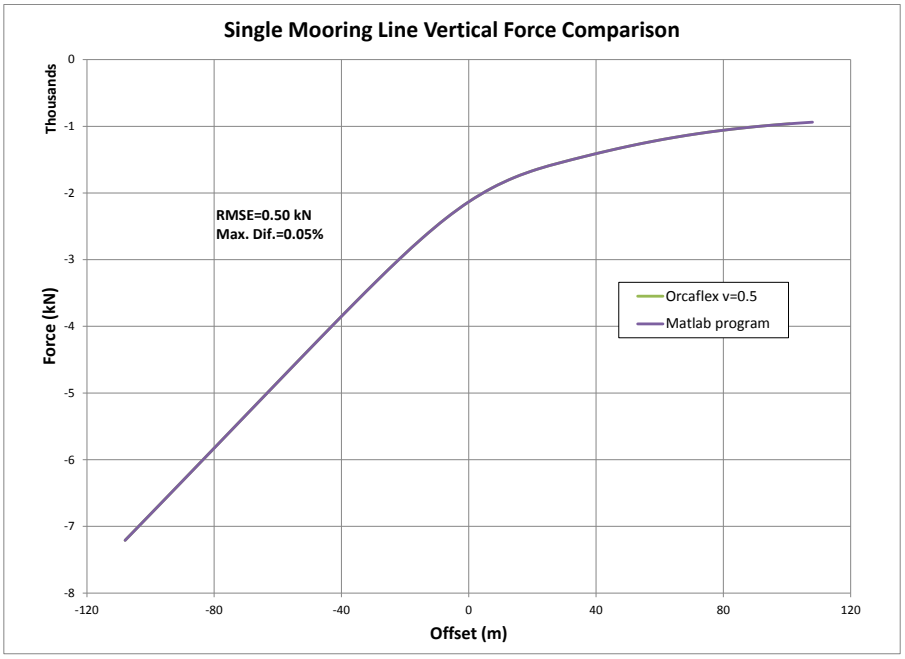

Figure 2.13. Single mooring line, vertical force comparison.

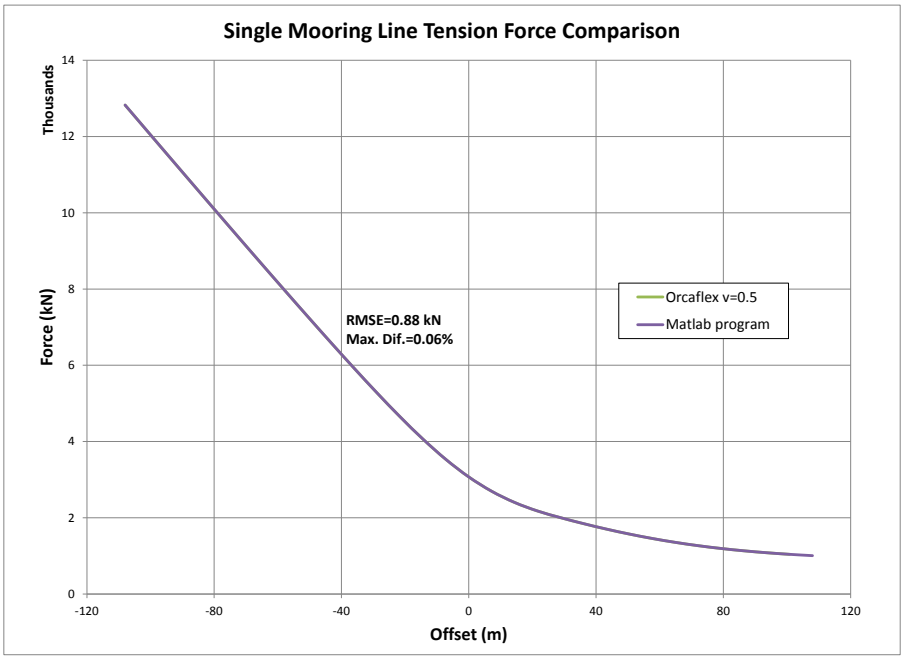

Figure 2.14. Single mooring line, tension force comparison.

2.3.2 Semisubmersible Mooring System

The second validation case considered is to compare the six degree of freedom static response of a semisubmersible with a symmetric 16-line mooring system, arranged in 4 groups of 4 mooring lines as shown in Figure 2.15.

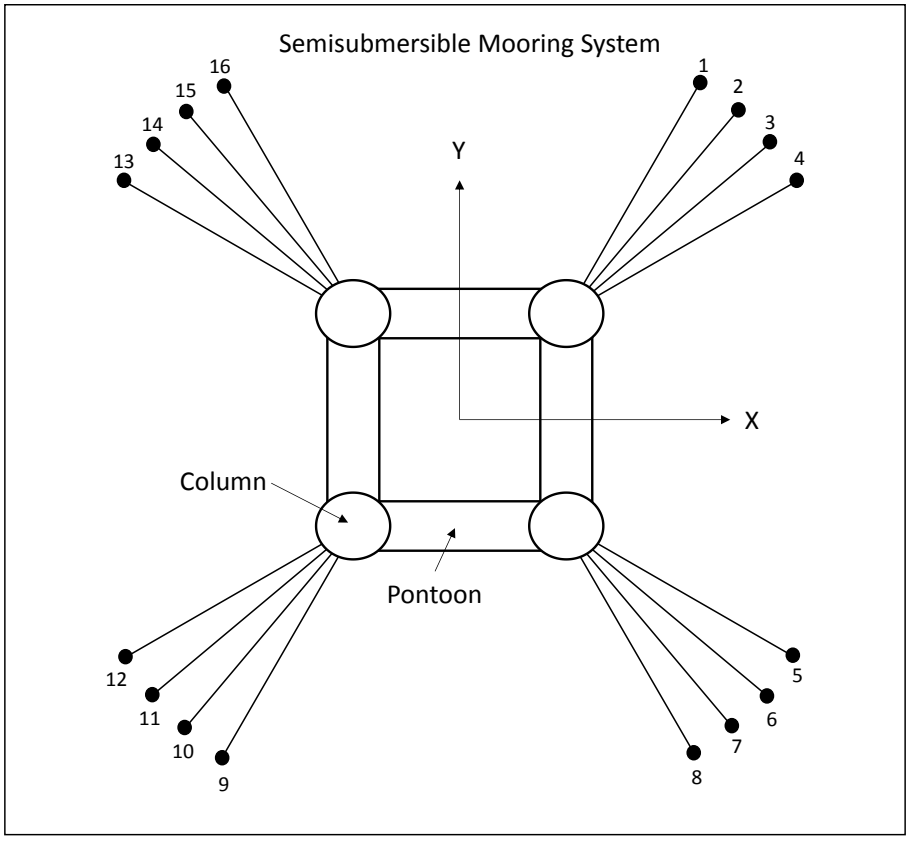

Figure 2.15. Semisubmersible mooring system configuration.

The semisubmersible hydrostatic stiffness characteristics and the mooring system properties are presented in Table 2.5. For this mooring system all mooring lines are

identical, so the values included in this table apply to all the mooring lines. The coordinates of the fairlead and anchor points for each mooring line are provided in Table 2.6.

Table 2.5. Semisubmersible and mooring system characteristics.

Property	Value			
Water Depth (m)	2,200			
Semisubmersible hydrostatic stiffness	Heave, K_z (N/m)	Roll, K_r (N m/rad)	Pitch, K_p (N m/rad)	
	22,690,000	4.233e10	4.233e10	
Elevation for applying acting force in X direction	18.74 m (above Sea Water Level)			
Number of Mooring Lines	16			
Number of Segment per Mooring Line	3			
Segment Properties	*L* (m)	*w* (N/m)	*AE* (N)	*Elements*
Platform Chain	150	4,648	2.303e9	15
Polyester	3,900	125.6	3.276e8	39
Anchor Chain	450	4,648	2.303e9	45

Table 2.6. Mooring lines coordinates at fairlead and anchor positions.

Mooring Line	Fairlead location			Anchoring location		
	X' (m)	Y' (m)	Z' (m)	X (m)	Y (m)	Z (m)
1	47.12	56.37	-17.68	2,449	3,187	-2,200
2	51.14	54.32	-17.68	2,717	2,964	-2,200
3	54.32	51.14	-17.68	2,964	2,717	-2,200
4	56.37	47.12	-17.68	3,187	2,449	-2,200
5	56.37	-47.12	-17.68	3,187	-2,449	-2,200
6	54.32	-51.14	-17.68	2,964	-2,717	-2,200
7	51.14	-54.32	-17.68	2,717	-2,964	-2,200
8	47.12	-56.37	-17.68	2,449	-3,187	-2,200
9	-47.12	-56.37	-17.68	-2,449	-3,187	-2,200
10	-51.14	-54.32	-17.68	-2,717	-2,964	-2,200
11	-54.32	-51.14	-17.68	-2,964	-2,717	-2,200
12	-56.37	-47.12	-17.68	-3,187	-2,449	-2,200
13	-56.37	47.12	-17.68	3,187	2,449	-2,200
14	-54.32	51.14	-17.68	2,964	2,717	-2,200
15	-51.14	54.32	-17.68	2,717	2,964	-2,200
16	-47.12	56.37	-17.68	2,449	3,187	-2,200

Using the Matlab fit-for-purpose program, the static response characteristics were calculated for a set of offsets from the calm water equilibrium position up to -176 m, which corresponds to -8% of the water depth. The six degree of freedom static responses for this case are calculated for a total of 40 offset positions.

As for the first validation case, in the Orcaflex model a Poisson's ratio (v) equal to 0.5 was applied since the mooring lines are considered incompressible. Using Orcaflex the semisubmersible six degree of freedom static response characteristics were calculated considering increments of -5,000 kN in the applied horizontal force in the surge direction (x) from the calm water equilibrium position (horizontal force equal to zero) up to a maximum horizontal force equal to -55,000 kN.

Figure 2.16, 2.17 and 2.18 compare the heave (floater set down), pitch and horizontal restoring force, respectively, calculated by Orcaflex and by the developed fit-for-purpose program. There is excellent correlation between both sets of results for the entire range of offsets.

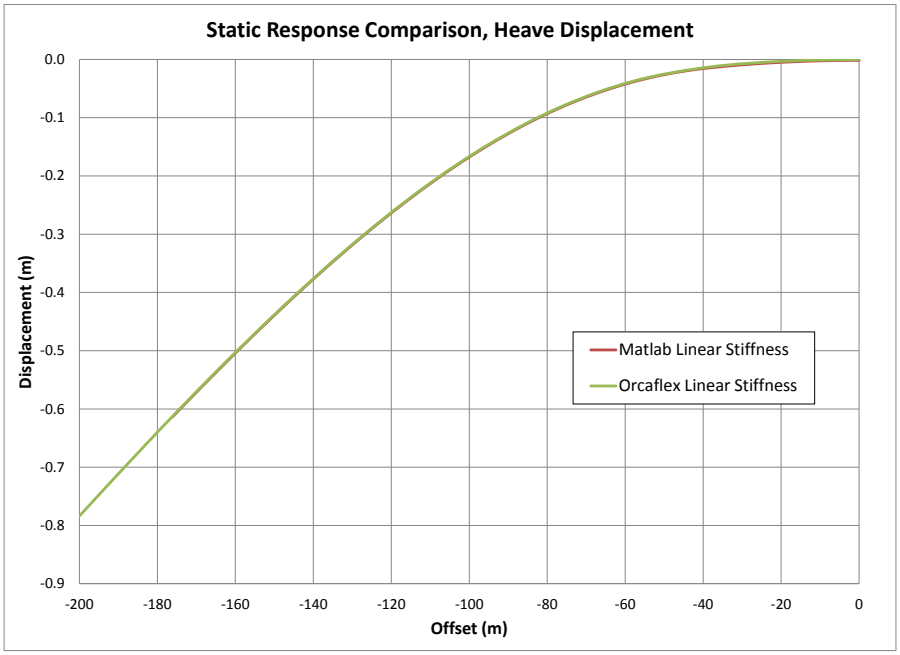

Figure 2.16. Semisubmersible static response comparison in heave.

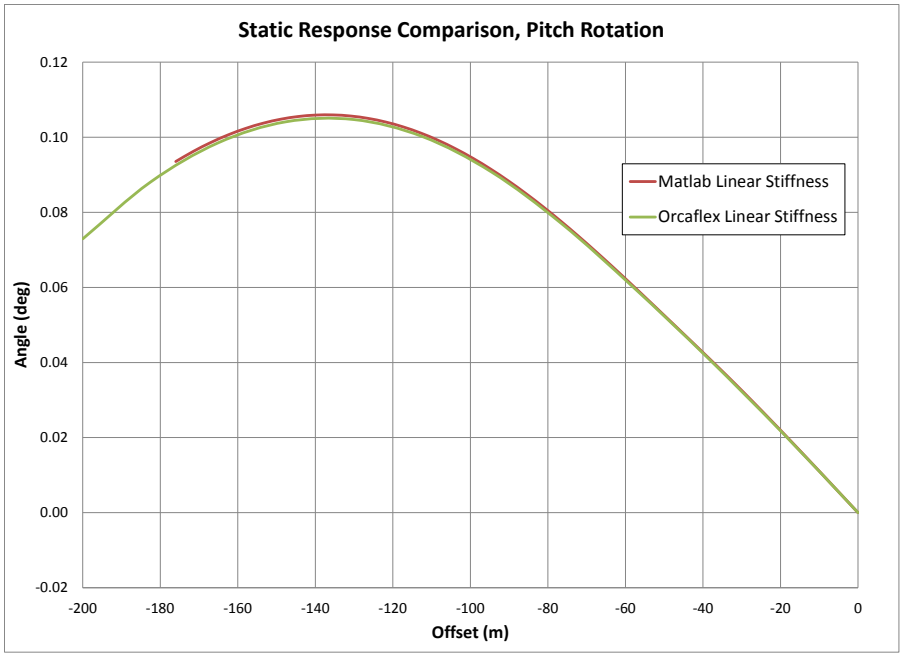

Figure 2.17. Semisubmersible static response comparison in pitch.

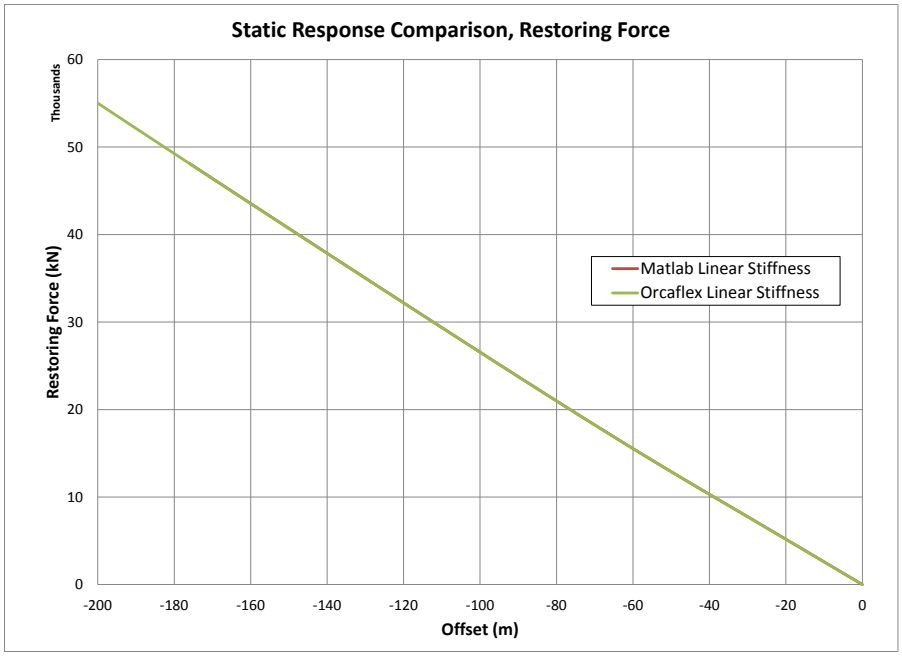

Figure 2.18. Semisubmersible static response comparison for restoring force.

3 GENETIC ALGORITHM FOR DESIGN OF STATICALLY EQUIVALENT MOORING AND RISER SYSTEMS

3.1 Fundamentals of Genetic Algorithms

The approach used in this research for the optimized design of the statically equivalent truncated mooring and riser system, considering the six degree of freedom static response characteristics, is based on a Genetic Algorithm (GA) using Matlab. This research work is taking advantage of the GA algorithm already embedded in Matlab. A Genetic Algorithm is a heuristic search approach used for optimization problems which simulates the process of natural evolution formulated by Charles Darwin in 1859 (Sivanandam and Deepa, 2008), which states that the strongest or best adapted individuals prevail, so their genes will be transmitted to future generations. On the other hand, the weak or less adapted individuals will perish, so their genes perish too. The information presented in this section is mainly based on Sivanandam and Deepa (2008) and Matlab (Mathworks).

The Genetic Algorithm was initially introduced by John Holland in 1975 (Sivanandam and Deepa, 2008). There are some basic concepts that must be explained in this procedure. The individual characteristics in the solution domain (i.e. design parameters) are called phenotype, which are commonly codified in a binary string referred to as a chromosome (genotype), and each individual characteristic in the chromosome is called a gene. As an example, Figure 3.1 (taken from Sivanandam and Deepa, 2008 and modified by the author) shows the relation between the individual characteristics (i.e.

design parameters) in the model (phenotype) and chromosome (genotype) representation for an individual in the population. The numbers shown represent a basic example of some values to be related between the phenotype and the genotype.

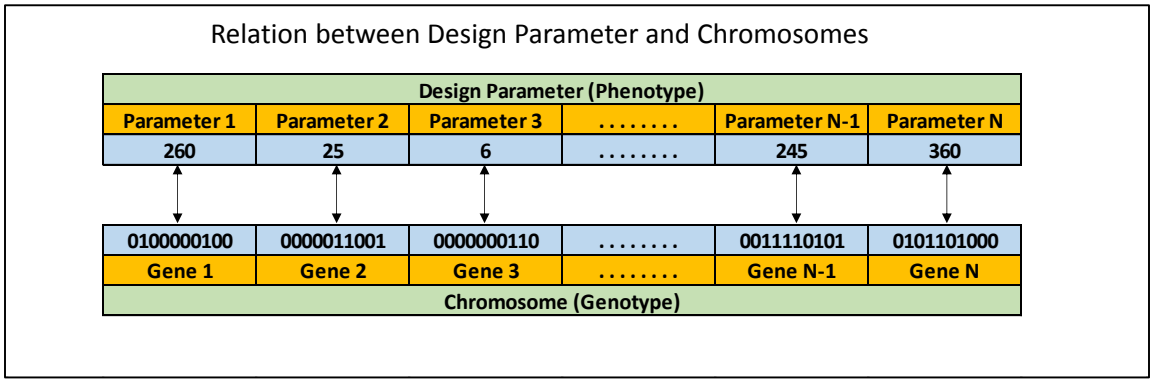

Figure 3.1. Relation between phenotype and genotype, model individual characteristics and genes.

The Genetic Algorithm procedure is based on an iterative process to allow the individuals in a population to evolve at each step. The fundamental elements of the GA procedure are:

1. **Initial Population**. An initial population is generated randomly.
2. **Selection**. Based on fitness function values, parents are selected to breed a new generation.
3. **Operators**. The crossover operator combines genes of the selected parents to create a new child and the mutation operator makes random changes to a single parent to create a new child.

4. **Replacement**. The current population is replaced with the children created to form the next generation.
5. **Termination**. The procedure finishes if it reaches the maximum number of generations specified or if differences between the previous and current generation are below a specified tolerance.

The parent selection process is defined randomly with a probability based on the relative fitness value of each individual, so the best individuals have a larger probability to be a parent than the worst individuals in the population. In this way the strongest genes can prevail in each generation. There can also be selected a number of elitist individuals in each generation; those selected elitist individuals are kept directly for the next generation.

The most commonly used operators to be applied to the parents, to breed a new offspring generation, are the crossover and mutation operators. The crossover operator is the reproduction between two parents which breed a new offspring generation; this operator swaps a sequence of parent's chromosomes into two offspring chromosomes. Figure 3.2 shows an example of the single point crossover operator between parent (a) chromosome and parent (b) chromosome which breed the offspring (c) and (d).

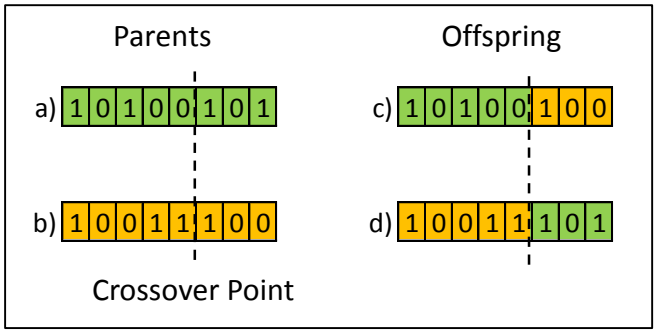

Figure 3.2. Parent reproduction by crossover operator, example.

The mutation operator is the change of a single bit in the parent chromosome, flipping its value from 0 to 1 or from 1 to 0. Figure 3.3 shows an example of how the mutation operator works in a parent's chromosome (a) to breed an offspring chromosome (b).

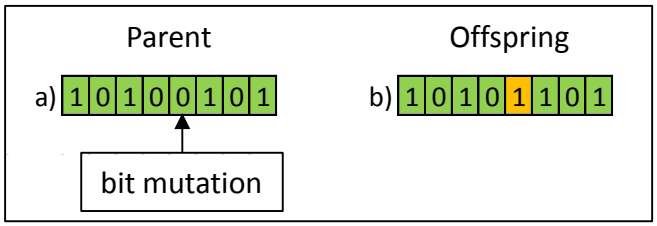

Figure 3.3. Parent chromosome mutation operator, example.

There are different methods for selecting parents to breed the new generation. Typically the selection algorithm works with the fitness values of the individuals. The fitness value is equivalent to the value of the objective function that is used to drive the optimization. Some of the selection methods are:

a) *Roulette wheel selection*. This is also known as fitness proportionate selection. There is assigned a relative probability of selection to each individual proportional to its fitness value, so that the sum of the individual probabilities is equal to 1. The roulette wheel is configured such that there are as many pockets as individuals and the size of each pocket is proportional to the probability of the assigned individual. When the wheel is "spun" the selection point will have a higher probability of landing on an individual with the highest fitness function value, although there will always be a probability of landing on an individual with a low probability. The selection of a parent with a low probability allows the possible survival of genetic information that may ultimately be useful in the breeding process.

b) *Random selection*. The parents are selected randomly from the population without considering their fitness values.

c) *Rank selection*. First, all the individuals in the population are ranked based on their fitness value, assigning 1 to the worst and N to the best individual. Then, two individuals are selected randomly from the ranked population and the individual with highest ranking is selected to be a parent. The same procedure is applied to select the second parent.

d) *Tournament selection*. A number N_u of individuals are selected randomly from the population, and from this set of individuals the one with the best fitness value is selected to be a parent.

e) *Elitism*. The best first or the few best individuals are kept for the new population.

Another important factor used in the breeding of offspring is the crossover factor which defines the percentage of the new generation that will be breeding using the crossover operator. The crossover factor doesn't include elitist children. Commonly, this crossover factor is set as 0.8.

The limits applied to stop the GA procedure are based on different criteria, which are:

a) *Maximum number of generations*. The GA procedure will stop when the indicated maximum number of generations is reached.
b) *Elapsed time*. The search process will end when the indicated elapsed time allowed is reached
c) *No change in fitness value*. The GA will stop when there is no change in the best individual's fitness value during an indicated number of generations.
d) *Stall generations*. The search process will end if there is no improvement in the fitness function for a specified number of generations.
e) *Stall time limit*. The GA will stop if there is no improvement in the fitness function for a predefined stall time limit.

3.2 Configuration of Genetic Algorithm

For this research work, the objective (fitness) function will be evaluated with the Root Mean Square Error (RMSE) between the prototype and the equivalent model static response for the six rigid body (floater) response characteristics (horizontal restoring force in surge, displacements in sway and heave, and rotations in roll, pitch and yaw), over a pre-defined range of horizontal offsets. A weighting factor will be applied for the RMSE associated with each static response characteristic considered and this will allow prioritizing a desired response for a certain static characteristic. The GA will be set up to minimize the fitness function described above. Figure 3.4 illustrates the general flow chart for the Genetic Algorithm used for the design of the statically equivalent truncated mooring and riser system.

The fitness function adopted is of the form

$$f(x) \rightarrow Min \left[\sum_{i=1}^{6} (Wf_i * RMSE_i)\right] \quad for\ i = 1,2,\dots,6$$

with constraints

$$x_j^L \leq x_j \leq x_j^U \quad for\ j = 1,2,..,m$$

$$g_k(x) \leq 0\ for\ k = 1,2,\dots,n$$

where:

f(x) = function of design parameters

Wf_i = weighting factor for static response characteristic i

$RMSE_i$ = root mean square error between prototype and model static response characteristic i

i=1 for horizontal restoring force; i=2 for sway; i=3 for heave; i=4 for roll; i=5 for pitch and i=6 for yaw

x_j = *design parameter j*

x_j^L = *lower bound value for* x_j

x_j^U = *upper bound value for* x_j

m = number of design parameters

$g_k(x)$ = *linear constraint equation*

k = number of linear constraint equation

n = total number of linear constraint equations

The root mean square error for each degree of freedom *i* is calculated with the static response values for the prototype and equivalent mooring/riser system at each discrete offset *j* considered,

$$RMSE_i = \sqrt{\frac{\sum_{j=1}^{N}(R_{prot_{ij}} - R_{equiv_{ij}})^2}{N}}$$

where,

$RMSE_i = root\ mean\ square\ error\ for\ rigid\ body\ degree\ of\ freedom\ i$

$R_{prot_{ij}} = prototype\ response\ for\ degree\ of\ freedom\ i\ at\ offset\ j$

$R_{equiv_{ij}} = equivalent\ system\ response\ for\ degree\ of\ freedom\ i\ at\ offset\ j$

$i = rigid\ body\ degree\ of\ freedom$

$j = offset\ position$

$N = total\ number\ of\ offsets\ considered\ from\ the\ calm\ water\ position\ up\ to\ the\ maximum\ offset\ position$

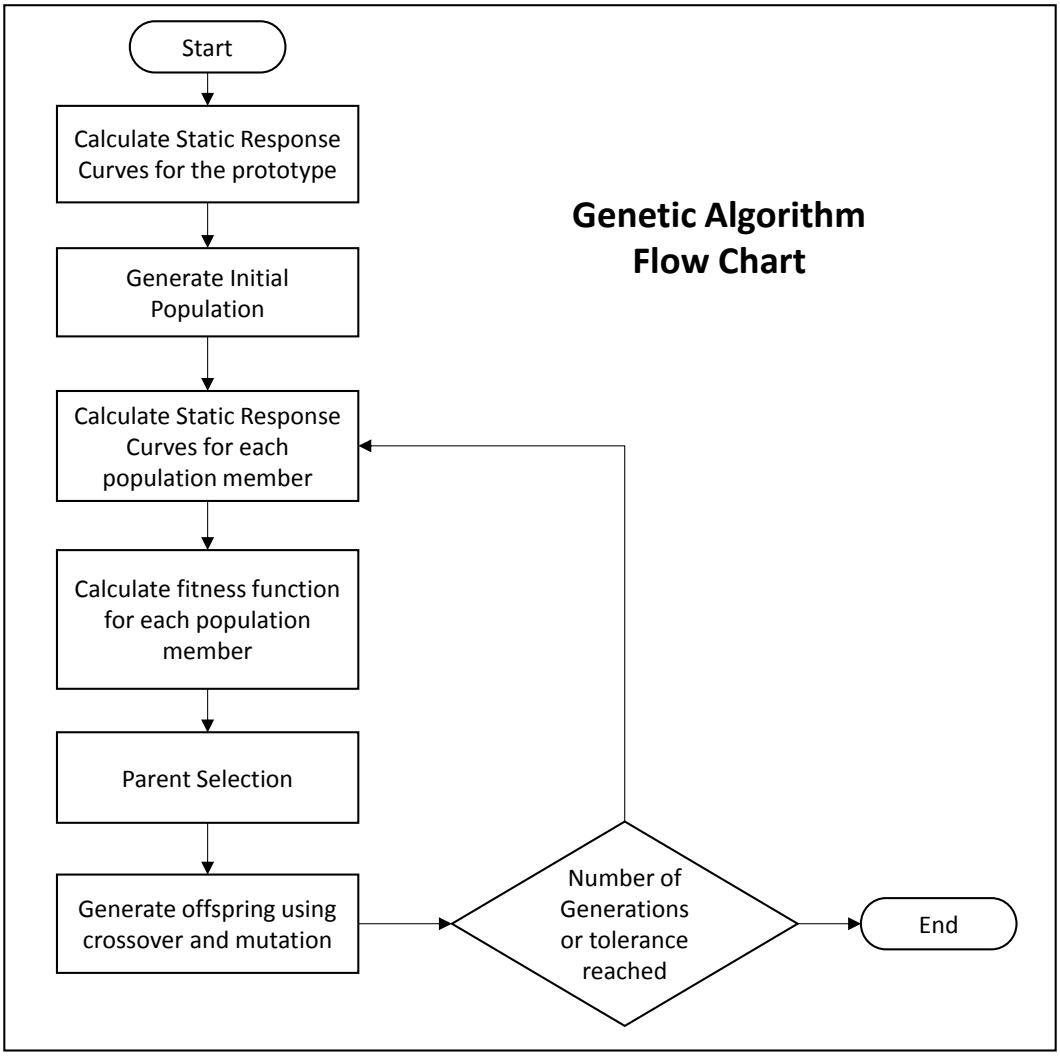

Figure 3.4. Flow chart for the Genetic Algorithm.

The solution domain of the design parameters is defined by the imposed constraints. The constraints are configured to reduce the search domain to feasible values

of the design parameters so that the candidate designs for the mooring and riser systems are feasible to be built and installed in the basin. For example, maximum and minimum values of the anchor radius are specified for the equivalent mooring lines so that the anchor points fall on the main floor of the basin outside of the pit but within the basin walls. Each design parameter has a specified lower and upper limit, and there are some linear inequalities to define the interaction between design parameters, in particular for the lengths of the different segments in the equivalent mooring line and riser.

There are some user defined input parameters to generate those constraints which are:

a) the minimum and maximum length for the spring as a percentage of the total mooring line/riser length
b) the minimum length for the anchoring cable as a percentage of the total mooring line/riser length
c) a minimum and maximum factor for the total mooring line/riser length as a percentage of the distance between the fairlead location and the anchoring point for the mooring line/riser
d) a minimum anchor radius for the mooring lines to avoid the pit in the basin
e) a maximum anchor radius to avoid being too close to the side walls in the basin or too close to the wave maker or to the wave absorber
f) a maximum angle variation about the initial defined heading angle for each mooring line/riser

g) for the riser design procedure, the maximum and minimum depth in the basin pit, and the longitudinal and transverse dimensions for the pit, so that the design space for the SCRs allows the anchor points to fall anywhere in the volume of the pit.

Four possible solution scenarios are considered for the equivalent mooring and riser system: symmetric equivalent mooring system, non-symmetric equivalent mooring system, six design parameters for each mooring line in the equivalent mooring system and six design parameters for each riser in the equivalent riser system. The solution scenarios are described in more detail in the following subsection of this dissertation.

When there are SCRs in the prototype system to be modeled, the equivalent mooring system is designed first considering the full depth prototype SCRs to be attached to the floater. Once, the equivalent mooring system is designed, the design of the equivalent truncated riser system is developed considering the previously designed equivalent mooring system to be attached to the floater. This approach is judged to yield the most robust design for the equivalent mooring/riser system.

3.2.1 Symmetric Solution for the Equivalent Mooring System

A Genetic Algorithm was developed for designing a symmetric equivalent mooring system, which considers that the characteristics for all mooring lines for the model are identical. Figure 3.5 shows the six design parameters defined for this solution:

1. length of cable segment at the bottom (X_1),
2. length of the spring segment (X_2),
3. length of the cable segment at the top (X_3),

4. spring property number (X_4), which identifies the associated values for the axial stiffness (*EA*) and unit submerged weight (*w*) of the spring,
5. angle variation for the anchor point with respect to the fairlead location (X_5),
6. radial distance to the anchor point (X_6).

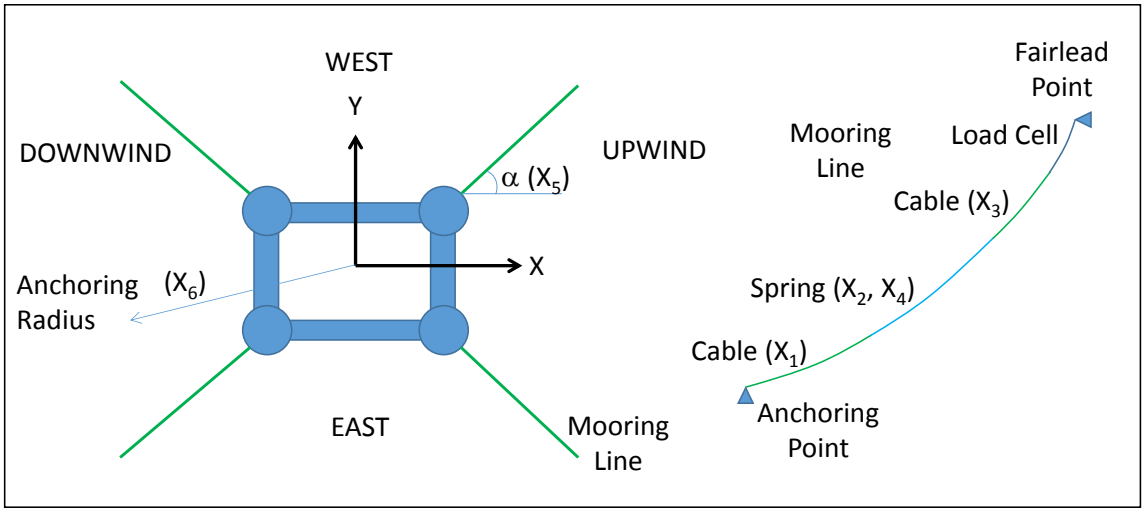

Figure 3.5. Mooring line design parameters for the symmetric solution.

The possible values of axial stiffness (*EA*) and unit submerged weight (*w*) for a spring are not only discrete but also fully correlated. Therefore the paired values of *EA* and *w* are considered a single independent variable in the design solution, identified by the "spring property number".

3.2.2 Non-symmetric Solution for the Equivalent Mooring System

A Genetic Algorithm was developed for designing a non-symmetric equivalent mooring system, which considers different design parameters between upwind and downwind mooring lines. Figure 3.6 shows the eleven design parameters defined for this solution:

1. length of cable segment at the bottom for the upwind mooring lines (X_1),
2. length of the spring segment for the upwind mooring lines (X_2),
3. length of the cable segment at the top for the upwind mooring lines (X_3),
4. spring property number for the upwind mooring lines (X_4),
5. length of cable segment at the bottom for the downwind mooring lines (X_5),
6. length of the spring segment for the downwind mooring lines (X_6),
7. length of the cable segment at the top for the downwind mooring lines (X_7),
8. spring property number for the downwind mooring lines (X_8),
9. angle variation for the anchor point with respect to the fairlead for the upwind mooring lines (X_9),
10. angle variation for the anchor point with respect to the fairlead for the downwind mooring lines (X_{10}),
11. Radial distance to the anchor point, assumed to be the same for the upwind and downwind mooring lines (X_{11}).

Note that even though the defined anchor radius is assumed to be the same for the upwind and downwind mooring lines, the calm water equilibrium position (zero offset position) of the floater can be different than the location of the geometric center of the

anchor pattern. This means that for the non-symmetric mooring in general the anchor radius relative to the calm water equilibrium position will be different for the upwind and downwind mooring lines.

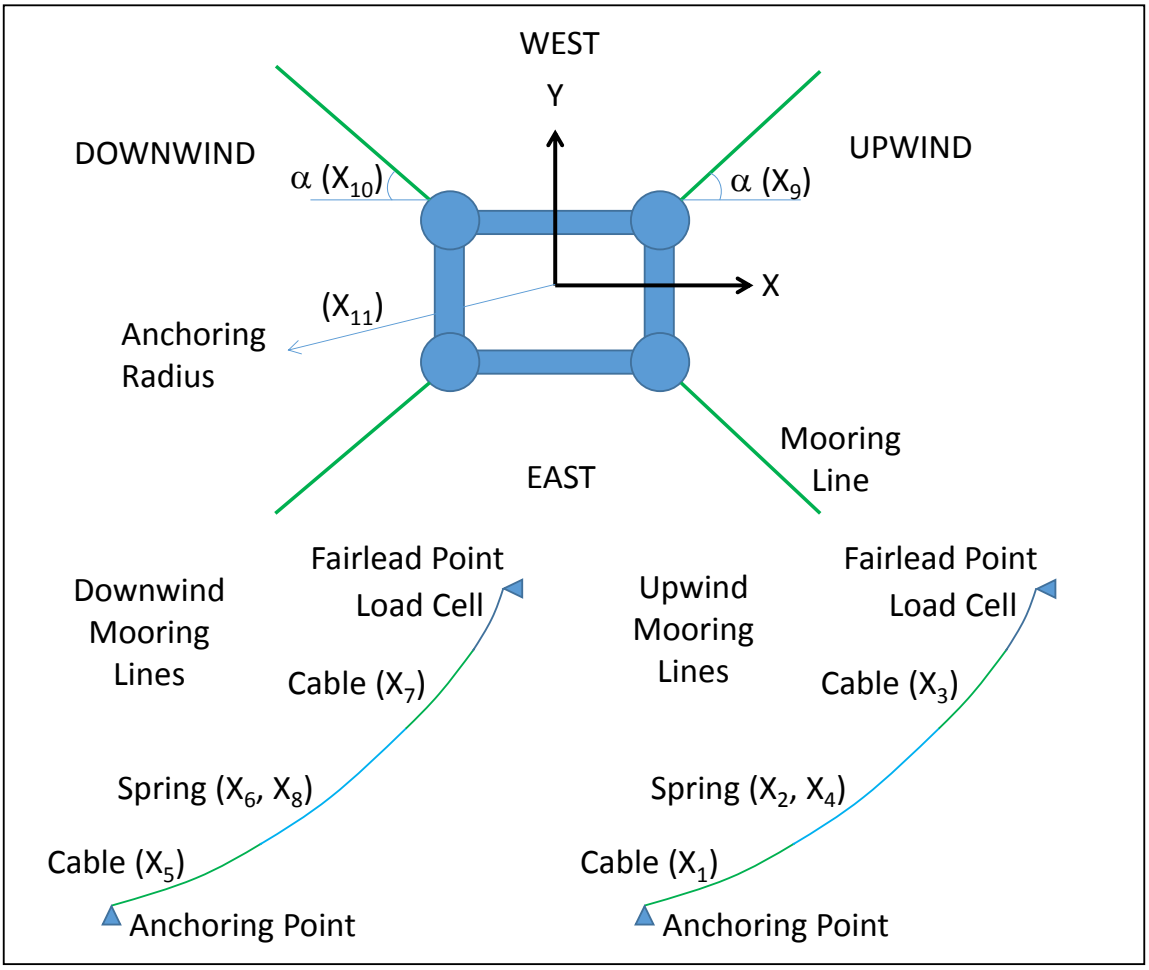

Figure 3.6. Mooring line design parameters for the non-symmetric solution.

3.2.3 General Solution for the Equivalent Mooring System

A Genetic Algorithm was developed for designing an equivalent mooring system allowing all lines to be different and considering six design parameters for each mooring line. Figure 3.7 shows the six design parameters defined for each mooring line:

1. length of cable segment at the bottom (X_1),
2. length of the spring segment (X_2),
3. length of the cable segment at the top (X_3),
4. spring property number (X_4),
5. angle variation for the anchor point with respect to the fairlead (X_5),
6. radial distance to the anchor point (X_6).

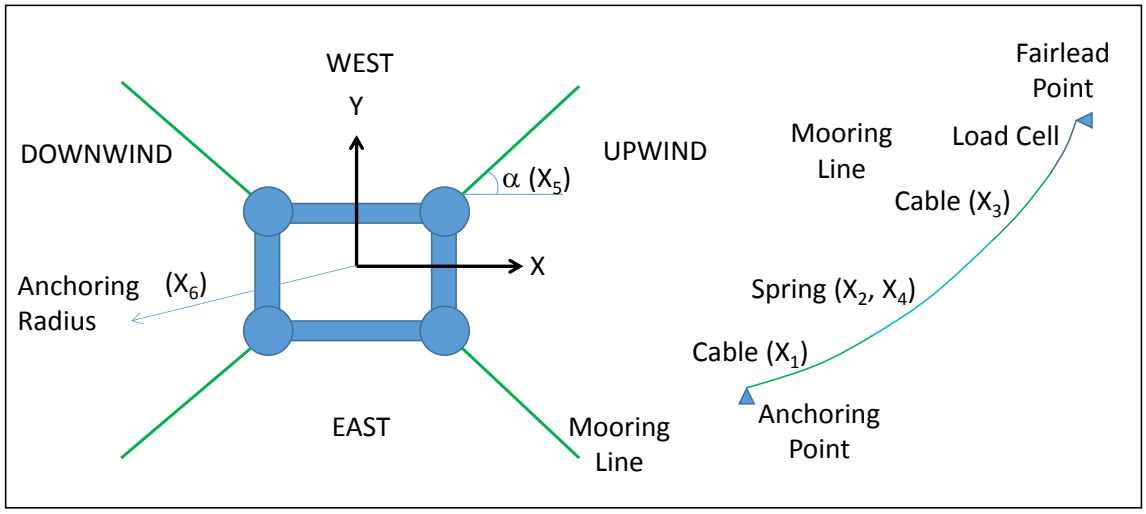

Figure 3.7. Mooring line design parameters for the general solution.

3.2.4 General Solution for the Equivalent Riser System

A Genetic Algorithm was developed for designing an equivalent catenary riser system considering six design parameters for each riser in the system. The six design parameters for each riser are:

1. length of cable segment at the bottom of the riser (X_1),
2. length of the spring segment (X_2),
3. spring property number (X_3),
4. angle variation for the anchor point with respect to the fairlead (X_4),
5. radial distance to the anchor point (X_5),
6. anchor point depth (the anchor point can be located at any depth in the basin pit or at the main basin floor) (X_6).

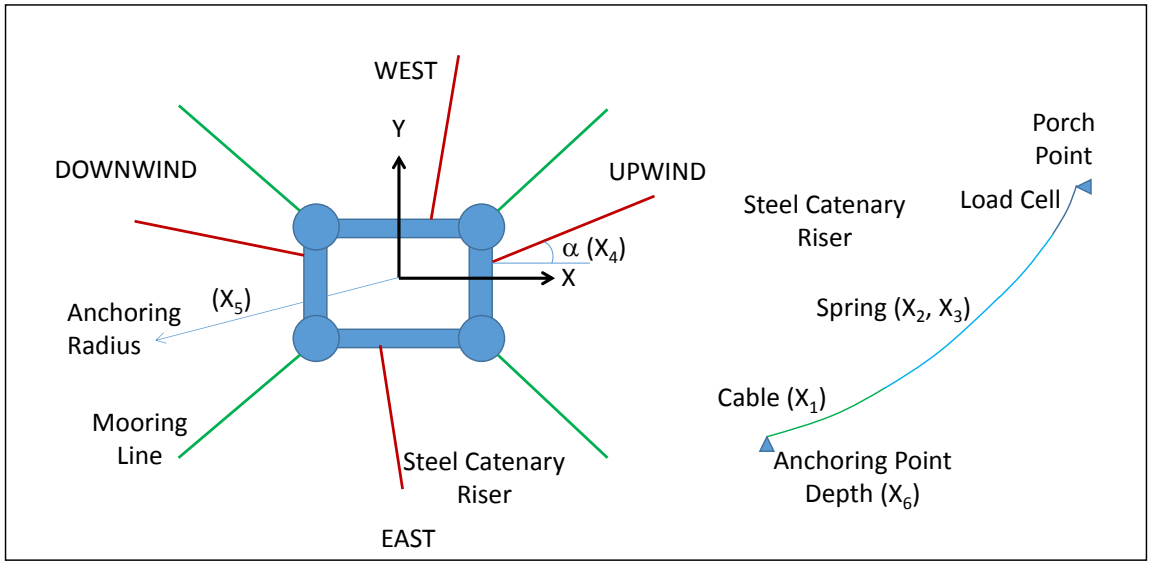

Figure 3.8. Steel catenary riser design parameters.

For the equivalent riser system two additional design parameters are considered that are related with the floater's horizontal position over the pit. The calm water equilibrium position of the floater is allowed to have a horizontal offset relative to the center of the pit so the coordinates of the offset represent two additional design parameters.

3.3 Study Cases

Four study cases are considered to evaluate and demonstrate the performance of the Genetic Algorithm solutions developed for the optimized design of the statically equivalent mooring and riser systems. The four study cases considered are:

1. semisubmersible with a symmetric 4x4 polyester mooring system,
2. semisubmersible with a symmetric 4x4 steel wire mooring system,
3. semisubmersible with a non-symmetric 4x3 polyester mooring system including 3 steel catenary risers,
4. spar structure with a non-symmetric 3x3 polyester mooring system including 2 steel catenary risers.

3.3.1 Semisubmersible with Polyester Mooring System

The first study case to validate the procedure for the optimized design of the equivalent mooring system is a semisubmersible with a polyester mooring system attached. The mooring for this semisubmersible is a symmetric system with a total of 16 lines, arranged in 4 groups of 4 lines, as is illustrated in Figure 3.9. It is important to mention that for this mooring system, the polyester stiffness behavior is non-linear, but currently the Matlab fit-for-purpose program is only capable of handling mooring lines with linear stiffness (i.e. constant *EA*). Therefore for this study case the static response curves for the prototype mooring were generated using Orcaflex with the nonlinear stiffness correctly modeled and they were used as input curves in the Genetic Algorithm procedure. This serves to illustrate that the target static offset curves for the prototype can be obtained from any source and do not have to be generated by the fit-for-purpose static equilibrium solver. However the design of the equivalent mooring system will rely on the fit-for-purpose static equilibrium solver, and the nonlinear stiffness behavior of the prototype will be reproduced through evolutionary optimization of the design parameters using the Genetic Algorithm.

The equivalent mooring system design will have 4 mooring lines with the same fairlead elevation as the prototype, but located in the X-Y plane in the middle of the location of the 4 prototype lines at each column. The initial anchor heading in the X-Y plane is between the anchor points for the middle prototype mooring lines at each column.

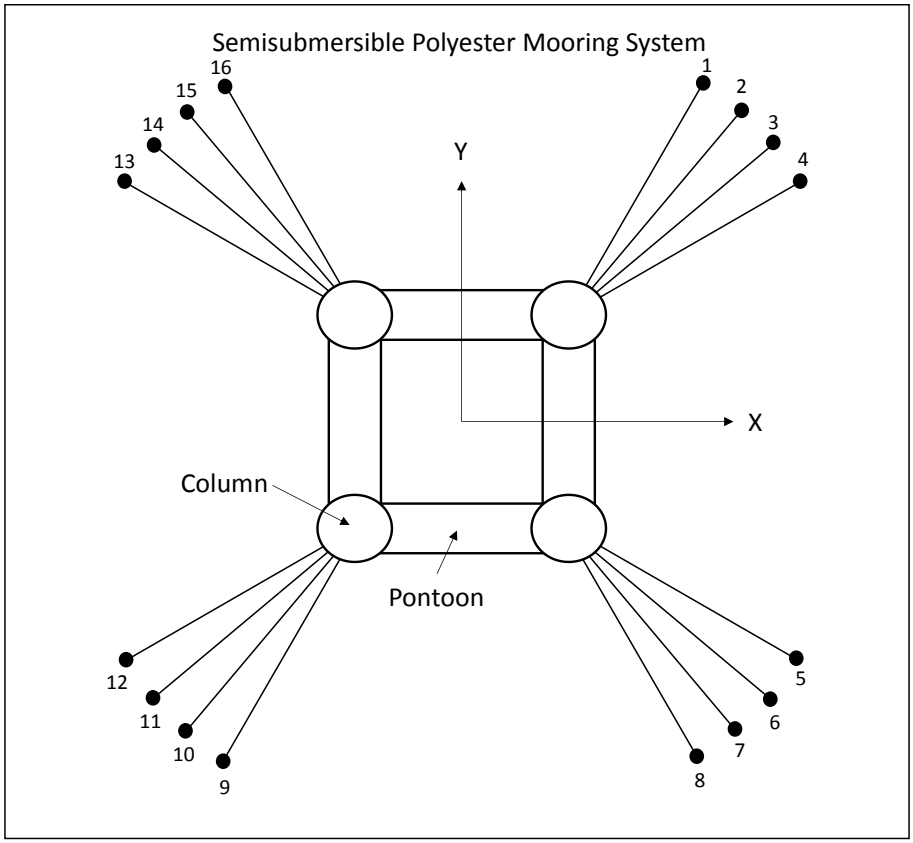

Figure 3.9. Semisubmersible polyester mooring system configuration, prototype.

The semisubmersible hydrostatic stiffness characteristics and the mooring system properties are presented in Table 3.1. For this prototype mooring system all lines are identical, so the values included in this table apply to all mooring lines. The coordinates for the fairlead and anchor points for each mooring line are shown in Table 3.2.

Table 3.1. Semisubmersible and prototype polyester mooring system characteristics.

Property	Value			
Water Depth (m)	2,200			
Semisubmersible hydrostatic stiffness	Heave, K_z (N/m)	Roll, K_r (N m/rad)	Pitch, K_p (N m/rad)	
	22,690,000	4.233e10	4.2336e10	
Elevation for applying acting force in X direction	18.74 m (above Sea Water Level)			
Number of Mooring Lines	16			
Number of Segments per Mooring Line	3			
Segment Properties	*L* (m)	*w* (N/m)	*AE* (N)	*Elements*
Platform Chain	150	4,648	2.303e9	15
Polyester	3,900	125.6	Non-linear	39
Anchor Chain	450	4,648	2.303e9	45

Figure 3.10 shows the nonlinear axial stiffness curve for the polyester rope, which was used in Orcaflex to calculate the rigid body six degrees of freedom static response for the prototype.

Table 3.3 provides the fixed input parameters for the design of the equivalent mooring system. Table 3.4 lists the coordinates of the fairlead locations and the initial mooring line heading angles with respect to the X axis for the equivalent mooring system.

Table 3.2. Fairlead and anchor coordinates, prototype polyester mooring system.

Mooring Line	Fairlead location			Anchor location		
	X' (m)	Y' (m)	Z' (m)	X (m)	Y (m)	Z (m)
1	47.12	56.37	-17.68	2,449	3,187	-2,200
2	51.14	54.32	-17.68	2,717	2,964	-2,200
3	54.32	51.14	-17.68	2,964	2,717	-2,200
4	56.37	47.12	-17.68	3,187	2,449	-2,200
5	56.37	-47.12	-17.68	3,187	-2,449	-2,200
6	54.32	-51.14	-17.68	2,964	-2,717	-2,200
7	51.14	-54.32	-17.68	2,717	-2,964	-2,200
8	47.12	-56.37	-17.68	2,449	-3,187	-2,200
9	-47.12	-56.37	-17.68	-2,449	-3,187	-2,200
10	-51.14	-54.32	-17.68	-2,717	-2,964	-2,200
11	-54.32	-51.14	-17.68	-2,964	-2,717	-2,200
12	-56.37	-47.12	-17.68	-3,187	-2,449	-2,200
13	-56.37	47.12	-17.68	3,187	2,449	-2,200
14	-54.32	51.14	-17.68	2,964	2,717	-2,200
15	-51.14	54.32	-17.68	2,717	2,964	-2,200
16	-47.12	56.37	-17.68	2,449	3,187	-2,200

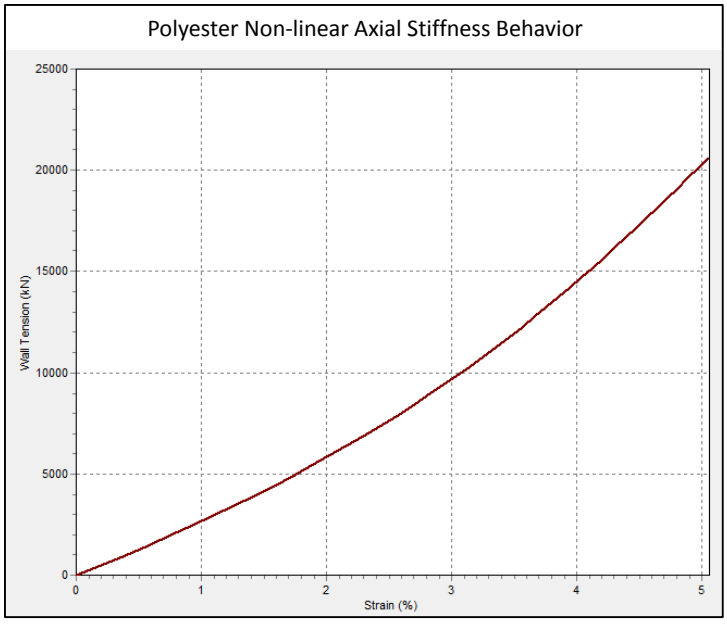

Figure 3.10. Polyester non-linear axial stiffness behavior.

Table 3.3. Equivalent mooring system design characteristics, polyester mooring system.

Property	Value			
Scale Factor	1:50			
Truncation Factor	7.578			
Number of individuals	320			
Number of generations	60			
Anchoring radius	Minimum (m)		Maximum (m)	
	254.9		712.5	
Semisubmersible hydrostatic stiffness	Heave, K_z (N/m)	Roll, K_r (N m/rad)	Pitch, K_p (N m/rad)	
	22,690,000	4.233e10	4.2336e10	
Elevation for applying acting force in X direction	18.74 m (above Sea Water Level)			
Maximum Offset in Surge	8% of Full Water Depth			
Number of Mooring Lines	4			
Number of Segments per Mooring Line	4			
Segment Properties	*L* (m)	*w* (N/m)	*AE* (N)	*Elements*
Platform Load Cell	3.81	42,250	1.228e11	1
Cable Segment	---	255.9	3.810e10	1
Spring Segment	---	---	---	20
Anchor Cable Segment	---	255.9	3.810e10	1

Table 3.4. Fairlead coordinates and initial mooring line heading for the equivalent mooring design, polyester mooring system.

Mooring Line	Fairlead location			Initial mooring line heading (deg)
	X' (m)	Y' (m)	Z' (m)	
1	52.73	52.73	-17.68	45
2	52.73	-52.73	-17.68	315
3	-52.73	-52.73	-17.68	225
4	-52.73	52.73	-17.68	135

For this study case the symmetric and non-symmetric Genetic Algorithm solutions were investigated, considering different values for the weighting factors in the fitness

function. Table 3.5 lists the values for the weighting factors applied to the fitness function for each one of the cases considered. The weighting factors are used to bias the relative priority of achieving a certain RMS error in matching the prototype static offset curve for each response.

For example, for case C1 (symmetric and non-symmetric) the weighting factors assigned to heave and pitch in Table 3.5 are of the same order of magnitude, indicating a desire for equal weighting in matching those responses, even though heave is measured in meters and pitch is measured in radians. This doesn't necessarily mean that the optimal design will exhibit heave and pitch responses that match the prototype behavior with the same fidelity. Indeed working with the objective function in the GA is itself an iterative procedure. After obtaining an initial optimal design it is often necessary or desirable to adjust the weighting factors in order to seek a new optimal design that provides a better overall match to the prototype static offset curves. Relative to case C1 then, in Table 3.5 the weighting factors for C2 are assigned values with the intent of achieving a better match of the heave response at the expense of the pitch response. Similarly the weighting factors for case C3 are assigned values with the intent of achieving a better match of the pitch response at the expense of the heave response, relative to the C1 design.

Table 3.5. Fitness function weight factors per each case considered, polyester mooring system.

Static Response	Fitness Function Weight Factors Considered					
	Symmetric solutions			Non-symmetric solutions		
	PM-S-C1	PM-S-C2	PM-S-C3	PM-N-C1	PM-N-C2	PM-N-C3
Restoring Force	1.0	1.0	1.0	1.0	1.0	1.0
Heave	10,000	10,000	1,000	10,000	10,000	1,000
Pitch	10,000	1,000	100,000	10,000	1,000	100,000

The results for the symmetric cases are presented first. Figure 3.11, Figure 3.12 and Figure 3.13 compare the restoring force, setdown and pitch static offset curves, respectively, for the prototype and the equivalent mooring system considering the different sets of weighting factors.

The fairlead and anchor coordinates for the best symmetric mooring design for each set of weighting factors in the fitness function are provided in Table 3.6. The anchor coordinates in the X-Y plane are the result of considering the anchor radius and line angle variations as design parameters; those results are highlighted in green in the table. It is evident that the anchor locations for each one of the different cases considered are different, due to the effect of the different weighting factors considered for the fitness function in each case.

Table 3.7 lists the properties for each mooring line segment for the best fitness function solution. The design parameters are highlighted in green. As expected, there is a variation in the segment lengths and in the spring properties due the weight factors applied to the fitness function.

Table 3.6. Fairlead and anchor coordinates, symmetric solutions, polyester mooring system.

Case	Mooring Line	Fairlead location			Anchor location		
		X' (m)	Y' (m)	Z' (m)	X (m)	Y (m)	Z (m)
PM-S-C1	1	52.73	52.73	-17.68	270.16	429.43	-290.32
	2	52.73	-52.73	-17.68	270.16	-429.43	-290.32
	3	-52.73	-52.73	-17.68	-270.16	-429.43	-290.32
	4	-52.73	52.73	-17.68	-270.16	429.43	-290.32
PM-S-C2	1	52.73	52.73	-17.68	282.08	416.76	-290.32
	2	52.73	-52.73	-17.68	282.08	-416.76	-290.32
	3	-52.73	-52.73	-17.68	-282.08	-416.76	-290.32
	4	-52.73	52.73	-17.68	-282.08	416.76	-290.32
PM-S-C3	1	52.73	52.73	-17.68	231.89	481.40	-290.32
	2	52.73	-52.73	-17.68	231.89	-481.40	-290.32
	3	-52.73	-52.73	-17.68	-231.89	-481.40	-290.32
	4	-52.73	52.73	-17.68	-231.89	481.40	-290.32

Table 3.7. Mooring line properties for best fitness function solutions, polyester mooring system.

Case	Segment	Value			
		L (m)	*w* (N/m)	*AE* (N)	*Elements*
PM-S-C1	Platform Load Cell	3.81	42,250	1.228e11	1
	Cable Segment	78.23	255.9	3.810e10	1
	Spring Segment	201.10	33,870	6.047e07	20
	Anchor Cable Segment	203.07	255.9	3.810e10	1
PM-S-C2	Platform Load Cell	3.81	42,250	1.228e11	1
	Cable Segment	90.21	255.9	3.810e10	1
	Spring Segment	200.03	33,870	6.047e07	20
	Anchor Cable Segment	190.25	255.9	3.810e10	1
PM-S-C3	Platform Load Cell	3.81	42,250	1.228e11	1
	Cable Segment	114.13	255.9	3.810e10	1
	Spring Segment	248.30	22,725	9.081e07	20
	Anchor Cable Segment	138.79	255.9	3.810e10	1

Figure 3.11 compares the horizontal restoring force curve for the prototype mooring with each of the three symmetric solutions for the equivalent mooring. For each solution (i.e. each set of weighting factors used) there is a really good correlation with the prototype response, with root mean square error (RMSE) for the restoring force of 271 kN for PM-S-C1, 205 kN for PM-S-C2 and 231 kN for PM-S-C3 with maximum errors for small offsets (up to the mean offset value) of 7.1%, 5.0% and 5.8%, respectively and with maximum errors for large offset (greater than the mean offset value) of 1.1%, 0.8% and 1.4%.

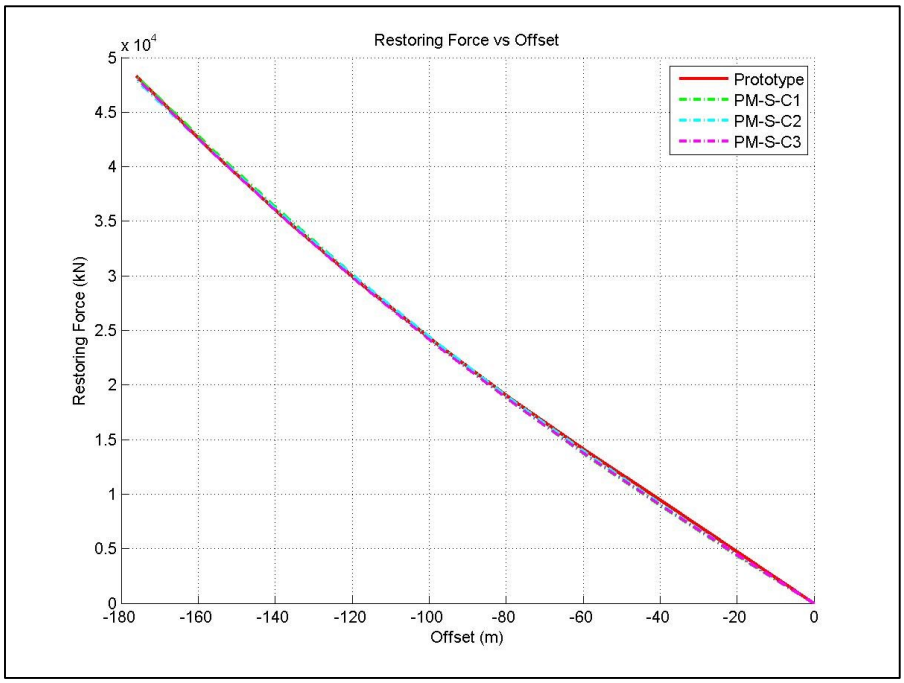

Figure 3.11. Restoring force vs offset plot, symmetric solutions, polyester mooring system.

Figure 3.12 compares the setdown curve for the prototype mooring with each of the three symmetric solutions for the equivalent mooring. Here the correlation with the prototype is not as good as for the restoring force but it is still quite acceptable. The largest deviation in setdown between the prototype and any of the three equivalent mooring designs is about 0.1 m.

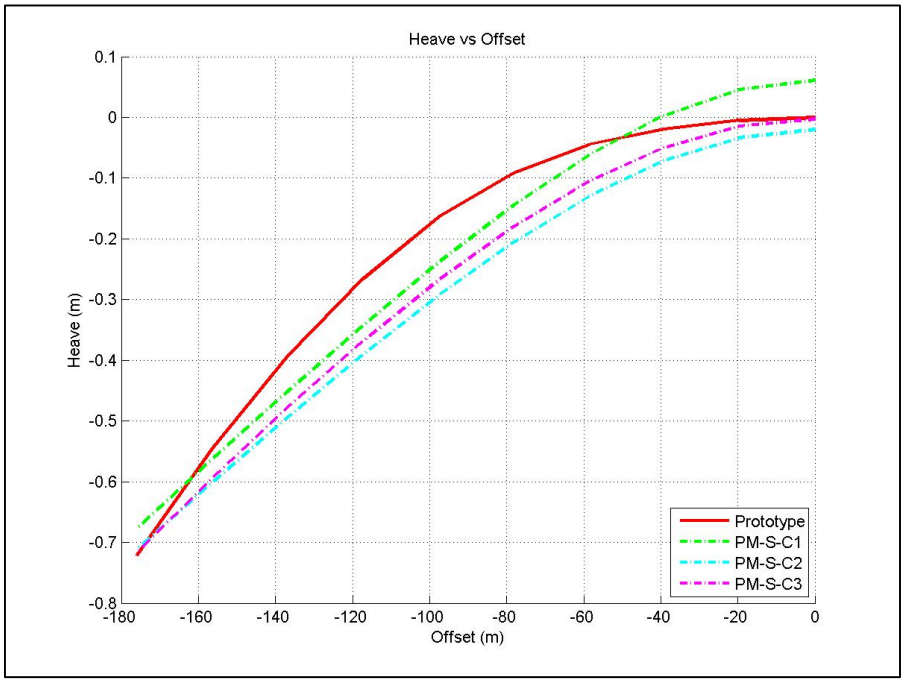

Figure 3.12. Heave vs offset plot, symmetric solutions, polyester mooring system.

Figure 3.13 compares the pitch rotation curves for the symmetric solutions. With increasing offset the curves for the equivalent moorings diverge from that for the prototype mooring, reaching a difference of 0.6 to 0.8 degrees at the maximum offset, depending on the case.

The evolution of the best value of the fitness function among the 320 samples of the population for each of the three cases considered in the symmetric solution scenario is plotted in Figure 3.14. It is evident that there is strong improvement in the fitness function best value in the first 30 generations of the evolution for the three cases considered and the improvement beyond that generation is small. In fact for the case PM-S-C2 there is no improvement in the fitness function best value beyond the 31st generation.

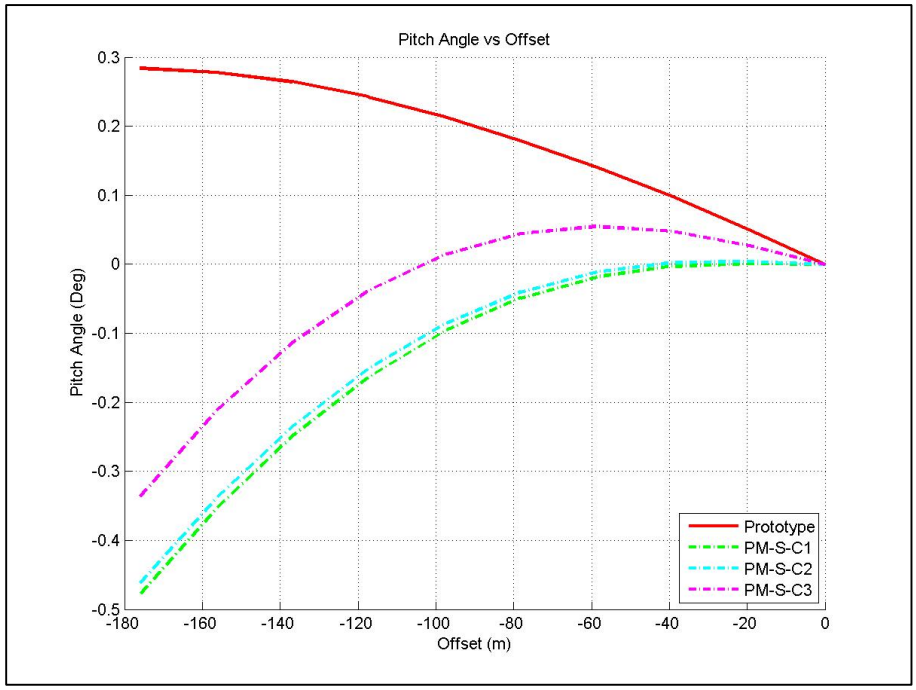

Figure 3.13. Pitch vs offset plot, symmetric solutions, polyester mooring system.

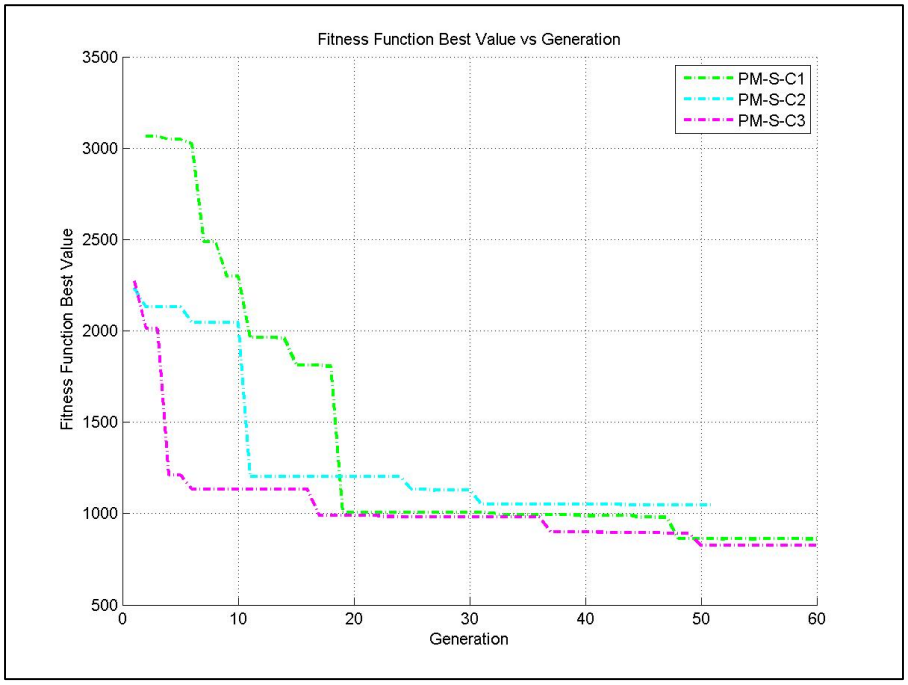

Figure 3.14. Fitness function best value evolution, symmetric solutions, polyester mooring system.

The evolution of the mean fitness function value of the 320 samples for the three symmetric cases considered is plotted in Figure 3.15. The improvement in the quality of the population of designs is generally continuous, especially for the first 30 generations. Beyond that generation there is a small change in the fitness mean value, because the GA is evolving to move all the samples in the population to the fitness function best value, even if there is not an improvement in the fitness function best value. In other words, eventually all sample designs evolve to the best design as influenced by the weighting factors in the fitness function.

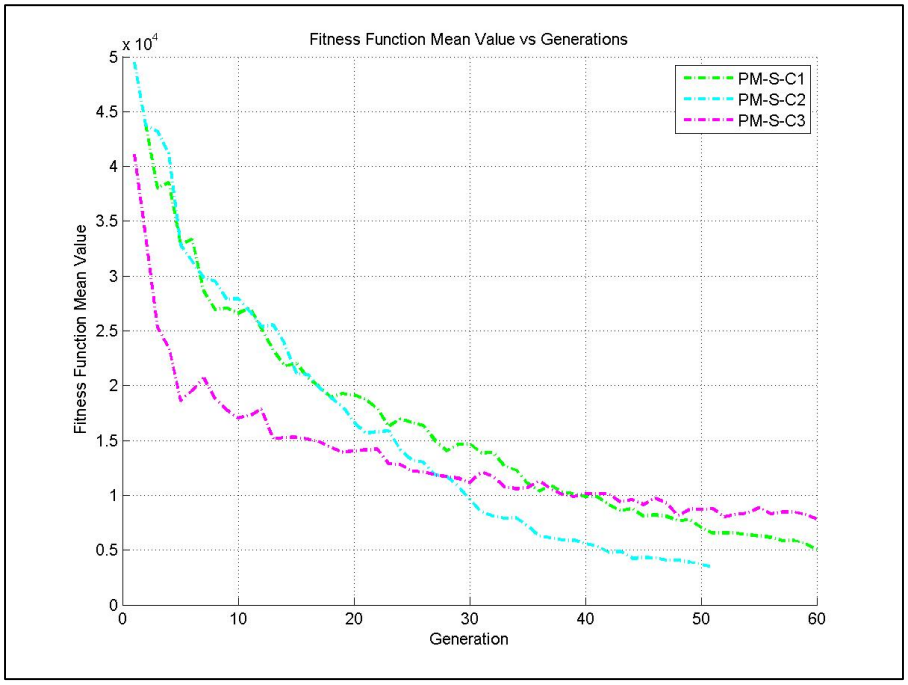

Figure 3.15. Fitness function mean value evolution, symmetric solutions, polyester mooring system.

While the symmetric design solutions exhibit acceptable behavior in restoring force and setdown, it is worth investigating whether a non-symmetric mooring solution would result in reduced error for the pitch response. Figure 3.16, Figure 3.17 and Figure 3.18 compare the static offset curves for the prototype and the solutions for the non-symmetric equivalent mooring system associated with the 3 sets of weighting factors listed in Table 3.5.

The fairlead and anchor coordinates for the best non-symmetric mooring design for each set of weighting factors are provided in Table 3.8. The properties for each segment

in the upwind and downwind mooring lines related with the best fitness function solution are listed in Table 3.9.

Table 3.8. Fairlead and anchor coordinates, non-symmetric solutions, polyester mooring system.

Case	Mooring Line	Fairlead location			Anchor location		
		X' (m)	Y' (m)	Z' (m)	X (m)	Y (m)	Z (m)
PM-N-C1	1	52.73	52.73	-17.68	321.92	338.75	-290.32
	2	52.73	-52.73	-17.68	321.92	-338.75	-290.32
	3	-52.73	-52.73	-17.68	-242.45	-396.64	-290.32
	4	-52.73	52.73	-17.68	-242.45	396.64	-290.32
PM-N-C2	1	52.73	52.73	-17.68	150.39	417.16	-290.32
	2	52.73	-52.73	-17.68	150.39	-417.16	-290.32
	3	-52.73	-52.73	-17.68	-274.59	-357.90	-290.32
	4	-52.73	52.73	-17.68	-274.59	357.90	-290.32
PM-N-C3	1	52.73	52.73	-17.68	333.63	307.30	-290.32
	2	52.73	-52.73	-17.68	333.63	-307.30	-290.32
	3	-52.73	-52.73	-17.68	-257.17	-371.97	-290.32
	4	-52.73	52.73	-17.68	-257.17	371.97	-290.32

Figure 3.16 compares the horizontal restoring force curves. As for the symmetric solutions, there is really good correlation for the three different non-symmetric solutions with the prototype response, with maximum errors for small offsets (up to the mean offset value) of 4.6% for PM-N-C1, 2.2% PM-N-C2 and 4.6% for PM-N-C3, respectively; and with maximum errors for large offsets (greater than the mean offset value, around 90m) of 1.0%, 0.6% and 1.6%, respectively.

Table 3.9. Mooring line properties for best solution, non-symmetric cases, polyester mooring system.

Case	Mooring Lines	Segment	Value			
			***L* (m)**	***w* (N/m)**	***AE* (N)**	***Elements***
PM-N-C1	Upwind (1,2)	Load Cell	3.81	42,250	1.228e11	1
		Cable	70.19	255.9	3.810e10	1
		Spring	196.83	47,860	5.049e07	20
		Anchor Cable	188.56	255.0	3.810e10	1
	Downwind (3,4)	Load Cell	3.81	42,250	1.228e11	1
		Cable	107.53	255.9	3.810e10	1
		Spring	166.13	33,870	6.047e07	20
		Anchor Cable	182.30	255.9	3.810e10	1
PM-N-C2	Upwind (1,2)	Load Cell	3.81	42,250	1.228e11	1
		Cable	72.37	255.9	3.810e10	1
		Spring	174.53	17,200	8.224e07	20
		Anchor Cable	165.54	255.9	3.810e10	1
	Downwind (3,4)	Load Cell	3.81	42,250	1.228e11	1
		Cable	87.68	255.9	3.810e10	1
		Spring	170.30	8,772	3.655e07	20
		Anchor Cable	178.39	255.9	3.810e10	1
PM-N-C3	Upwind (1,2)	Load Cell	3.81	42,250	1.228e11	1
		Cable	92.33	255.9	3.810e10	1
		Spring	196.29	31,860	4.921e07	20
		Anchor Cable	159.93	255.9	3.810e10	1
	Downwind (3,4)	Load Cell	3.81	42,250	1.228e11	1
		Cable	109.03	255.9	3.810e10	1
		Spring	172.81	22,730	9.081e07	20
		Anchor Cable	179.10	255.9	3.810e10	1

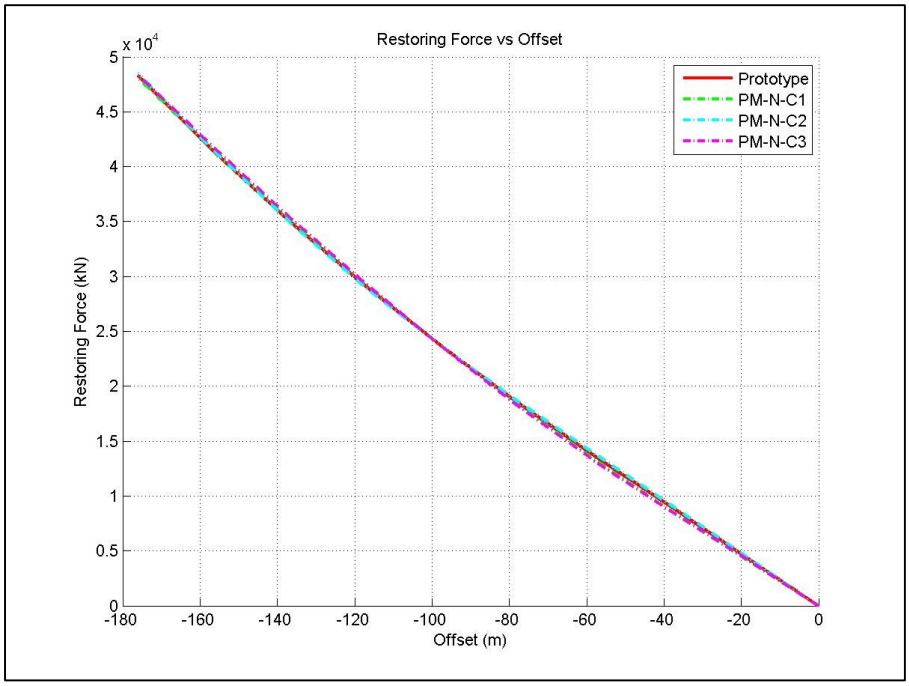

Figure 3.16. Restoring force vs offset plot, non-symmetric solutions, polyester mooring system.

In the case of setdown, Figure 3.17 shows that non-symmetric solutions C1 and C2 are in very good agreement with the prototype curve, with a maximum error less than 0.1 m. As a result of the increased weighting on pitch and reduced weighting on heave (see Table 3.5), the correlation for the C3 solution is not as good as for C1 and C2, with a maximum error of about 0.5 m.

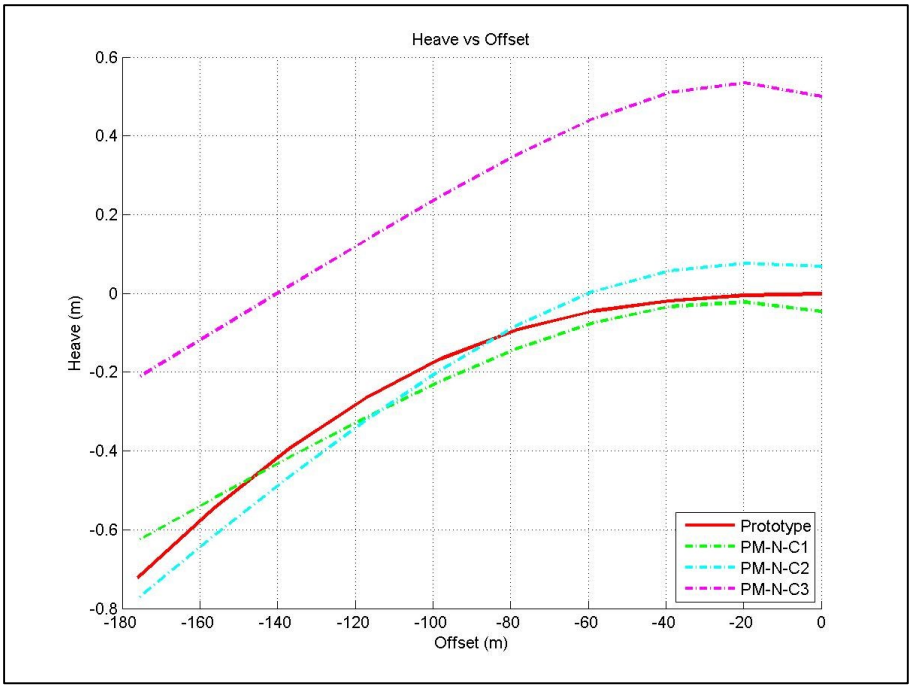

Figure 3.17. Heave vs offset plot, non-symmetric solutions, polyester mooring system.

Figure 3.18 compares the pitch static offset curves for the non-symmetric solutions. There is good correlation for the C1 and C3 solutions, with a maximum error of about 0.6 degrees. The pitch curve for case C2 shows a maximum error of about 1.2 degrees.

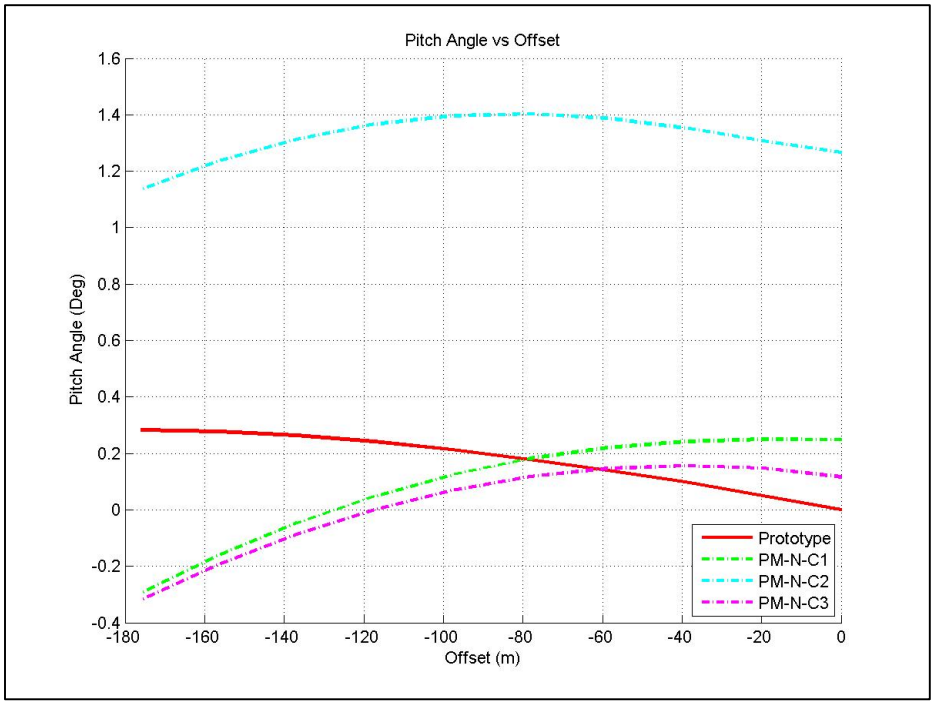

Figure 3.18. Pitch vs offset plot, non-symmetric solutions, polyester mooring system.

Figure 3.19 is a plot of the evolution of the best value of the 320 samples of the fitness function at each generation for the three non-symmetric cases considered. There is a really good improvement in the fitness function best value in the first 30 generations for the cases C1 and C2, beyond which the improvement is small. For the C3 case the maximum improvement is reached in the first 7 generations and beyond that generation the improvement is small.

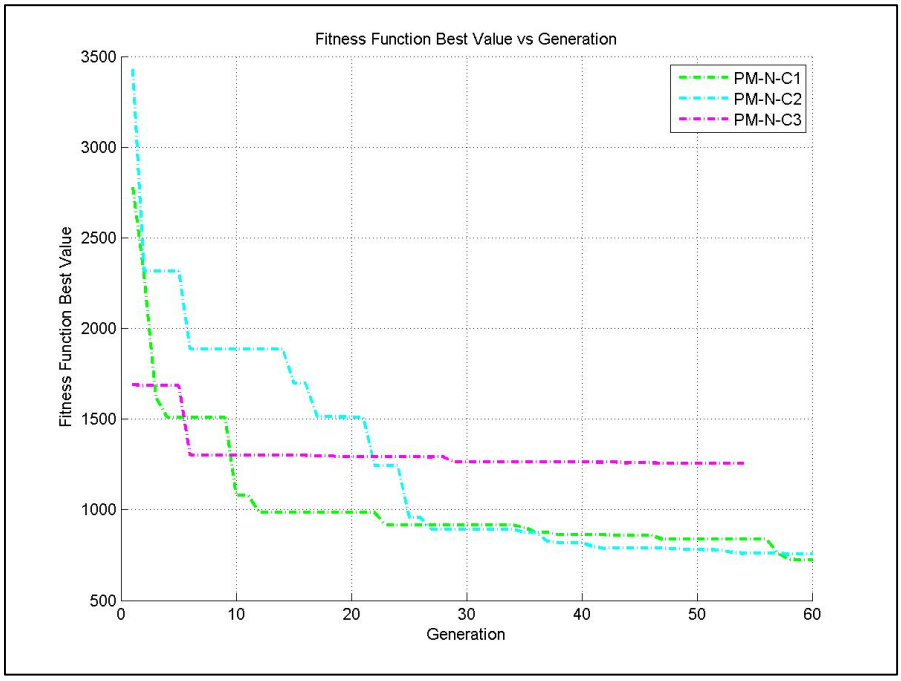

Figure 3.19. Fitness function best value evolution, non-symmetric solutions, polyester mooring system.

Figure 3.20 is a plot of the mean value of the 320 sample values of the fitness function mean value at each generation for the three non-symmetric cases considered. There is a constant improvement in the fitness function mean value for all the generations, because the GA is moving all the samples in the population to the best fitness function value, even if there is no improvement in the fitness function best value.

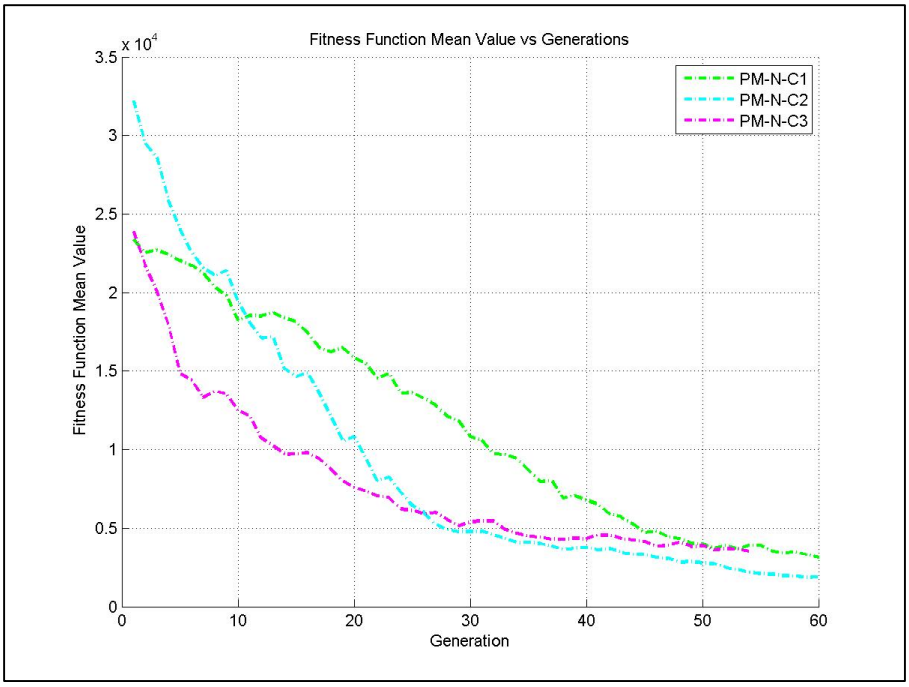

Figure 3.20. Fitness function mean value evolution, non-symmetric solutions, polyester mooring system.

Table 3.10 is a summary of the main Genetic Algorithm process characteristics for the solutions for the equivalent polyester mooring system. The computing time is based on a parallel computing implementation of the Genetic Algorithm program on a laptop using eight processors. It appears that the computing time is directly proportional to the number of design parameters. The changes in the RMS errors for the various responses and design solutions tend to track the changes in the relative weighting factors in the fitness function. Based on the plots and the RMSE values, the best solution for the equivalent mooring system is the non-symmetric case PM-N-C1 and the second best solution is the symmetric case PM-S-C3. The weighting factors applied to the pitch angle

consider the angle in radians which is the units used internally in the procedures developed.

Table 3.10. Summary results equivalent mooring system, polyester mooring system.

CONCEPT	VALUE					
Case	PM-S-C1	PM-S-C2	PM-S-C3	PM-N-C1	PM-N-C2	PM-N-C3
Design Parameters	6			11		
Individuals	320			320		
Generations	60			60		
Comp. Time (hrs)*	3.45	2.92	3.71	5.23	6.62	5.18
Fitness Function Weighting Factor						
Restoring Force	1.0	1.0	1.0	1.0	1.0	1.0
Heave Motion	10,000	10,000	1,000	10,000	10,000	1,000
Pitch Angle	10,000	1,000	100,000	10,000	1,000	100,000
Root Mean Square Error						
Rest. Force (kN)	270.6	205.2	231.0	214.97	126.7	286.5
Heave Motion (m)	0.052	0.084	0.066	0.046	0.061	0.471
Pitch Angle (deg)	0.399	0.389	0.303	0.282	1.151	0.286
Fit. Func. Value	861	1048	825	725	755	1256

* Using parallel computing with 8 processors

Figure 3.21 shows the mooring line configuration at the calm water equilibrium position and at the maximum offset position for the prototype, the symmetric equivalent mooring system (PM-S-C3) and the non-symmetric equivalent mooring system (PM-N-C1). The maximum offset position (176 m) is equal to 8% of the prototype water depth (2,200 m). For the equivalent mooring systems the water depth is equal to 290.32 m, which amounts to a truncation factor of 7.58. In the maximum offset position the down-weather lines of the equivalent mooring system are almost vertical at the top, whereas this is

obviously not the case for the prototype system. The up-weather lines of the equivalent mooring systems therefore have to compensate for the fact that the down-weather lines will slacken faster in the equivalent mooring system than in the prototype.

Additionally, for this specific case, a design of the equivalent mooring system was developed at the OTRC by Dr. Richard Mercier using a manual iterative procedure, with the same design objectives and constraints. Dr. Mercier's design was completed for an actual model test project that was performed prior to the development of the GA described herein, so this represents a blind comparison between human and machine (GA-based) design. Figure 3.22 shows the restoring force response comparison of the equivalent mooring systems designed with the automatic procedure developed in this research work (PM-S-C3 and PM-N-C1) and the manual iterative design by Dr. Mercier at the OTRC. The equivalent mooring designs from the automatic procedure yield restoring forces that are closer to the prototype response than Dr. Mercier's design at large offsets (larger than 120m), although clearly all designs yield acceptable results.

Figure 3.23 shows the setdown response comparison between the equivalent mooring systems. Significantly better setdown results were obtained with the designs from the automated procedure developed in this research (PM-S-C3 and PM-N-C1) than with Dr. Mercier's equivalent mooring design.

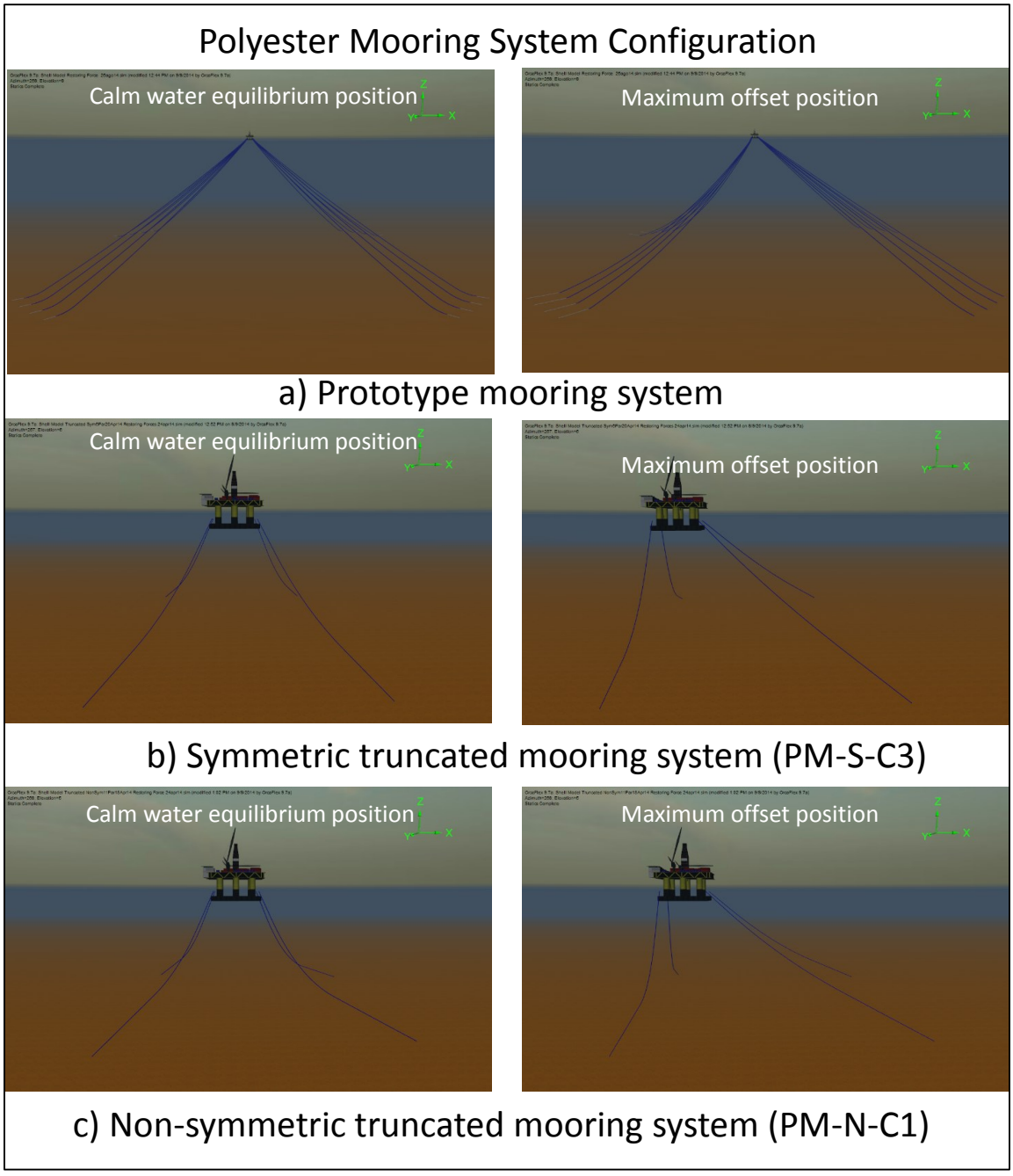

Figure 3.21. Polyester mooring system configuration at calm water equilibrium position and at maximum offset. a) Prototype, b) symmetric, and c) non-symmetric.

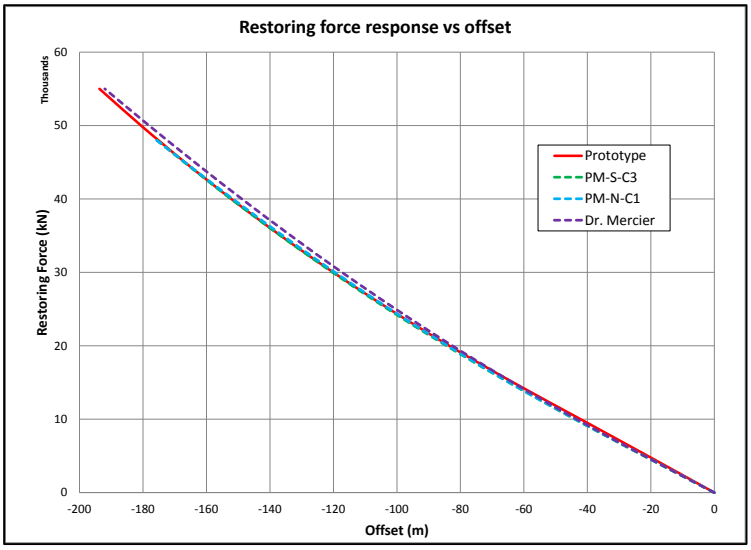

Figure 3.22. Restoring force response comparison automatic procedure vs manual iterative procedure, polyester mooring system.

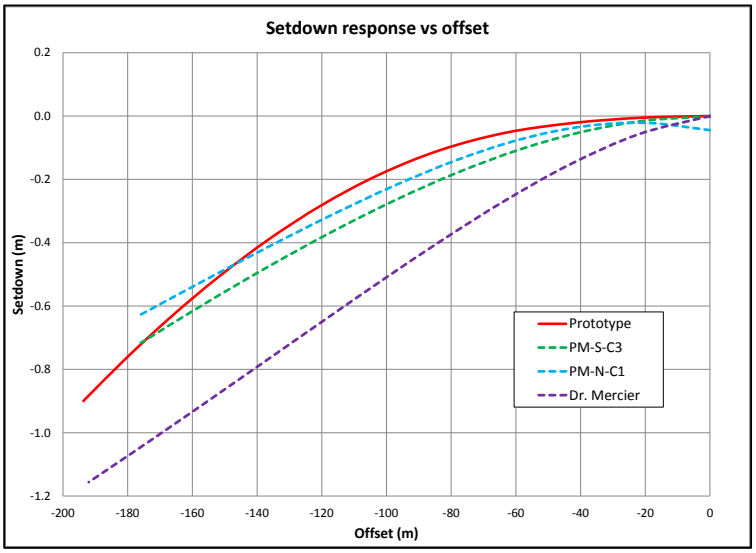

Figure 3.23. Setdown response comparison automatic procedure vs manual iterative procedure, polyester mooring system.

Figure 3.24 shows the pitch response comparison for the equivalent mooring system designs. The equivalent mooring system designed by Dr. Mercier has a closer response to the prototype than the equivalent mooring systems designed with the procedure developed in this research.

Compared to the GA designs, evidently Dr. Mercier placed higher priority on matching the pitch static offset curve at the expense of the setdown and restoring force responses, but clearly on an overall basis the best GA designs are as good as Dr. Mercier's design. This serves as a strong validation of the GA algorithms developed in this research.

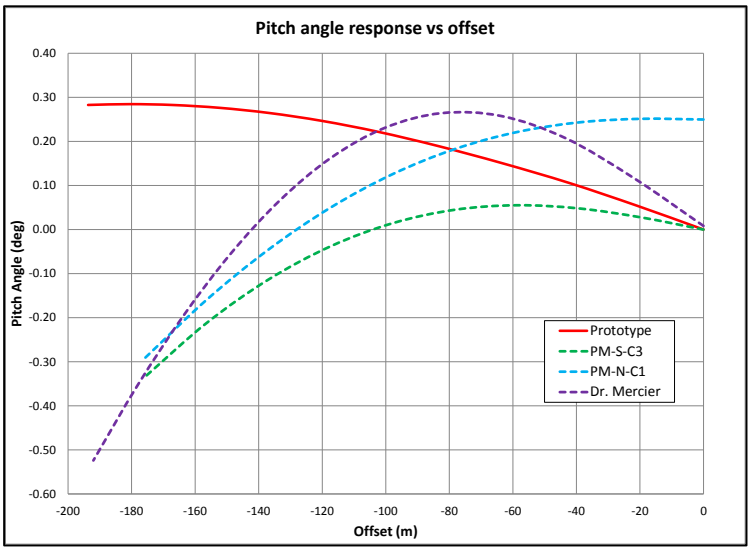

Figure 3.24. Pitch response comparison automatic procedure vs manual iterative procedure, polyester mooring system.

Table 3.11 lists the fairlead and anchor coordinates for the manual design of the equivalent mooring system developed by Dr. Mercier. Table 3.12 shows the equivalent mooring line properties for Dr. Mercier's design.

Table 3.11. Fairlead and anchor coordinates, Dr. Mercier equivalent design.

Mooring Line	Fairlead location			Anchor location		
	X' (m)	Y' (m)	Z' (m)	X (m)	Y (m)	Z (m)
1	52.15	52.15	-19.42	178.53	191.50	-292.06
2	52.15	-52.15	-19.42	178.53	-191.55	-292.06
3	-52.15	-52.15	-19.42	-289.56	-297.62	-292.06
4	-52.15	52.15	-19.42	-289.56	297.62	-292.06

Table 3.12. Mooring line properties, Dr. Mercier equivalent design.

Mooring Lines	Segment	Value			
		L **(m)**	***w*** **(N/m)**	***AE*** **(N)**	***Elements***
Upwind (1,2)	Load Cell	3.81	42,020	1.240e11	1
	Cable	78.32	254.1	3.800e10	8
	Spring	233.00	33,870	6.047e07	23
Downwind (3,4)	Load Cell	3.81	42,020	1.240e11	1
	Spring	235.00	33,870	6.047e07	23
	Anchor Cable	181.35	254.1	3.800e10	18

3.3.2 Semisubmersible with Steel Wire Mooring System

The second study case developed is a semisubmersible with a mooring system based on steel wire rope for a 1,900 m water depth. The mooring system is composed of 4 groups with 4 mooring lines each for a total of 16 mooring lines. Figure 3.25 shows the configuration of the mooring system.

The equivalent mooring system design considers 4 mooring lines with fairlead position at each semisubmersible column at the same elevation as for the prototype. The model fairlead is located at the middle point between the four prototype fairlead positions and the initial mooring line heading in the X-Y plane is in the middle of each group of four prototype lines.

The semisubmersible hydrostatic stiffness characteristics and the mooring system properties are listed in Table 3.13. Since all mooring lines are identical the values included in this table apply to all mooring lines. Table 3.14 lists the prototype mooring system coordinates for the fairlead and anchor points.

The catenary effect is more important for steel mooring systems than for polyester mooring systems due to the substantially higher unit submerged weight of wire rope compared to comparable strength polyester rope. In order to address this behavior in the equivalent mooring system three additional cases are considered using heavier chain segments instead of cable segments for the lower and upper segments. This is over and above the three cases investigated using cable segments. The order of these segments from the anchor point to the fairlead is:

- cable segment, spring, cable segment and load cell, or

- chain segment, spring, chain segment and load cell.

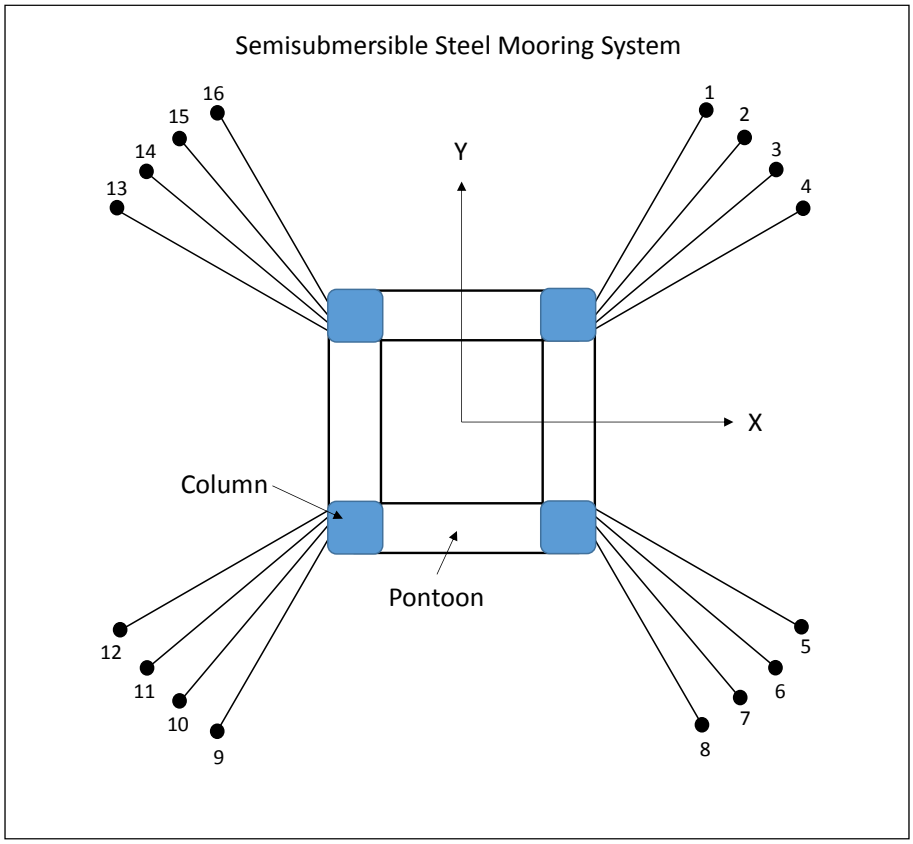

Figure 3.25. Semisubmersible mooring system configuration, prototype steel wire mooring lines.

Table 3.13. Semisubmersible and prototype mooring system characteristics, steel wire mooring system.

Property	Value			
Water Depth (m)	1,900			
Semisubmersible hydrostatic stiffness	Heave, K_z (N/m)	Roll, K_r (N m/rad)	Pitch, K_p (N m/rad)	
	11,740,000	1.246e10	1.246e10	
Elevation for applying acting force in X direction	15.62 m (above Sea Water Level)			
Number of Mooring Lines	16			
Number of Segment per Mooring Line	3			
Segment Properties	*L* (m)	*w* (N/m)	*AE* (N)	*Elements*
Platform Chain	100	2,613	1.238e9	10
Steel Wire Rope	2,800	539.9	1.222e9	280
Anchor Chain	350	2,233	1.060e9	35

Table 3.14. Fairlead and anchor coordinates, prototype steel wire mooring system.

Mooring Line	Fairlead location			Anchor location		
	X' (m)	Y' (m)	Z' (m)	X (m)	Y (m)	Z (m)
1	45.00	38.60	-24.38	1,545	2,007	-1,900
2	45.00	34.20	-24.38	1,713	1,864	-1,900
3	45.00	29.80	-24.38	1,868	1,708	-1,900
4	45.00	25.40	-24.38	2,009	1,539	-1,900
5	45.00	-25.40	-24.38	2,009	-1,539	-1,900
6	45.00	-29.80	-24.38	1,868	-1,708	-1,900
7	45.00	-34.20	-24.38	1,713	-1,864	-1,900
8	45.00	-38.60	-24.38	1,545	-2,007	-1,900
9	-45.00	-38.60	-24.38	-1,545	-2,007	-1,900
10	-45.00	-34.20	-24.38	-1,713	-1,864	-1,900
11	-45.00	-29.80	-24.38	-1,868	-1,708	-1,900
12	-45.00	-25.40	-24.38	-2,009	-1,539	-1,900
13	-45.00	25.40	-24.38	-2,009	1,539	-1,900
14	-45.00	29.80	-24.38	-1,868	1,708	-1,900
15	-45.00	34.20	-24.38	-1,713	1,864	-1,900
16	-45.00	38.60	-24.38	-1,545	2,007	-1,900

Table 3.15 lists the design parameters used in the Genetic Algorithm for designing the equivalent mooring system. The values highlighted in green are part of the GA solution. The coordinates of the fairlead location for the equivalent mooring system, and the initial equivalent mooring line headings are presented in Table 3.16.

Table 3.15. Equivalent mooring system design characteristics, steel wire mooring system.

Property	**Value**			
Scale Factor	1:60			
Truncation Factor	5.468			
Number of individuals	500			
Number of generations	60			
Anchoring radius	Minimum (m)		Maximum (m)	
	305.9		914.4	
Semisubmersible hydrostatic stiffness	Heave, K_z (N/m)	Roll, K_r (N m/rad)	Pitch, K_p (N m/rad)	
	11,740,000	1.246e10	1.246e10	
Elevation for applying acting force in X direction	15.62 m (above Sea Water Level)			
Maximum Offset in Surge	12% of Full Water Depth			
Number of Mooring Lines	4			
Number of Segment per Mooring Line	4			
Considering Cable Segments				
Segment Properties	*L* (m)	*w* (N/m)	*AE* (N)	*Elements*
Platform Load Cell	4.57	60,840	2.123e11	1
Cable Segment	---	368.4	6.584e10	20
Spring Segment	---	---	---	20
Anchor Cable Segment	---	368.4	6.584e10	20
Considering Chain Segments				
Segment Properties	*L* (m)	*w* (N/m)	*AE* (N)	*Elements*
Platform Load Cell	4.57	60,840	2.123e11	1
Chain Segment	---	15,050	1.292e11	20
Spring Segment	---	---	---	20
Anchor Chain Segment	---	15,050	1.292e11	20

The Genetic Algorithm scenarios used are the symmetric and non-symmetric solutions, considering different values for the weighting factors in the fitness function. Table 3.17 list the values for the weighting factors applied to the fitness function for each case considered.

Table 3.16. Fairlead coordinates and initial mooring line heading for the equivalent mooring design, steel wire mooring system.

Mooring Line	Fairlead location			Initial mooring line heading (deg)
	X' (m)	Y' (m)	Z' (m)	
1	45.00	32.00	-24.38	45.15
2	45.00	-32.00	-24.38	314.85
3	-45.00	-32.00	-24.38	225.15
4	-45.00	32.00	-24.38	134.85

The results for the symmetric cases are presented first followed by those for the non-symmetric cases.

Table 3.17. Fitness function weight factors per each case considered, steel wire mooring system.

Static Response	Fitness Function Weight Factors Considered					
	Using Cable Segments					
	Symmetric solutions			Non-symmetric solutions		
	SM-S-C1	SM-S-C2	SM-S-C3	SM-N-C1	SM-N-C2	SM-N-C3
Restoring Force	1.0	1.0	1.0	1.0	1.0	1.0
Heave	100	1,000	1,000	100	1,000	1,000
Pitch	1,000	10,000	1,000	1,000	10,000	1,000
Static Response	**Using Chain Segments**					
	Symmetric solutions			**Non-symmetric solutions**		
	SM-SC-C1	**SM-SC-C2**	**SM-SC-C3**	**SM-NC-C1**	**SM-NC-C2**	**SM-NC-C3**
Restoring Force	1.0	1.0	1.0	1.0	1.0	1.0
Heave	100	1,000	1,000	100	1,000	1,000
Pitch	1,000	10,000	1,000	1,000	10,000	1,000

The coordinates for the equivalent mooring line fairlead and anchoring points for the best solutions for each symmetric case considered are presented Table 3.18. The anchor coordinates in the X-Y plane are the result of considering the anchor radius and line angle variations as design parameters; those results are highlighted in green in the table. The properties for each mooring line segment for the best solution are listed in Table 3.19. The design parameters obtained from the GA are highlighted in green.

Table 3.18. Fairlead and anchor coordinates, symmetric solutions, steel wire mooring system.

Case		Mooring Line	Fairlead location			Anchor location		
			X' (m)	Y' (m)	Z' (m)	X (m)	Y (m)	Z (m)
Using Cable Segments	SM-S-C1	1	45.00	32.00	-24.38	448.74	575.02	-347.47
		2	45.00	-32.00	-24.38	448.74	-575.02	-347.47
		3	-45.00	-32.00	-24.38	-448.74	-575.02	-347.47
		4	-45.00	32.00	-24.38	-448.74	575.02	-347.47
	SM-S-C2	1	45.00	32.00	-24.38	358.21	675.05	-347.47
		2	45.00	-32.00	-24.38	358.21	-675.05	-347.47
		3	-45.00	-32.00	-24.38	-358.21	-675.05	-347.47
		4	-45.00	32.00	-24.38	-358.21	675.05	-347.47
	SM-S-C3	1	45.00	32.00	-24.38	220.98	706.68	-347.47
		2	45.00	-32.00	-24.38	220.98	-706.68	-347.47
		3	-45.00	-32.00	-24.38	-220.98	-706.68	-347.47
		4	-45.00	32.00	-24.38	-220.98	706.68	-347.47
Using Chain Segments	SM-SC-C1	1	45.00	32.00	-24.38	360.91	632.68	-347.47
		2	45.00	-32.00	-24.38	360.91	-632.68	-347.47
		3	-45.00	-32.00	-24.38	-360.91	-632.68	-347.47
		4	-45.00	32.00	-24.38	-360.91	632.68	-347.47
	SM-SC-C2	1	45.00	32.00	-24.38	402.50	630.75	-347.47
		2	45.00	-32.00	-24.38	402.50	-630.75	-347.47
		3	-45.00	-32.00	-24.38	-402.50	-630.75	-347.47
		4	-45.00	32.00	-24.38	-402.50	630.75	-347.47
	SM-SC-C3	1	45.00	32.00	-24.38	344.03	640.64	-347.47
		2	45.00	-32.00	-24.38	344.03	-640.64	-347.47
		3	-45.00	-32.00	-24.38	-344.03	-640.64	-347.47
		4	-45.00	32.00	-24.38	-344.03	640.64	-347.47

Table 3.19. Mooring line properties for best fitness function solutions, steel wire mooring system.

Case		Segment	Value			
			L **(m)**	***w*** **(N/m)**	***AE*** **(N)**	***Elements***
Using Cable Segments	**SM-S-C1**	Load Cell	4.57	60,840	2.123e11	1
		Cable Segment	233.22	368.4	6.584e10	20
		Spring Segment	306.46	12,630	6.316e07	20
		Cable Segment	293.42	368.4	6.584e10	20
	SM-S-C2	Load Cell	4.57	60,840	2.123e11	1
		Cable Segment	128.28	368.4	6.584e10	20
		Spring Segment	300.71	24,760	1.421e08	20
		Cable Segment	445.59	368.4	6.584e10	20
	SM-S-C3	Load Cell	4.57	60,840	2.123e11	1
		Cable Segment	192.92	368.4	6.584e10	20
		Spring Segment	274.37	29,480	6.711e07	20
		Cable Segment	325.39	368.4	6.584e10	20
Using Chain Segments	**SM-SC-C1**	Load Cell	4.57	60,840	2.123e11	1
		Chain Segment	372.69	15,050	1.292e11	20
		Spring Segment	292.54	24,760	1.421e08	20
		Chain Segment	206.83	15,050	1.292e11	20
	SM-SC-C2	Load Cell	4.57	60,840	2.123e11	1
		Chain Segment	176.19	15,050	1.292e11	20
		Spring Segment	514.00	24,760	1.421e08	20
		Chain Segment	200.86	15,050	1.292e11	20
	SM-SC-C3	Load Cell	4.57	60,840	2.123e11	1
		Chain Segment	236.18	15,050	1.292e11	20
		Spring Segment	353.29	24,760	1.421e08	20
		Chain Segment	274.50	15,050	1.292e11	20

Figure 3.26 shows the restoring force response for the symmetric solutions using cable (a) and chain (b) segments. There is a very good correlation in the restoring force response for the six solutions considered with respect to the prototype response. In general, the cases with cable segments are closer to the prototype response that the cases with chain segments. The maximum absolute errors for large offsets (greater than the mean offset value, above 115m) are 5.4% for SM-S-C1, 4.3% for SM-S-C2, 13.2% for SM-S-C3, 14.5% for SM-SC-C1, 9.7% for SM-SC-C2 and 9.2% for SM-SC-C3, respectively.

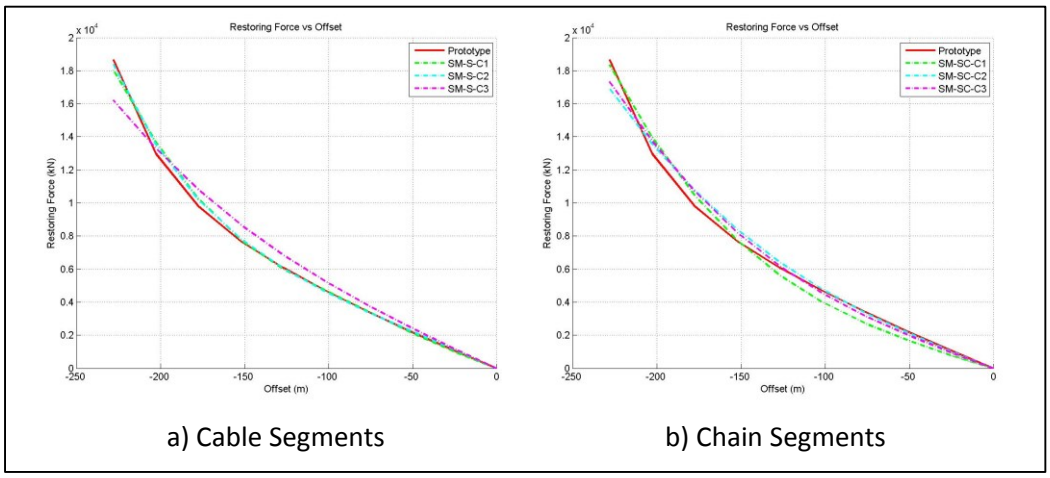

Figure 3.26. Restoring force vs offset plot, symmetric solutions, steel wire mooring system.

Figure 3.27 shows the setdown response for the symmetric solutions considered. The setdown is improved when chain segments are used instead of cable segments in the equivalent mooring system. The best solutions considering just the setdown response are

the SM-SC-C2 and SM-SC-C3 with maximum differences relative to the prototype of about 0.1 m.

Figure 3.28 shows the pitch response for the symmetric solutions considered. There is a significant improvement in the pitch response when the chain segments are used instead of cable segments. The designs SM-SC-C2 and SM-SC-C3 have the best pitch response with respect to the prototype.

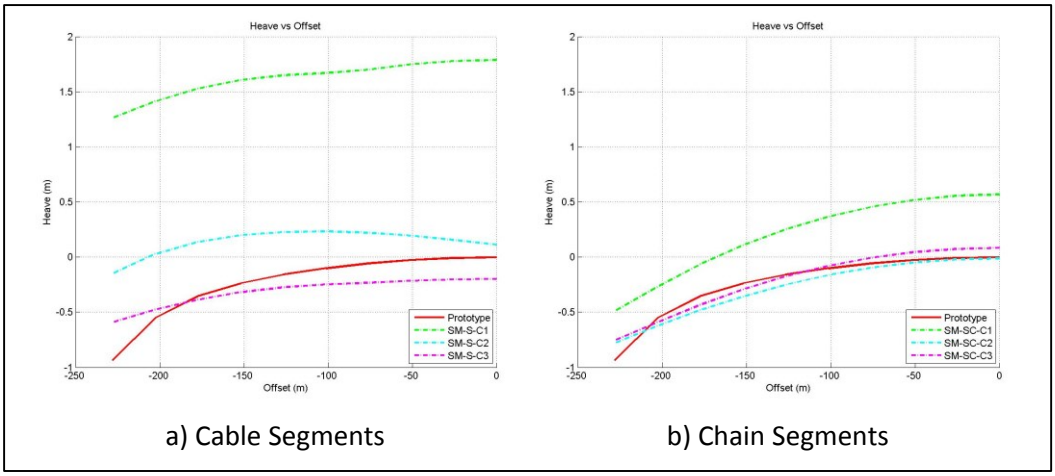

Figure 3.27. Heave vs offset plot, symmetric solutions, steel wire mooring system.

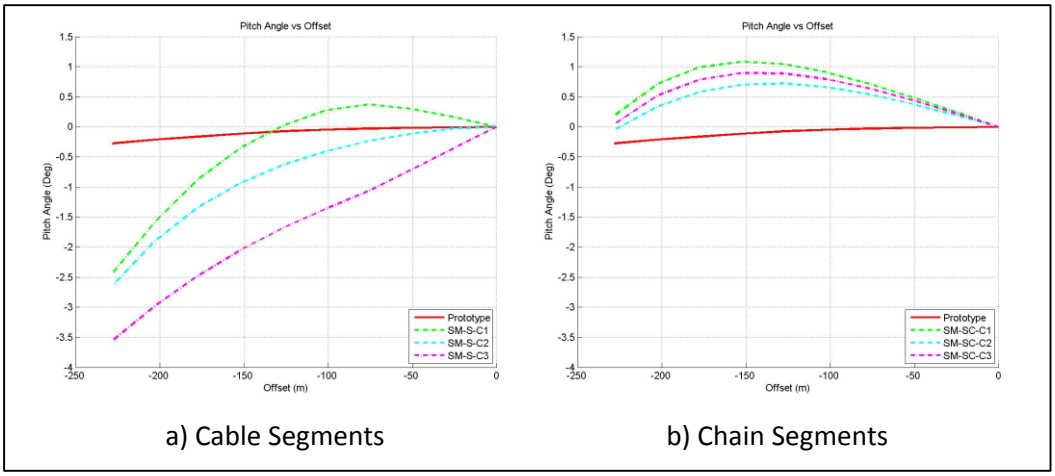

a) Cable Segments b) Chain Segments

Figure 3.28. Pitch vs offset plot, symmetric solutions, steel wire mooring system.

Based on the results presented above, as it is expected for this study case which considers a prototype steel mooring system, the submerged weight catenary effect plays an important role in the static response, so using chain segments instead of cable segments in the equivalent mooring system design significantly improves the setdown and pitch responses compared with the prototype. Although there is some loss of accuracy in the restoring force response, we can say that overall, considering the three degrees of freedom, the design is improved with the use of chain instead of cable for the equivalent mooring system. Note that the submerged weight (i.e. the size) of the chain was fixed at the outset and not considered a design variable. Had the chain size been allowed to vary as part of the GA optimization it is likely that better equivalent mooring designs would have resulted. The point here is that for steel prototype moorings the equivalent mooring design should incorporate heavier chain segments rather than cable segments.

Figure 3.29 shows the evolution of the best fitness function value in the GA at each generation for the symmetric solution cases considered. For the cases with cable segments the most important improvement is in the first 20 generations while for the cases with chain segments the optimal design is reached in less than 10 generations. In general, the initial fitness function best value is smaller for all the cases when chain segments are considered instead of cable segments.

The fitness function mean value at each generation for the symmetric cases is plotted in Figure 3.30. The fitness function mean value is significantly improved in the first 20 generations for the cases with cable segments and within around 30 generations for the cases with chain segments. Based on these results, it can be assumed that an acceptable solution will be reached if just 30 generations are used in the Genetic Algorithm solution.

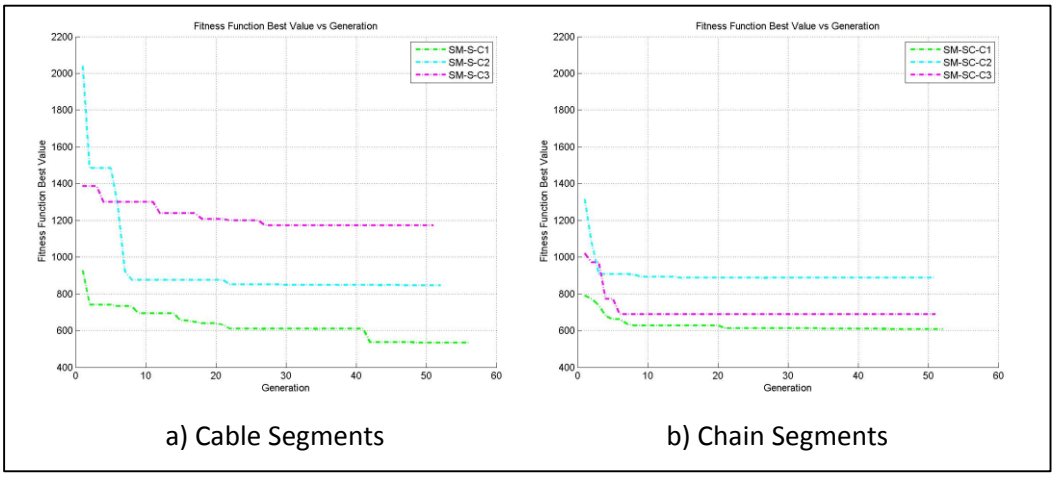

Figure 3.29. Fitness function best value evolution, symmetric solutions, steel wire mooring system.

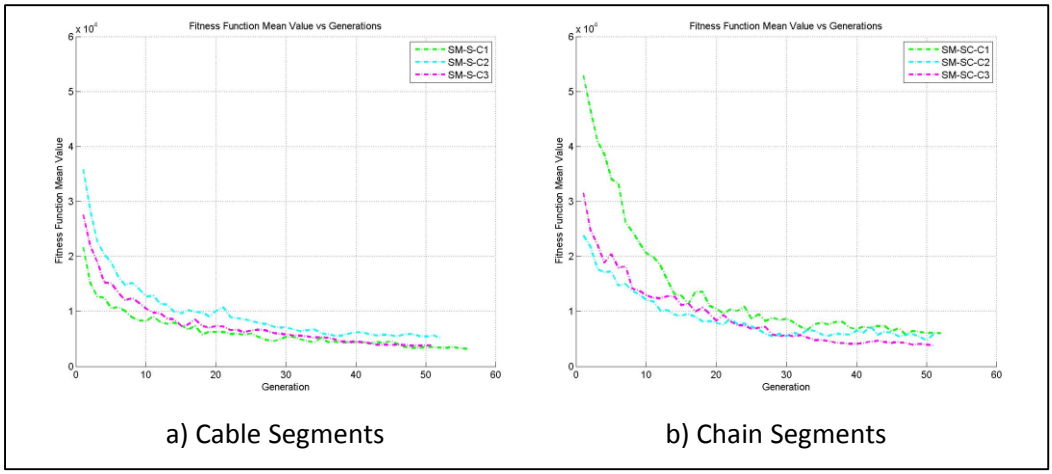

Figure 3.30. Fitness function mean value evolution, symmetric solutions, steel wire mooring system.

Figure 3.31, Figure 3.32 and Figure 3.33 show the results for restoring force, setdown and pitch, respectively, for the prototype and the equivalent non-symmetric mooring system responses. The coordinates for the fairlead and anchor points for the best solutions are included in Table 3.20.

Table 3.21 and Table 3.22 list the properties for each mooring line segment for the upwind and downwind mooring lines for the best solutions, with cable segments and chain segments, respectively.

Table 3.20. Fairlead and anchor coordinates, non-symmetric solutions, steel wire mooring system.

Case		Mooring Line	Fairlead location			Anchor location		
			X' (m)	Y' (m)	Z' (m)	X (m)	Y (m)	Z (m)
Using Cable Segments	SM-N-C1	1	45.00	32.00	-24.38	303.59	679.45	-347.47
		2	45.00	-32.00	-24.38	303.59	-679.45	-347.47
		3	-45.00	-32.00	-24.38	-658.17	-363.78	-347.47
		4	-45.00	32.00	-24.38	-658.17	363.78	-347.47
	SM-N-C2	1	45.00	32.00	-24.38	457.48	633.94	-347.47
		2	45.00	-32.00	-24.38	457.48	-633.94	-347.47
		3	-45.00	-32.00	-24.38	-299.78	-715.78	-347.47
		4	-45.00	32.00	-24.38	-299.78	715.78	-347.47
	SM-N-C3	1	45.00	32.00	-24.38	430.25	610.03	-347.47
		2	45.00	-32.00	-24.38	430.25	-610.03	-347.47
		3	-45.00	-32.00	-24.38	-306.99	-675.35	-347.47
		4	-45.00	32.00	-24.38	-306.99	675.35	-347.47
Using Chain Segments	SM-NC-C1	1	45.00	32.00	-24.38	310.50	661.76	-347.47
		2	45.00	-32.00	-24.38	310.50	-661.76	-347.47
		3	-45.00	-32.00	-24.38	-531.47	-512.04	-347.47
		4	-45.00	32.00	-24.38	-531.47	512.04	-347.47
	SM-NC-C2	1	45.00	32.00	-24.38	522.07	535.01	-347.47
		2	45.00	-32.00	-24.38	522.07	-535.01	-347.47
		3	-45.00	-32.00	-24.38	-214.59	-704.20	-347.47
		4	-45.00	32.00	-24.38	-214.59	704.20	-347.47
	SM-NC-C3	1	45.00	32.00	-24.38	547.08	512.88	-347.47
		2	45.00	-32.00	-24.38	547.08	-512.88	-347.47
		3	-45.00	-32.00	-24.38	-235.50	-700.61	-347.47
		4	-45.00	32.00	-24.38	-235.50	700.61	-347.47

Table 3.21. Mooring line properties for best solution using cable segments, non-symmetric cases, steel wire mooring system.

Case	Mooring Lines	Segment	Value			
			L **(m)**	***w*** **(N/m)**	***AE*** **(N)**	***Elements***
SM-N-C1	Upwind (1,2)	Load Cell	4.57	60,840	2.123e11	1
		Cable	357.26	368.4	6.584e10	20
		Spring	244.91	12,630	6.316e07	20
		Cable	239.91	368.4	6.584e10	20
	Downwind (3,4)	Load Cell	4.57	60,840	2.123e11	1
		Cable	124.62	368.4	6.584e10	20
		Spring	266.41	9,018	1.678e07	20
		Cable	433.49	368.4	6.584e10	20
SM-N-C2	Upwind (1,2)	Load Cell	4.57	60,840	2.123e11	1
		Cable	154.92	368.4	6.584e10	20
		Spring	567.53	29,480	6.711e07	20
		Cable	280.95	368.4	6.584e10	20
	Downwind (3,4)	Load Cell	4.57	60,840	2.123e11	1
		Cable	145.93	368.4	6.584e10	20
		Spring	303.85	10,090	3.454e07	20
		Cable	264.02	368.4	6.584e10	20
SM-N-C3	Upwind (1,2)	Load Cell	4.57	60,840	2.123e11	1
		Cable	160.53	368.4	6.584e10	20
		Spring	544.29	24,760	1.421e08	20
		Cable	464.49	368.4	6.584e10	20
	Downwind (3,4)	Load Cell	4.57	60,840	2.123e11	1
		Cable	135.64	368.4	6.584e10	20
		Spring	287.45	12,630	6.316e07	20
		Cable	254.60	368.4	6.584e10	20

Figure 3.31 plots the restoring force responses for the non-symmetric solutions considered. In general, the restoring forces for the cases with cable segments are closer to the prototype response than for the cases with chain segments. The only case where the restoring force response is improved using chain instead of cable is for the second case

(SM-C-C2 and SM-NC-C2). The maximum absolute errors for large offsets (greater than the mean offset value) between the prototype and the equivalent non-symmetric mooring systems are: 6.2% for SM-N-C1, 18.9% for SM-N-C2, 8.4% for SM-N-C3, 9.6% for SM-NC-C1, 11.5% for SM-NC-C2 and 12.1% for SM-NC-C3.

Table 3.22. Mooring line properties for best solution using chain segments, non-symmetric cases, steel wire mooring system.

Case	Mooring Lines	Segment	Value			
			L **(m)**	***w*** **(N/m)**	***AE*** **(N)**	***Elements***
SM-NC-C1	Upwind (1,2)	Load Cell	4.57	60,840	2.123e11	1
		Chain	180.10	15,050	1.292e11	20
		Spring	290.29	24,760	1.421e08	20
		Chain	531.10	15,050	1.292e11	20
	Downwind (3,4)	Load Cell	4.57	60,840	2.123e11	1
		Chain	215.63	15,050	1.292e11	20
		Spring	307.07	29,480	6.711e07	20
		Chain	258.78	15,050	1.292e11	20
SM-NC-C2	Upwind (1,2)	Load Cell	4.57	60,840	2.123e11	1
		Chain	180.86	15,050	1.292e11	20
		Spring	236.18	12,630	6.316e07	20
		Chain	223.68	15,050	1.292e11	20
	Downwind (3,4)	Load Cell	4.57	60,840	2.122e11	1
		Chain	418.03	15,050	1.292e11	20
		Spring	294.55	6,020	5.823e06	20
		Chain	218.31	15,050	1.292e11	20
SM-NC-C3	Upwind (1,2)	Load Cell	4.57	60,840	2.123e11	1
		Chain	172.77	15,050	1.292e11	20
		Spring	266.83	29,480	6.711e07	20
		Chain	679.68	15,050	1.292e11	20
	Downwind (3,4)	Load Cell	4.57	60,840	2.123e11	1
		Chain	183.78	15,050	1.292e11	20
		Spring	316.17	10,090	3.454e07	20
		Chain	204.96	15,050	1.292e11	20

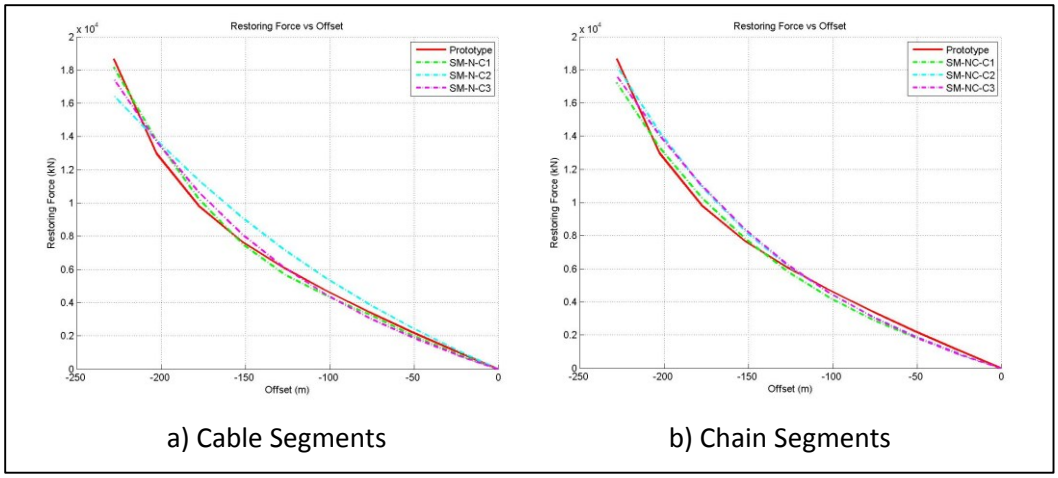

Figure 3.31. Restoring force vs offset plot, non-symmetric solutions, steel wire mooring system.

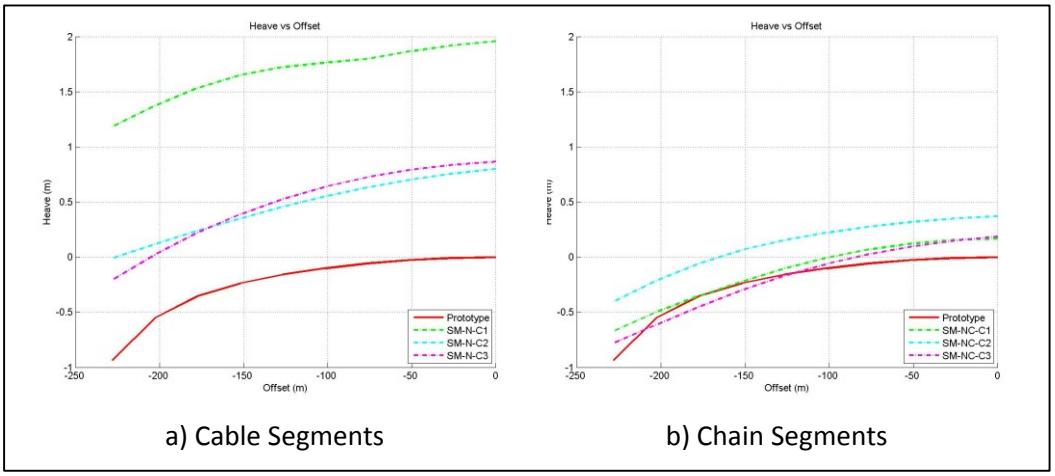

Figure 3.32. Heave vs offset plot, non-symmetric solutions, steel wire mooring system.

Figure 3.32 shows the setdown responses for the non-symmetric solutions. There is a marked improvement for the cases with chain segments instead of cable segments.

The best solutions for the setdown are for SM-NS-C1 and SM-NS-C3 designs with maximum differences with the prototype of about 0.10 m.

The pitch responses for the non-symmetric solutions are plotted in Figure 3.33. Here again there is an improvement in the pitch response for the cases with chain segments instead of cable segments. For the pitch response the best solutions are reached with the cases SM-NC-C1 and SM-NC-C2 with maximum differences with the prototype for the pitch angle of around 1 degree.

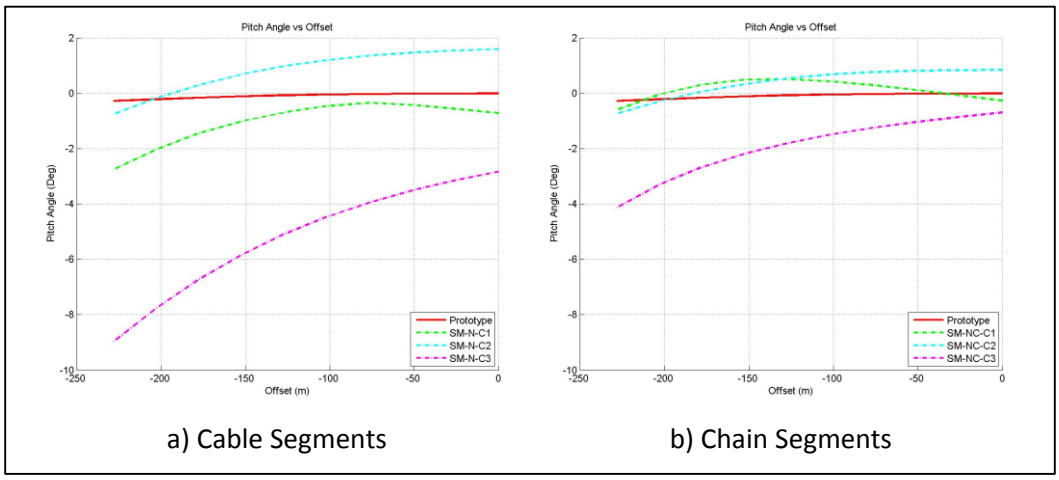

Figure 3.33. Pitch vs offset plot, non-symmetric solutions, steel wire mooring system.

The evolution of the Genetic Algorithm for the fitness function best value for the non-symmetric solutions is plotted in Figure 3.34. For the cases with cable segments in the design, most of the improvement in the fitness function best value is reached in the

first 20 generations, and for the cases with chain segments instead of cable segments most of the improvement is reached in less than 40 generations.

Figure 3.35 shows the fitness function mean value evolution for the non-symmetric solutions. For the six cases, using cable and chain, most of the improvement is reached in less than 30 generations.

Considering the evolution of the fitness function best and mean values, we can say that for this study case and for the non-symmetric scenarios 30 generations is sufficient to have an acceptable solution.

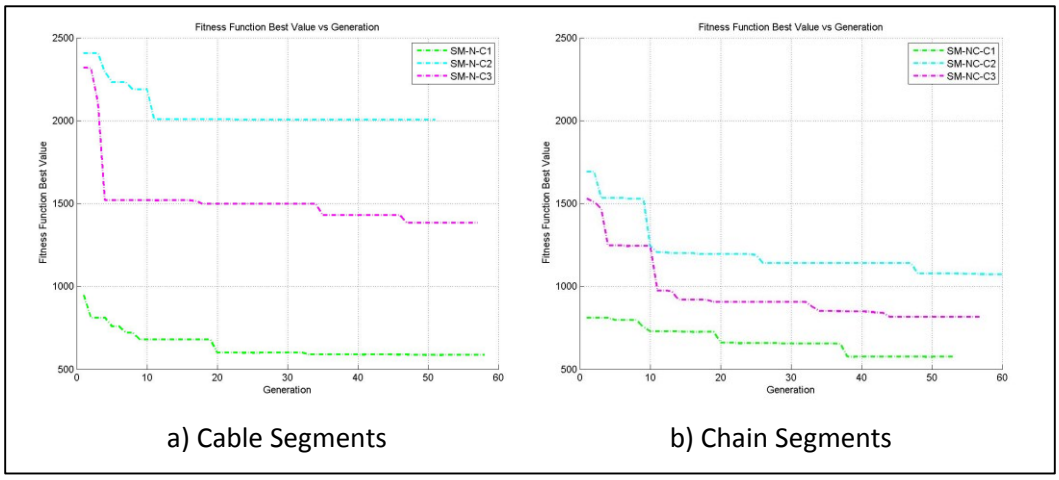

Figure 3.34. Fitness function best value evolution, non-symmetric solutions, steel wire mooring system.

Table 3.23 and Table 3.24 summarize the results for the cases with cable segments and the cases with chain segments, respectively. The tables include the main characteristics used in the GA procedure, the weight factors used for the fitness function,

the computing times for each solution, the RMSE values for each static response associated with the best solution and their fitness function best value. The computing time considers a parallel computing implementation for the GA procedure in a laptop using eight processors. As it is mentioned previously, there is shown in the RMSE values and the fitness function best value the effect of considering different weight factors for each static response in the fitness function. The weighting factors applied to pitch angles consider that those angles are in radians which is the unit used internally for angles in the codes developed.

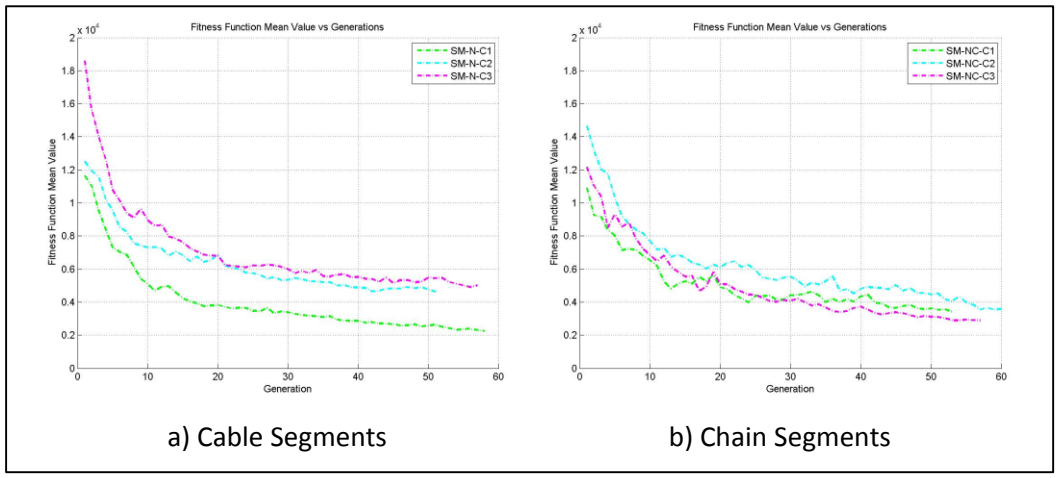

Figure 3.35. Fitness function mean value evolution, non-symmetric solutions, steel wire mooring system.

Table 3.23. Summary results equivalent mooring system, using cable segments in the design, steel wire mooring system.

CONCEPT	VALUE					
Case	SM-S-C1	SM-S-C2	SM-S-C3	SM-N-C1	SM-N-C2	SM-N-C3
Design Parameters	6			11		
Individuals	500			500		
Generations	60			60		
Comp. Time (hrs)*	8.46	9.22	8.31	12.71	11.23	12.17
Fitness Function Weighting Factors						
Restoring Force	1.0	1.0	1.0	1.0	1.0	1.0
Heave	100	1,000	1,000	100	1,000	1,000
Pitch	1,000	10,000	1,000	1,000	10,000	1,000
Root Mean Square Error						
Rest. Force (kN)	333.3	237.4	963.3	372.2	1,096.9	556.3
Heave (m)	1.863	0.427	0.177	1.923	0.710	0.732
Pitch (deg)	0.863	1.047	1.829	1.159	1.133	5.453
Fit. Func. Value	535	847	1,172	585	2,005	1,383

* Using parallel computing with 8 processors

Figure 3.36 shows the mooring line configuration at the calm water equilibrium position and at the maximum offset position for the prototype, symmetric (SM-SC-C3) and non-symmetric (SM-NC-C1) equivalent mooring system, respectively. The maximum offset position is equal to 12% of the prototype water depth (1,900 m) which is equal to 228 m. For the equivalent truncated mooring systems the water depth is equal to 347.47 m which implies a truncation factor of 5.47. For the symmetric and non-symmetric equivalent mooring systems there are long segments laying on the seabed. This is due to the important effect of the submerged weight in the prototype mooring system, which is compensated in the equivalent mooring by the process of lifting chain from the basin floor.

Table 3.24. Summary results equivalent mooring system, using chain segments in the design, steel wire mooring system.

CONCEPT	VALUE					
Case	SM-SC-C1	SM-SC-C2	SM-SC-C3	SM-NC-C1	SM-NC-C2	SM-NC-C3
Design Parameters	6			11		
Individuals	500			500		
Generations	60			60		
Comp. Time (hrs)*	7.52	7.97	7.55	10.71	11.93	11.38
Fitness Function Weighting Factors						
Restoring Force	1.0	1.0	1.0	1.0	1.0	1.0
Heave	100	1,000	1,000	100	1,000	1,000
Pitch	1,000	10,000	1,000	1,000	10,000	1,000
Root Mean Square Error						
Rest. Force (kN)	547.5	701.3	596.0	554.5	601.6	666.7
Heave (m)	0.456	0.086	0.082	0.134	0.358	0.113
Pitch (deg)	0.828	0.567	0.699	0.385	0.642	2.086
Fit. Func. Value	607	887	689	575	1,071	816

* Using parallel computing with 8 processors

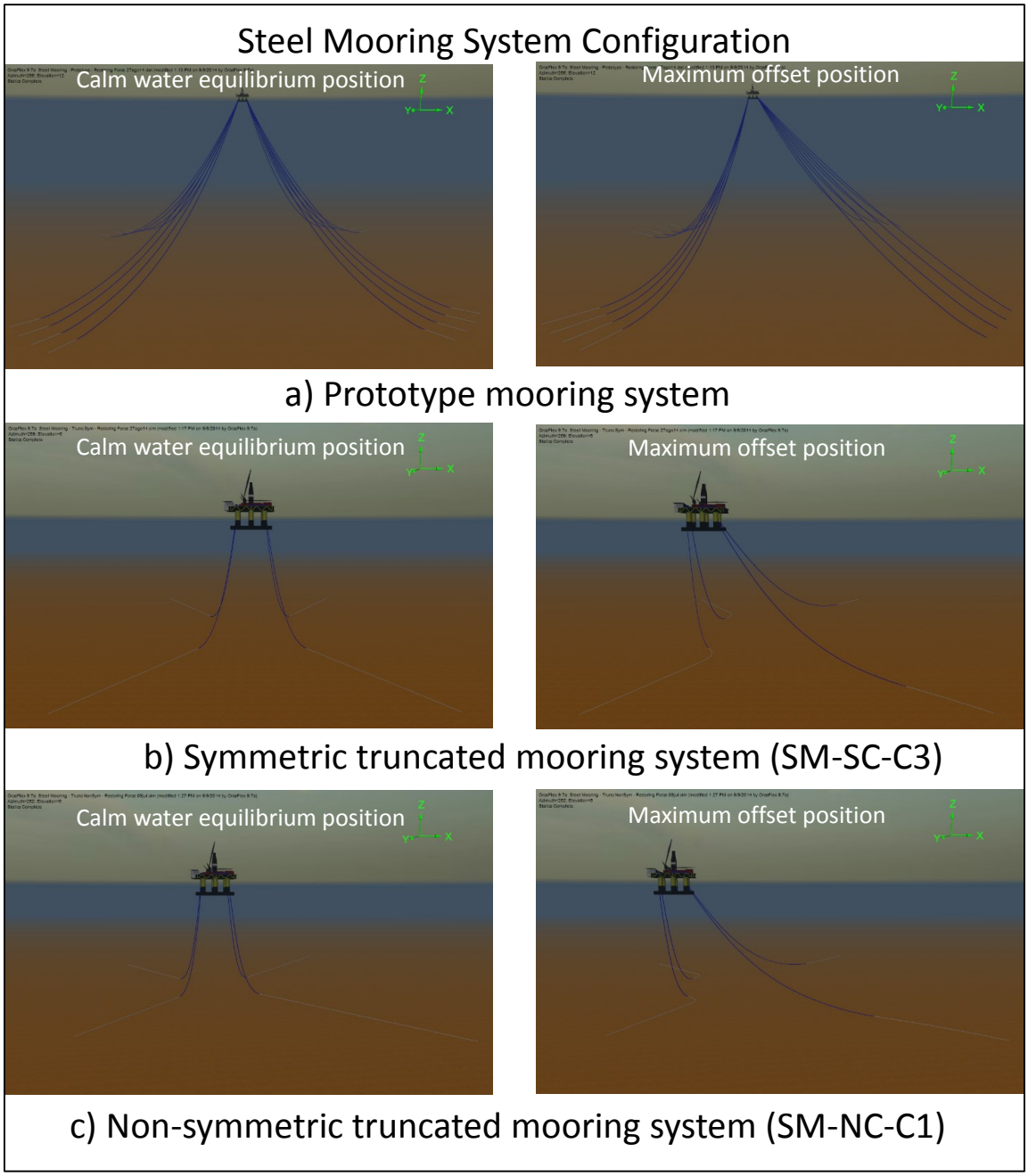

Figure 3.36. Steel mooring system configuration at calm water equilibrium position and at maximum offset. a) Prototype, b) symmetric, and c) non-symmetric.

3.3.3 Semisubmersible with SCRs Attached

The third study case to validate the procedure for the optimized design of the equivalent mooring and steel catenary riser system is a semisubmersible with a polyester mooring system and three SCRs attached. The mooring system for this semisubmersible is a non-symmetric system (for balancing the SCR forces) with a total of 12 mooring lines, arranged in 4 groups of 3 mooring lines. There are three SCRs attached to the semisubmersible (West, North and East pontoons, Figure 3.37). For this case it is considered that the testing heading (i.e. the heading of the environment) will be in the northeastern direction of the platform, so the semisubmersible body-fixed coordinate system is rotated to have the positive X axis oriented upwind, as is illustrated in Figure 3.37. It is important to highlight that for this case, as mentioned before, the procedure followed is to design first the equivalent mooring system considering the prototype SCRs attached, and then once the equivalent mooring system is designed the equivalent riser system is designed with the equivalent mooring system designed in the previous step attached.

The equivalent mooring system design will have 4 mooring lines with the same fairlead elevation as the prototype and those will be located, in the X-Y plane, at the same position as for the middle prototype mooring line at each column (mooring lines 2, 5, 8 and 11 in Figure 3.37). The initial anchor heading is the same as that for the middle prototype line at each column. The equivalent riser system design will consider 2 SCRs. The SCR porch locations are the same as those for the risers SCR 1 and SCR 2 in the

prototype. The initial heading for these equivalent risers are the headings of the SCR 1 and SCR 2 risers in the prototype.

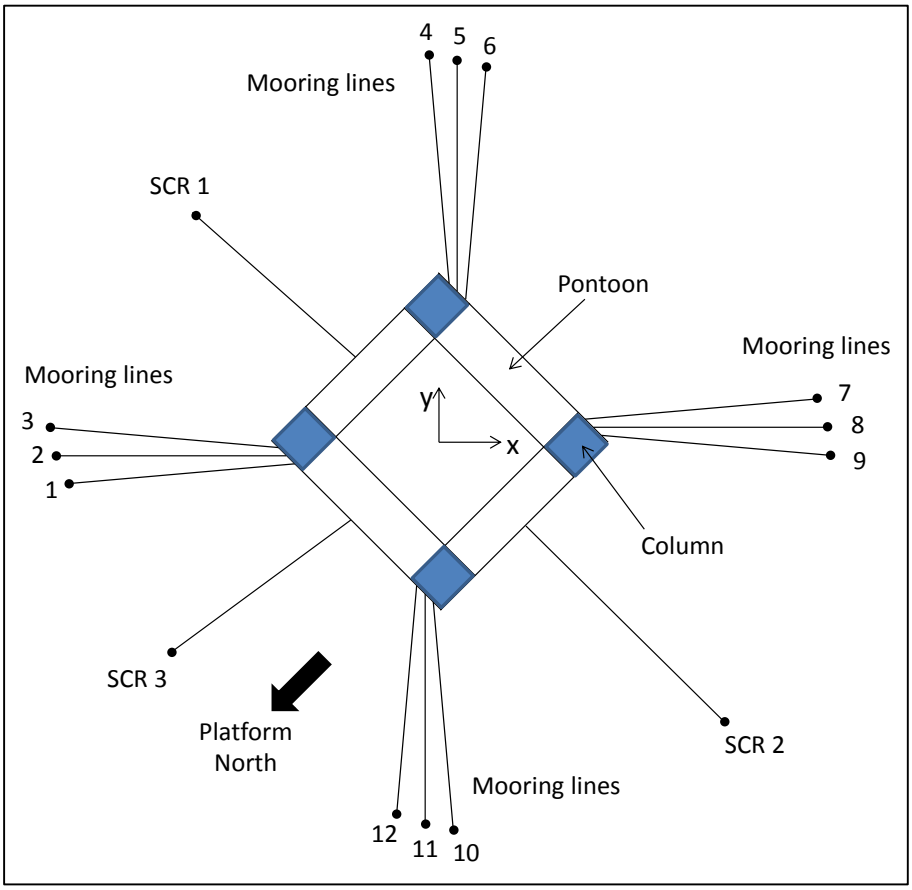

Figure 3.37. Semisubmersible mooring and riser system configuration, prototype.

The semisubmersible hydrostatic stiffness characteristics and the mooring and riser system properties are presented in Table 3.25. In the prototype, all the mooring lines have three segments which are: platform chain, polyester rope and anchor chain, while the SCRs have only one segment. The anchor chain and platform chain have the same mechanical properties. The prototype fairlead/porch and anchor point coordinates for each

mooring line and SCR are listed in Table 3.26. The fairlead and porch coordinates are referenced to the vessel's fixed coordinate system which in this case has its origin at the vessel's center of gravity (CG). The CG is located at the center of the platform and 7.62 m below the sea water level (SWL).

Table 3.25. Semisubmersible and prototype mooring and riser system characteristics.

Property	Value			
Water Depth (m)	1,219			
Semisubmersible hydrostatic stiffness	Heave, K_z (N/m)	Roll, K_r (N m/rad)	Pitch, K_p (N m/rad)	
	9,486,000	1.356e9	1.356e9	
Elevation for applying acting force in X direction	30.48 m (above the CG)			
Number of Mooring Lines	12			
Number of Segments per Mooring Line	3			
Mooring Segments Properties	*L* (m)	*w* (N/m)	*AE* (N)	*Elements*
Platform Chain	Variable	3,179	1.557e9	Variable
Polyester	1,981.2	110.5	6.672e8	20
Anchor Chain	243.8	3,179	1.557e9	24
Platform Chain Length and Number of Elements				
Mooring Lines Number	1,2,3	4,5,6	7,8,9	10,11,12
Platform Chain Length (m)	126.5	124.97	121.92	137.16
Number of Elements	13	12	12	14
Number of SCRs	3			
Number of Segments per SCR	1			
SCR Properties	*L* (m)	*w* (N/m)	*AE* (N)	*Elements*
SCR 1	2,895.6	10,910	3.114e10	289
SCR 2	2,895.6	11,970	3.114e10	289
SCR 3	2,895.6	1,998	6.672e09	289

Table 3.26. Fairlead/porch and anchor coordinates, prototype mooring and riser system.

Mooring Line/SCR	Fairlead location			Anchor location		
	X' (m)	Y' (m)	Z' (m)	X (m)	Y (m)	Z (m)
1	-49.00	-8.23	-23.06	-2,038	-182.2	-1,219
2	-51.58	-5.46	-23.06	-2,048	-5.46	-1,219
3	-54.17	-2.69	-23.06	-2,043	171.3	-1,219
4	2.69	54.17	-23.06	-171.3	2,043	-1,219
5	5.46	51.58	-23.06	5.46	2,048	-1,219
6	8.23	49.00	-23.06	182.2	2,038	-1,219
7	49.00	8.23	-23.06	2,038	182.2	-1,219
8	51.58	5.46	-23.06	2,045	5.46	-1,219
9	54.17	2.69	-23.06	2,043	-171.3	-1,219
10	-2.69	-54.17	-23.06	171.3	-2,043	-1,219
11	-5.46	-51.58	-23.06	-5.46	-2,048	-1,219
12	-8.23	-49.00	-23.06	-182.2	-2,038	-1,219
SCR 1	-27.80	27.80	-23.29	-1,611	1,458	-1,219
SCR 2	27.80	-27.80	-23.29	1,550	-1,523	-1,219
SCR 3	-31.04	-24.57	-23.29	-1,729	-1,317	-1,219

Table 3.27 provides the fixed parameters for the equivalent mooring and riser system. The design parameters that are part of the solution in the GA procedure are highlighted in green. Table 3.28 lists the coordinates of the fairlead and porch locations and the initial mooring line and riser headings with respect to the X axis.

For this study case, the GA procedure for the general solution scenario was applied to design the equivalent mooring and riser system design. Each equivalent mooring line and each equivalent SCR was allowed to have an independent design as determined by six design parameters. It is important to mention that several trials were used for the design of the equivalent mooring and riser system, but here only the best solution for those different trials will be presented. For the best solution, Table 3.29 lists the values for the

weighting factors applied to the fitness function for each one of the design phases considered (i.e. the mooring design phase and the SCR design phase).

Table 3.27. Equivalent mooring and riser system design characteristics.

Property	Value			
Scale Factor	1:55			
Truncation Factor	3.818			
Design Phase	Equi Moor + Prot SCR		Equi Moor + Equi SCR	
Number of individuals	480		320	
Number of generations	30		30	
Number of Equivalent Mooring Lines/SCR	4		2	
Number of Segments per Equivalent Mooring Line/SCR	4		3	
Anchor radius	Minimum (m)		Maximum (m)	
	280.4		838.2	
Semisubmersible hydrostatic stiffness	Heave, K_z (N/m)	Roll, K_r (N m/rad)	Pitch, K_p (N m/rad)	
	9,486,000	1.356e9	1.356e9	
Elevation for applying acting force in X direction	30.48 m (above the CG)			
Maximum Offset in Surge	10% of Full Water Depth			
Equivalent Mooring Line Segment Properties	*L* (m)	*w* (N/m)	*AE* (N)	*Elements*
Platform Load Cell	4.19	51,130	1.635e11	1
Cable Segment	---	309.6	5.071e10	5
Spring Segment	---	---	---	40
Anchor Cable Segment	---	309.6	5.071e10	5
Basin Pit Dimension (Prototype Scale)	Water Depth (m)		Length (m)	Width (m)
	Minimum	Maximum		
	318.52	922.02	502.92	251.46
Equivalent SCR Segment Properties	*L* (m)	*w* (N/m)	*AE* (N)	*Elements*
Platform Load Cell	4.19	51,130	1.635e11	1
Spring Segment	---	---	---	40
Anchor Cable Segment	---	309.6	5.071e10	5

Table 3.28. Fairlead and porch coordinates and initial mooring line and riser heading, equivalent mooring and riser system.

Mooring Line/SCR	Fairlead location			Initial mooring line/SCR heading (deg)
	X' (m)	Y' (m)	Z' (m)	
1	-51.58	-5.46	-23.06	180
2	5.46	51.58	-23.06	90
3	51.58	5.46	-23.06	0
4	-5.46	-51.58	-23.06	270
SCR 1	-27.80	27.80	-23.29	137.9
SCR 2	27.80	-27.80	-23.29	315.5

Table 3.29. Fitness function weight factors per each case considered, equivalent mooring and riser system.

Static Response	Fitness Function Weight Factors	
	Equivalent Mooring System	Equivalent Riser System
Restoring Force	1	1
Sway	600	600
Heave	1,500	5,000
Roll	15,000	17,000
Pitch	10,000	15,000
Yaw	15,000	23,000

The results for the prototype, for the equivalent mooring with the prototype SCRs attached, and for the equivalent mooring and equivalent riser systems are presented in Figure 3.38, Figure 3.39, Figure 3.40, Figure 3.41, Figure 3.42 and Figure 3.43, compare the restoring force, sway, setdown, roll, pitch and yaw response curves, respectively.

The anchor coordinates for the best design are provided in Table 3.30. Table 3.31 lists the properties for each equivalent mooring line/SCR segment for the best fitness function solution. The design parameters are highlighted in green. The best design for the equivalent SCRs has the anchor points located at different depths in the basin pit. Note that the maximum available scaled depth in the pit is 922 m and the anchor points for the mooring lines are on the basin main floor at 319 m depth. As expected, the equivalent risers are almost vertical and they are very soft; each riser has a spring with unstretched length that is about 4 to 7 times longer than the cable segment.

Table 3.30. Fairlead/porch and anchor coordinates, equivalent mooring and riser system.

Case	Mooring Line/SCR	Fairlead/porch location			Anchor location		
		X' (m)	Y' (m)	Z' (m)	X (m)	Y (m)	Z (m)
Mooring Line	1	-51.58	-5.46	-23.06	-576.35	6.02	-319.35
	2	5.46	51.58	-23.06	-20.63	564.82	-319.35
	3	51.58	5.46	-23.06	552.36	-8.33	-319.35
	4	-5.46	-51.58	-23.06	-11.90	-561.53	-319.35
SCR	1	-27.80	27.80	-23.29	-111.00	118.25	-770.06
	2	27.80	-27.80	-23.29	149.76	-105.61	-591.31

Figure 3.38 compares the horizontal restoring force curves. For both solution designs, there is an acceptable correlation with the prototype response; the absolute percentage error for the equivalent designs and the prototype for large offsets are: 11.9% for the equivalent mooring system with the full depth prototype SCRs (Trunc Moor + Prot SCR) and 8.5% for the equivalent mooring and riser system (Trunc Moor + Trunc SCR).

Table 3.31. Mooring line/SCR properties for best fitness function solutions.

Case	Segment	Value			
		L **(m)**	***w*** **(N/m)**	***AE*** **(N)**	***Elements***
Mooring Line 1	Platform Load Cell	4.19	51,130	1.635e11	1
	Cable Segment	87.90	309.6	5.071e10	5
	Spring Segment	321.38	6,503	3.573e07	40
	Anchor Cable Segment	167.05	309.6	5.071e10	5
Mooring Line 2	Platform Load Cell	4.19	51,130	1.635e11	1
	Cable Segment	89.96	309.6	5.071e10	5
	Spring Segment	177.34	4,243	7.069e06	40
	Anchor Cable Segment	169.80	309.6	5.071e10	5
Mooring Line 3	Platform Load Cell	4.19	51,130	1.635e11	1
	Cable Segment	85.87	309.6	5.071e10	5
	Spring Segment	172.78	20,810	1.095e08	40
	Anchor Cable Segment	319.77	309.6	5.071e10	5
Mooring Line 4	Platform Load Cell	4.19	51,130	1.635e11	1
	Cable Segment	238.49	309.6	5.071e10	5
	Spring Segment	174.25	20,810	1.095e08	40
	Anchor Cable Segment	167.67	309.6	5.071e10	5
SCR 1	Platform Load Cell	4.19	51,130	1.635e11	1
	Spring Segment	489.96	13,500	4.713e07	40
	Anchor Cable Segment	111.18	309.6	5.071e10	5
SCR 2	Platform Load Cell	4.19	51,130	1.635e11	1
	Spring Segment	490.28	39,550	3.793e07	40
	Anchor Cable Segment	72.47	309.6	5.071e10	5

Figure 3.39 compares the sway static offset curves. The correlation with the prototype is acceptable; the largest deviation in sway between the prototype and the equivalent mooring and riser system is about 1.5 m. In general, the design of the equivalent SCR system improved the sway response when compared with the design of the mooring system with the full depth prototype SCRs attached.

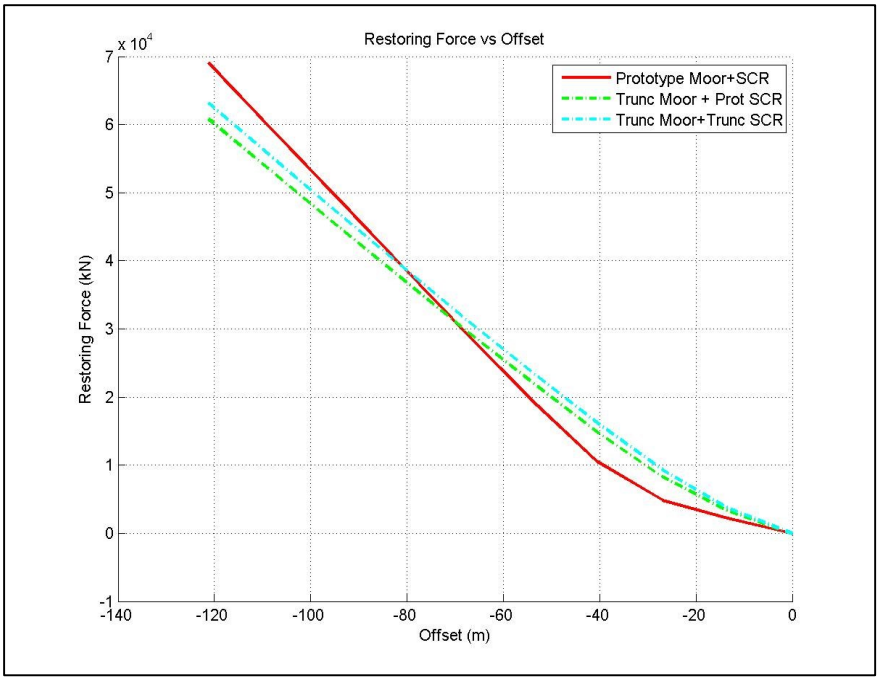

Figure 3.38. Restoring force vs offset plot, semisubmersible mooring/riser system.

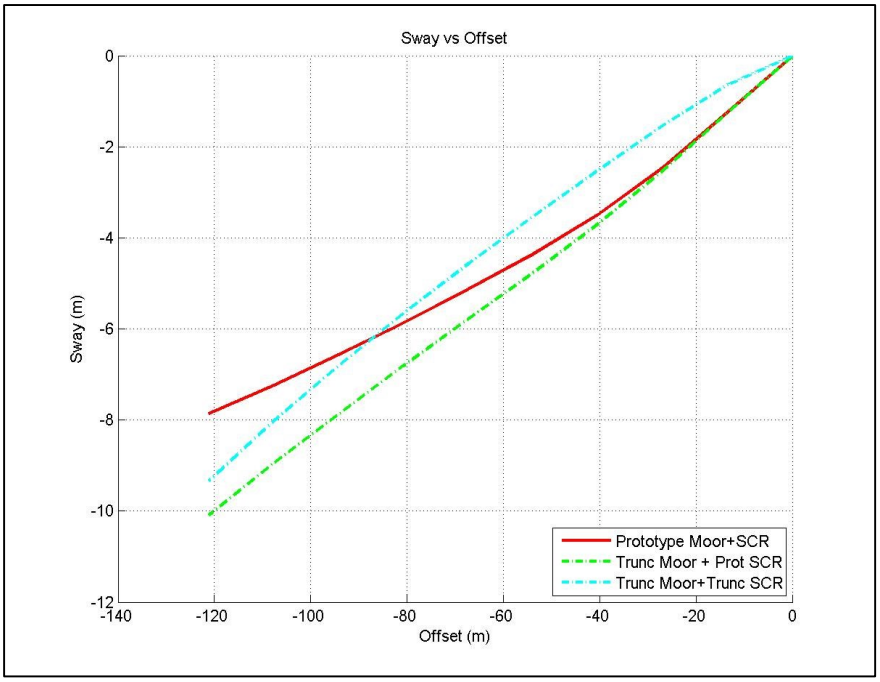

Figure 3.39. Sway vs offset plot, semisubmersible mooring/riser system.

Figure 3.40 compares the setdown curves. Here the correlation with the prototype is acceptable. The largest deviation in setdown between the prototype and the equivalent mooring and riser system design is about 0.6 m. The setdown responses for the equivalent mooring system with the prototype SCR and the equivalent mooring and riser system are almost the same.

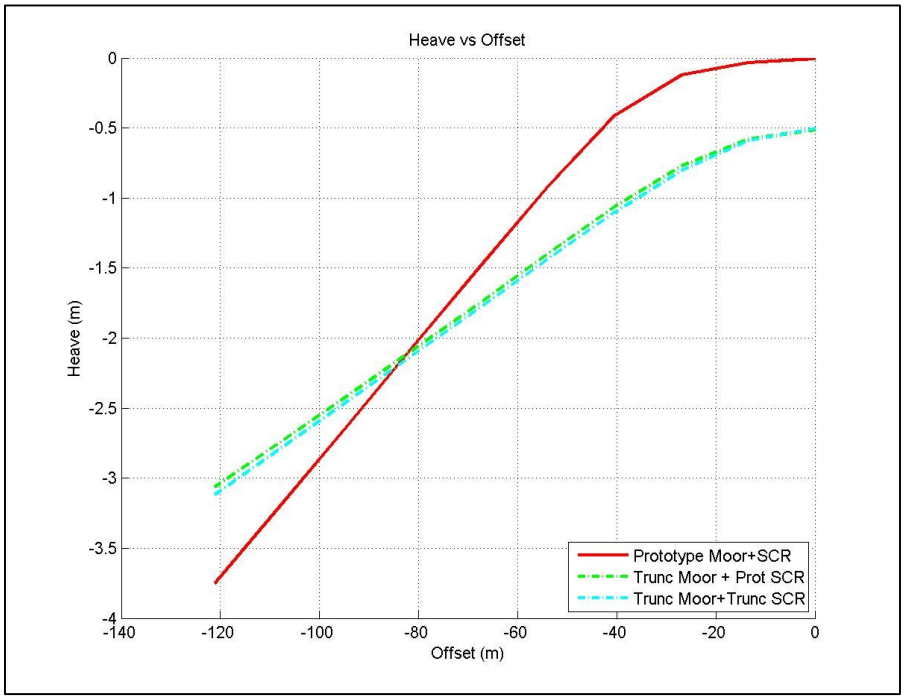

Figure 3.40. Setdown vs offset plot, semisubmersible mooring/riser system.

Figure 3.41 compares the roll static offset curves. Here again the correlation with the prototype is quite acceptable. The largest deviation in roll between the prototype and the equivalent mooring and riser design is about 0.6 degrees. The roll response for the

equivalent mooring system with the prototype SCRs is improved with the design of the equivalent SCR system.

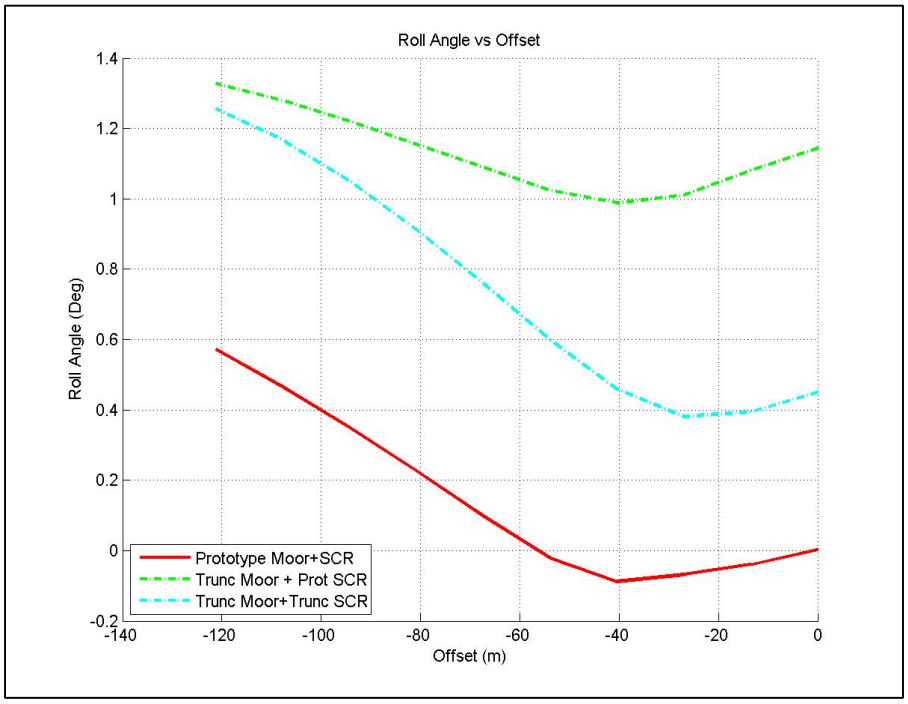

Figure 3.41. Roll vs offset plot, semisubmersible mooring/riser system.

Figure 3.42 compares the pitch static offset curves. There is an acceptable correlation between the prototype and the equivalent mooring and riser system. The largest deviation in pitch between the prototype and the equivalent mooring and riser system designs is about 2 degrees. The pitch responses for the design of the equivalent mooring system with the prototype SCRs attached and the equivalent mooring and riser system are almost equal for large offsets, but close to the calm water position the maximum deviation is around 2 degrees between those two responses.

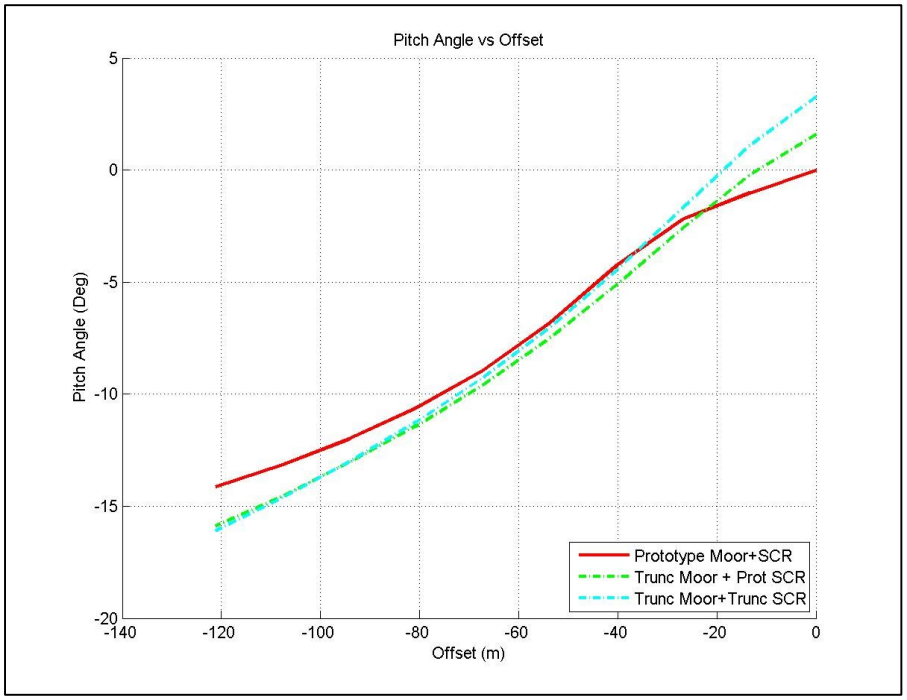

Figure 3.42. Pitch vs offset plot, semisubmersible mooring/riser system.

Finally Figure 3.43 compares the yaw static offset curves. There is a very good correlation between the prototype and the equivalent mooring and riser system. The largest deviation in yaw between the prototype and the equivalent mooring and riser system design is about 0.8 degrees at the calm water equilibrium position, and the response is closer to the prototype at large offsets. The yaw rotation response for the design of the equivalent mooring system with the prototype SCRs attached is improved with the design of the equivalent SCR system.

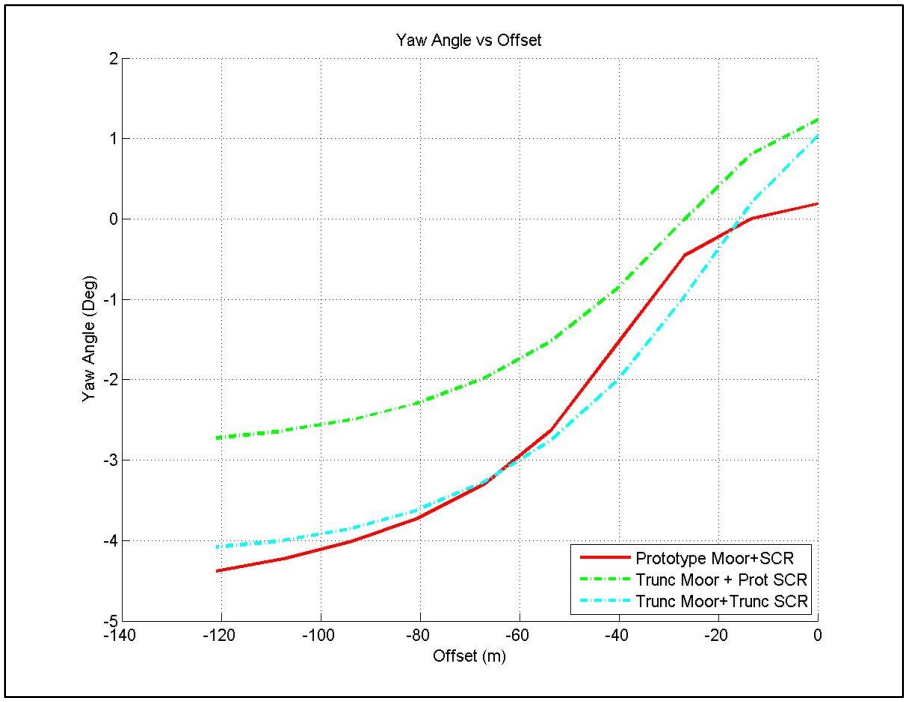

Figure 3.43. Yaw vs offset plot, semisubmersible mooring/riser system.

Table 3.32 is a summary of the main Genetic Algorithm process characteristics for the solutions for the equivalent mooring system with prototype SCRs attached and for the equivalent mooring and riser system. The computing time is based on a parallel computing implementation of the Genetic Algorithm program on a laptop using eight processors. The responses for the equivalent mooring and riser system are sufficiently close to the prototype responses that we consider this design solution to be acceptable for reproducing the floater's static response for the offset range from the calm water equilibrium position to a maximum offset of 10% of the water depth. As it is shown, the weighting factors used for the design of the equivalent mooring system with the full depth prototype SCRs attached to the floater are different than those used for the design of the equivalent SCR

system with the equivalent mooring system attached. Comparing the overall response for the equivalent mooring system with the prototype SCRs and the equivalent mooring and riser system, the response is improved with the design of the equivalent SCRs.

Table 3.32. Summary results equivalent mooring and riser system, semisubmersible.

CONCEPT	VALUE	
Case	Trunc Moor + Prot SCR	Trunc Moor + Trunc SCR
Design Parameters	24	14
Individuals	480	320
Generations	30	30
Comp. Time (hrs)*	22.32	15.19
Fitness Function Weighting Factors		
Restoring Force	1	1
Sway	600	600
Setdown	1,500	5,000
Roll	15,000	17,000
Pitch	10,000	15,000
Yaw	15,000	23,000
Root Mean Square Error		
Rest. Force (kN)	4,042	3,632
Sway (m)	1.05	0.78
Setdown (m)	0.49	0.50
Roll (deg)	0.99	0.60
Pitch (deg)	1.09	1.51
Yaw (deg)	1.23	0.38
Fit. Func. Value	6181	7303

* Using parallel computing with 8 processors

3.3.4 Spar with SCRs Attached

The fourth and last study case to validate the procedure for the optimized design of the statically equivalent mooring and steel catenary riser system is a spar with a polyester mooring system and two SCRs attached. The mooring system is symmetric with a total of 9 mooring lines arranged in 3 groups of 3 lines and there are two SCRs attached to the spar (Figure 3.44). For this case the environment (testing) heading will be in the minus X axis direction, as is illustrated in Figure 3.44.

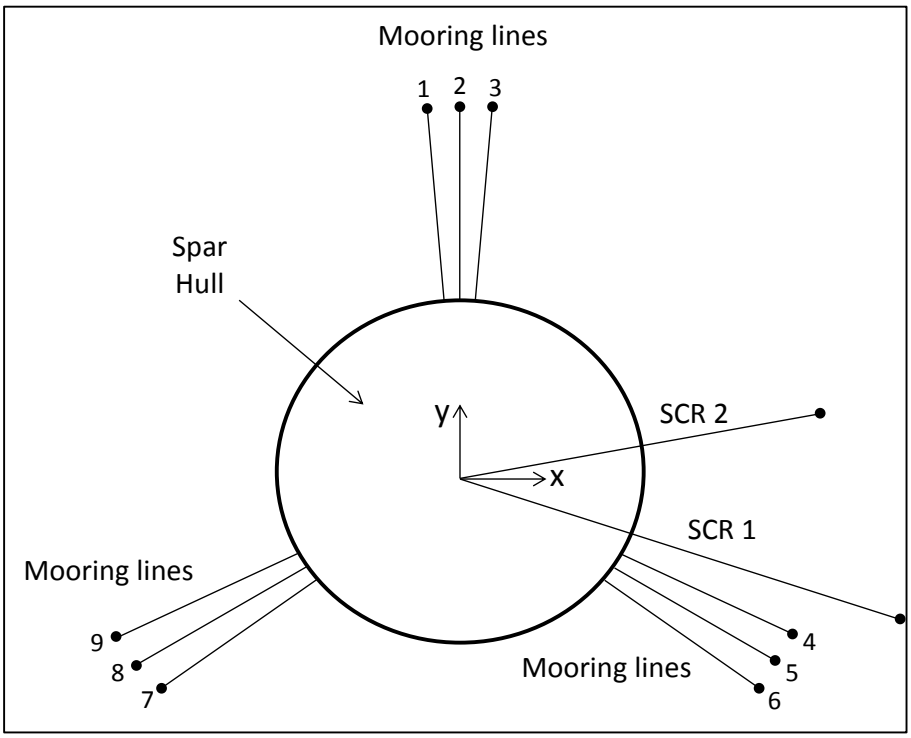

Figure 3.44. Spar mooring and riser system configuration, prototype.

The equivalent mooring system design will have 3 mooring lines with the same fairlead elevation as the prototype and those will be located (X-Y plane) at the same

position as the middle prototype mooring line in each group (mooring lines 2, 5 and 8 in Figure 3.44). The initial anchor headings are the same as those for the middle prototype mooring lines in each group. The equivalent riser system design will consider one SCR; the porch location is the same as that for riser SCR 1 in the prototype, and the initial heading for this equivalent riser is the heading of SCR 1 in the prototype.

Table 3.33. Spar and mooring and riser system characteristics, prototype.

Property	Value			
Water Depth (m)	1,219			
Spar hydrostatic stiffness	Heave, K_z (N/m)	Roll, K_r (N m/rad)	Pitch, K_p (N m/rad)	
	7,336,000	4.259e8	4.259e8	
Elevation for applying acting force in X direction	82.30 m (above the CG)			
Number of Mooring Lines	9			
Number of Segments per Mooring Line	2			
Mooring Segments Properties	*L* (m)	*w* (N/m)	*AE* (N)	*Elements*
Platform Chain	121.9	2,798	1.112e9	12
Polyester	1,475.2	76.47	1.779e8	148
Anchor Chain	152.4	2,798	1.112e9	15
Number of SCRs	2			
Number of Segments per SCR	1			
SCR Properties	*L* (m)	*w* (N/m)	*AE* (N)	*Elements*
SCR 1	1,981.2	2,381	8.896e9	198
SCR 2	1,981.2	2,477	8.896e6	198

The spar hydrostatic stiffness characteristics and the mooring and riser system properties are presented in. In the prototype, all the mooring lines have three segments which are: platform chain, polyester rope and anchor chain; and the SCRs have only one

segment. The anchor chain and platform chain have the same mechanical properties. The prototype fairlead/porch and anchor location coordinates for each mooring line and SCR are shown in. The fairleads and porches coordinates are referenced to the vessel's fixed coordinate system that in this case is the vessel's center of gravity (CG) which is located at the center of the platform (in the X-Y plane) and 82.296m below the sea water level (SWL).

Table 3.34. Fairlead and anchor coordinates, spar prototype mooring and SCRs.

Mooring Line/SCR	Fairlead location			Anchor location		
	X' (m)	Y' (m)	Z' (m)	X (m)	Y (m)	Z (m)
1	-1.33	15.18	54.86	-114.8	1,312	1,219
2	0.00	15.24	54.86	0.000	1,317	1,219
3	1.33	15.18	54.86	114.8	1,312	1,219
4	13.81	-6.44	54.86	1,187	-553.6	1,219
5	13.20	-7.62	54.86	1,13	-655.0	1,219
6	12.48	-8.74	54.86	1,073	-751.4	1,219
7	-12.48	-8.74	54.86	-1,081	-757.0	1,219
8	-13.20	-7.62	54.86	-1,143	-660.0	1,219
9	-13.81	-6.44	54.86	-1,196	-557.8	1,219
SCR 1	0.00	0.00	-67.06	1,304	-423.8	1,219
SCR 2	0.00	0.00	-67.06	1,350	238.2	1,219

Table 3.35 provides the fixed parameters for the equivalent mooring and riser system. The properties that are part of the solution in the GA procedure are highlighted in green.

Table 3.36 lists the coordinates of the fairlead and porch locations and the initial mooring line and riser headings with respect to the X axis.

Table 3.35. Spar equivalent mooring and riser system design characteristics.

Property	Value			
Scale Factor	1:60			
Truncation Factor	3.500			
Design Phase	Equi Moor + Prot SCR		Equi Moor + Equi SCR	
Number of individuals	480		240	
Number of generations	30		30	
Number of Equivalent Mooring Lines/SCR	3		1	
Number of Segments per Equivalent Mooring Line/SCR	4		3	
Anchor radius	Minimum (m)		Maximum (m)	
	305.9		914.4	
Spar hydrostatic stiffness	Heave, K_z (N/m)	Roll, K_r (N m/rad)	Pitch, K_p (N m/rad)	
	7,336,000	4.259e8	4.259e8	
Elevation for applying acting force in X direction	82.30 m (above the CG)			
Maximum Offset in Surge	6% of Full Water Depth			
Equivalent Mooring Line Segment Properties	*L* (m)	*w* (N/m)	*AE* (N)	*Elements*
Platform Load Cell	4.57	60,840	2.123e11	1
Cable Segment	---	368.4	6.584e10	5
Spring Segment	---	---	---	30
Anchor Cable Segment	---	368.4	6.584e10	5
Basin Pit Dimension (Prototype Scale)	Water Depth (m)		Length (m)	Width (m)
	Minimum	Maximum		
	265.18	923.54	548.64	274.32
Equivalent SCR Segment Properties	*L* (m)	*w* (N/m)	*AE* (N)	*Elements*
Platform Load Cell	4.57	60,840	2.123e11	1
Spring Segment	---	---	---	30
Anchor Cable Segment	---	368.4	6.584e10	5

For this study case, the equivalent mooring design was attempted using both the general solution scenario and the symmetric solution scenario, while the design of the

equivalent SCR system was performed using the specific GA procedure for SCR design. It is important to mention that several trials were used for the design of the equivalent mooring and riser system but here just the best solution is presented. The best solution for the design of the equivalent mooring system was one that used the symmetric solution scenario. Table 3.37 lists the values for the weighting factors applied to the fitness function for each one of the design phases considered.

Table 3.36. Spar fairlead/porch coordinates and initial mooring line/riser heading, equivalent mooring and riser system.

Mooring Line/SCR	Fairlead location			Initial mooring line/SCR heading (deg)
	X' (m)	Y' (m)	Z' (m)	
1	0.0	15.24	54.86	90
2	13.20	-7.62	54.86	330
3	-13.20	-7.62	54.86	210
SCR 1	0.0	0.0	-67.06	342

The results for the prototype, for the equivalent mooring with the prototype SCRs attached, and for the equivalent mooring and equivalent riser systems are presented in Figure 3.45, Figure 3.46, Figure 3.47, Figure 3.48, Figure 3.49 and Figure 3.50, comparing the restoring force, sway, setdown, roll, pitch and yaw response curves, respectively.

Table 3.37. Fitness function weight factors per each case considered, spar mooring/riser system.

Static Response	Fitness Function Weight Factors Considered	
	Equivalent Mooring System	Equivalent Riser System
Restoring Force	1	1
Sway	600	1,000
Heave	1,500	3,000
Roll	20,000	20,000
Pitch	10,000	15,000
Yaw	18,000	20,000

The fairlead/porch and anchor coordinates for the best solution design are provided in Table 3.38. Table 3.39 lists the properties for each equivalent mooring line/SCR segment for the best fitness function solution. The design parameters are highlighted in green. The best design of the equivalent SCR has the anchor point located in the basin pit.

Table 3.38. Fairlead/porch and anchor coordinates, spar equivalent mooring and riser system.

Case	Mooring Line/SCR	Fairlead location			Anchor location		
		X' (m)	Y' (m)	Z' (m)	X (m)	Y (m)	Z (m)
Mooring Line	1	1	0.0	15.24	54.86	-43.55	779.90
	2	2	13.20	-7.62	54.86	648.63	-418.98
	3	3	-13.20	-7.62	54.86	-645.52	-418.98
SCR	2	2	0.0	0.0	-67.06	54.49	-85.20

Table 3.39. Spar mooring line/SCR properties for best fitness function solutions.

Case	Segment	Value			
		L **(m)**	***w*** **(N/m)**	***AE*** **(N)**	***Elements***
Mooring Lines 1,2,3	Platform Load Cell	4.57	60,840	2.123e11	1
	Cable Segment	171.16	368.4	6.584e10	5
	Spring Segment	219.41	16,100	6.12e7	30
	Anchor Cable Segment	412.17	368.4	6.584e10	5
SCR 1	Platform Load Cell	4.57	60,840	2.123e11	1
	Spring Segment	374.23	4,080	1.78e7	30
	Anchor Cable Segment	94.80	368.4	6.584e10	5

Figure 3.45 compares the horizontal restoring force curves. There is a good correlation with the prototype response for both solution designs. The absolute percentage error for large offsets (greater than the mean offset value) between the equivalent designs and the prototype are: 7.0% for the equivalent mooring system with the prototype SCRs and 7.7% for the equivalent mooring and riser system.

Figure 3.46 compares the sway curves. The correlation with the prototype is acceptable. The largest deviation in sway between the prototype and the equivalent mooring and riser system is about 1m.

Figure 3.47 compares the setdown curves. Here the correlation with the prototype is good. The largest deviation in setdown between the prototype and the equivalent mooring and riser system design is about 0.3 m. The setdown responses for the equivalent mooring system with the prototype SCR and the equivalent mooring and riser system are almost the same.

Figure 3.48 compares the roll curves. The correlation of the equivalent designs with the prototype is acceptable. The largest deviation in roll between the prototype and the equivalent mooring and riser design is about 0.6 degrees.

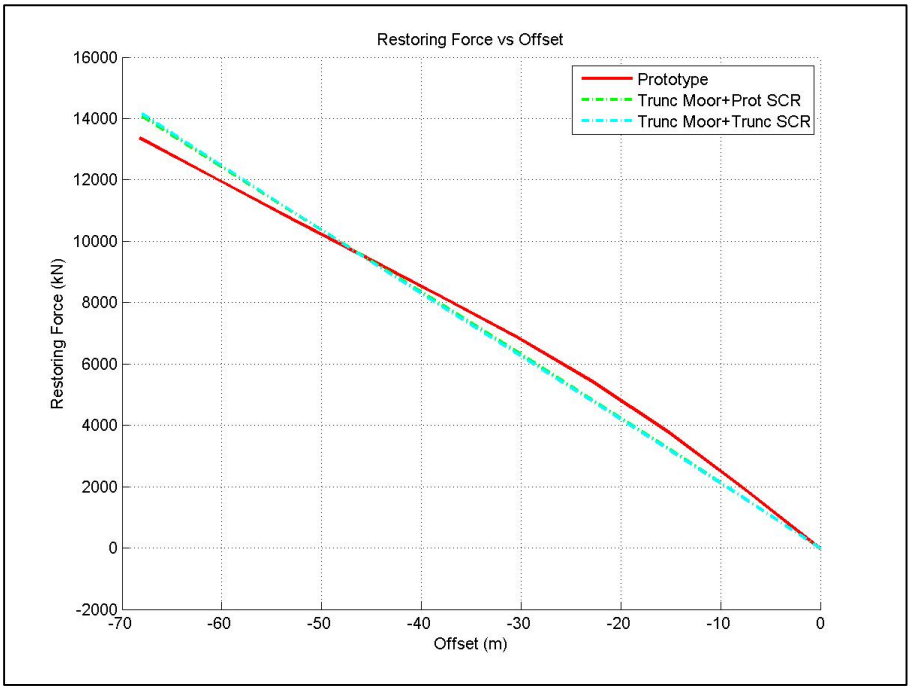

Figure 3.45. Restoring force vs offset plot, spar mooring/riser system.

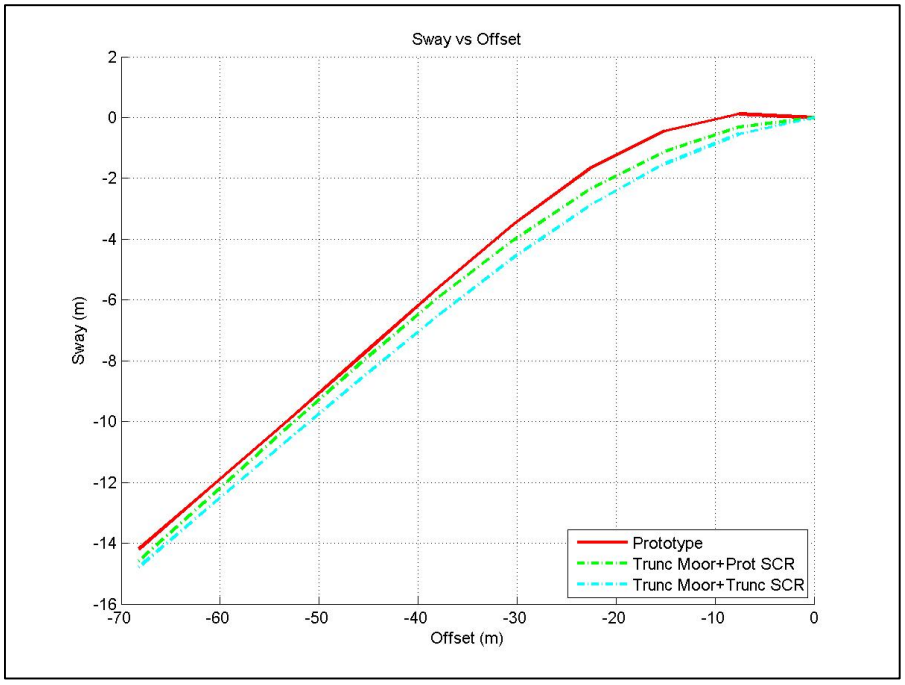

Figure 3.46. Sway vs offset plot, spar mooring/riser system.

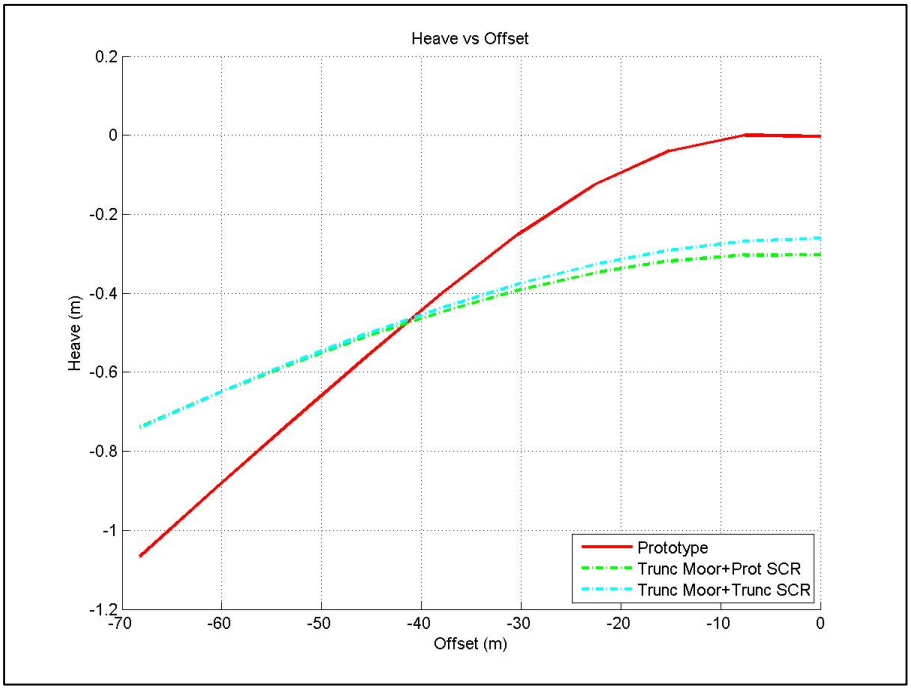

Figure 3.47. Setdown vs offset plot, spar mooring/riser system.

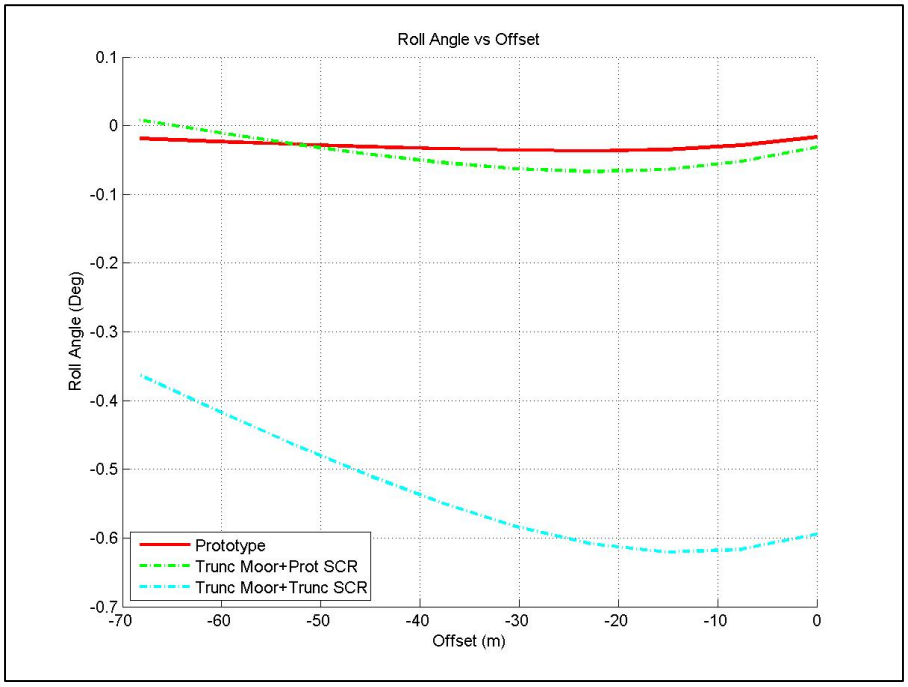

Figure 3.48. Roll vs offset plot, spar mooring/riser system.

Figure 3.49 compares the pitch curves. There is an acceptable correlation between the prototype and the equivalent mooring and riser system. The largest deviation in pitch between the prototype and the equivalent mooring and riser system designs is about 1 degree.

Figure 3.50 compares the yaw curves. There is very good correlation between the prototype and the equivalent mooring and riser system. The largest deviation in yaw between the prototype and the equivalent mooring and riser system design is about 1.5 degrees at the calm water equilibrium position, and the response is closer to the prototype at large offsets.

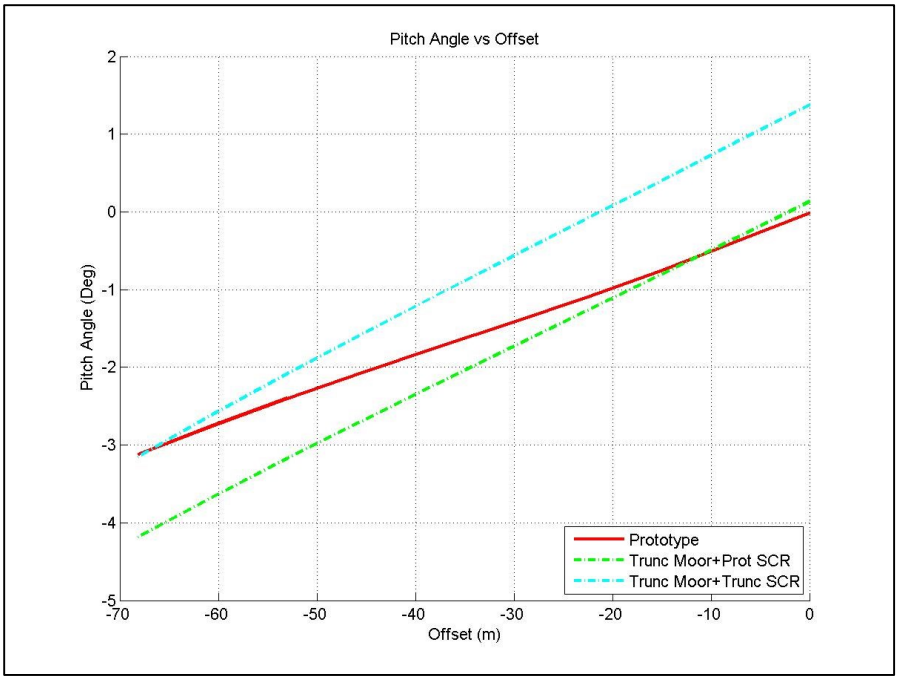

Figure 3.49. Pitch vs offset plot, spar mooring/riser system.

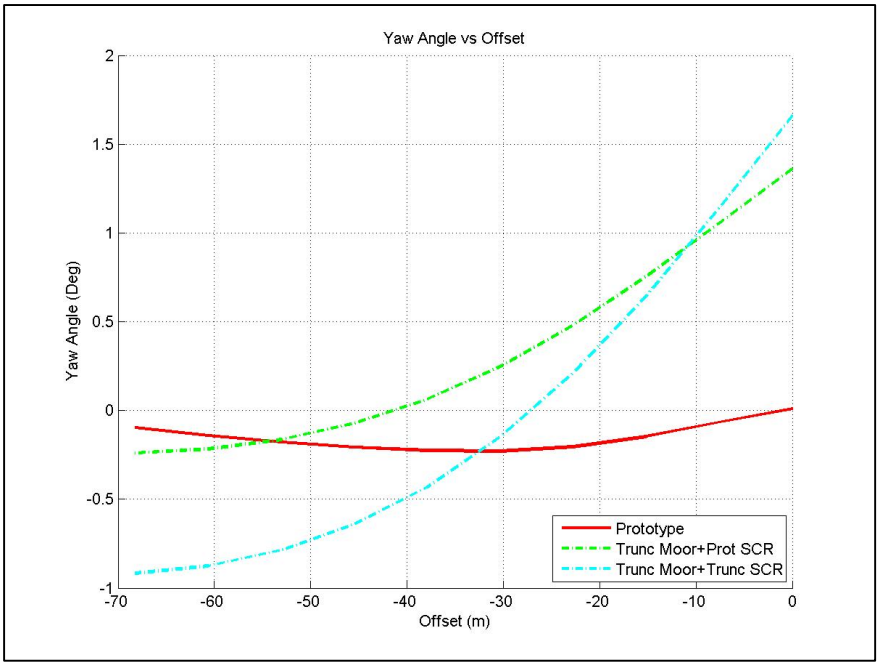

Figure 3.50. Yaw vs offset plot, spar mooring/riser system.

Table 3.40 is a summary of the GA process characteristics for the equivalent mooring system with the prototype SCRs and for the equivalent mooring and riser system. The computing time is based on a parallel computing implementation of the GA program using eight processors. The responses for the equivalent mooring and riser system is close enough to the prototype responses that we consider that this design solution is acceptable for offsets out to 6% of the water depth. As it is shown, the weighting factors used for the design of the equivalent mooring system with the full depth prototype SCR attached are different than the weighting factors used for the design of the equivalent SCR system with the equivalent mooring system attached.

Table 3.40. Summary results for spar equivalent mooring and riser system.

CONCEPT	VALUE	
Case	Trunc Moor + Prot SCR	Trunc Moor + Trunc SCR
Design Parameters	18	8
Individuals	480	240
Generations	30	30
Comp. Time (hrs)	17.71	7.00
Fitness Function Weighting Factors		
Restoring Force	1	1
Sway	600	1,000
Setdown	1,500	3,000
Roll	20,000	20,000
Pitch	10,000	15,000
Yaw	18,000	20,000
Root Mean Square Error		
Rest. Force (kN)	437.3	476.6
Sway (m)	0.427	0.824
Setdown (m)	0.228	0.211
Roll (deg)	0.0215	0.5102
Pitch (deg)	0.578	0.864
Yaw (deg)	0.688	0.826
Fit. Func. Value	1,360	2,627

4 ASSESSMENT OF DYNAMIC MOORING FORCES EXERTED ON FLOATER

The current practice in the design of equivalent mooring systems is only to seek static equivalence of net mooring system forces and moments imparted to the floater. The state of the art is to seek a design that matches the static offset performance of the prototype in all 6 rigid body degrees of freedom of the floater, as characterized by a set of static offset curves. As demonstrated in the previous chapter, this is already quite a challenging design problem, even when using a Genetic Algorithm to perform a thorough search of the design space in order to arrive at an optimum design. Having arrived at an optimum statically equivalent mooring design, it is of interest to assess the dynamic behavior of the equivalent system and compare it with that of the prototype mooring system.

Consistent with the design objective of seeking equivalence of net mooring system forces and moments imparted to the floater, the dynamic behavior that is of interest here is simply the net dynamic forces and moments obtained by summing the top tension contributions from all mooring lines. The nonlinear elastic restoring forces have already been well matched as a result of the statically equivalent design process, and these force contributions can be readily removed from the total dynamic forces, leaving behind forces and moments that contribute only inertia and damping to the motion response of the floater.

For this research only the net horizontal dynamic force in the surge direction imparted by the mooring to the floater is considered. Upon removing the elastic restoring force and decomposing the remainder into inertia and damping contributions, various procedures for examining these contributions are explored, for purposes of characterizing how the dynamic behavior of the equivalent mooring system differs from that of the prototype.

4.1 Methodology

The procedure developed to assess the inertia and damping forces exerted by the mooring system to the vessel involves using Orcaflex to perform dynamic forced vibration simulations for the prototype and equivalent mooring systems, specifically simulations where the vessel motion in the surge direction is prescribed and the vessel motion in the other 5 degrees of freedom is constrained to zero. This approach is chosen because the largest range of dynamic forces imparted by the mooring is in the horizontal direction. The procedures explored herein are general and can also be applied in the other modes of motion, but for this research only the surge mode is considered.

The horizontal displacement signals for the vessel are synthesized from prescribed spectra. Four surge displacement power spectra are used:

- three band limited white noise spectra:
    - the first one spans the slow drift frequency range,
    - the second spans the wave frequency range, and

    - the third spectrum is for the full range (slow drift and wave frequencies)
- a representative surge spectrum for a storm condition, where the spectral shape, frequency range, and energy levels in the slow drift and wave frequency bands are realistic.

The displacement power spectra are used to generate the surge motion time series about a specified mean offset position which the vessel is forced to undergo, in order to calculate the associated total horizontal force exerted by the mooring system in response to that forced motion. The procedure to assess and compare the inertia and damping forces exerted by the prototype and the static equivalent mooring systems is outlined in Figure 4.1.

In order to verify the robustness and effectiveness of the procedure developed, two study cases are considered. The two study cases considered correspond to the first two mooring system examples from Chapter III, namely a semisubmersible deployed in 2,200m water depth with a polyester mooring system and a semisubmersible deployed in 1,900m water depth with a steel wire mooring system.

For convenience and simplicity, the realistic surge spectrum is modeled analytically as the superposition of two spectra, each of JONSWAP spectral form. The JONSWAP spectrum is a 3-parameter spectrum developed and used to model wave elevation spectra, however its analytic form may be adapted to approximately represent either the slow drift surge spectrum or the wave frequency surge spectrum of a moored semisubmersible in deep water. The analytical form of the JONSWAP spectrum is (ITTC, 2002)

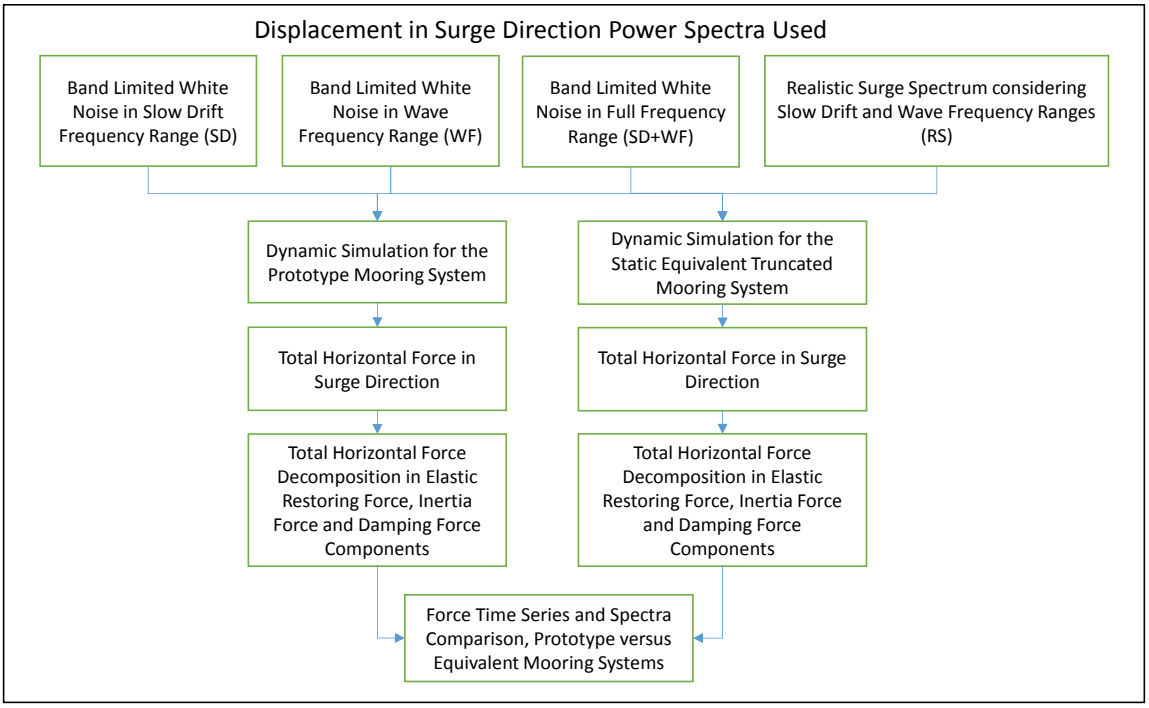

Figure 4.1. Flow chart for assessment of inertia and damping contributions.

$$S_{xx}(f) = 2\pi X_S \frac{f^{-5}}{{f_p}^{-4}} \exp\left[-\frac{5}{4}\left(\frac{f}{f_p}\right)^{-4}\right] \gamma^{\exp\left[\frac{(f-f_p)^2}{2\tau^2 {f_p}^2}\right]} \tag{4.1}$$

where:

$$\alpha^* = \frac{0.0624}{0.230 + 0.0336\gamma - 0.185(1.9+\gamma)^{-1}}$$

$\tau = 0.07, f \leq f_p$

$\tau = 0.09, f > f_p$

X_S = significant value of process X (i.e. surge motion in this case)

f_p = frequency associated with the maximum spectral density

$\gamma =$ spectral peakedness parameter

The values of the spectral parameters X_S, $T_p = 1/f_p$ and γ are provided in Table 4.1 for each one of the superposed spectra. Subscript 1 refers to the slow drift spectrum while subscript 2 refers to the wave frequency spectrum.

The main characteristics of the power spectra used to generate the surge motion time series are provided in Table 4.1.

Table 4.1. Surge power spectra used for the dynamic analysis.

Surge Motion Power Spectrum	Lower Frequency Limit (f_l)	Upper Frequency Limit (f_u)	Spectrum Main Characteristic
Band Limited White Noise for Slow Drift Motion (SD)	0.004 Hz	0.04 Hz	σ=1.524 m
Band Limited White Noise for Wave Frequency Motion (WF)	0.04 Hz	0.4 Hz	σ=1.524 m
Band Limited White Noise for Full Range Frequency Motion (SD+WF)	0.004 Hz	0.4 Hz	σ=2.1554 m
Realistic Spectrum (RS-P) for the polyester mooring system	0.001 Hz	1.0 Hz	γ_1=3.3; γ_2=1.0 X_{S1}=X_{S2}=9.144m T_{p1}=188.6792s and T_{p2}=15.5s
Realistic Spectrum (RS-S) for the steel mooring system	0.001 Hz	1.0 Hz	γ_1=3.3; γ_2=1.0 X_{S1}=X_{S2}=9.144m T_{p1}=238.0952s and T_{p2}=15.5s

The analytical model for the band-limited white noise spectrum is

$$S_{xx}(f) = \sigma^2/(f_u - f_l) \quad (4.2)$$

where:

$\sigma =$ standard deviation of process X

$f_u =$ upper frequency limit

$f_l =$ lower frequency limit

Given a set of equally-spaced frequencies with spacing Δf, the displacement amplitude at each frequency $A(f)$ can be obtained as:

$$A(f) = \sqrt{2\, S_{xx}(f)\, \Delta f} \tag{4.3}$$

Finally, the displacement time series can be calculated as a sum of sine series at any time, considering the displacement amplitude at each frequency and introducing a random phase angle (ϵ_f), as:

$$x(t) = \sum_{f=f_l}^{f_u} A(f) \sin(2\pi f t + \epsilon_f) \tag{4.4}$$

where:

$x(t) =$ displacement time series

$A(f) =$ displacement amplitude at each frequency f

$t =$ time

$\epsilon_f =$ random phase angle at each frequency f

The displacement time series, for each one of the power spectra considered, is calculated from 0.0 seconds up to 9999.5 seconds with a 0.5 second increment. In order to eliminate any transient response an initial ramp-up of duration 249.5 seconds was included in the Orcaflex dynamic simulations.

Figure 4.2 shows the displacement power spectra used to generate the displacement time series, in particular: a) band limited white noise for the Slow Drift (SD) frequency range; b) band limited white noise for the Wave (WF) frequency range; c) band limited white noise for the Full Range (SD+WF), which includes Slow Drift and Wave frequency ranges; d) realistic surge spectrum (RS-P) for the polyester mooring system; and e) realistic surge spectrum (RS-S) for the steel mooring system. The main characteristics of those displacement power spectra are defined in Table 4.1. The realistic surge spectra for the polyester and steel mooring systems have a different peak frequency for the slow drift partition, otherwise the other 5 JONSWAP parameters are identical. This difference reflects the fact that the horizontal stiffness of the steel mooring system is considerably less than that of the polyester mooring system, and this difference is reflected in the natural frequency of the slow drift motion.

Figure 4.3 shows the displacement time series used for the dynamic simulations in Orcaflex. The initial ramp-up period is not displayed as the simulation data in this period was not included in the analysis. In order to highlight the differences in the character of the time series considered, Figure 4.4 shows a snapshot of each one from 2000 seconds up to 2250 seconds.

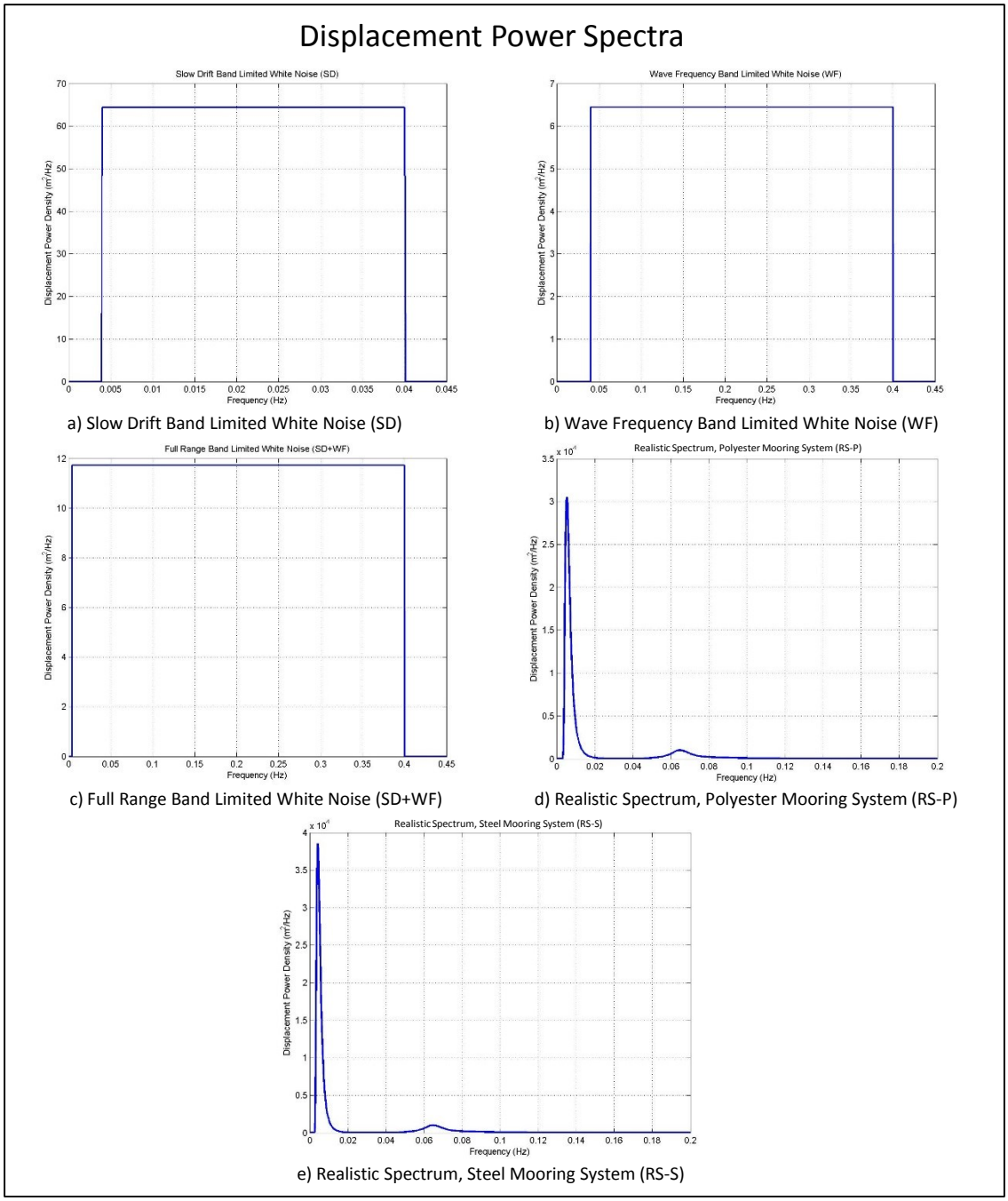

Figure 4.2. Displacement power spectra used to generate displacement time series for dynamic simulations in Orcaflex.

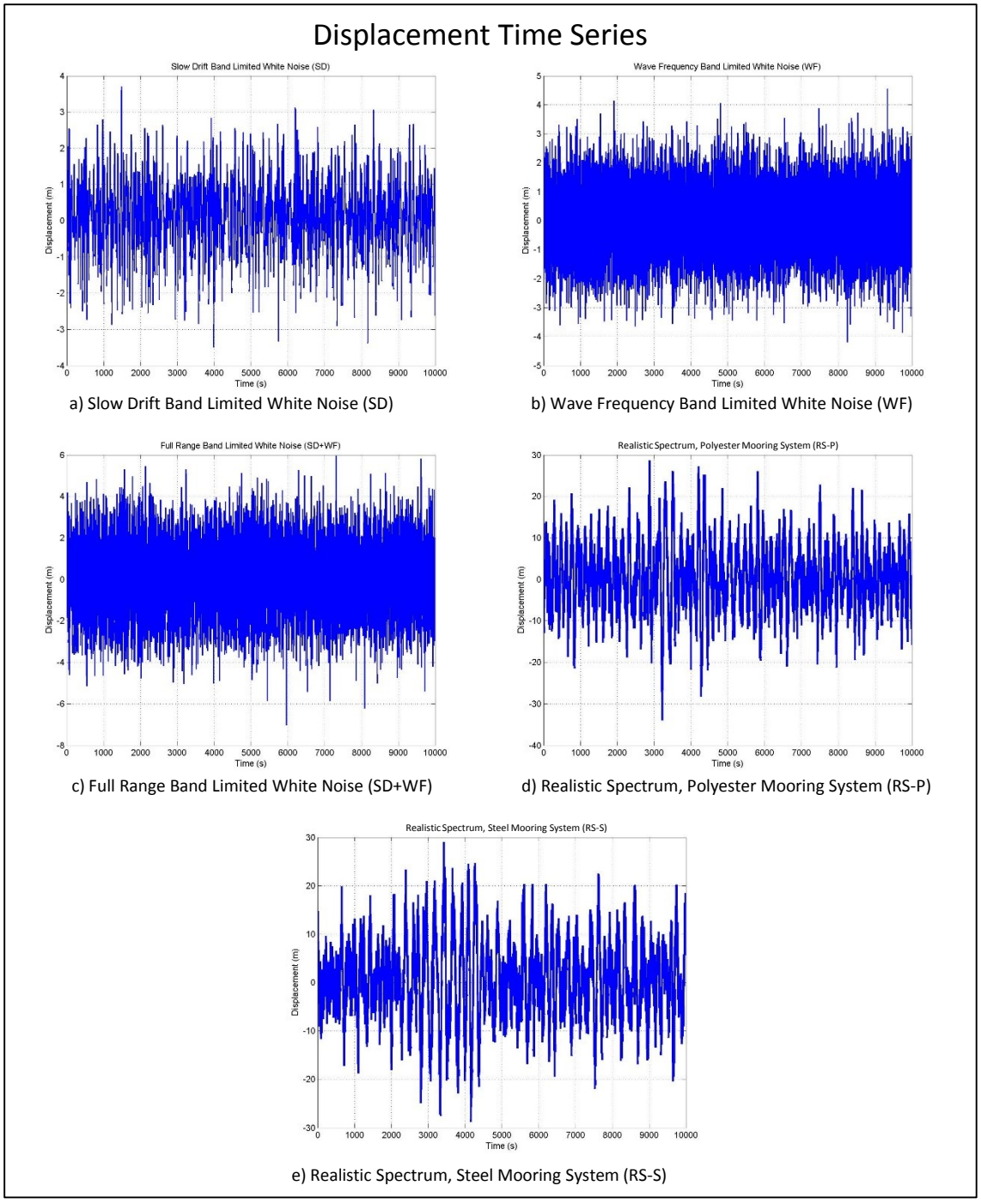

Figure 4.3. Displacement time series generated for the dynamic simulations.

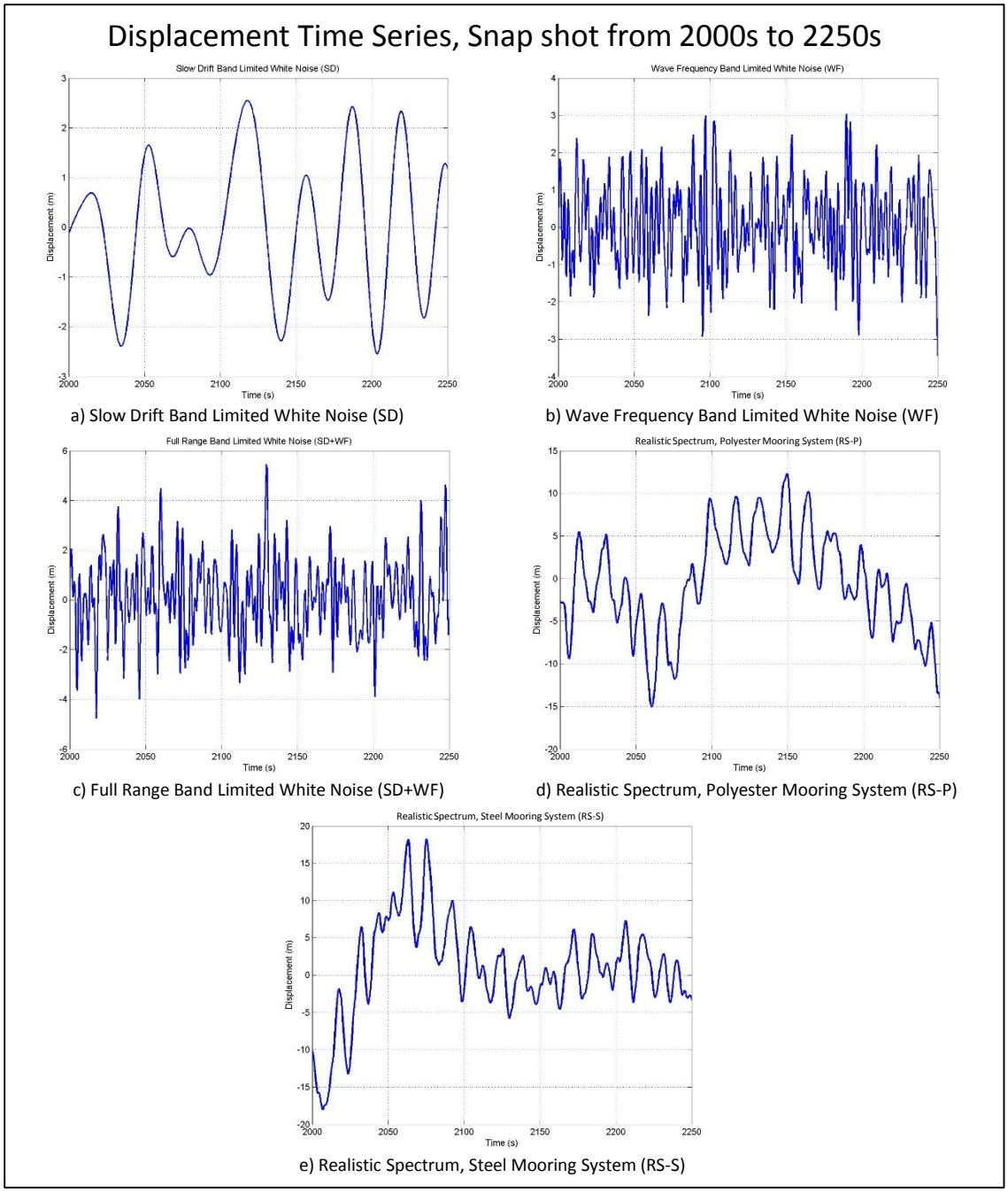

Figure 4.4. Displacement time series snapshot between 2,000 s and 2,250 s.

The time series calculated for the five displacement power spectra mentioned above were used to run dynamic simulations in Orcaflex for the prototype, equivalent symmetric and equivalent non-symmetric mooring systems. With the results obtained from those dynamic simulations the procedure described in the following section was applied to assess the mooring system inertia and damping force contributions to the floater, so that those contributions from the prototype and the equivalent mooring systems could be compared.

4.2 Force Decomposition

Considering the forced oscillation simulations where the input is the displacement time series for the vessel $x(t)$ and the output is the total top horizontal mooring force time series $f_h(t)$, the total mooring force imparted on the floater can be considered as the sum of three components: a nonlinear elastic mooring force component that is proportional to the vessel displacement, a damping force component that is proportional to the vessel velocity, and an inertia force component that is proportional to the vessel acceleration. This can be represented with the following equation:

$$f_h = M\ddot{x} + \beta\dot{x} + k(x)x \tag{4.5}$$

where,

$M = mooring\ system\ virtual\ mass\ contribution$

$\beta = mooring\ system\ damping\ contribution$

$k(x) = nonlinear\ mooring\ system\ stiffness$

$f_h = total\ horizontal\ mooring\ force\ in\ surge\ direction$

$x = induced\ horizontal\ displacement\ of\ floater\ in\ surge\ direction$

$\dot{x} = induced\ horizontal\ velocity\ of\ floater\ in\ surge\ direction$

$\ddot{x} = induced\ horizontal\ acceleration\ of\ floater\ in\ surge\ direction$

In Equation (4.5) the term *k(x)x* is the elastic restoring force (f_{spring}) exerted by the mooring system, so it is equal to the total mooring system restoring force at any location defined by the horizontal displacement *x*. The restoring force time series is calculated from the known displacement time series using an accurate polynomial approximation for the nonlinear static restoring force curve (f_{spring} vs *x*) obtained by exercising Orcaflex. Subtracting the restoring force contribution from the total force,

$$f_{dyn} = M\ddot{x} + \beta\dot{x} \tag{4.6}$$

where:

$f_{dyn} = f_h - f_{spring}$

$f_{spring} = k(x)x$

We will refer to f_{dyn} as the dynamic force, even though strictly speaking f_{spring} is also a dynamic force since the position *x* varies with time.

Assuming that *M* and β are time-invariant, equation (4.6) can be transformed from the time domain to the frequency domain according to

$$F_{dyn} = (M\omega^2 + i\beta\omega)\,X \tag{4.7}$$

where:

$\omega = 2\pi f;\ \omega\ is\ the\ circular\ frequency\ and\ f\ is\ the\ cyclic\ frequency$

$X = A_X + iB_X;\ \ X\ is\ complex\ valued\ for\ any\ frequency\ f$

$F_{dyn}\ = A_F + iB_F;\ F_{dyn}\ is\ complex\ valued\ for\ any\ frequency\ f$

In equation (4.7), let's refer to the frequency-dependent term ($-M\omega^2$) as the inertia factor (C_{iner}) and to the frequency-dependent term ($\beta\,\omega$) as the damping factor (C_{damp}). Using the Fourier coefficients for the displacement and the dynamic force, equation (4.7) can be rewritten as:

$$(C_{iner} + iC_{damp})(A_X + iB_X) = A_F + iB_F \tag{4.8}$$

Equation (4.8) can be re-written as:

$$\left(C_{iner} + iC_{damp}\right) = \frac{(A_F + iB_F)}{(A_X + iB_X)}$$

Multiplying and dividing with the denominator's complex conjugate, and expanding the multiplications,

$$\left(C_{iner} + iC_{damp}\right) = \frac{(A_F + iB_F)(A_X - iB_X)}{(A_X + iB_X)(A_X - iB_X)} = \frac{A_F A_X + iB_F A_X - iA_F B_X + B_F B_X}{\left({A_X}^2 + {B_X}^2\right)}$$

Grouping the real and imaginary parts,

$$\left(C_{iner} + iC_{damp}\right) = \frac{A_F A_X + B_F B_X}{\left({A_X}^2 + {B_X}^2\right)} + i\frac{B_F A_X - A_F B_X}{\left({A_X}^2 + {B_X}^2\right)} \tag{4.9}$$

From equation (4.9) the inertia and damping factors can be identified as:

$$C_{iner} = \frac{A_F A_X + B_F B_X}{\left({A_X}^2 + {B_X}^2\right)} \tag{4.10}$$

$$C_{damp} = \frac{B_F A_X - A_F B_X}{\left({A_X}^2 + {B_X}^2\right)} \tag{4.11}$$

Once the frequency-dependent inertia and damping factors have been calculated for the range of frequencies considered, the inertia and damping force contributions in the frequency domain are obtained using equation (4.8) by expanding the left hand side as

$$C_{iner}(A_X + iB_X) + C_{damp}(iA_X - B_X) = A_F + iB_F$$

So, the inertia force and damping force contributions at any frequency *f* in the frequency domain can be written as:

$$F_{iner} = C_{iner}(A_X + iB_X) \tag{4.12}$$

$$F_{damp} = C_{damp}(iA_X - B_X) \tag{4.13}$$

Transforming equations (4.12) and (4.13) from the frequency domain to the time domain, the inertia and damping force time series can be written as sums of sine and cosine series as

$$f_{iner} = \sum_f C_{iner}\,(A_X \cos(2\pi f t) - B_X \sin(2\pi f t)) \tag{4.14}$$

$$f_{damp} = \sum_f C_{damp}\,(-A_X \sin(2\pi f t) - B_X \cos(2\pi f t)) \tag{4.15}$$

The mooring forces f_{iner} and f_{damp} are orthogonal (90 degrees out of phase) with each other. The force f_{iner} is in phase with the acceleration of the vessel and therefore contributes to its inertia. The force f_{damp} is in phase with the velocity of the vessel and therefore contributes to its retardation (damping).

4.3 Results

Two study cases are considered to assess the mooring system inertia and damping contributions to the floater and demonstrate the effectiveness and robustness of the procedure developed. For each of the study cases the inertia and damping contributions for the prototype mooring and for one symmetric and one non-symmetric statically equivalent mooring system are considered. The study cases are those used to demonstrate the effectiveness and robustness of the Genetic Algorithm procedure developed for the optimized design of the statically equivalent mooring system, included in Chapter III, section 3.3.1 and section 3.3.2. The first case is a semisubmersible with a polyester mooring system deployed in 2,200 m water depth and the second case is a semisubmersible with a steel wire mooring system deployed in 1,900 m water depth.

4.3.1 Polyester Mooring System

The prototype, as it is described in Chapter III, section 3.3.1, is a semisubmersible with a polyester mooring system, with a configuration of four groups of four mooring lines, and this semisubmersible is deployed in 2,200m water depth. The statically equivalent mooring systems selected for the dynamic analysis are: PM-S-C3 for the symmetric mooring system and PM-N-C1 for the non-symmetric mooring system. The polyester mooring system prototype configuration is shown in Figure 3.9 in Chapter III, the prototype mooring line properties are included in Table 3.1, and the fairlead and anchor coordinates are included in Table 3.2. The main design characteristics for the equivalent mooring systems are included in Table 3.3. For the symmetric equivalent mooring system

PM-S-C3, the fairlead and anchor coordinates are listed in Table 3.6 and the mooring line characteristics are included in Table 3.7. For the non-symmetric equivalent mooring system PM-N-C1, the fairlead and anchor coordinates are provided in Table 3.8 and the mooring line properties are included in Table 3.9

The dynamic simulations in Orcaflex required additional data for each segment in the mooring system. The additional data for each segment are: equivalent outer diameter (OD), unit mass in air (m), drag coefficient (C_d) and added mass coefficient (C_m). The OD is set to a value that, in combination with the unit mass in air, results in the desired unit submerged weight. The values of these additional parameters used for the dynamic simulations are listed in Table 4.2.

Table 4.2. Polyester mooring system, additional data required for the dynamic simulations in Orcaflex.

Mooring System	Segment	Outer Diameter (m)	Mass per unit length (t/m)	Drag Coefficient (C_d)	Added Mass Coefficient (C_m)
Prototype	Platform chain	0.2970	0.5450	1.2	1.0
	Polyester rope	0.2150	0.0500	1.2	1.0
	Anchor chain	0.2970	0.5450	1.2	1.0
Symmetric equivalent, PM-S-C3	Load cell	0.8915	4.9480	1.2	1.0
	Cable segment	0.0804	0.0313	1.2	1.0
	Spring	0.6576	2.6654	1.2	1.0
Non-symmetric equivalent, PM-N-C1	Load cell	0.8915	4.9479	1.2	1.0
	Cable segments	0.0804	0.0313	1.2	1.0
	Upwind springs	0.9595	5.6214	1.2	1.0
	Downwind springs	0.7881	3.9535	1.2	1.0

Initially, the effect of the Morison added mass and damping coefficients was investigated. Three time domain simulations were executed for each one of the prototype, the symmetric equivalent (PM-S-C3) and the non-symmetric equivalent (PM-N-C1) mooring system using a realistic spectrum (RS-P) vessel forced motion. The differences in the mooring system models are:

A) the first model considers the added mass (C_m) and damping (C_d) coefficients for the mooring lines components, shown in Table 4.2;

B) the second model just considers the damping coefficient (C_d) for the mooring line components as shown in Table 4.2 (C_m is set to zero);

C) the third model just considers the added mass coefficient (C_m) for the mooring lines components as shown in Table 4.2 (C_d is set to zero).

Figure 4.5 compares for the prototype mooring system the total force (a), restoring force (b), and dynamic force (c) time series for a snapshot from 2000 seconds up to 2050 seconds, for the cases where the imposed vessel motion is a realistic spectrum (RS-P). For the total force (a) and dynamic force (c), the effect of just considering the mooring line drag (C_d) is similar to the effect of considering both the added mass and drag (C_m+C_d), while considering just the added mass (C_m) without the drag results in a large difference in the total and dynamic horizontal force exerted by the mooring system. As expected, the horizontal restoring force (b) is unaffected by whether added mass or drag effects are included.

For the same realistic spectrum vessel motion, Figure 4.6 shows the power spectrum for the prototype mooring system total force (a), restoring force (b), and dynamic

force (c), for the low frequency (LF) and high frequency (HF) ranges. As mentioned above, the effect of considering just the mooring line drag (C_d) is similar to the effect of including both the added mass and drag (C_m+C_d). Therefore based on these observations it is concluded that, for this study case, the prototype mooring system contribution to the dynamic force and, indeed, to the total force, is dominated by the mooring line drag coefficient (C_d). This behavior was initially observed by Huse *et al* (1988).

Comparing in Figure 4.6 just the response for the prototype mooring system using the C_d and C_m shown in Table 4.2, at low frequencies the total force exerted by the mooring system is dominated by the restoring force, while the inertia and damping force contributions are smaller than the restoring force. On the other hand, at wave frequencies, the dynamic force contribution exerted by the mooring system is the same order of magnitude as the restoring force, but the dynamic force contribution is larger than the mooring restoring force contribution.

Figure 4.7 and Figure 4.8 compare for the equivalent mooring systems PM-S-C3 and PM-N-C1, respectively, the total force (a), restoring force (b), and dynamic force (c) time series for a snapshot from 2000 seconds up to 2050 seconds, for the cases where the imposed vessel motion is a realistic spectrum (RS-P). As for the prototype response, in the total force (a) and dynamic force (c), the effect of just considering the mooring line drag (C_d) is similar to the effect of considering both the added mass and drag (C_m+C_d), while considering just the added mass (C_m) without the drag results in a large difference in the total and dynamic horizontal force exerted by the mooring system.

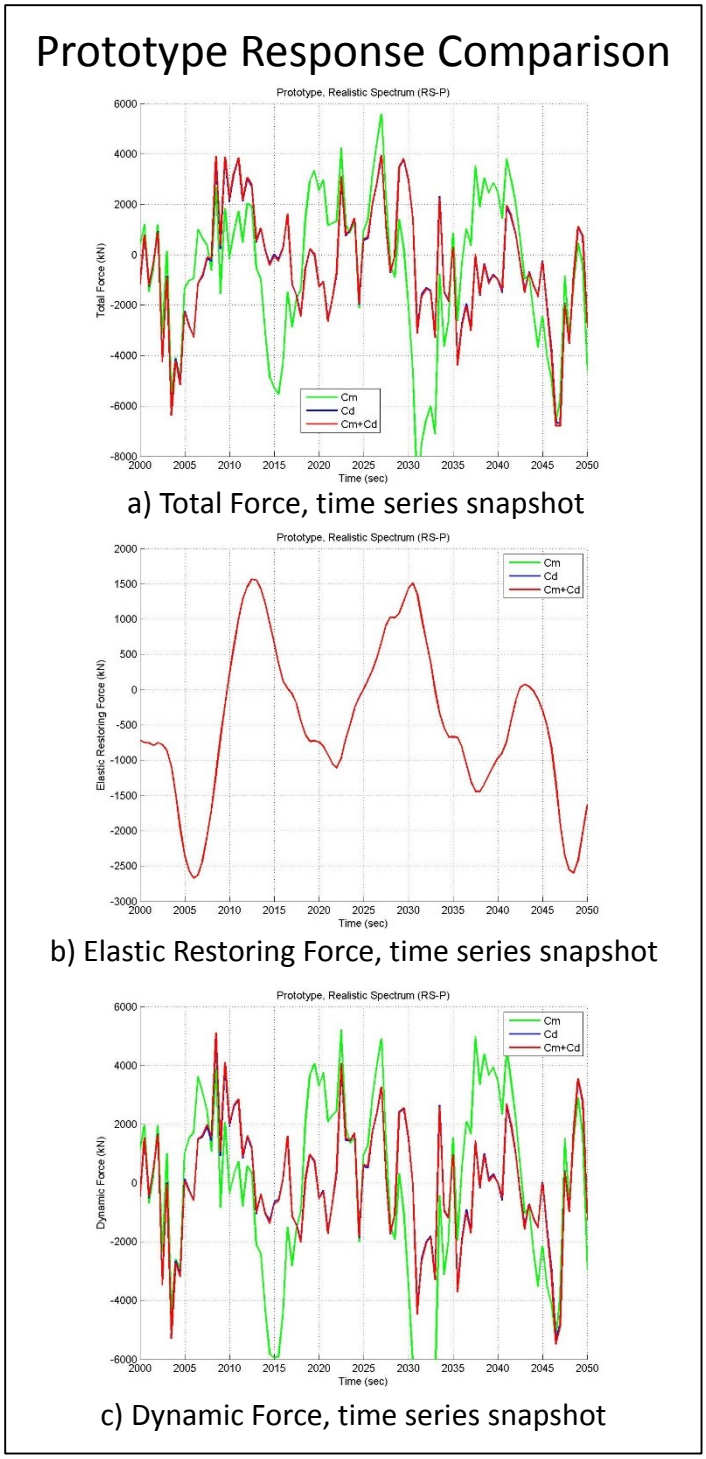

Figure 4.5. Prototype response comparison, force time series snapshot, polyester mooring system.

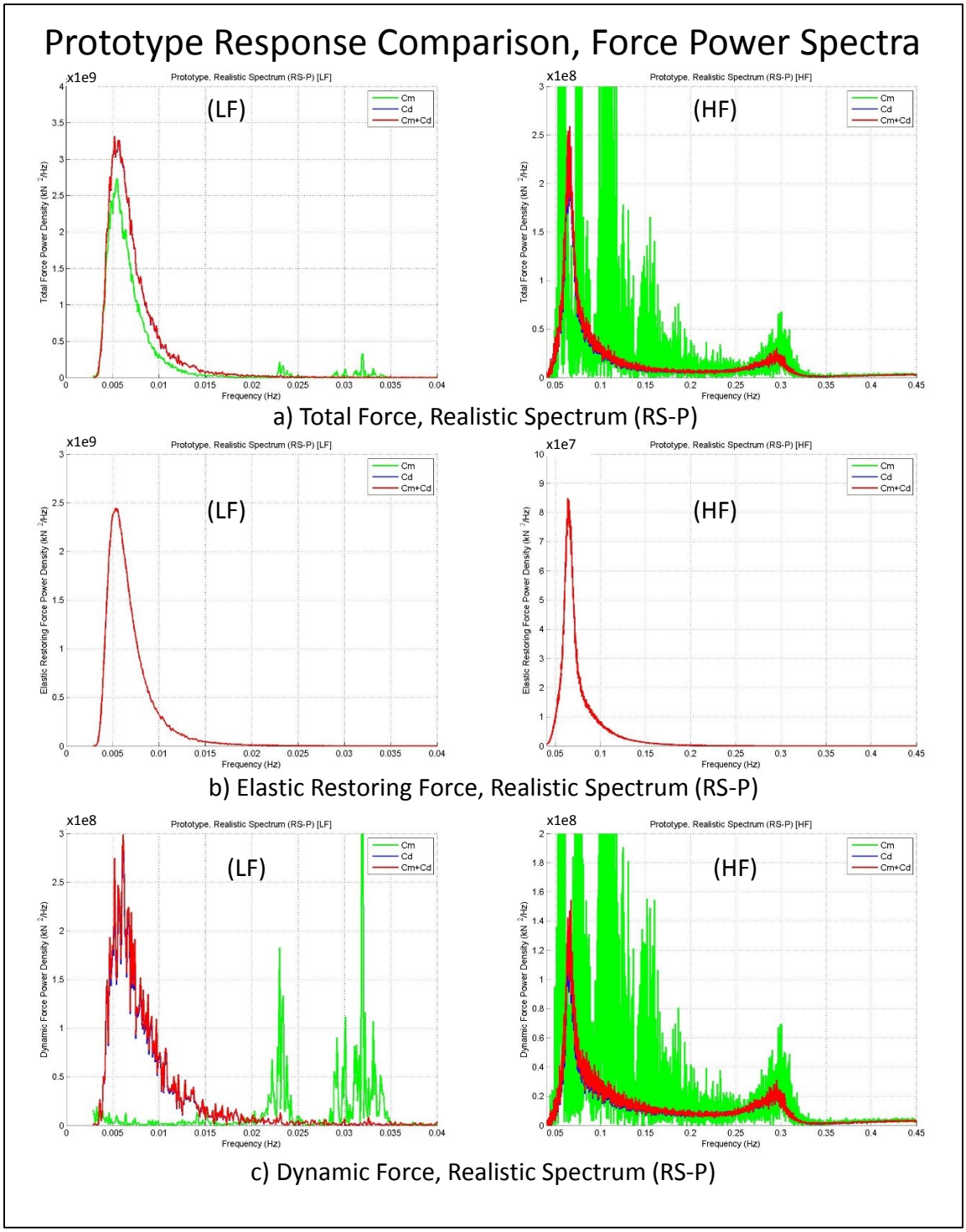

Figure 4.6. Prototype response comparison, force power spectra, low frequency (LF) and high frequency (HF) ranges, polyester mooring system.

Figure 4.9 and Figure 4.10 show for the equivalent mooring system PM-S-C3 and PM-N-C1, respectively, the power spectrum of the total force (a), restoring force (b), and dynamic force (c), for the low frequency (LF) and high frequency (HF) ranges. As for the prototype response, the effect of considering just the mooring line drag (C_d) is similar to the effect of including both the added mass and drag (C_m+C_d). Therefore, as for the prototype response, based on these observations for this study case, it is evident that the equivalent mooring system contribution to the dynamic force and, indeed, to the total force is also dominated by the mooring line drag coefficient (C_d). Considering the equivalent mooring system responses using C_d and C_m shown in Table 4.2, at low frequencies the restoring force is the main component of the total force, while the dynamic force contribution is three orders of magnitude smaller than the restoring force exerted by the mooring system. For the wave frequency range, the dynamic force is the same order of magnitude as the mooring restoring force, but the mooring restoring force contribution is smaller (at rms level) than the dynamic force contribution.

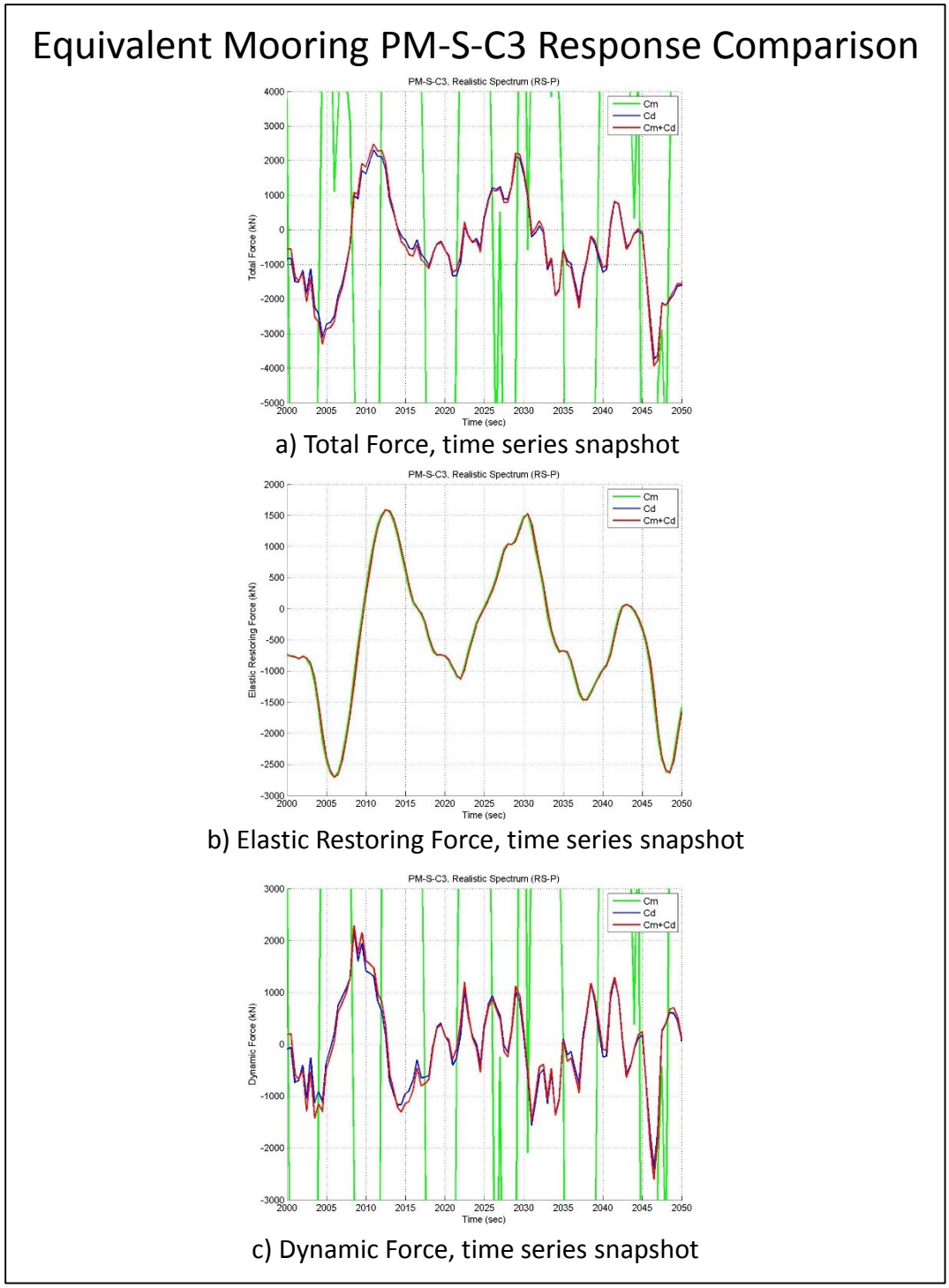

Figure 4.7. Equivalent mooring system (PM-S-C3) response comparison, force time series snapshot.

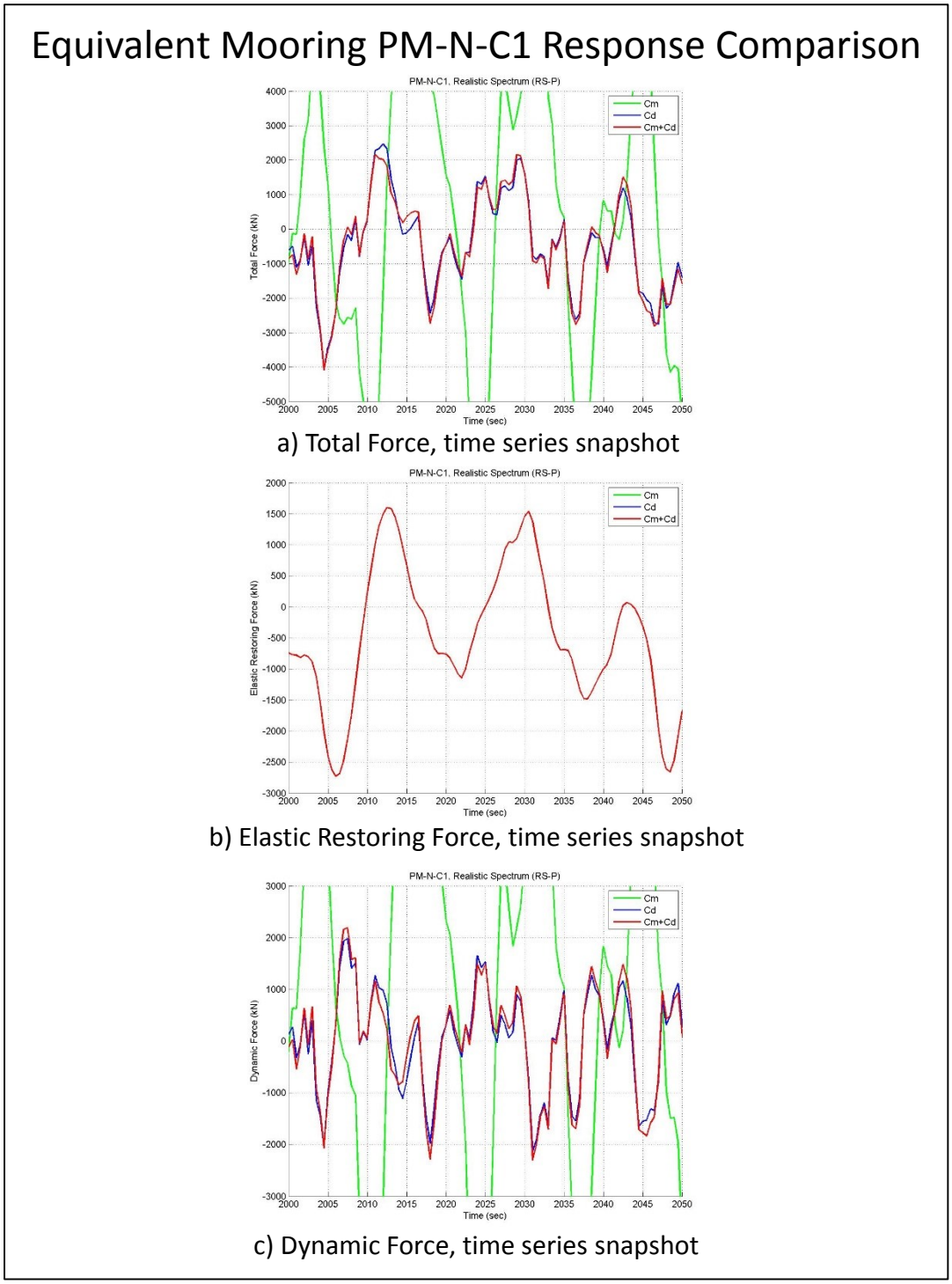

Figure 4.8. Equivalent mooring system (PM-N-C1) response comparison, force time series snapshot.

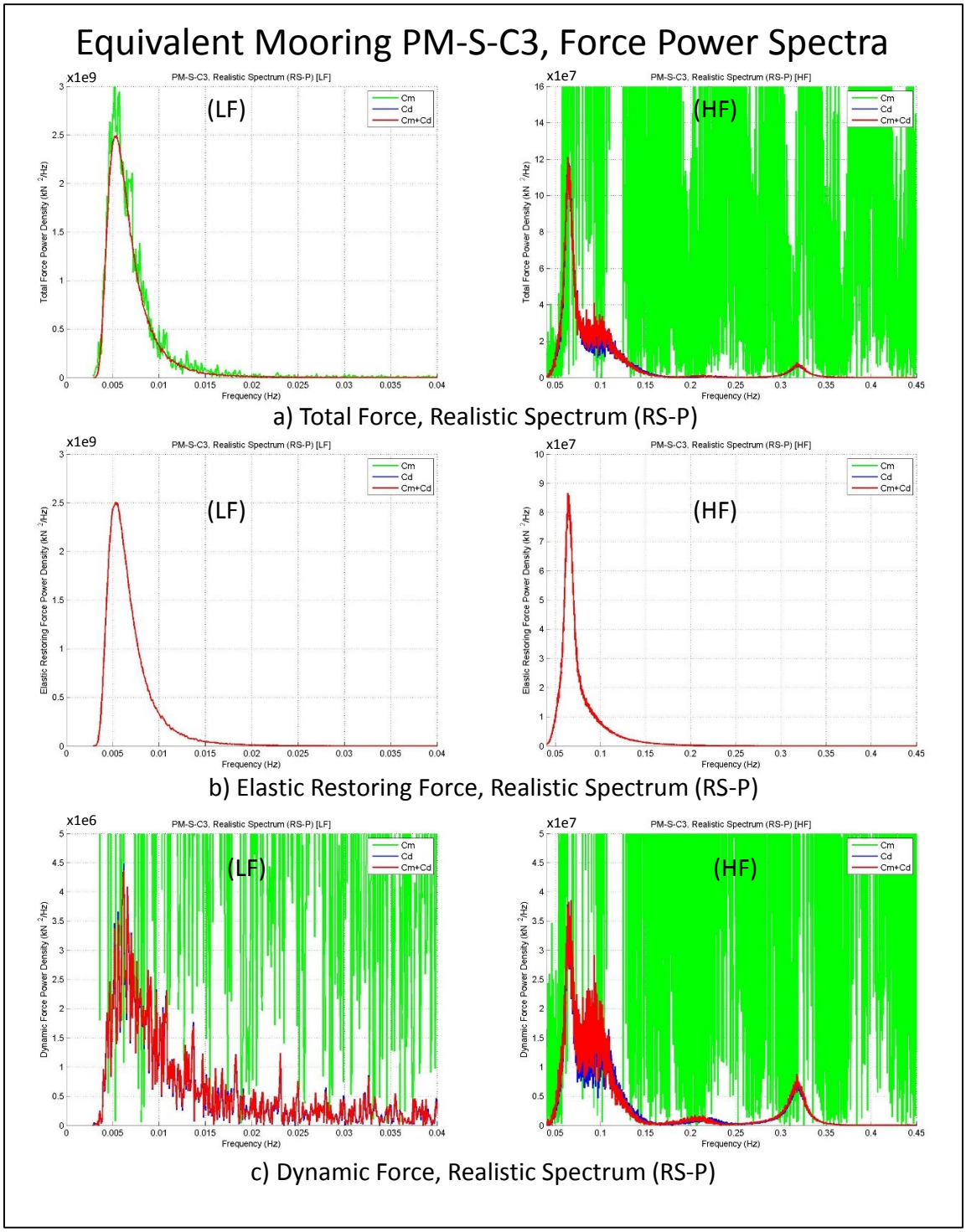

Figure 4.9. Equivalent mooring system (PM-S-C3) response comparison, force power spectra, low frequency (LF) and high frequency (HF) ranges.

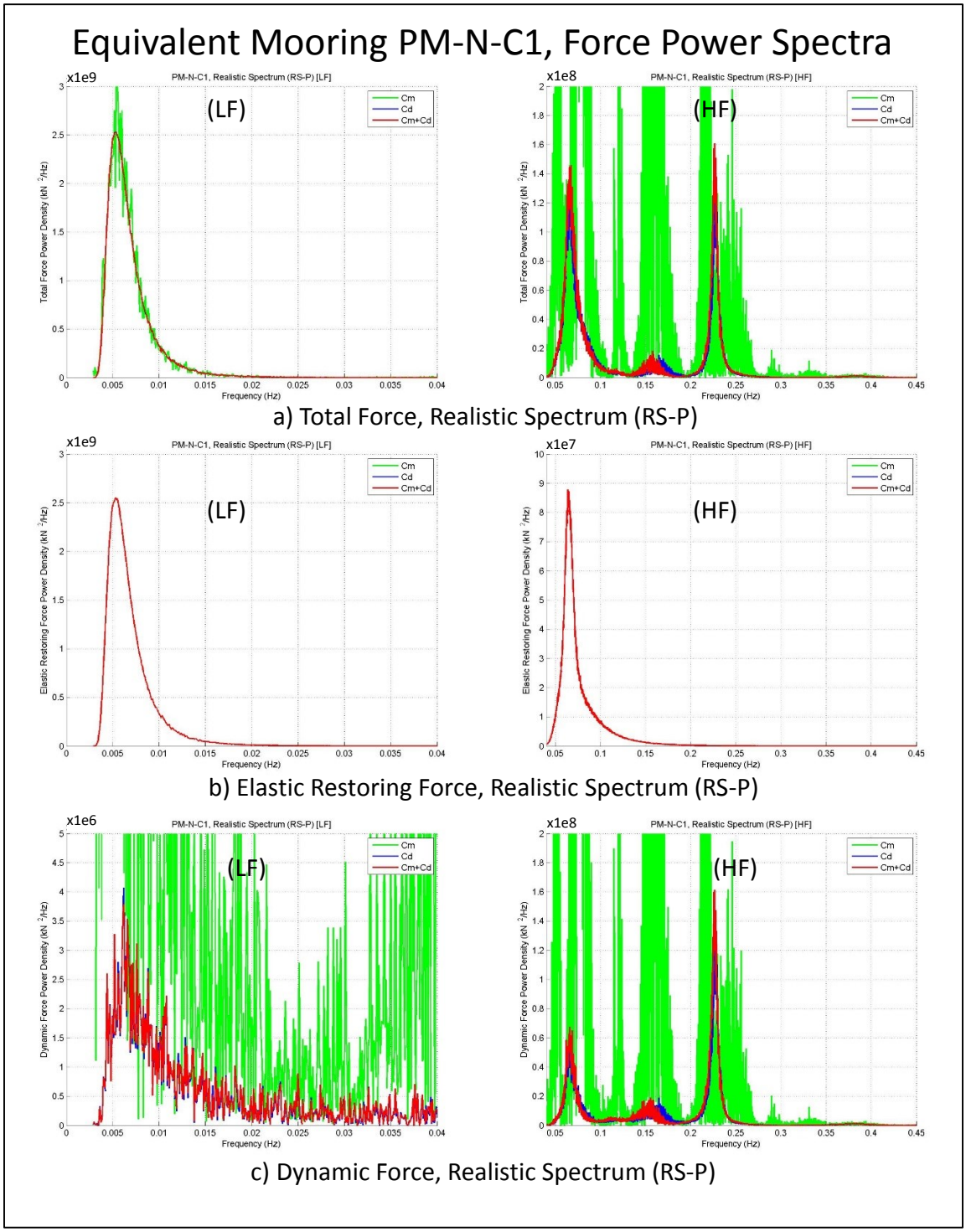

Figure 4.10. Equivalent mooring system (PM-N-C1) response comparison, force power spectra, low frequency (LF) and high frequency (HF) ranges.

In the following figures are plotted the results comparison for the prototype mooring system and the two equivalent mooring systems selected for this study case to assess the inertia and damping contributions. As mentioned above, the equivalent mooring systems are PM-S-C3 for the symmetric case and PM-N-C1 for the non-symmetric case. Figure 4.11 compares snapshots from 2000 seconds up to 2050 seconds of the total horizontal mooring force relative to its mean value, for the four different vessel displacement spectra considered: slow drift band limited white noise (SD), wave frequency band limited white noise (WF), full range band limited white noise (SD+WF) and the realistic spectrum (RS-P). With the exception of the slow drift band limited white noise (SD) spectrum, it is evident that the total mooring force is quite different for the three mooring systems, for each of the vessel surge spectra considered.

As expected, the restoring force snapshots for the three mooring systems are almost identical, as shown in Figure 4.12. The small differences in the restoring force are due to the fact that the restoring force vs offset curve used for the design of the equivalent mooring systems is based on three unconstrained degrees of freedom (surge, heave and pitch), while the dynamic simulations considered just the surge motion around a mean offset position with heave and pitch constrained to zero values.

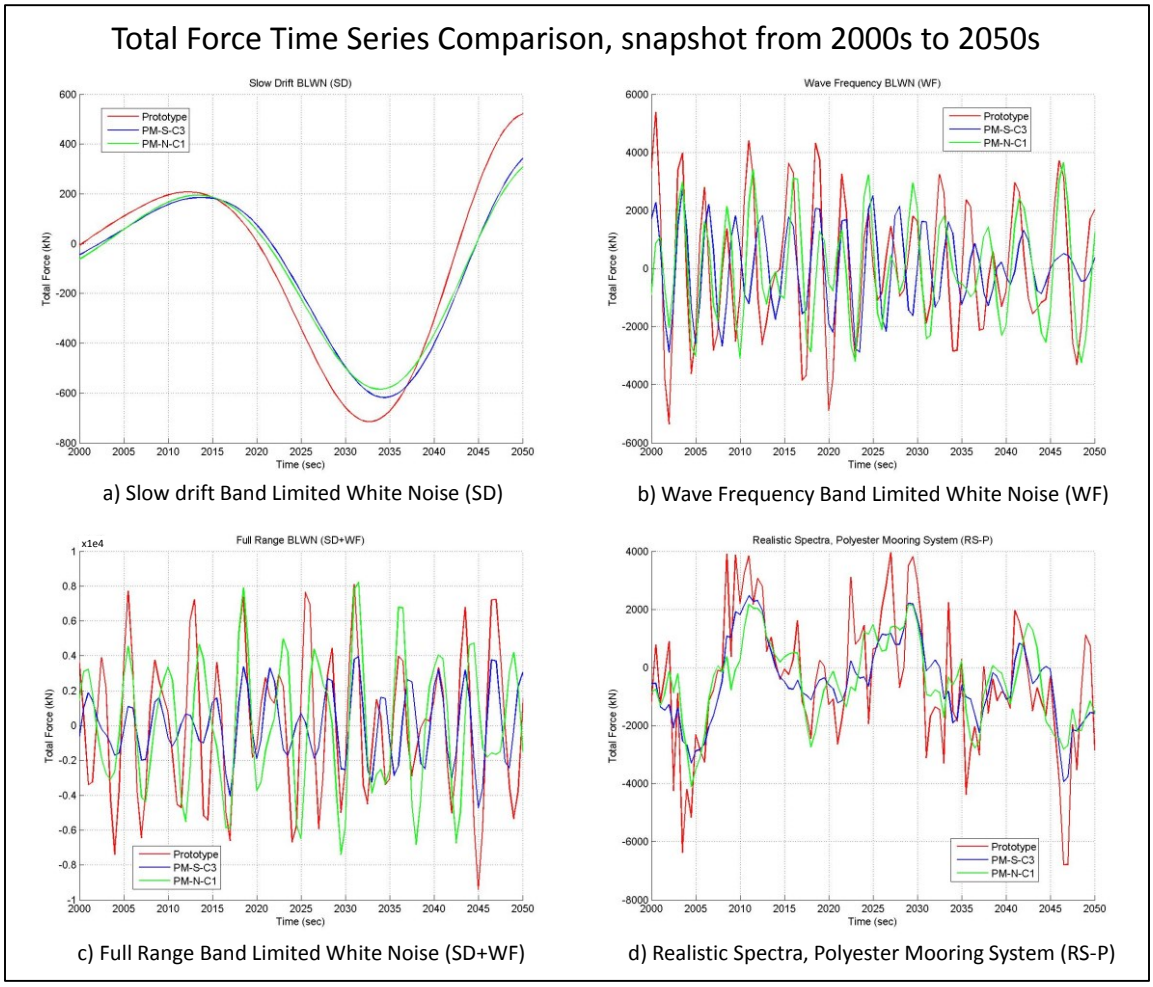

Figure 4.11. Total force time series comparison snapshot, polyester mooring system.

The dynamic horizontal force exerted by the mooring system is quite different between the prototype and the two equivalent mooring systems considered for this study case, as is shown in the time series snapshots in Figure 4.13.

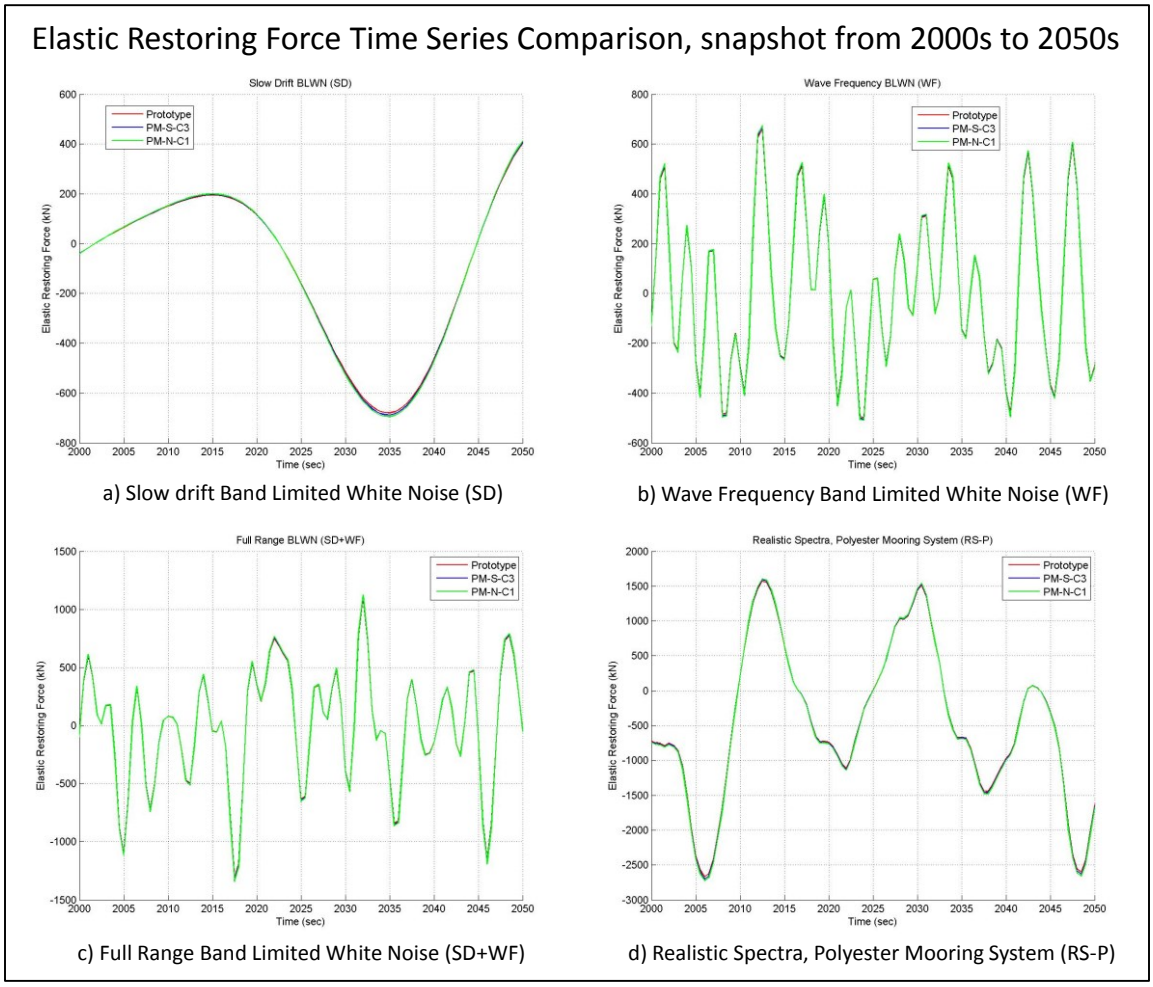

Figure 4.12. Restoring force time series comparison snapshot, polyester mooring system.

As expected from the force time series comparison, the power spectra for the total force exerted by the moorings systems are different for all but the very lowest frequencies (say, frequencies larger than 0.013 Hz), as is shown in Figure 4.14. For the dynamic force Figure 4.16 shows that all three mooring systems have spectra that are quite different for the entire frequency range, but particularly in the high frequency range where the peaks

and valleys do not occur at the same frequencies. The restoring force spectra for the equivalent mooring systems match that of the prototype mooring quite well, as shown in Figure 4.15. Therefore the differences in the spectra for the total force are related to the dynamic force component.

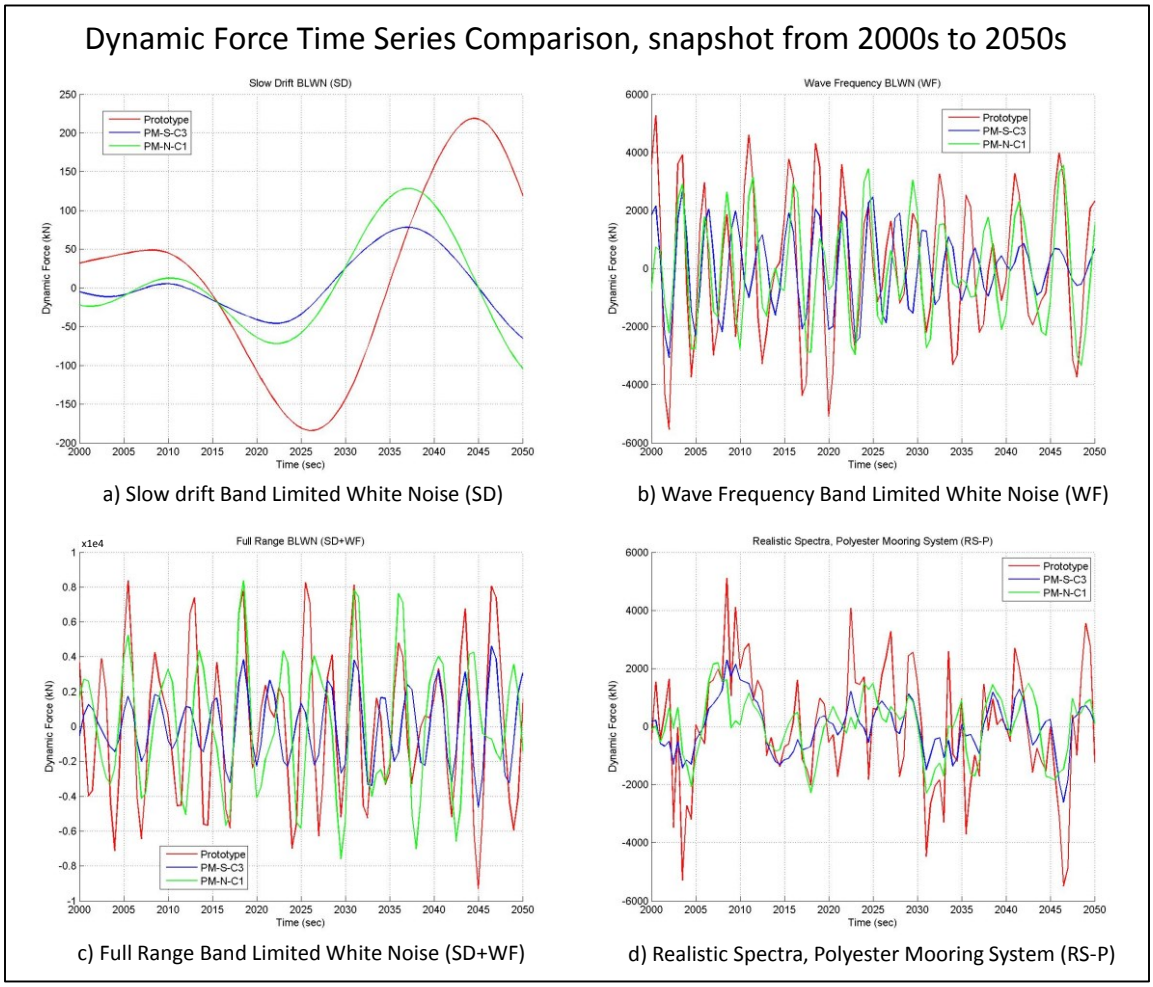

Figure 4.13. Dynamic force time series comparison snapshot, polyester mooring system.

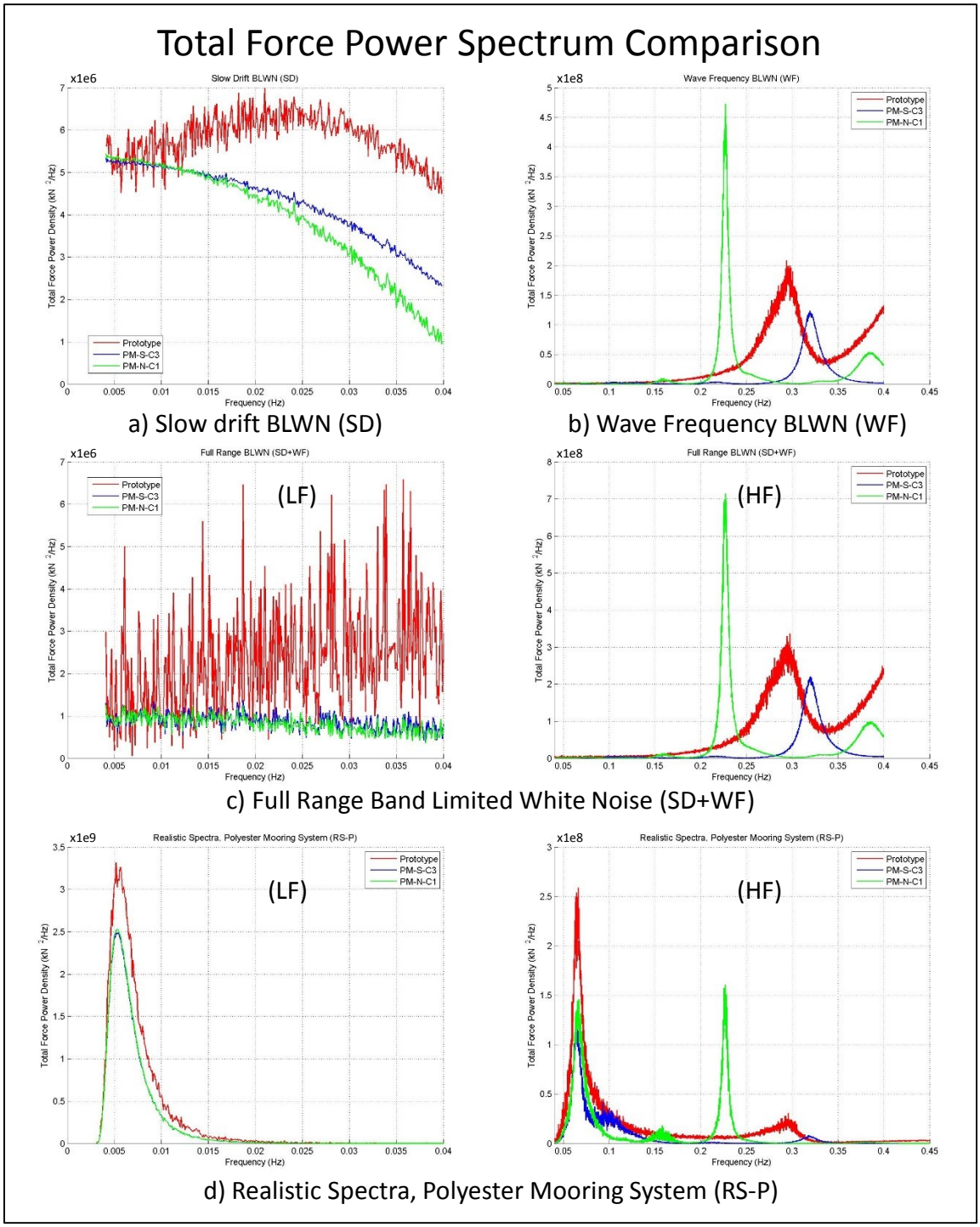

Figure 4.14. Total force power spectrum comparison, polyester mooring system.

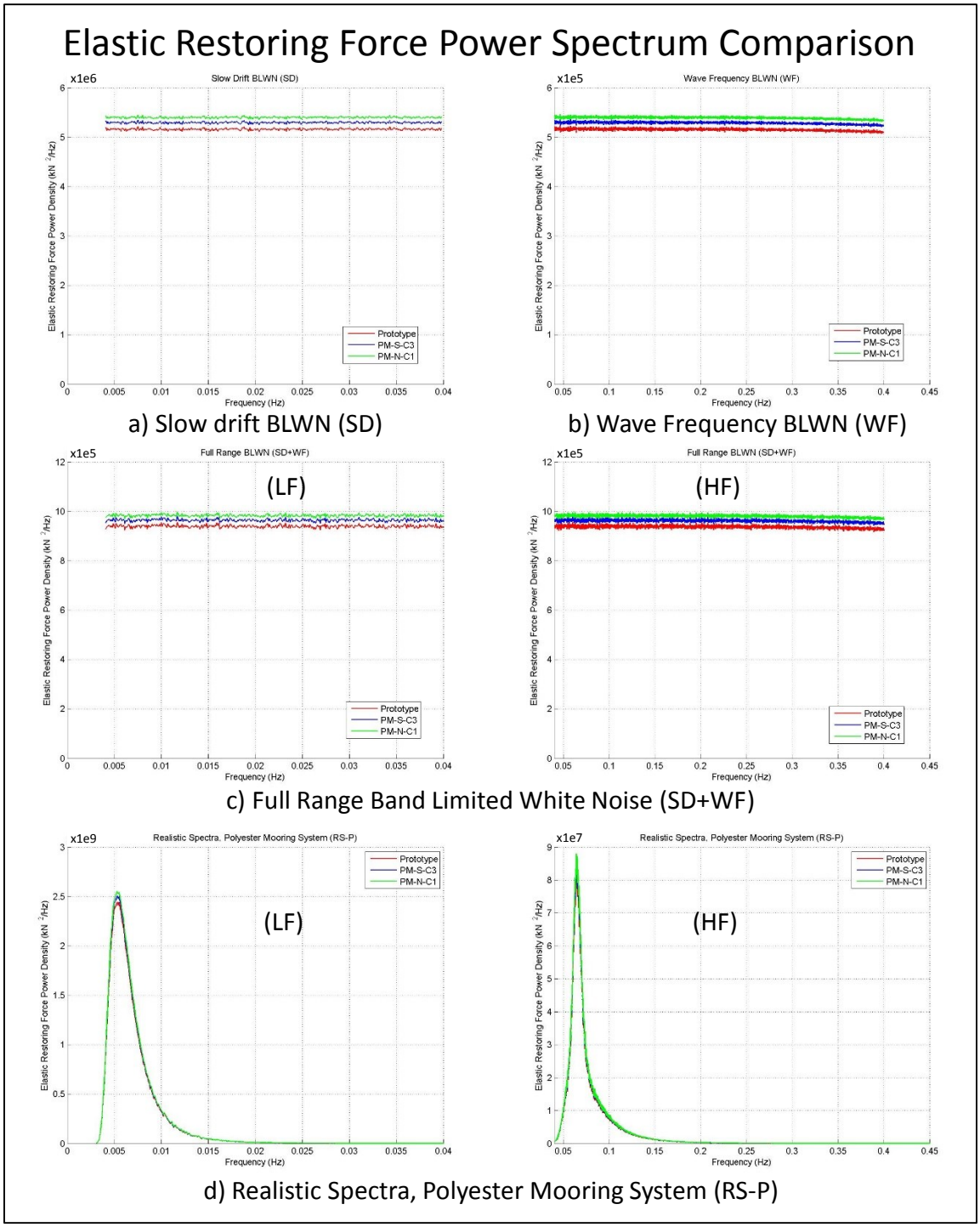

Figure 4.15. Restoring force power spectrum comparison, polyester mooring system.

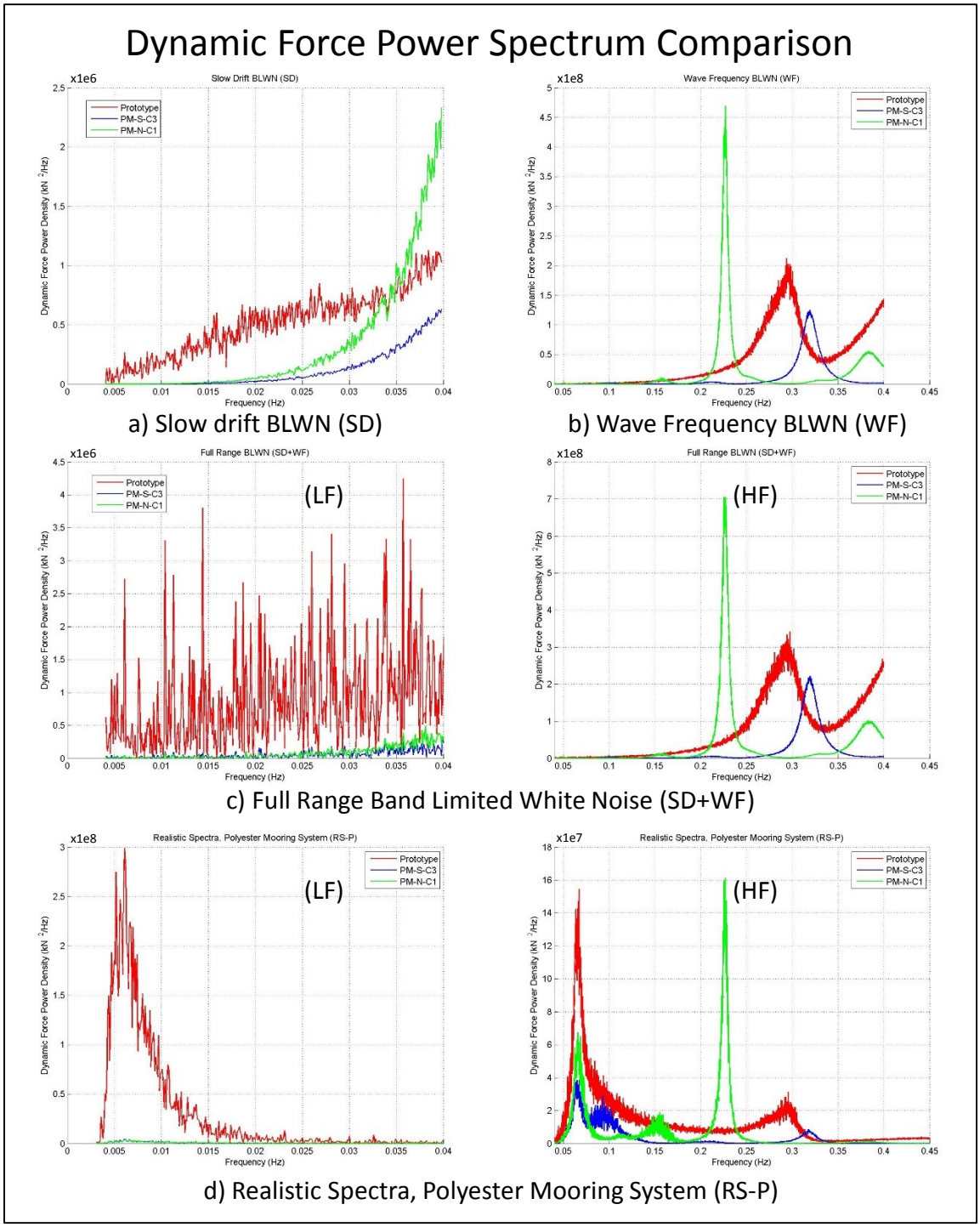

Figure 4.16. Dynamic force power spectrum comparison, polyester mooring system.

Considering the dynamic force spectrum comparison (Figure 4.16), for the realistic vessel surge spectrum (RS-P) (d) it is evident that at the slow drift resonant frequency (0.0053 Hz) there is a large difference in the power spectral density between the prototype and the equivalent mooring systems. Around the wave frequency response of the vessel (range between 0.05 Hz and 0.1 Hz) the differences are smaller than for the slow drift motion resonance frequency responses.

It should be noted that at the slow drift resonant frequency the total mooring force is dominated by the restoring force component, so the inability to reproduce the dynamic contribution of the prototype mooring may at first appear to be of little consequence. However the phasing of the dynamic force is of considerable importance, particularly that which contributes to damping of the resonant slow drift motion. In order to investigate this aspect it is necessary to decompose the dynamic force into orthogonal components that are in phase with the velocity and acceleration of the floater, in accordance with the procedure described in Section 4.2.

The decomposition procedure presented in Section 4.2 is used to calculate the frequency-dependent mooring system inertia contribution factor and the damping contribution factor, and these factors are compared between the prototype and the equivalent mooring systems. Figure 4.17 shows the inertia factors for the mooring systems while Figure 4.18 shows the damping factors. Consistent with the previous observations for the dynamic force time series and force spectra comparisons, the inertia and damping factors are different for most of the frequency range. However there are some observations that must be highlighted. There is a correlation at high frequencies (higher than 0.1 Hz)

between an abrupt change in the inertia factor, a negative inertia contribution occurrence and a peak in the damping factor (physical phenomenon studied by Vinje, 1989) and this peak is also correlated with a peak in the dynamic force power spectrum. For example, considering the prototype mooring, it can be seen that there is an abrupt change in the inertia factor around 0.3 Hz (Figure 4.17), there is a peak in the damping factor (Figure 4.18) around the same frequency, and there is also a peak around this frequency in the dynamic force power spectrum (Figure 4.16). The same behavior is evident in equivalent mooring PM-N-C1 around 0.23 Hz and 0.38 Hz, and in equivalent mooring PM-N-C3 around 0.32 Hz.

Vinje (1989) mentioned that the occurrence of negative added mass is related to a hydrodynamic resonance exerted by a structure close to its vicinity (i.e. the resonance column response in a short gap between a ship and the quayside, the response of the water in a FPSO moonpool, moving bodies close to the free surface). He also mentioned that the negative added mass occurrence is coupled with a peak in the damping curve, as it is highlighted above for the results obtained in this research. Vinje (1989) studied this phenomenon by reducing an oscillating plate close to the free surface to a two degree of freedom dynamic system. He concluded that the negative added mass and a sharp peak in the damping curve are closely related and "*one cannot appear without the other*". In his conclusions, he mentioned that the negative added mass may occur in multi-degree of freedom systems, but the description of these systems is more complex than single degree of freedom systems, so it is more complicated to explain the occurrence of negative added mass.

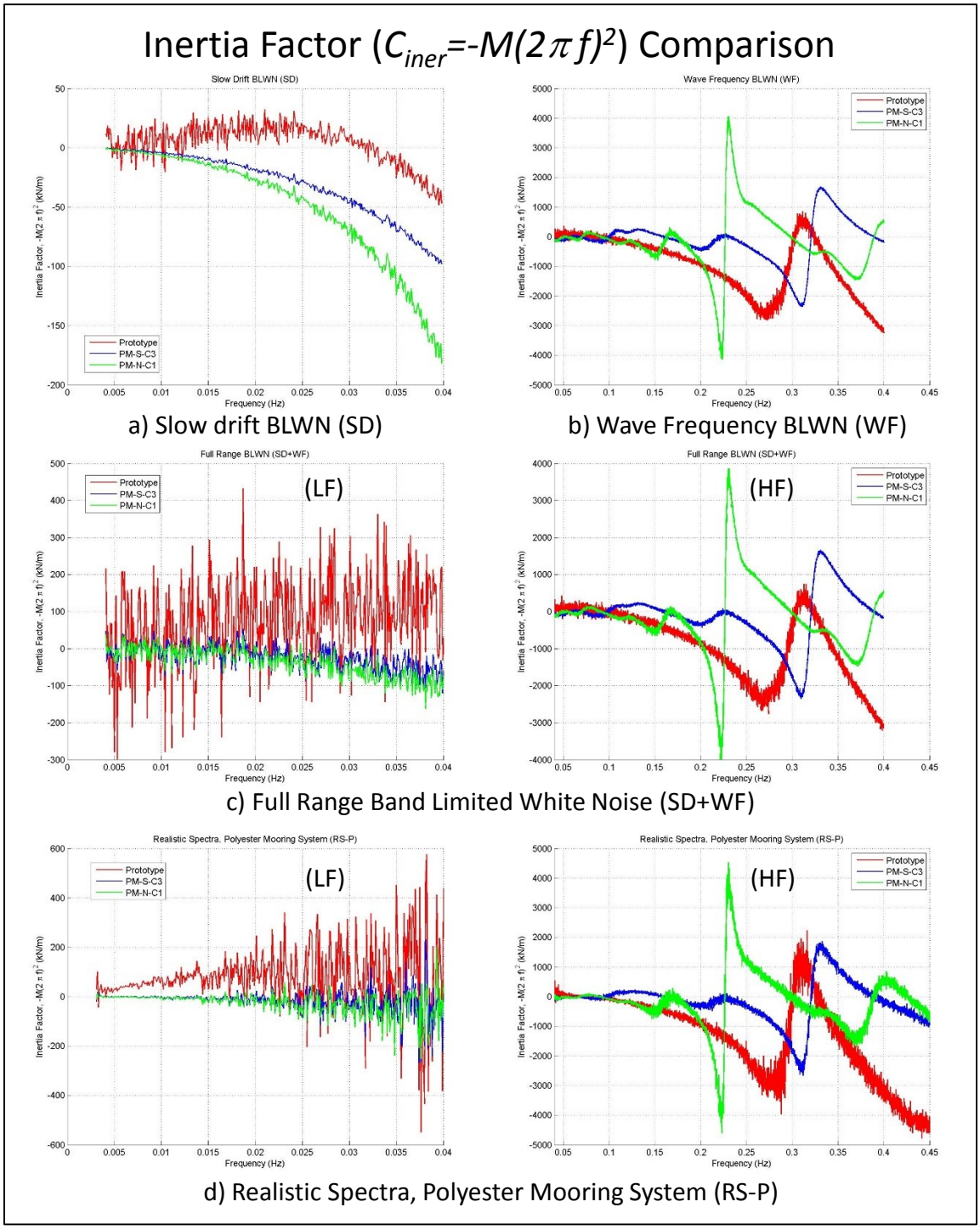

Figure 4.17. Inertia factor (C_{iner}) comparison, polyester mooring system.

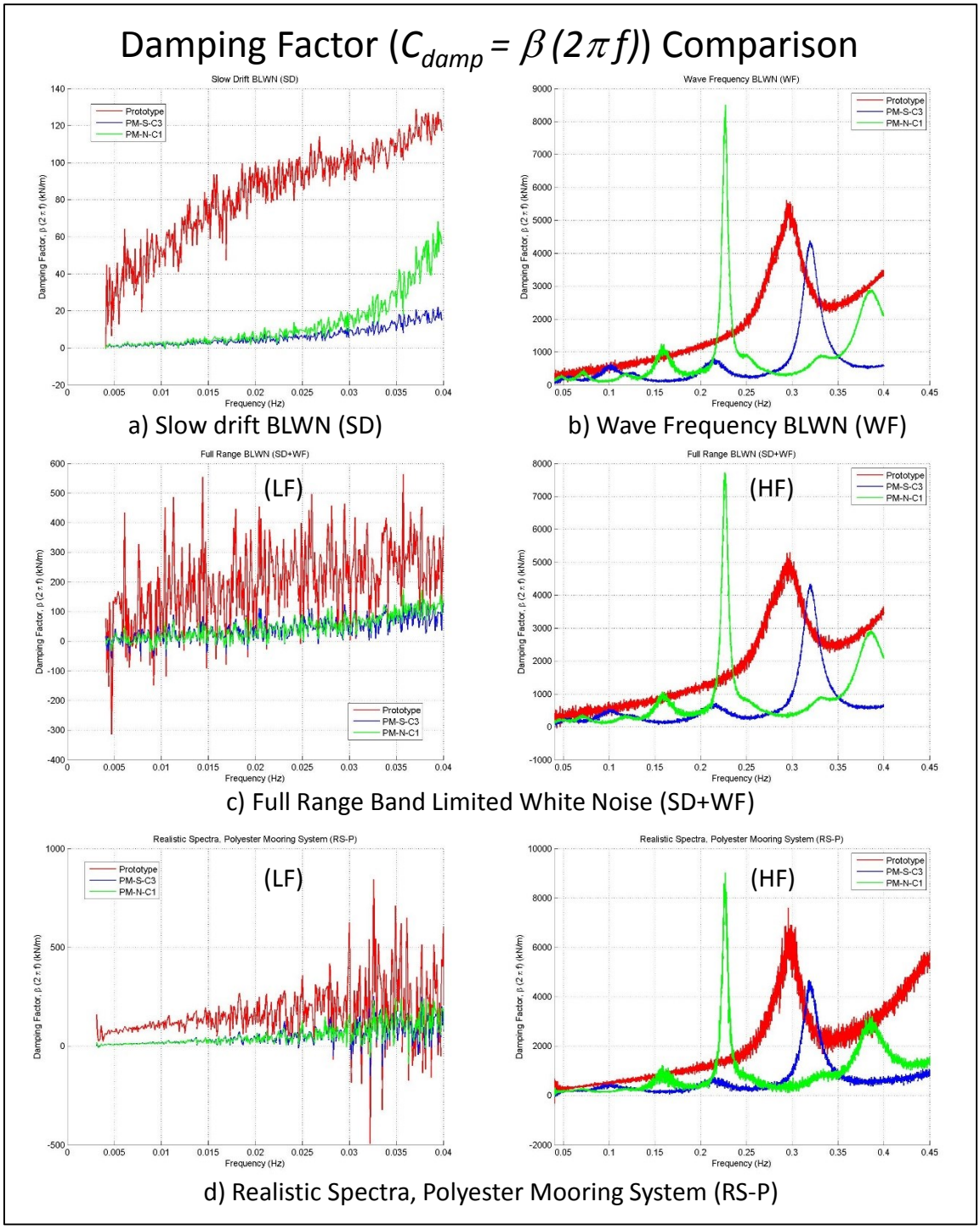

Figure 4.18. Damping factor (C_{damp}) comparison, polyester mooring system.

The mooring system inertial (f_{iner}) and damping (f_{damp}) force contributions are calculated based on the inertia and damping factors shown in Figure 4.17 and Figure 4.18, respectively, and the procedure described previously in Section 4.2. Figure 4.19 shows the mooring system inertia and damping contributions to the dynamic force at low and high frequencies for each one of the three mooring systems considered in this study for the realistic vessel displacement spectrum. The mooring system damping force contribution is the main component of the dynamic force at any frequency related with the slow drift motion and in the wave frequency range. For the prototype mooring as well as the two equivalent mooring designs the dynamic horizontal force exerted by the mooring system to the floater is clearly damping dominated with the inertia contribution being much smaller.

Figure 4.20 shows the inertia force contribution (f_{iner}) time series comparison and Figure 4.21 shows the damping force contribution (f_{damp}) time series comparison, between the prototype response and the equivalent mooring systems.

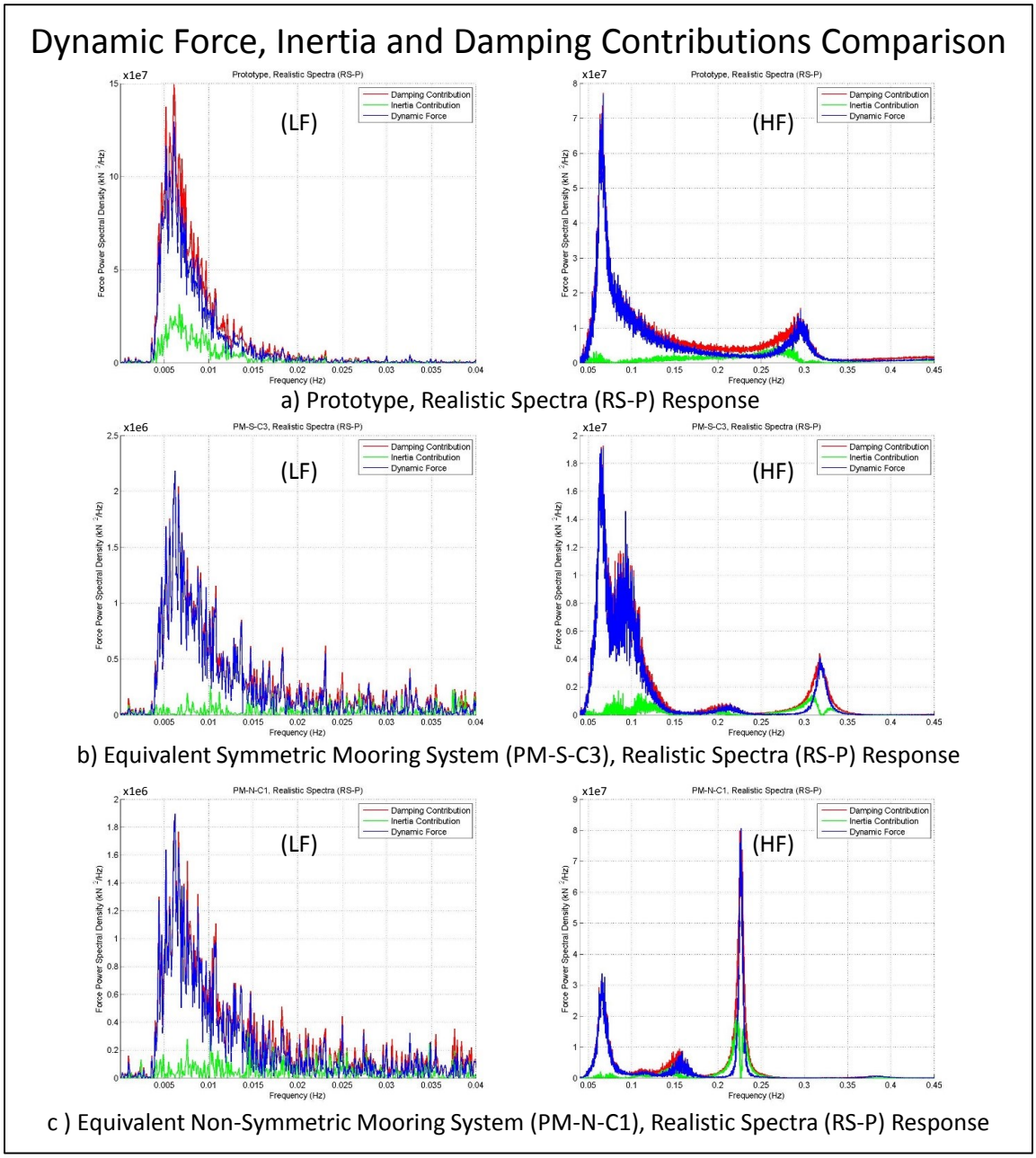

Figure 4.19. Dynamic force component, inertia and damping contributions comparison, polyester mooring system.

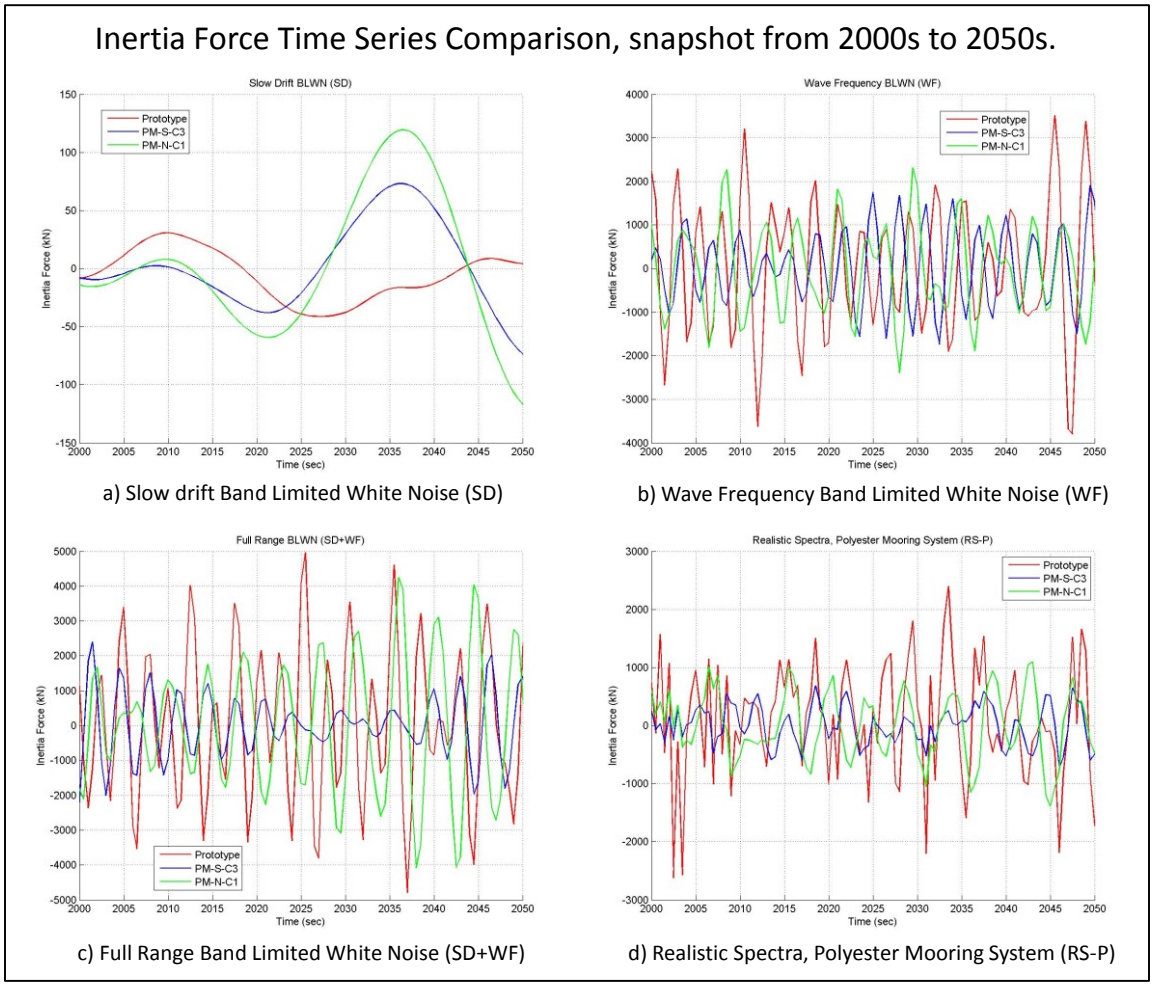

Figure 4.20. Inertia force contribution time series comparison snapshot, polyester mooring system.

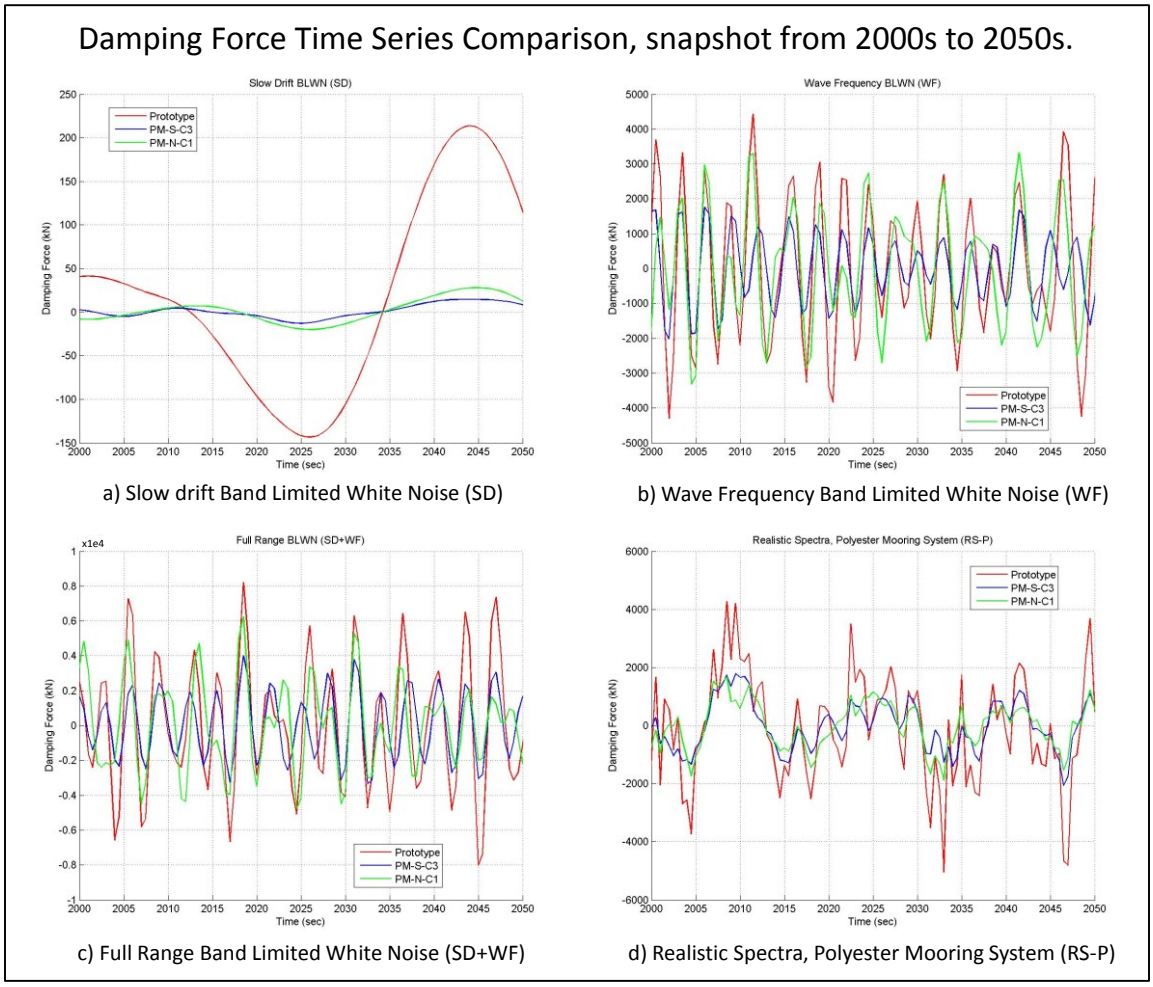

Figure 4.21. Damping force contribution time series comparison snapshot, polyester mooring system.

Figure 4.22 and Figure 4.23 provide the associated power spectra. As it is shown, the inertia and damping force contributions have a frequency dependence that is different among the three mooring systems.

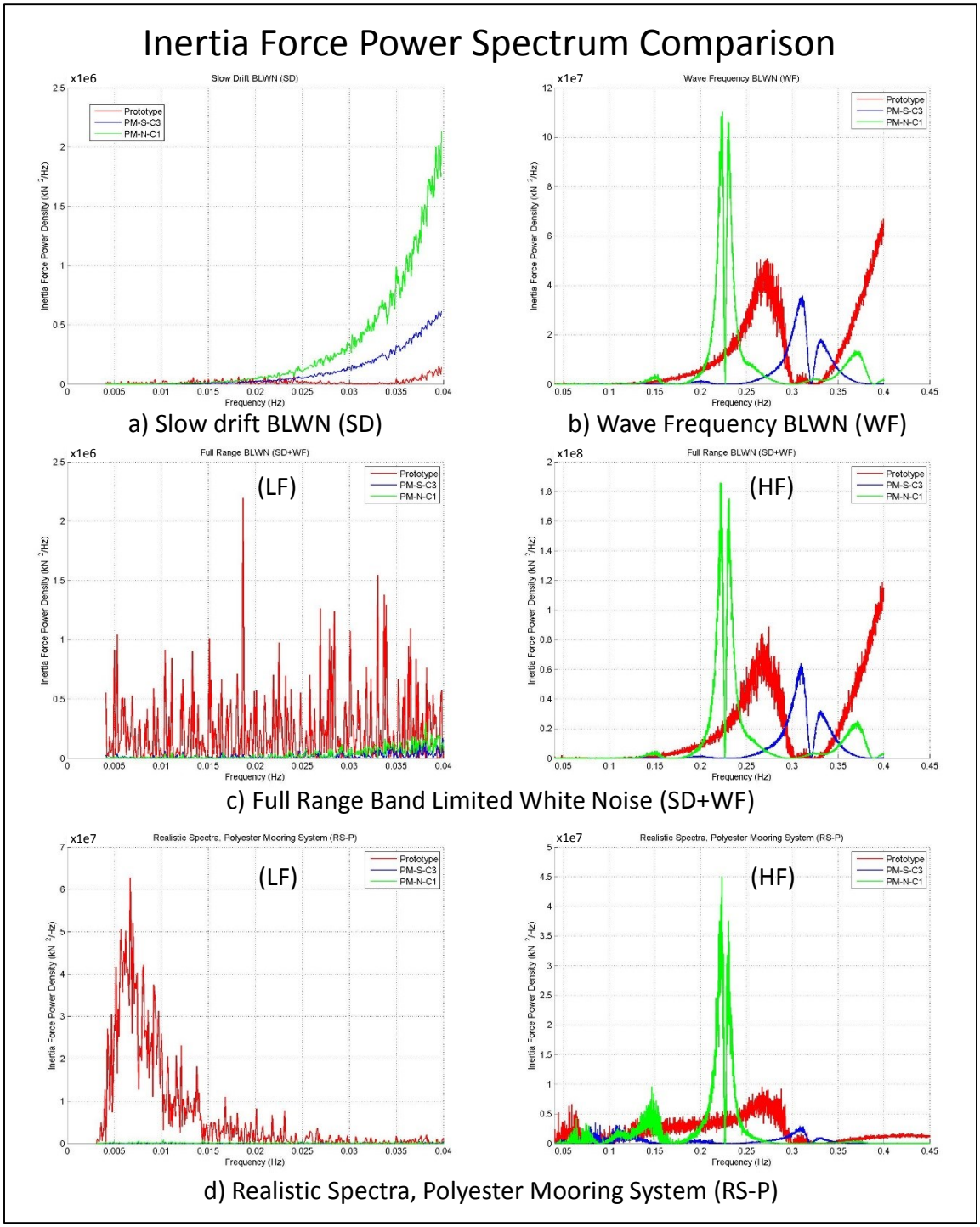

Figure 4.22. Inertial force contribution power spectrum comparison, polyester mooring system.

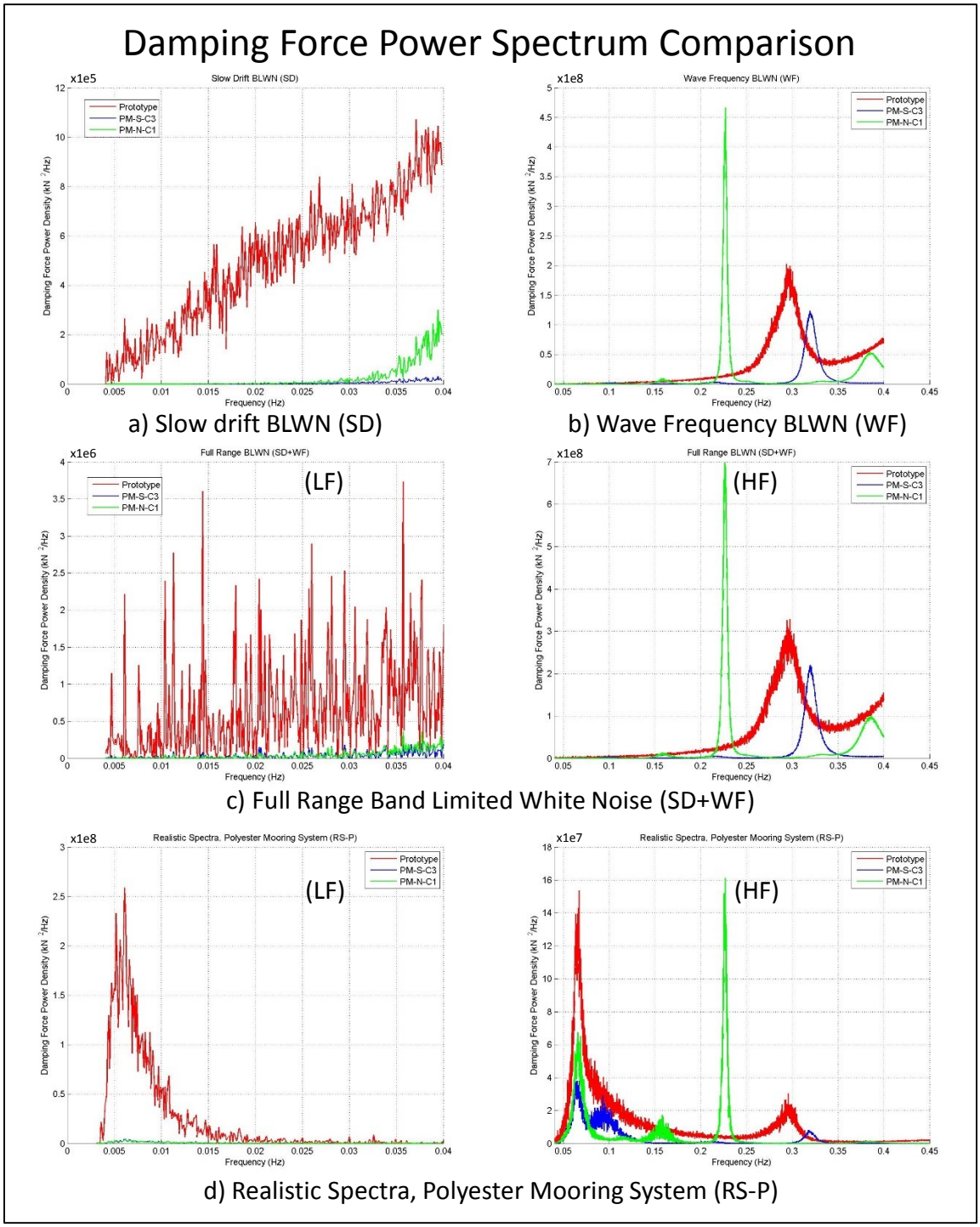

Figure 4.23. Damping force contribution power spectrum comparison, polyester mooring system.

Assuming that the net horizontal mooring force transmitted to the floater is linearly proportional to the horizontal motion of the floater, one can calculate the response amplitude operator (RAO) relating the force output to the displacement input.

In the following figures are shown the comparison of the mooring system force contribution Response Amplitude Operators (RAO's) for each one of the mooring systems considered. The response comparison for each one of the mooring systems is taking into account the different energy levels for the excitation displacement used at each frequency f, associated with the different types of displacement excitation: slow drift band limited white noise (SD); wave frequency band limited white noise (WF); full range band limited white noise (SD+WF) and realistic spectrum (RS-P)).

For the prototype mooring system Figure 4.24 compares the RAOs for the total mooring force (a), the restoring force (b), and the dynamic force contribution. In the total force and dynamic force contributions at low frequency there is a significant difference in the RAO's between 0.0035Hz and 0.045Hz. This difference in RAO magnitudes at low frequencies, which is associated with different energy levels of vessel displacement, is indicative of a nonlinear dynamic mooring force response. Since the RAOs for the different types of vessel motion excitation are pretty much the same in the wave frequency range, it appears that the horizontal dynamic mooring force is effectively linearly related to the vessel motion is this range.

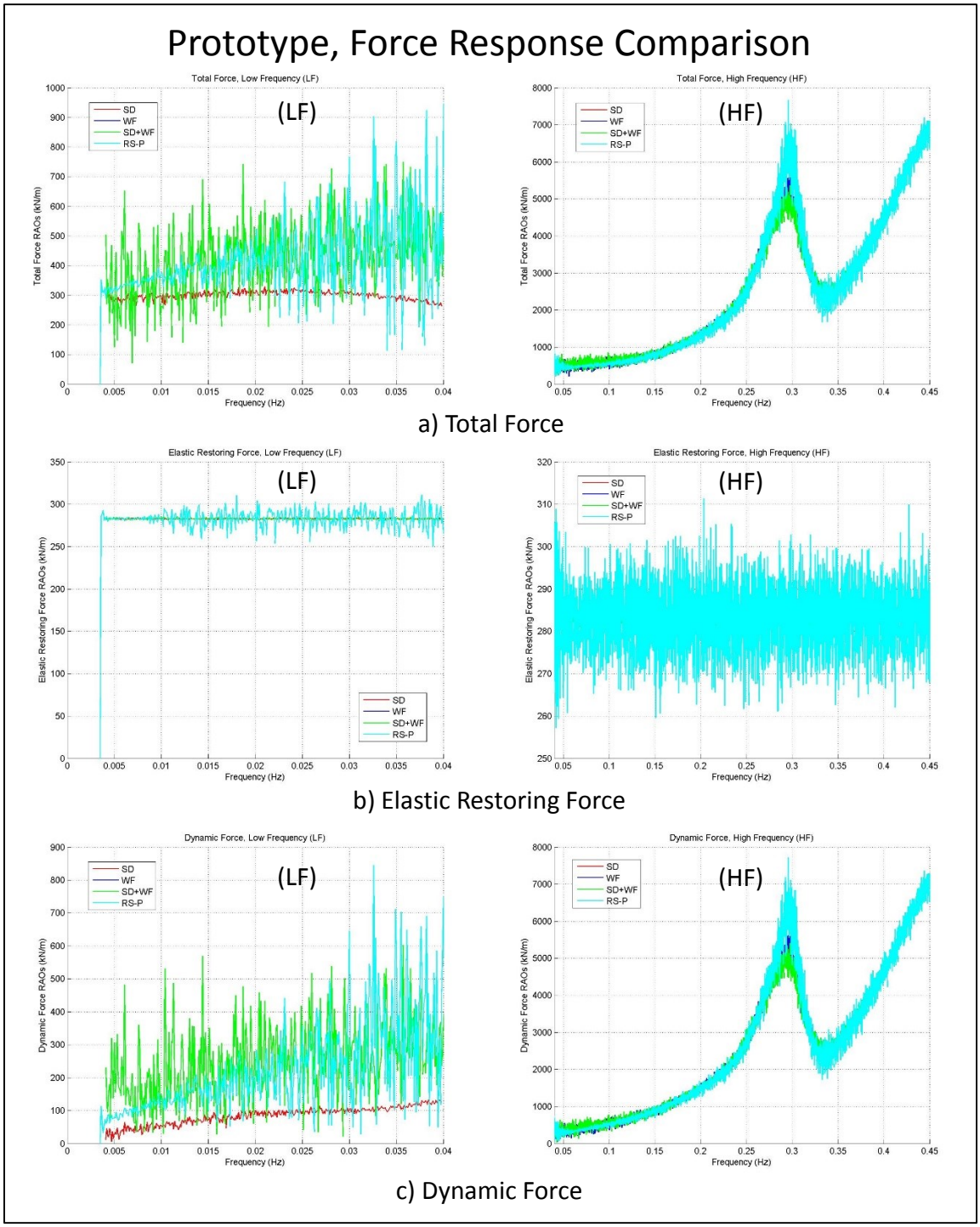

Figure 4.24. Prototype, force response amplitude operator comparison, polyester mooring system.

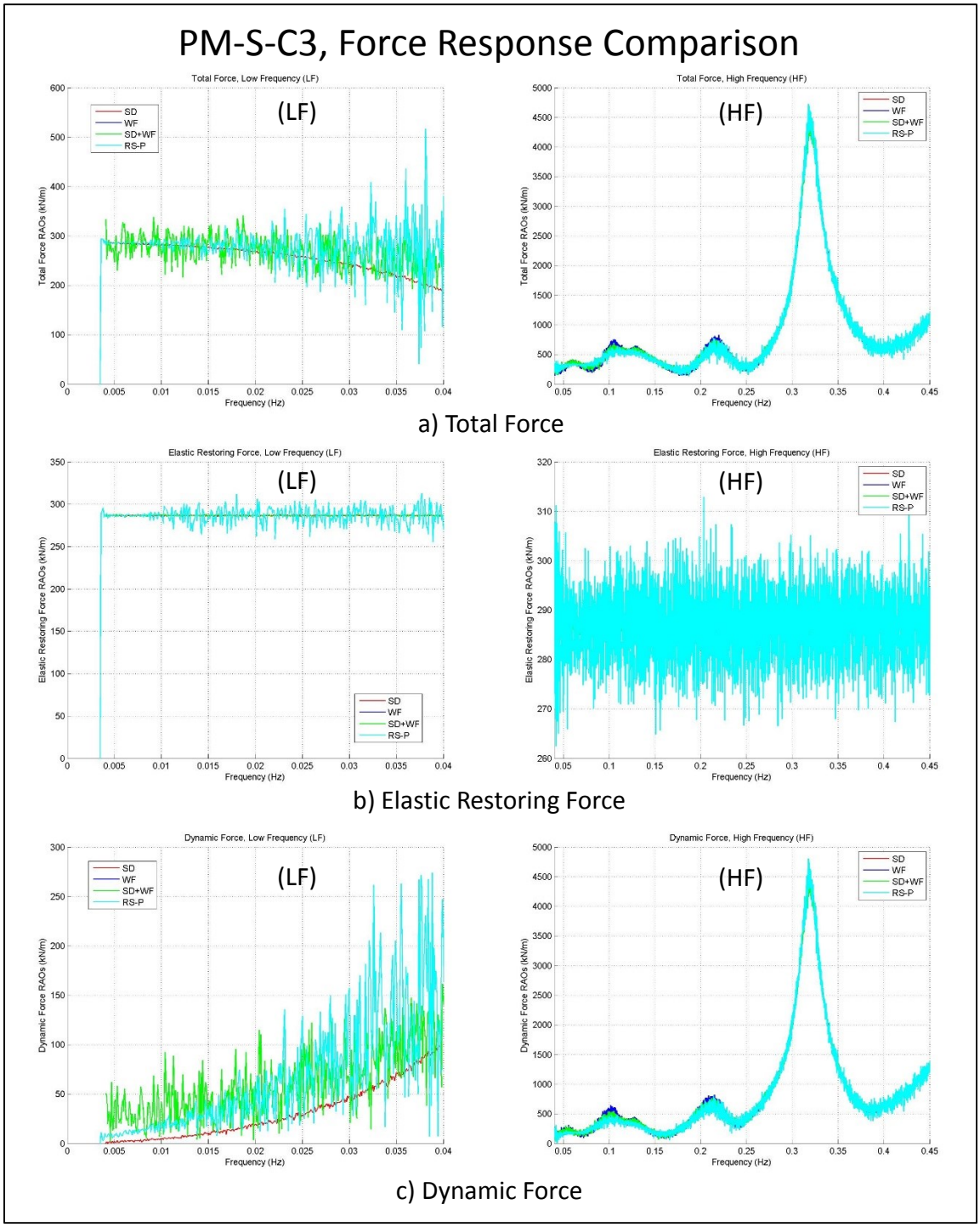

Figure 4.25. Equivalent symmetric mooring system (PM-S-C3), force response amplitude operator comparison.

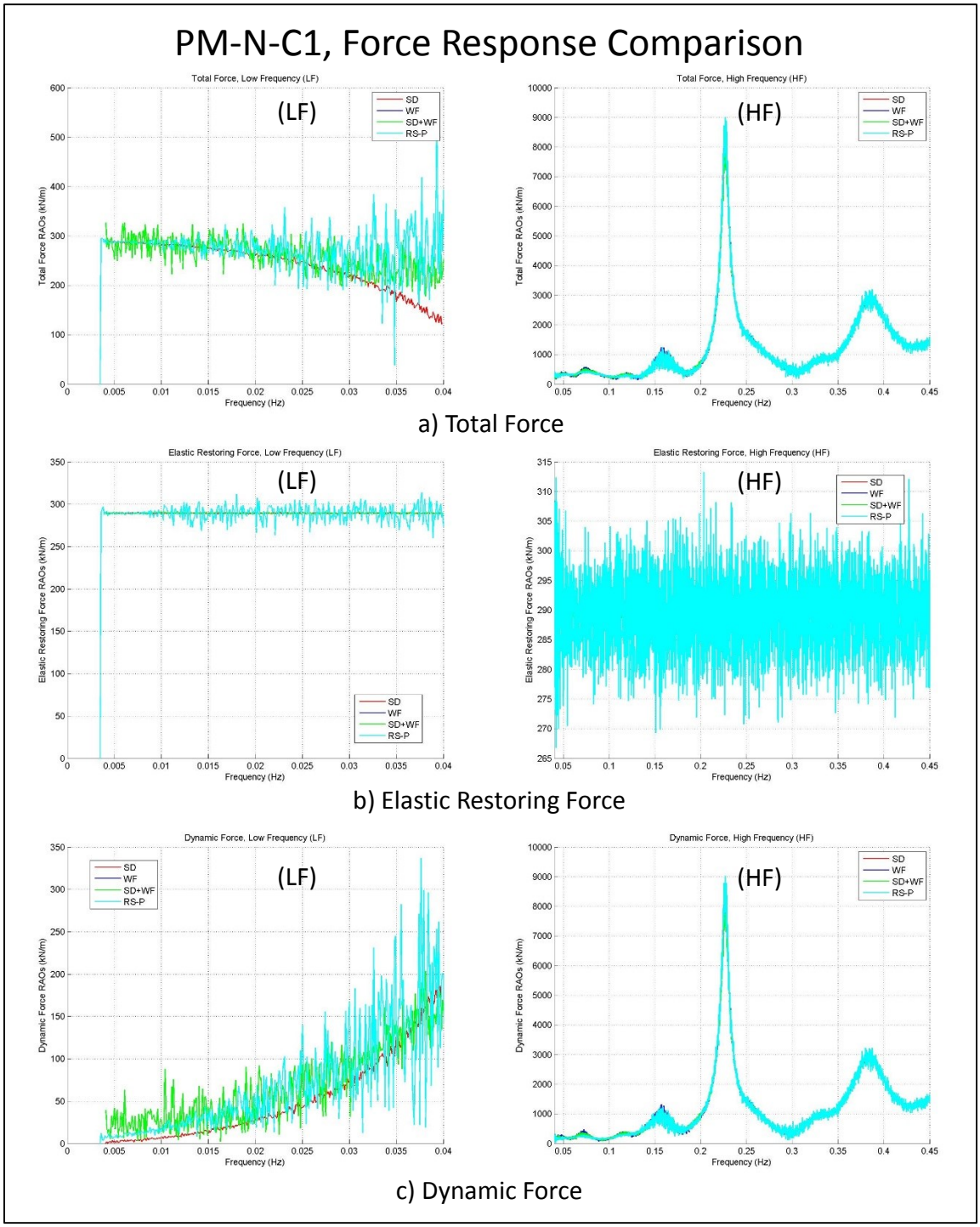

Figure 4.26. Equivalent non-symmetric mooring system (PM-N-C1), force response amplitude operator comparison.

Figure 4.25 and Figure 4.26 show the RAO comparisons for the symmetric and non-symmetric equivalent mooring systems, respectively. Although the RAOs are different from each other and from the prototype mooring, we again see that they overlap in the wave frequency range, indicating linear behavior, while being dependent on the type of vessel excitation in the low frequency range (0.0035 Hz to 0.045 Hz), indicating nonlinear behavior.

For the three different mooring systems, the RAOs for the mooring system total force, restoring force and dynamic force are compared in Figure 4.27, Figure 4.28 and Figure 4.29, respectively. As expected, the restoring force RAOs are in good agreement and they are effectively constant over the applicable frequency range since the mooring stiffness is essentially constant over the range of simulated motion. In fact the value of the restoring force RAO corresponds to the mooring system stiffness (K) at the mean offset position considered for the simulations. As expected from the observations noted previously, the total force and dynamic force RAOs are completely different for the equivalent mooring systems and the prototype system; however for all three mooring systems the RAOs have the largest values at high frequencies (higher than 0.2 Hz), indicating that the dynamic behavior of each mooring line plays an important role in the mooring system total force exerted on the floater.

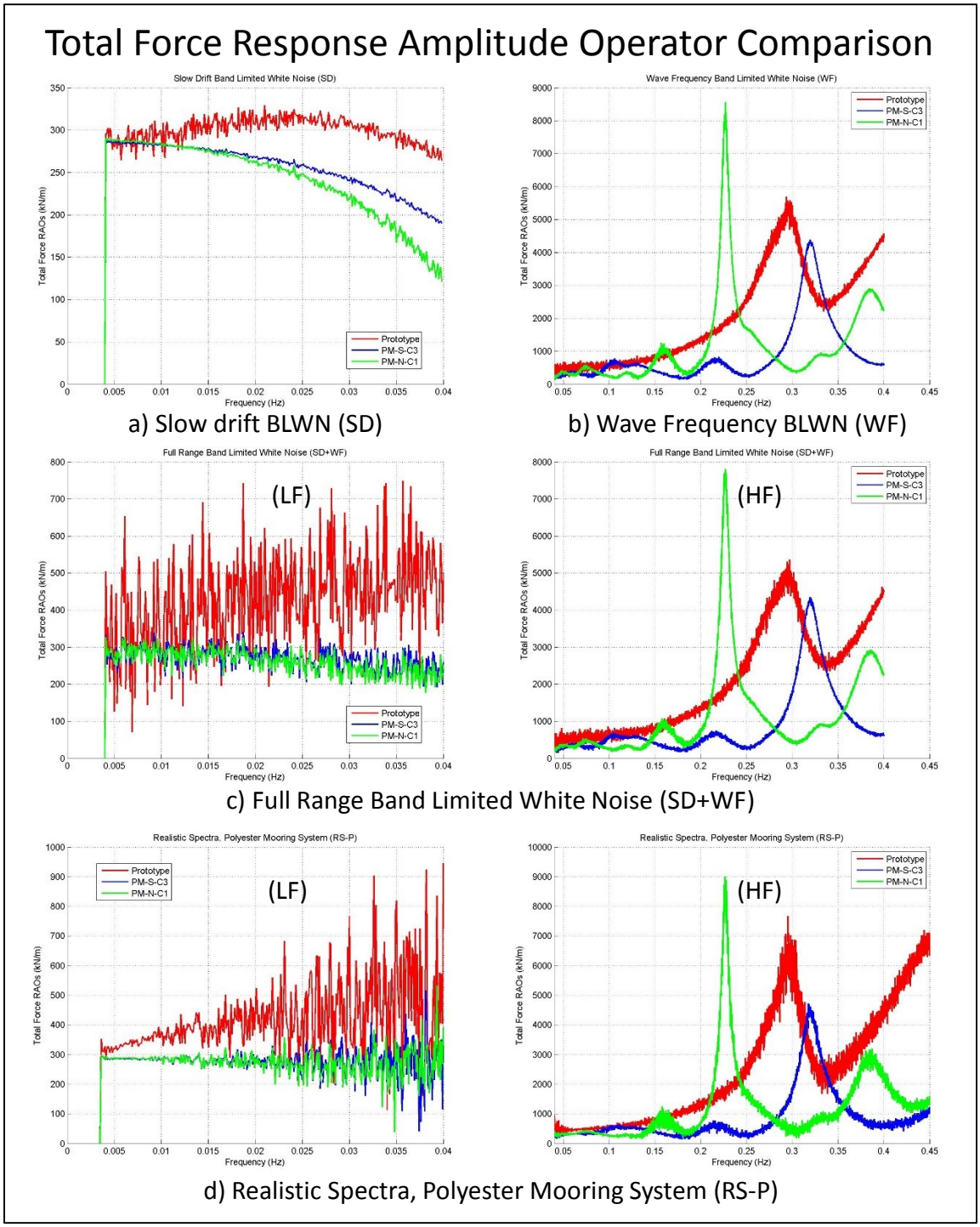

Figure 4.27. Total force response amplitude operators (RAO's) comparison, polyester mooring system.

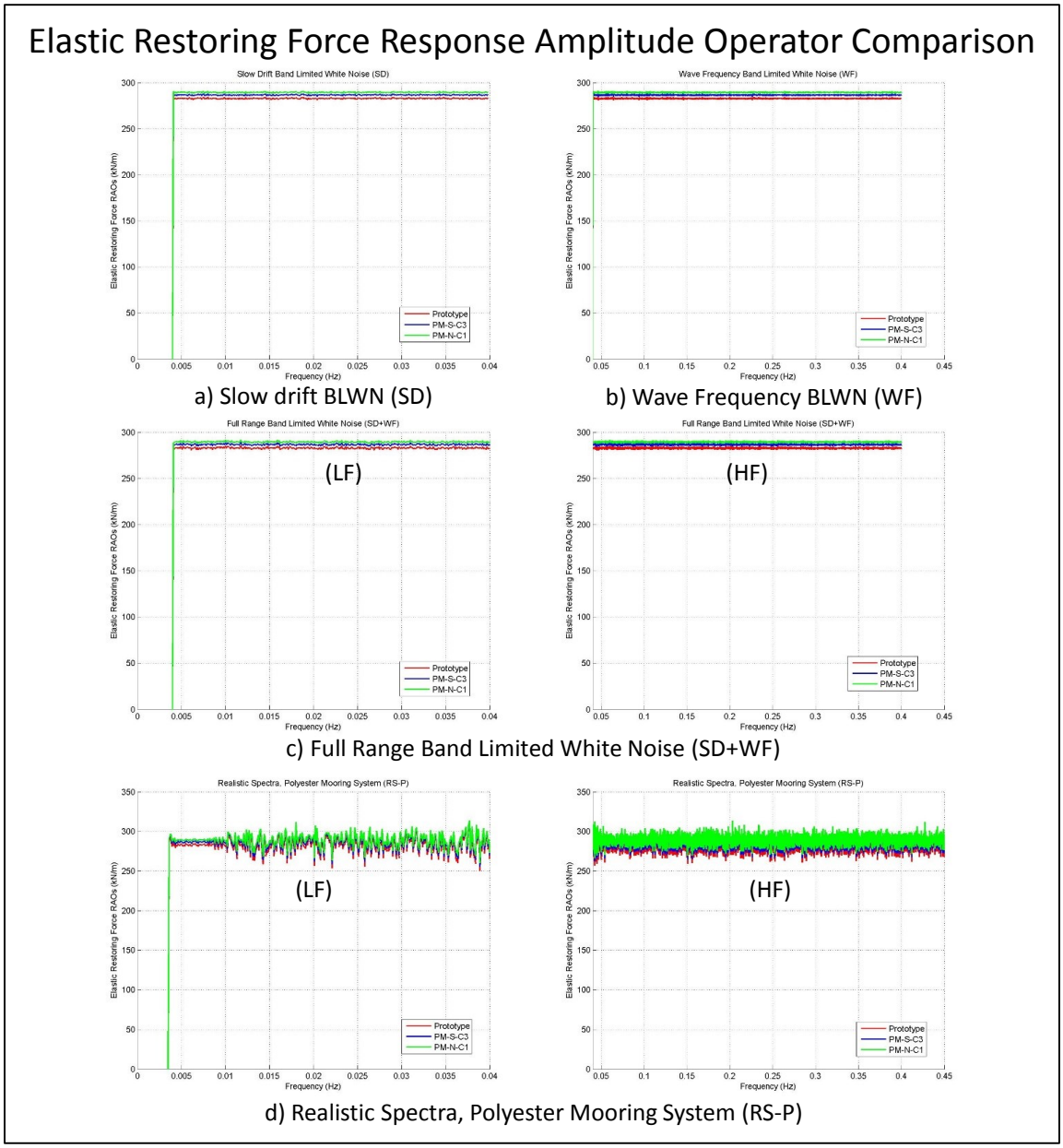

Figure 4.28. Restoring force response amplitude operators (RAO's) comparison, polyester mooring system.

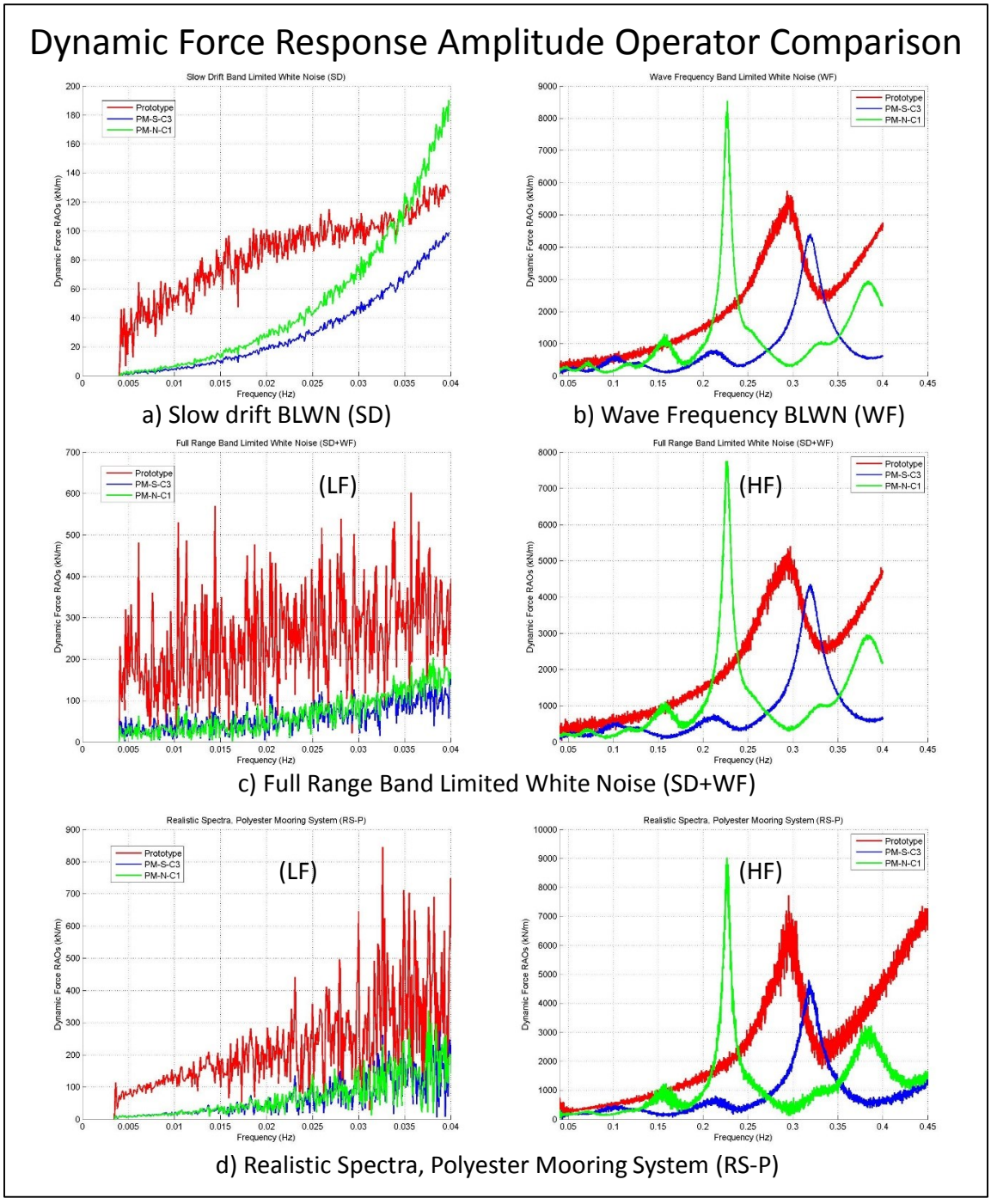

Figure 4.29. Dynamic force response amplitude operators (RAO's) comparison, polyester mooring system.

Continuing with the linear system analogy, Figure 4.30 shows the phase shift between the mooring system total horizontal force and the vessel surge displacement. Phase shifts near 0 degrees indicate that the dynamic force is negligible while phase shifts near 180 degrees indicate the inertia force contribution is dominant. Phase shifts equal to 90 degrees indicate that the restoring force and inertia force contribution are in balance so that the total force is due exclusively to the damping force contribution. As expected we see that at very low frequencies the phase shift is consistent with the total force that is dominated by the restoring force and that the phase shift increases with increasing frequency in the LF range. At high frequencies (HF), the phase shifts between the total force contribution and the displacement excitation are completely different between the equivalent mooring systems and the prototype responses. Figure 4.31 shows the phase shift between the elastic restoring force and the displacement excitation for the three mooring systems considered. The phase shift between the restoring force and the displacement exhibits similar behavior for all three mooring systems, as expected from the static equivalence.

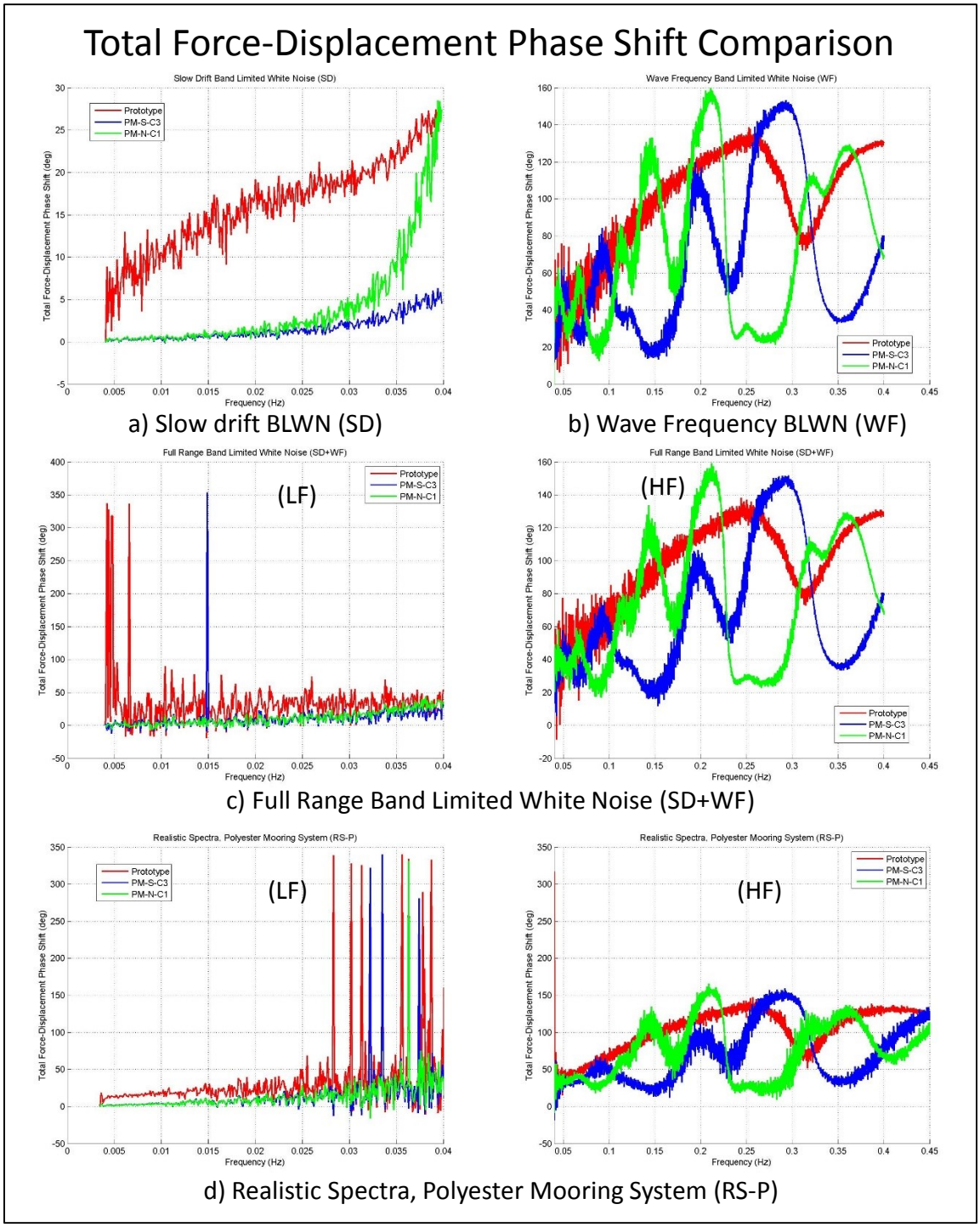

Figure 4.30. Phase shift between total force and displacement comparison, polyester mooring system.

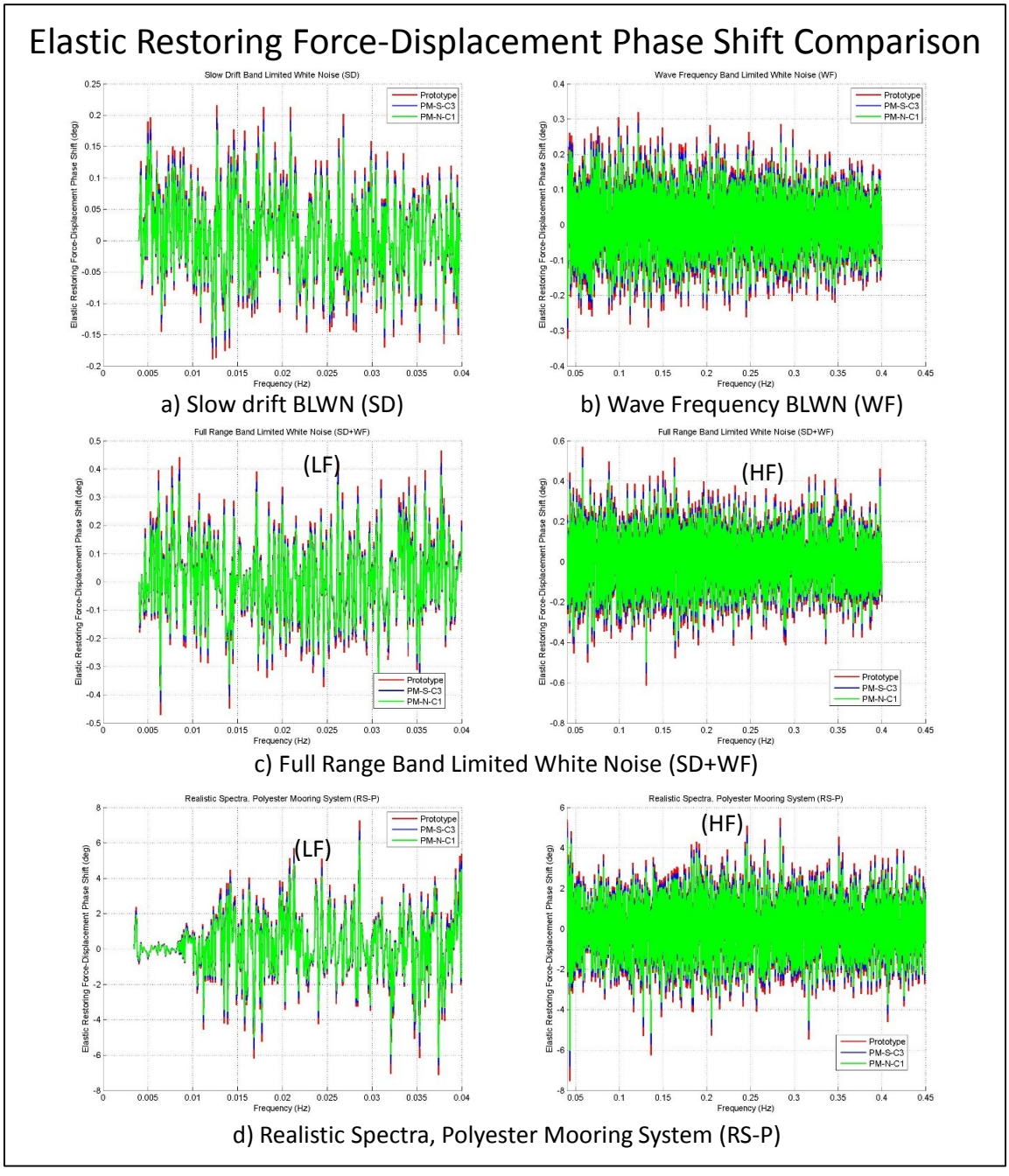

Figure 4.31. Phase shift between restoring force and displacement comparison, polyester mooring system.

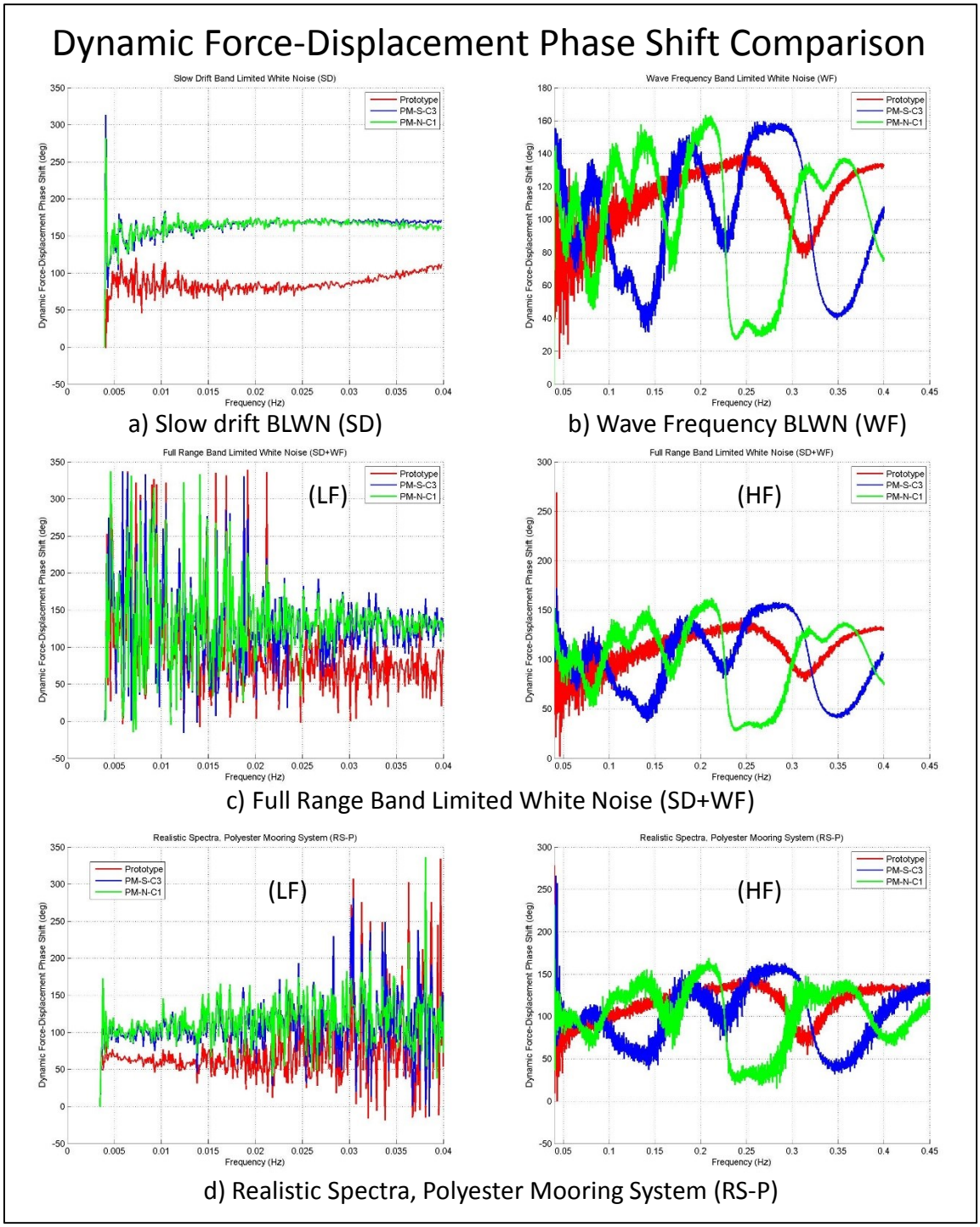

Figure 4.32. Phase shift between dynamic force and displacement comparison, polyester mooring system.

Figure 4.32 shows the phase shift between the mooring system dynamic force contribution and the displacement excitation. For those plots a value of 90 degrees means that the inertia force contribution coefficient ($-M\omega^2$) is balanced by the restoring force, so that the dynamic force component is entirely due to the damping force contribution. For the dynamic force, a phase shift between the force and the displacement of less than 90 degrees means that the inertia force contribution is in phase with the displacement, which indicates a negative virtual added mass contribution, in this case instead of generating a retardation effect to the motion the mooring is contributing to the motion. We see that the two equivalent mooring designs have a greater propensity toward negative virtual added mass than the prototype mooring.

In the following figures are plotted the linear coherence between the displacement excitation, which in this case is the input signal, and the mooring system force contributions signal, which is the output signal. The coherence between two signals is defined as:

$$C_{xy} = \frac{\left|G_{xy}\right|^2}{G_{xx}\, G_{yy}} \tag{4.16}$$

where;

$C_{xy} = coherence\ between\ the\ signals\ x\ and\ y, values\ [0,1]$;

$G_{xy} = cross\ spectral\ density\ function\ between\ signals\ x\ and\ y$;

$G_{xx} = auto\ spectral\ density\ function\ for\ signal\ x$;

$G_{yy} = auto\ spectral\ density\ function\ for\ signal\ y$;

Coherence values close to 1 means that the two signals are linearly correlated, or there is a linear dependency between the input signal and the output signal. Coherence values significantly less than 1 means that there is a non-linear dependency between the input signal and the output signal or the signal-to-noise ratio in either the input or the output is sufficiently low that the coherence cannot be accurately resolved.

Figure 4.33 shows the coherence between the total force and the displacement excitation for the three mooring systems considered and for each one of the excitations considered. For the realistic spectrum (RS-P) displacement excitation, the coherence values at frequencies ranging from 0.030Hz to 0.045Hz are showing a non-linear dependency between the displacement excitation and the mooring system total force. This is to be expected since there is essentially no forcing (vessel motion) in this frequency range so any response has to be from nonlinear mechanisms. For the full range white noise spectrum (SD + WF) there is also indication of nonlinear dependency at very low frequencies. Evidently this nonlinear response originates from interactions in the wave frequency range, since the coherence for the slow drift white noise spectrum (SD) does not show this behavior.

The coherence functions for the restoring force shown in Figure 4.34 indicate a linear dependency between both signals, as expected. Therefore the non-linear dependency shown in the total force contribution is due to the dynamic force contribution, as is shown in Figure 4.35. Here we see quite clearly the nonlinear response behavior evident with the full range white noise spectrum (SD + WF) excitation.

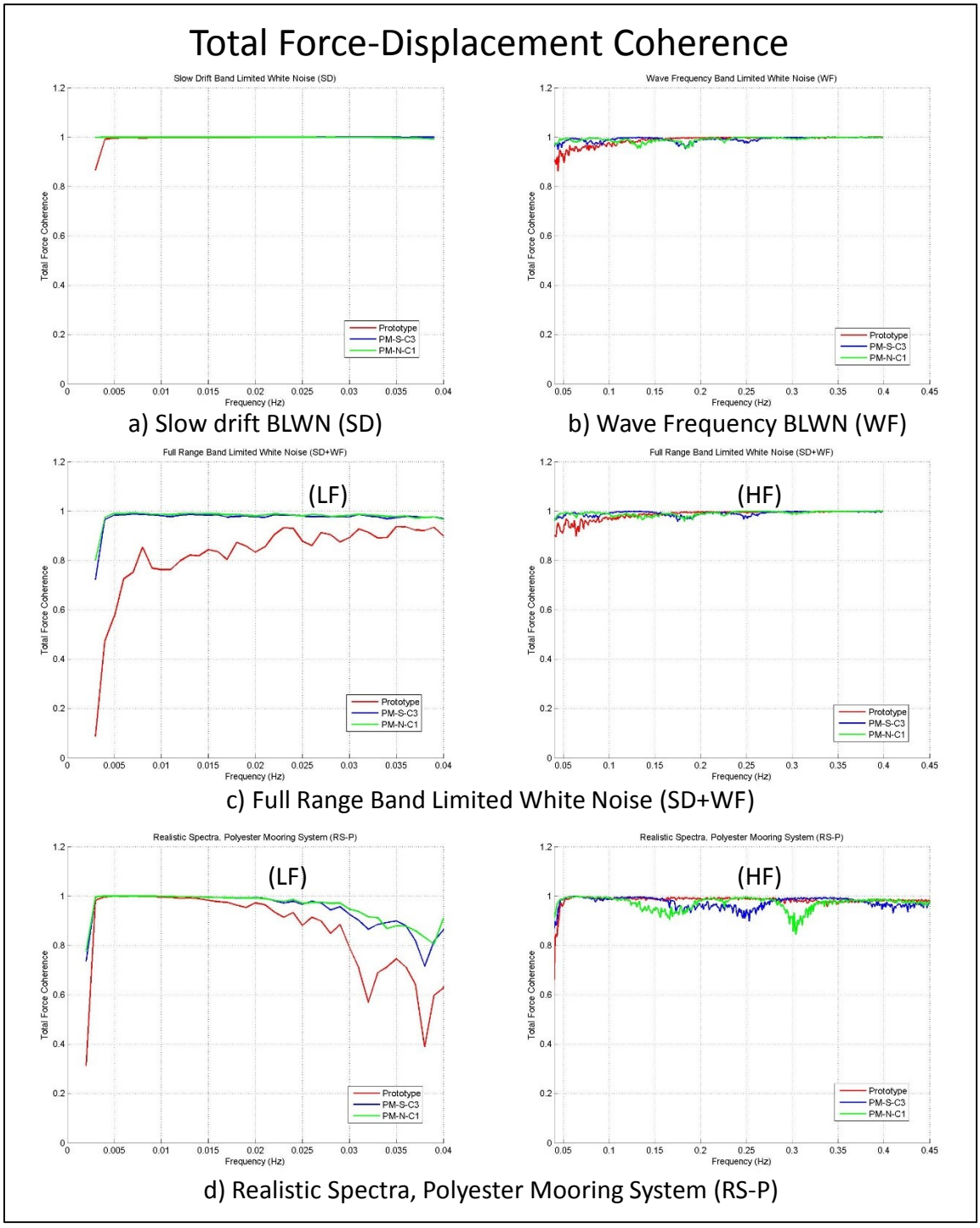

Figure 4.33. Total force and displacement coherence comparison, polyester mooring system.

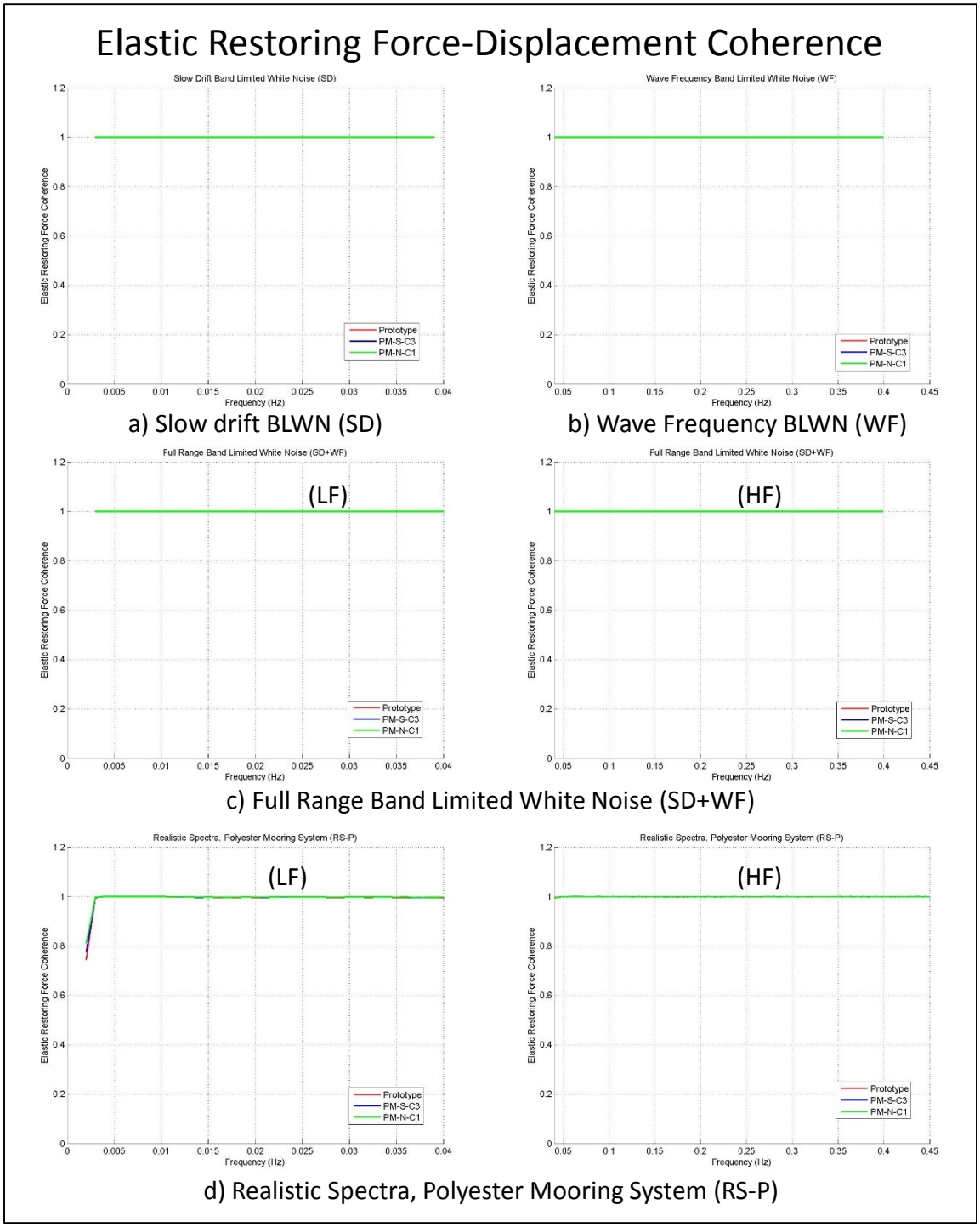

Figure 4.34. Restoring force and displacement coherence comparison, polyester mooring system.

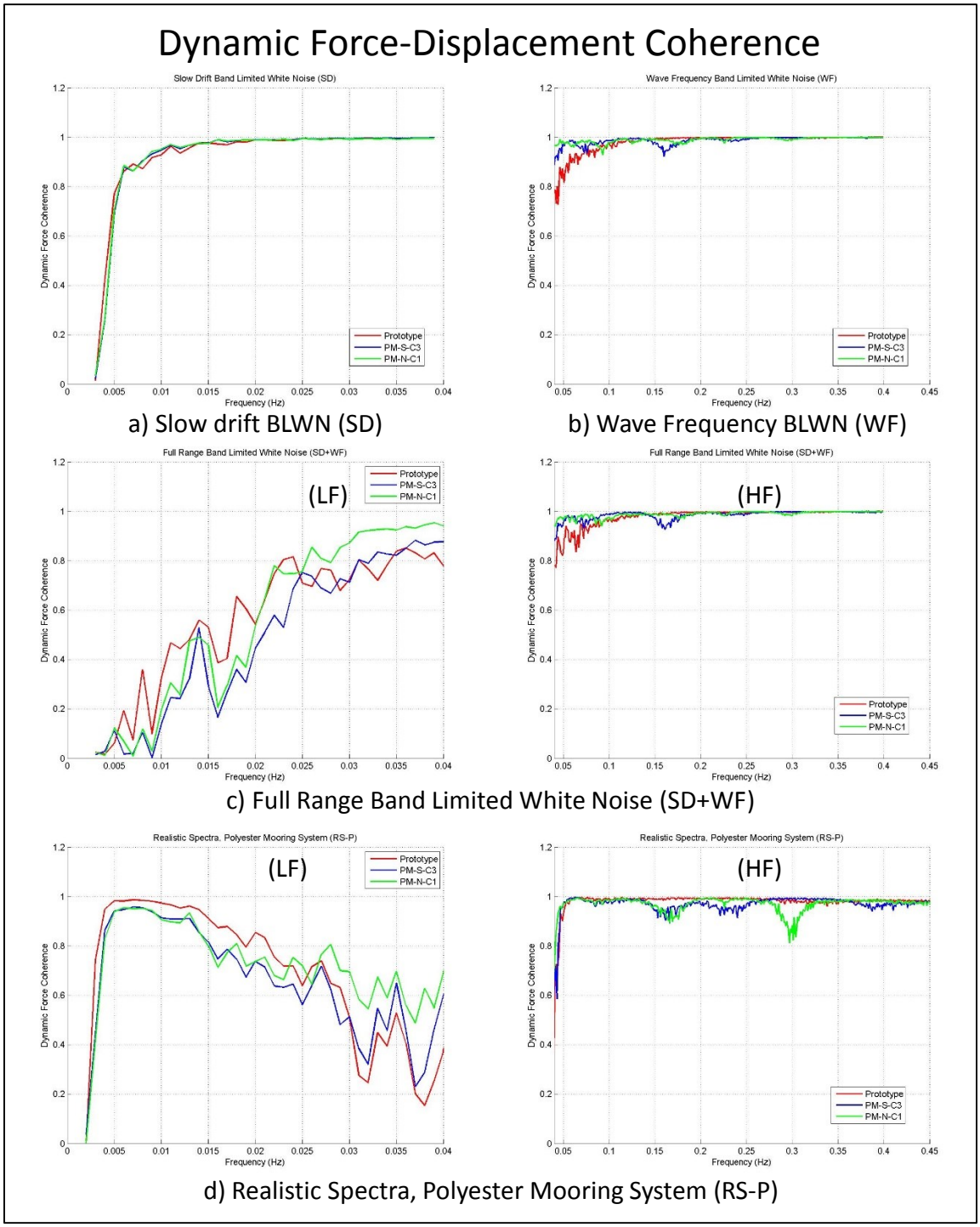

Figure 4.35. Dynamic force and displacement coherence comparison, polyester mooring system.

In order to have a perspective of the values associated with the mooring system damping contribution to the floater, the damping factor $C_{damp}=\beta\,(2\pi f)$, is normalized by the critical damping value, β_{cr}, associated with the slow drift resonance motion, multiplied by the circular frequency ($\omega=2\pi f$) in order to determine an equivalent critical damping ratio contribution from the total horizontal mooring force in the surge direction. The complete system characteristics used to calculate the values for the normalization of the mooring system damping factor are included in Table 4.3.

Table 4.3. Moored floating system dynamic characteristics, polyester mooring system.

Characteristic	Value
Floater Total Mass at Slow Drift resonance ($M_t=M_f+M_a$)	255,000 ton
Mooring System Horizontal Stiffness (K)	283 kN/m
Natural Angular Frequency (ω_n)	0.0333 rad/sec
Natural Frequency (f_n)	0.0053 Hz
Natural Period (T_n)	189 sec
Critical Damping ($\beta_{cr}=2\,M_t\,\omega_n$)	17,000 kN s/m

The mooring system damping force contribution is plotted as a frequency dependent critical damping ratio in Figure 4.36. There is a large difference between the equivalent mooring systems and the prototype mooring system damping responses at low frequencies less than 0.04 Hz and at high frequencies greater than 0.10 Hz. The differences in damping contributions between the equivalent mooring systems and the prototype are

smaller in the wave frequency range. In the wave frequency range (0.04Hz–0.10Hz), the critical damping ratio for the prototype mooring system is around 5%, while the equivalent mooring system contributions are around 3%. At low frequencies, the maximum critical damping ratio contribution for the prototype is around 15%, while the equivalent mooring system contributions are around 2%.

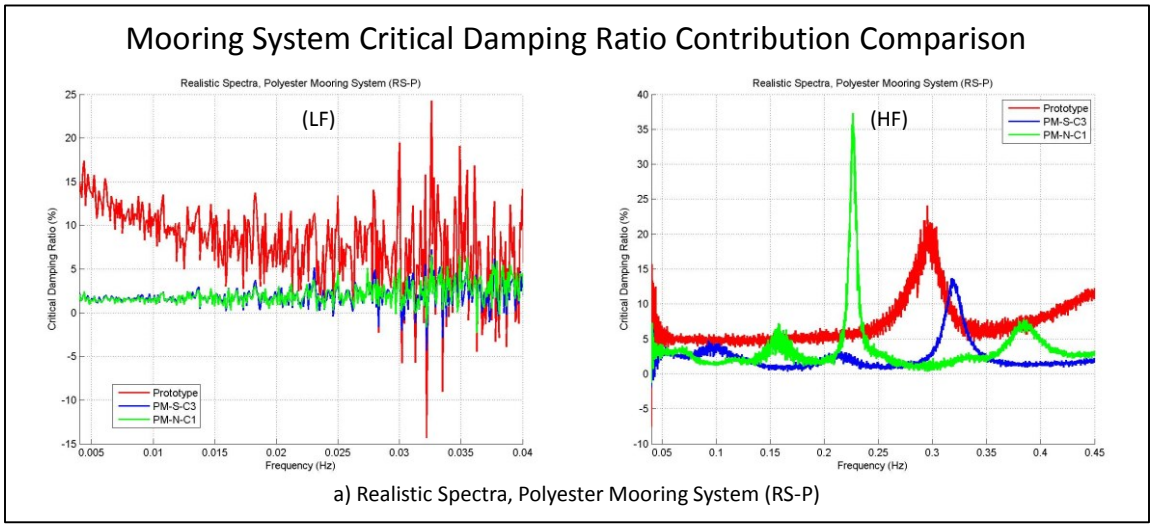

Figure 4.36. Polyester mooring system critical damping ratio contribution comparison, low frequency (LF) and high frequency (HF) ranges.

In the above assessment the damping ratio at low frequencies contains contributions from nonlinear interactions at wave frequencies. In a surge free vibration response the vessel will oscillate at its surge natural frequency without nonlinear contributions from wave frequencies. In order to quantify the damping level without the nonlinear contribution, the mooring forces associated with a single frequency forced vessel displacement were calculated. The single frequency selected corresponds to the

slow drift resonance response, in this case 0.0053Hz. At this frequency the floater was oscillated in surge with an amplitude of 30 m. Following the procedure to assess the damping contributions, Table 4.4 summarizes the results for the equivalent and prototype mooring systems and for the hull, for single frequency vessel motion at 0.0053Hz.

The model tests are designed and executed based on Froude number similarity with the full scale prototype, which leads to a Reynolds number difference for the viscous forces on the model hull relative to the full scale prototype hull. This Reynolds number difference implies that the drag forces on the model and prototype hulls will be different, which means that the drag coefficients for the hull will be different. For this study case, the floater's hull damping contribution is calculated considering the drag coefficient (*Cd*) at the model scale based on the plot of drag coefficient (*Cd*) vs Reynold's number (*Re*) for various values of Keulegan-Carpenter's number (*KC*) developed by Sarpkaya (1976). The Keulegan-Carpenter's number is calculated as $KC=2\pi A/D$, where: A is the motion displacement amplitude and D is the cylinder diameter associated with the column or pontoon. The Reynold's number is calculated as $Re=U_m D/\nu$, where: $U_m = A\omega$ (U_m is the characteristic velocity, A is the motion displacement amplitude and ω is the motion circular frequency) and ν is the water's kinematic viscosity. With the calculated values of KC and Re, the drag coefficients for the columns and pontoons may be determined from Sarpkaya's plot.

Table 4.4 indicates that the damping contribution of the equivalent mooring systems at the slow drift frequency is pretty small (critical damping ratio of 0.455% for the symmetric equivalent mooring system and 0.464% for the non-symmetric equivalent

mooring system) compared with the hull damping contribution (critical damping ratio of 12.6%). The damping contribution for the prototype mooring system (critical damping ratio of 9.3%) is more significant compared with the hull contribution at this frequency.

Table 4.4. Damping contributions comparison at slow drift resonance response, polyester mooring system.

SYSTEM	Damping Contribution	
	Coefficient (kN s/m)	Critical Damping Ratio (%)
Prototype Mooring System	1,581	9.304
Equivalent Symmetric Truncated Mooring System (PM-S-C3)	77.28	0.455
Equivalent Non-Symmetric Truncated Mooring System (PM-N-C1)	78.91	0.464
Floater's Hull	2,135	12.562

Regardless of the way the mooring system damping is quantified, it is evident that the damping contributed by the equivalent mooring systems is much less than that contributed by the prototype mooring system, although the majority of the damping of the slow drift surge motion is derived from the drag forces on the hull. In a model test situation with the statically equivalent polyester mooring it appears that the slow drift motion will be larger than that associated with the prototype mooring.

4.3.2 Steel Wire Mooring System

The prototype for this study case, as it is described in Chapter III, section 3.3.2, is a semisubmersible with a steel wire mooring system, with a configuration of four groups of four mooring lines, and this semisubmersible is deployed in 1,900m water depth. The statically equivalent mooring systems selected for the dynamic analysis are: SM-SC-C3 for the symmetric case and SM-NC-C1 for the non-symmetric case. The steel wire mooring system prototype configuration is shown in Figure 3.25, the prototype semisubmersible and mooring line properties are included in Table 3.13, and the fairlead and anchor coordinates are included in Table 3.14. The main design characteristics for the equivalent mooring systems are included in Table 3.15. The fairlead and anchor coordinates for the equivalent symmetric mooring system SM-SC-C3 are listed in Table 3.18 and the mooring line characteristics are included in Table 3.19. The fairlead and anchor coordinates for the equivalent non-symmetric mooring system SM-NC-C1 are listed in Table 3.20 and the mooring line properties for this case are included in Table 3.22.

The additional data used for developing the dynamic simulations in Orcaflex are provided in Table 4.5.

Initially the effect of the Morison added mass and damping coefficients was investigated, as for the polyester mooring system. Three time domain simulations were executed for each one of the prototype, the symmetric equivalent (SM-SC-C3) and the non-symmetric equivalent (SM-NC-C1) mooring systems using a forced vessel motion

represented by the realistic spectrum (RS-S). The differences in the mooring system models are:

Table 4.5. Steel wire mooring system, additional data required for the dynamic simulations in Orcaflex.

Mooring System	Segment	Outer Diameter (m)	Mass per unit length (t/m)	Drag Coefficient (C_d)	Added Mass Coefficient (C_m)
Prototype	Platform chain	0.22340	0.30660	1.2	1.0
	Steel wire rope	0.13600	0.06994	1.2	1.0
	Anchor chain	0.20620	0.26190	1.2	1.0
Equivalent symmetric, SM-SC-C3	Load cell	1.06978	6.20228	1.2	1.0
	Chain segments	0.53371	1.76393	1.2	1.0
	Spring	0.68642	2.90460	1.2	1.0
Equivalent non-symmetric, SM-NC-C1	Load cell	1.06978	6.20228	1.2	1.0
	Chain segments	0.53371	1.76393	1.2	1.0
	Upwind springs	0.68642	2.90460	1.2	1.0
	Downwind springs	0.74895	3.45664	1.2	1.0

A) the first model considers the added mass (C_m) and damping (C_d) coefficients for the mooring lines components, shown in Table 4.5.

B) the second model just considers the damping coefficient (C_d) for the mooring line components as shown in Table 4.5 (C_m is set to zero);

C) the third model just considers the added mass coefficient (C_m) for the mooring line components as shown in Table 4.5 (C_d is set to zero).

Figure 4.37 compares for the prototype mooring system the total force (a), restoring force (b), and dynamic force (inertia and damping force) (c) time series for a snapshot from 2000 seconds up to 2050 seconds. For the total force (a) and dynamic force

(c), the effect of just considering the mooring line drag (C_d) is similar to the effect of considering both the added mass and drag (C_m+C_d), while considering just the added mass (C_m) without the drag results in a large difference in the total and dynamic horizontal force exerted by the mooring system.

Figure 4.38 shows the power spectra for the total force (a), restoring force (b), and dynamic force (c), for the low frequency (LF) and high frequency (HF) ranges. As it is mentioned above, the effect of considering just the mooring line drag (C_d) is similar to the effect of including both the added mass and drag (C_m+C_d). Therefore, based on these observations, it is concluded that, for this study case, the prototype mooring system contribution to the dynamic force and, indeed, to the total force, is dominated by the mooring line drag coefficient (C_d). Considering just the prototype response using the C_d and C_m coefficients listed in Table 4.5, Figure 4.38 shows that at low frequencies the dynamic mooring force contribution is of the same magnitude as the mooring restoring force. At wave frequencies, the dynamic force contribution is much larger than the restoring force in the total force exerted by the mooring system. Evidently for the steel mooring system the weight of the mooring lines plays an important role in the total force exerted by the mooring system.

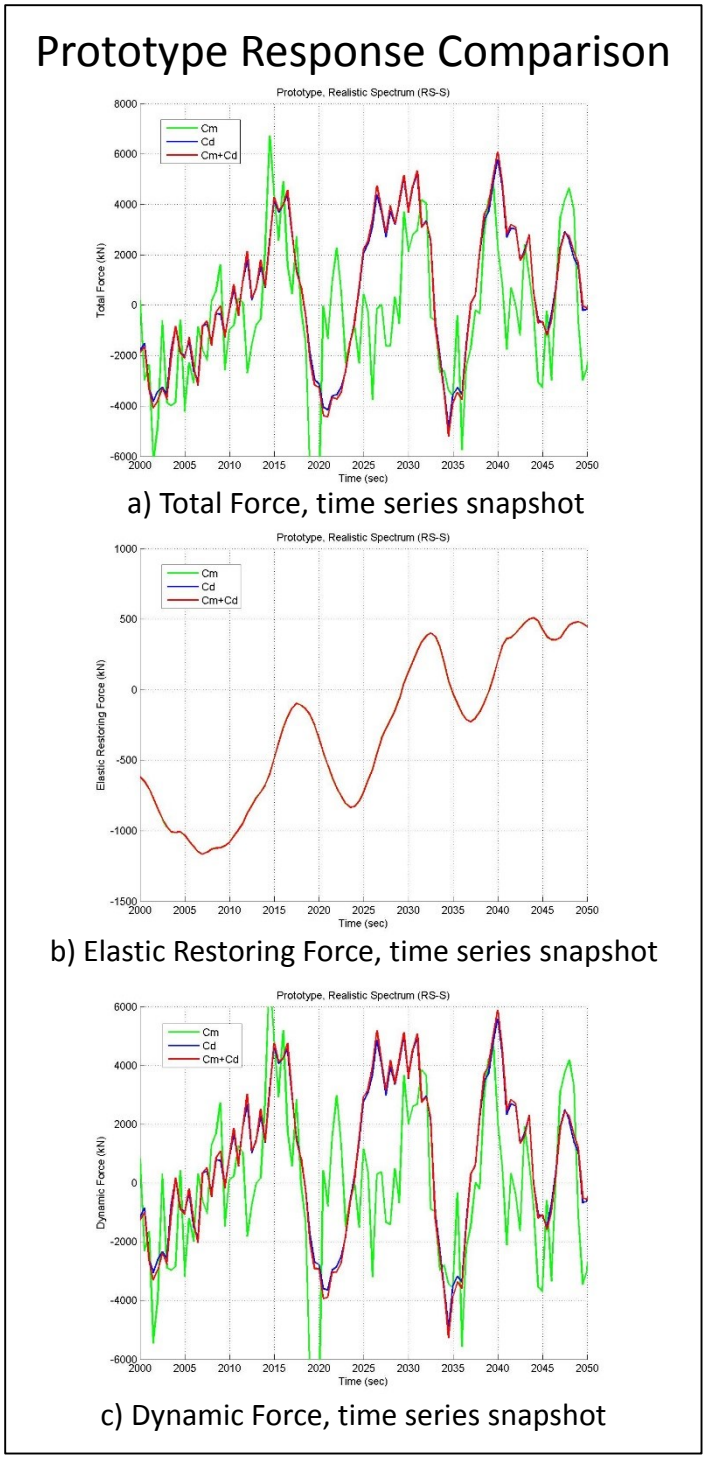

Figure 4.37. Prototype response comparison, force time series snapshot, steel wire mooring system.

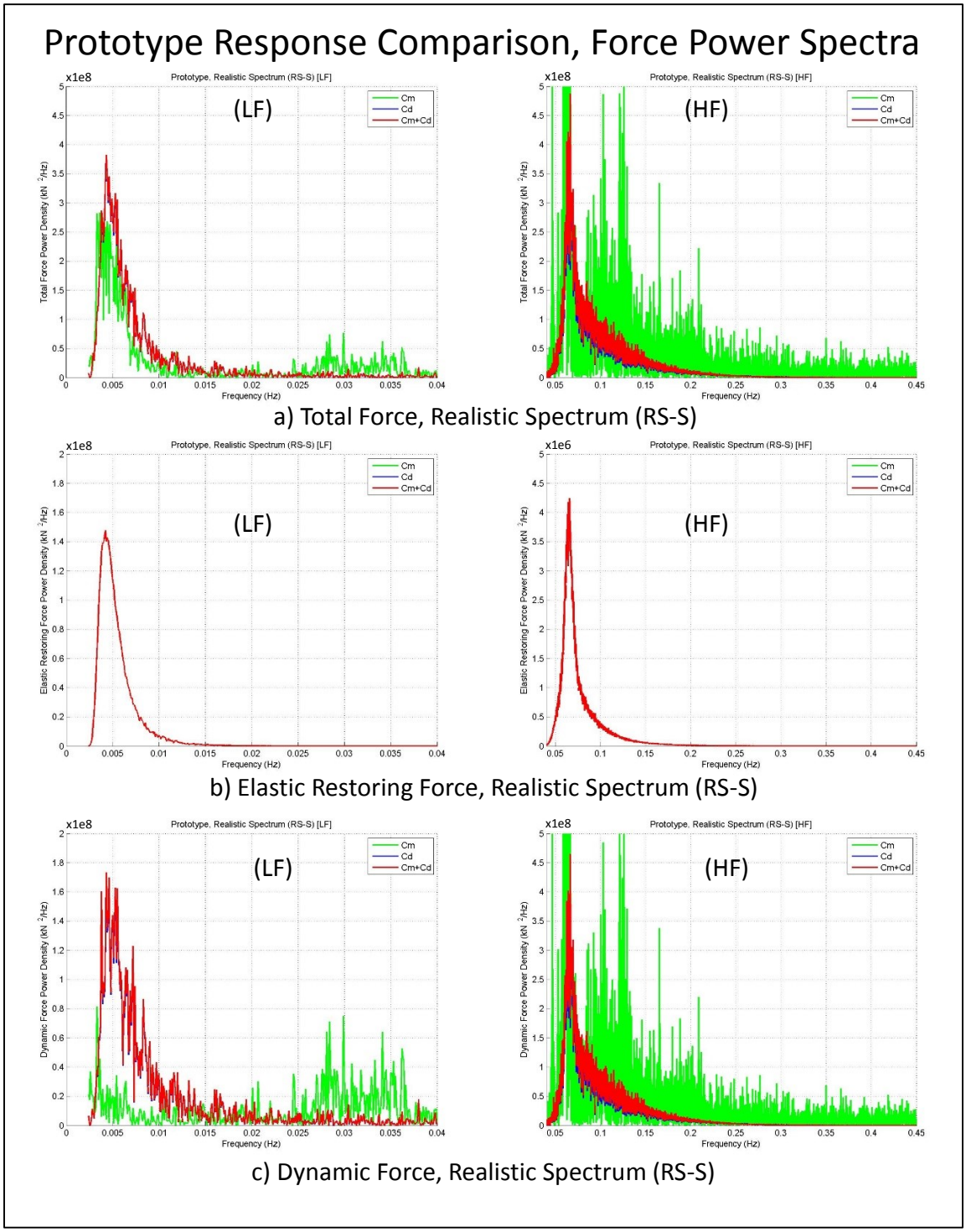

Figure 4.38. Prototype response comparison, force power spectra, low frequency (LF) and high frequency (HF) ranges, steel wire mooring system.

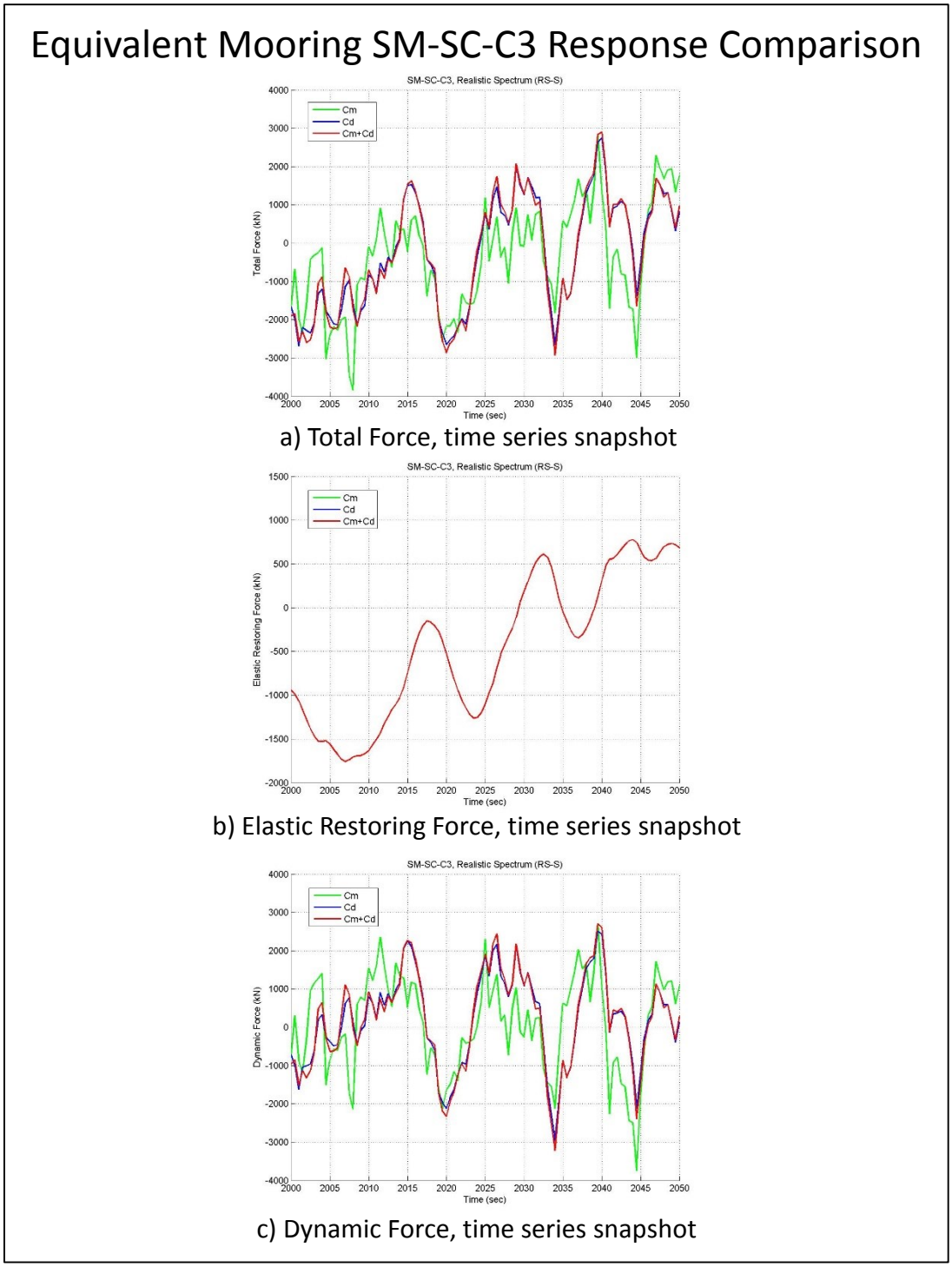

Figure 4.39. Equivalent mooring system (SM-SC-C3) response comparison, force time series snapshot

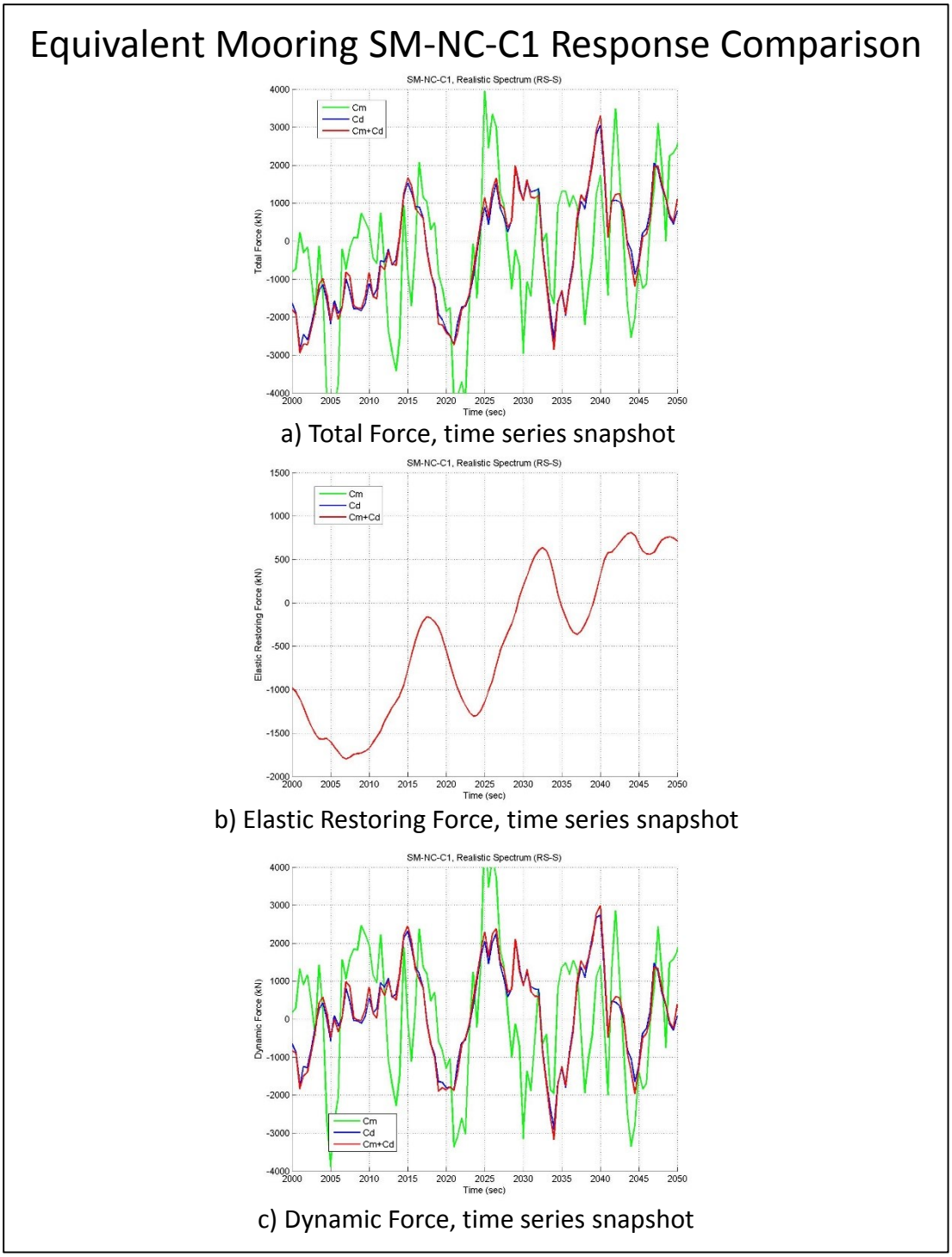

Figure 4.40. Equivalent mooring system (SM-NC-C1) response comparison, force time series snapshot.

Figure 4.39 and Figure 4.40 compare for the equivalent mooring systems SM-SC-C3 and SM-NC-C1, respectively, the total force (a), restoring force (b), and dynamic force (c) time series for a snapshot from 2000 seconds up to 2050 seconds, for the cases where the imposed vessel motion is a realistic spectrum (RS-S). As for the prototype response, in the total force (a) and dynamic force (c) the effect of just considering the mooring line drag (C_d) is similar to the effect of considering both the added mass and drag (C_m+C_d), while considering just the added mass (C_m) without the drag results in a large difference in the total and dynamic horizontal force exerted by the mooring system.

Figure 4.41 and Figure 4.42 for the equivalent mooring system SM-SC-C3 and SM-NC-C1, respectively, compare the power spectrum of the total force (a), restoring force (b), and dynamic force (c), for the low frequency (LF) and high frequency (HF) ranges. As for the prototype response, the effect of considering just the mooring line drag (C_d) is similar to the effect of including both the added mass and drag (C_m+C_d). Therefore, as for the prototype response, for this study case the equivalent mooring system contribution to the dynamic force and to the total force is dominated by the mooring line drag coefficient (C_d). Considering just the equivalent mooring system responses using C_d and C_m shown in Table 4.2, at low frequencies the restoring force is the main component in the total force, while the dynamic force contribution is considerably smaller than the mooring restoring force. On the other hand, in the wave frequency range the dynamic force contribution is considerably larger than the mooring restoring force.

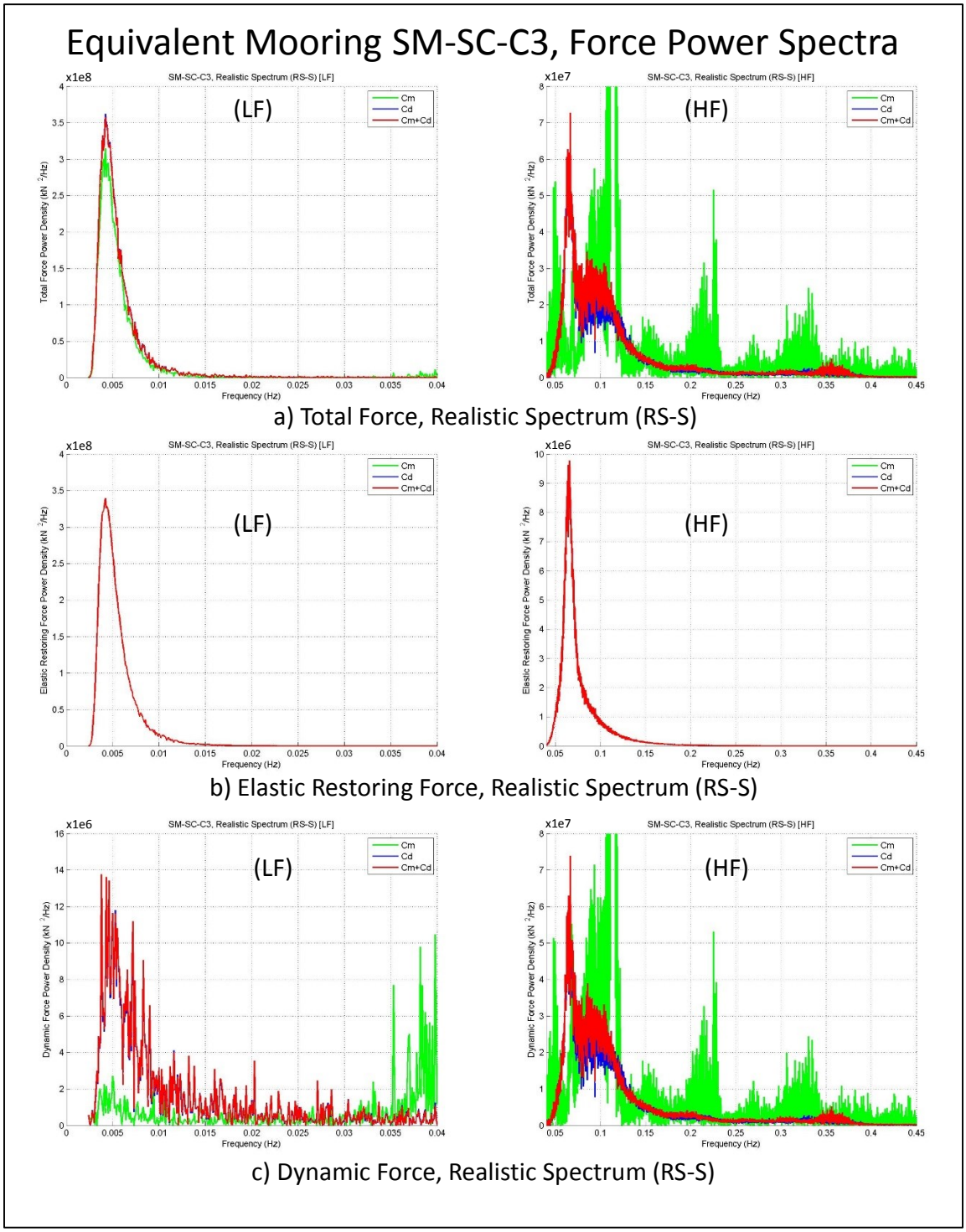

Figure 4.41. Equivalent mooring system (SM-SC-C3) response comparison, force power spectra, low frequency (LF) and high frequency (HF) ranges.

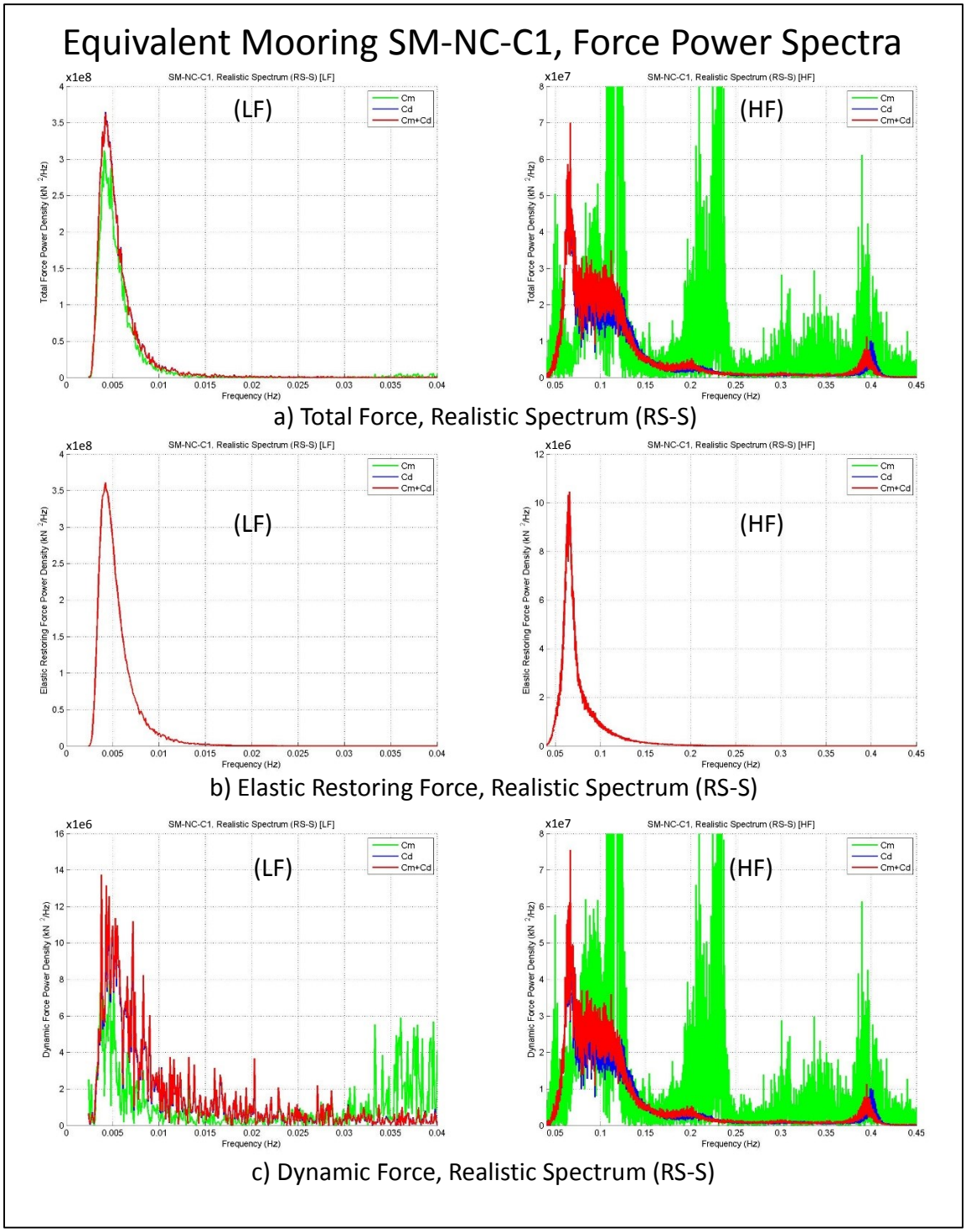

Figure 4.42. Equivalent mooring system (SM-NC-C1) response comparison, force power spectra, low frequency (LF) and high frequency (HF) ranges.

In the following figures are plotted the results comparison for the prototype mooring system and the two equivalent mooring systems selected for this study case to assess the inertia and damping contributions.

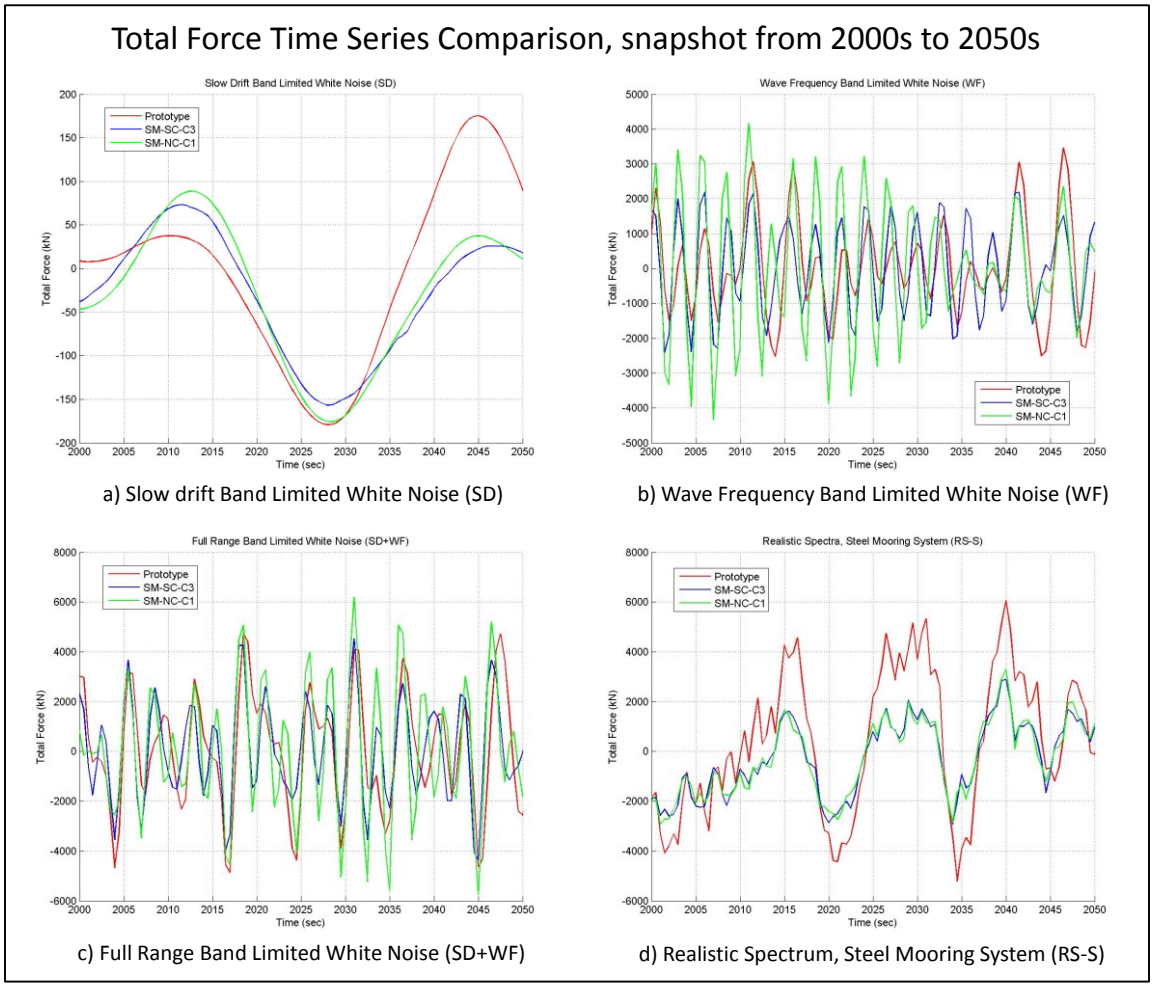

Figure 4.43. Total force time series comparison snapshot, steel wire mooring system.

In Figure 4.43 is shown the total horizontal force time series comparison for the four different displacement excitations for a snapshot from 2000 second up to 2050 seconds. It is evident that the total mooring force is quite different for the three mooring systems, for each of the vessel surge spectra considered.

The restoring force response of the equivalent mooring systems is also different than the prototype restoring force for the four different displacement excitations considered, as is shown in Figure 4.44. The differences in the restoring force are related to the design of the equivalent mooring systems which considers the static response of the floater for three degrees of freedom (surge, heave and pitch), while the dynamic simulations considered just the motion in the surge direction around a mean offset position with setdown and pitch set equal to zero. The more important factor responsible for the difference in, the restoring forces is that the design of the equivalent mooring systems neglected the friction between the mooring lines and the seabed whereas this effect is considered in the dynamic simulations. For equivalent steel mooring systems where there will be a tendency to have long lengths of chain lying on the basin floor it will be important to consider the frictional force.

The dynamic horizontal force exerted by the prototype mooring system is quite different than that exerted by the two equivalent mooring systems considered for this study case, as is shown in the time series snapshots in Figure 4.45.

The power spectra for the total force, shown in Figure 4.46, are completely different for almost any frequency for the different displacement excitations considered. For the total force response associated with the realistic spectrum, there is a good

correlation in the power spectral density values at low frequencies (less than 0.03Hz). The total force power spectral density values for the equivalent mooring systems (Figure 4.46.d at low frequencies) in this frequency range are dominated by the restoring force contribution (Figure 4.47.d), so the dynamic force contributions for the equivalent mooring systems are small (Figure 4.48.d). On the other hand, the prototype restoring force response is smaller than that for the equivalent mooring systems but the prototype dynamic force response is much larger than that for the equivalent mooring systems, so there is a good correlation in the total force at those low frequencies between the equivalent and the prototype mooring system.

The power spectra for the restoring force and dynamic force exerted by the equivalent mooring systems are completely different than those for the prototype, for almost any frequency in the range considered, as is shown in Figure 4.47 for the restoring force and in Figure 4.48 for the dynamic force.

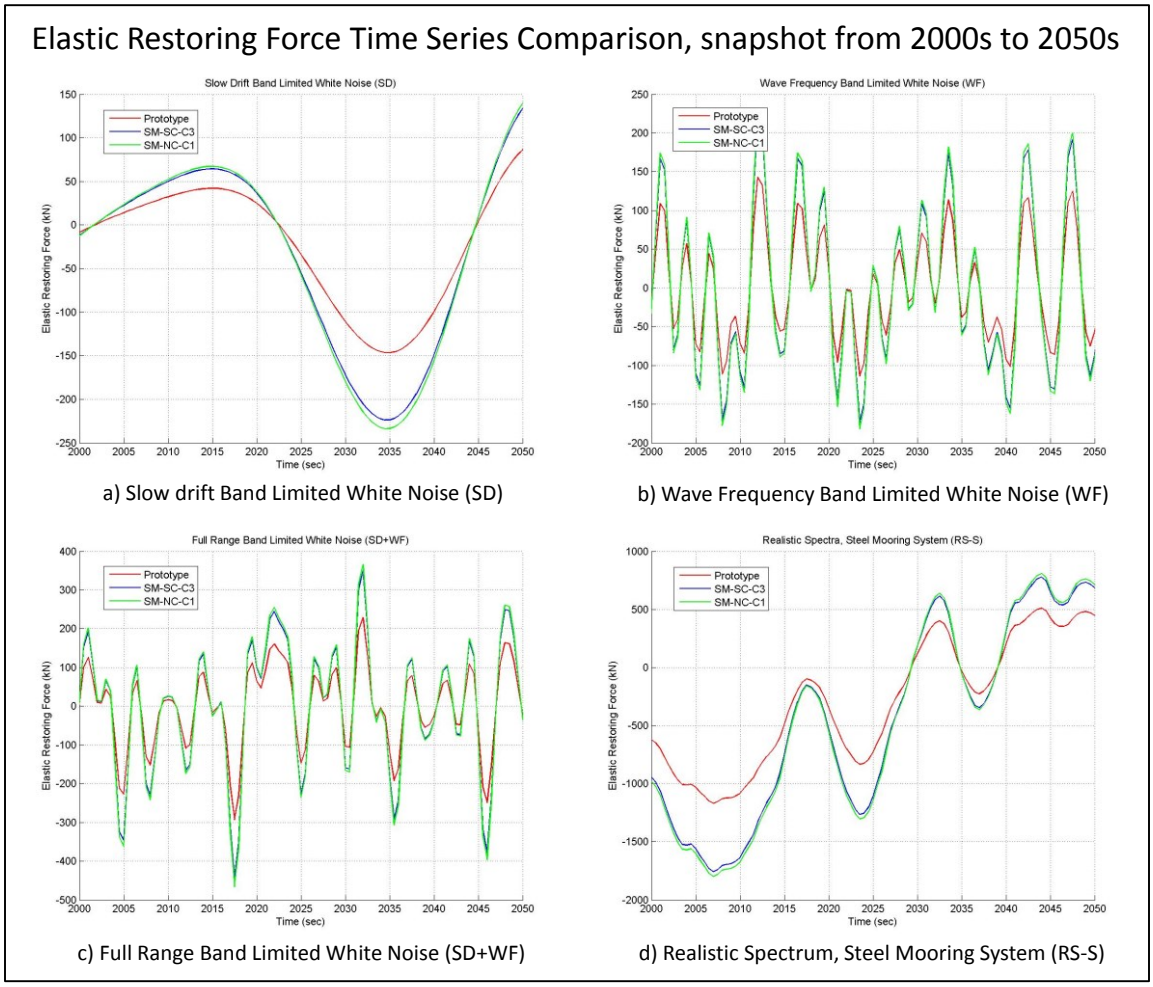

Figure 4.44. Restoring force time series comparison snapshot, steel wire mooring system.

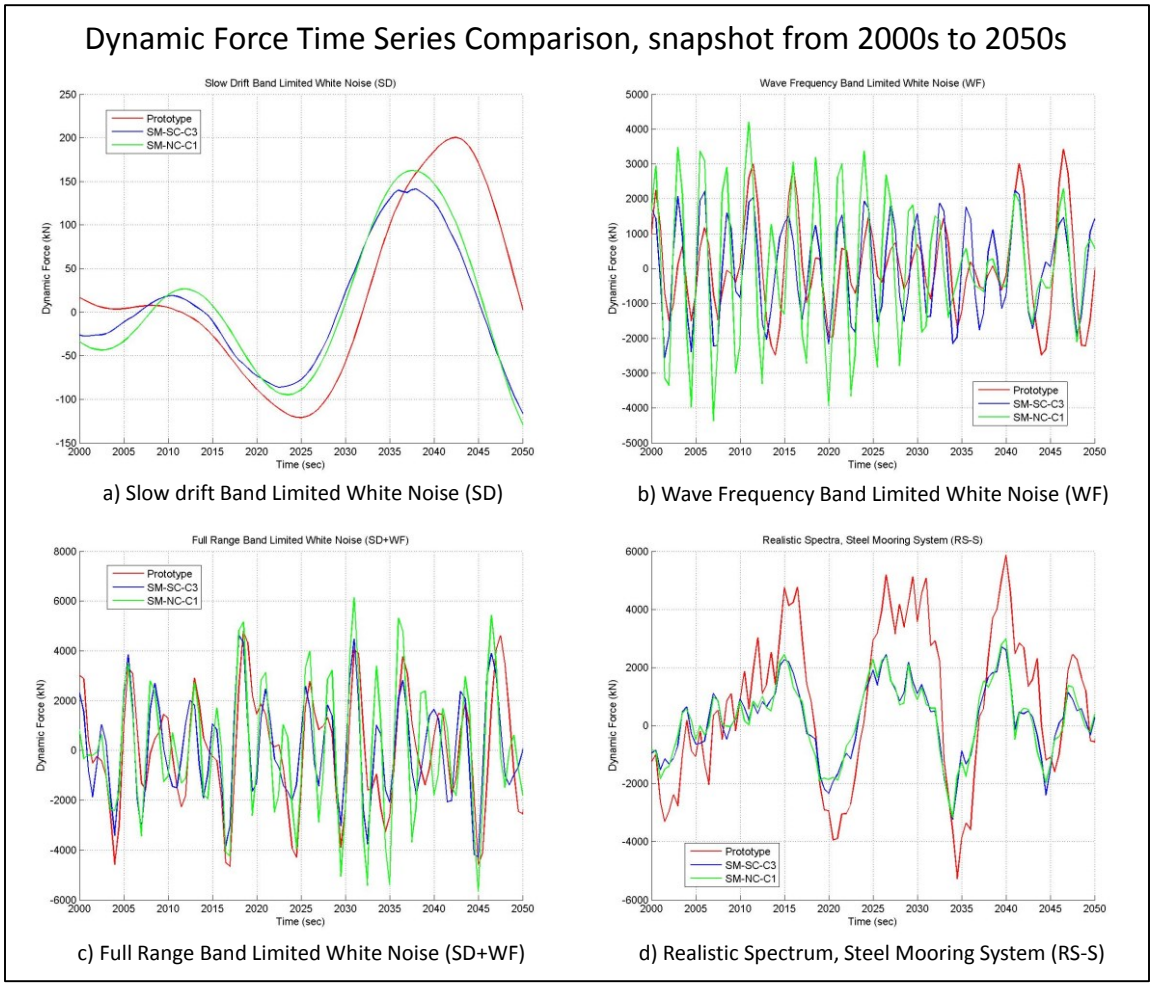

Figure 4.45. Dynamic force time series comparison snapshot, steel wire mooring system.

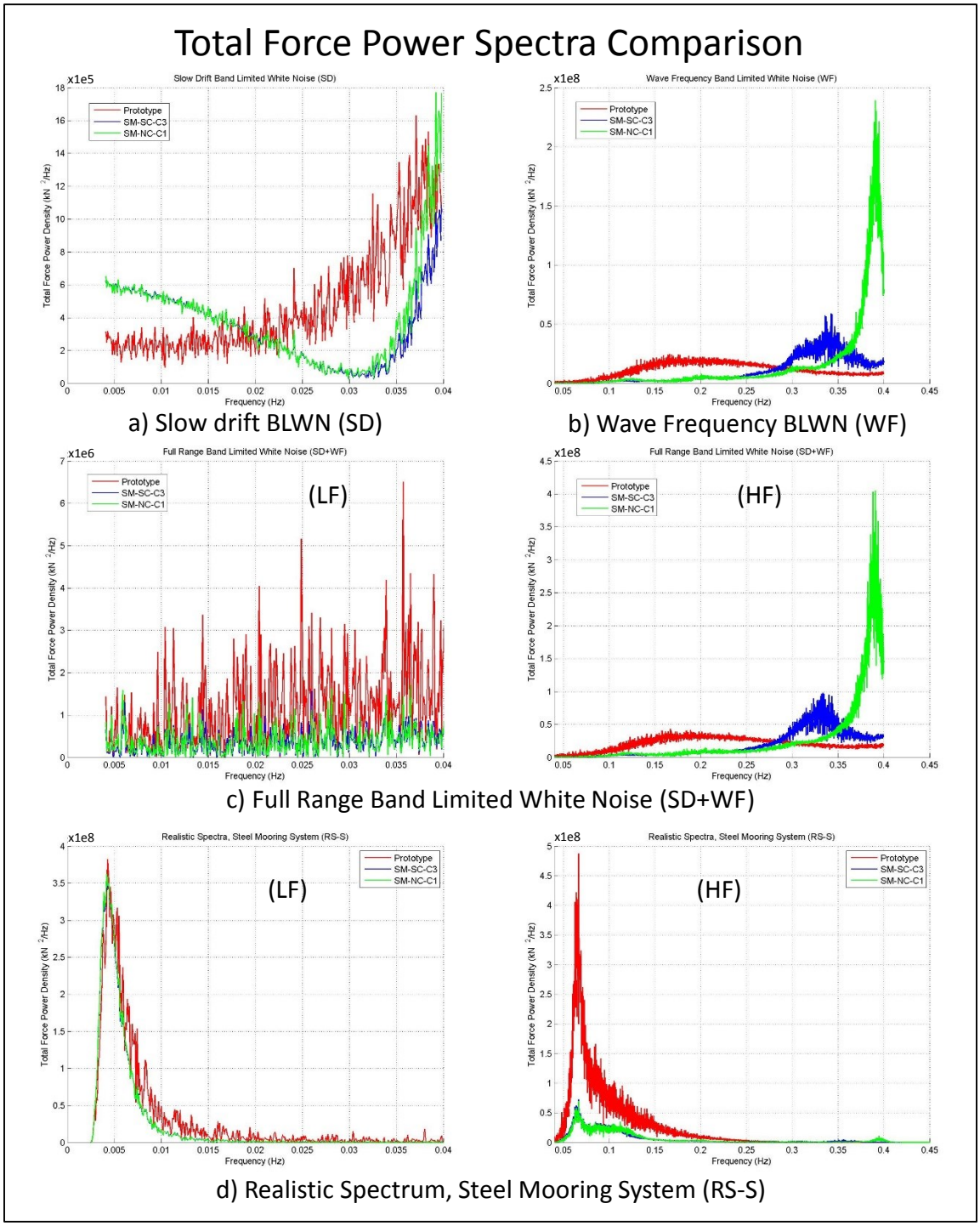

Figure 4.46. Total force power spectra comparison, steel wire mooring system.

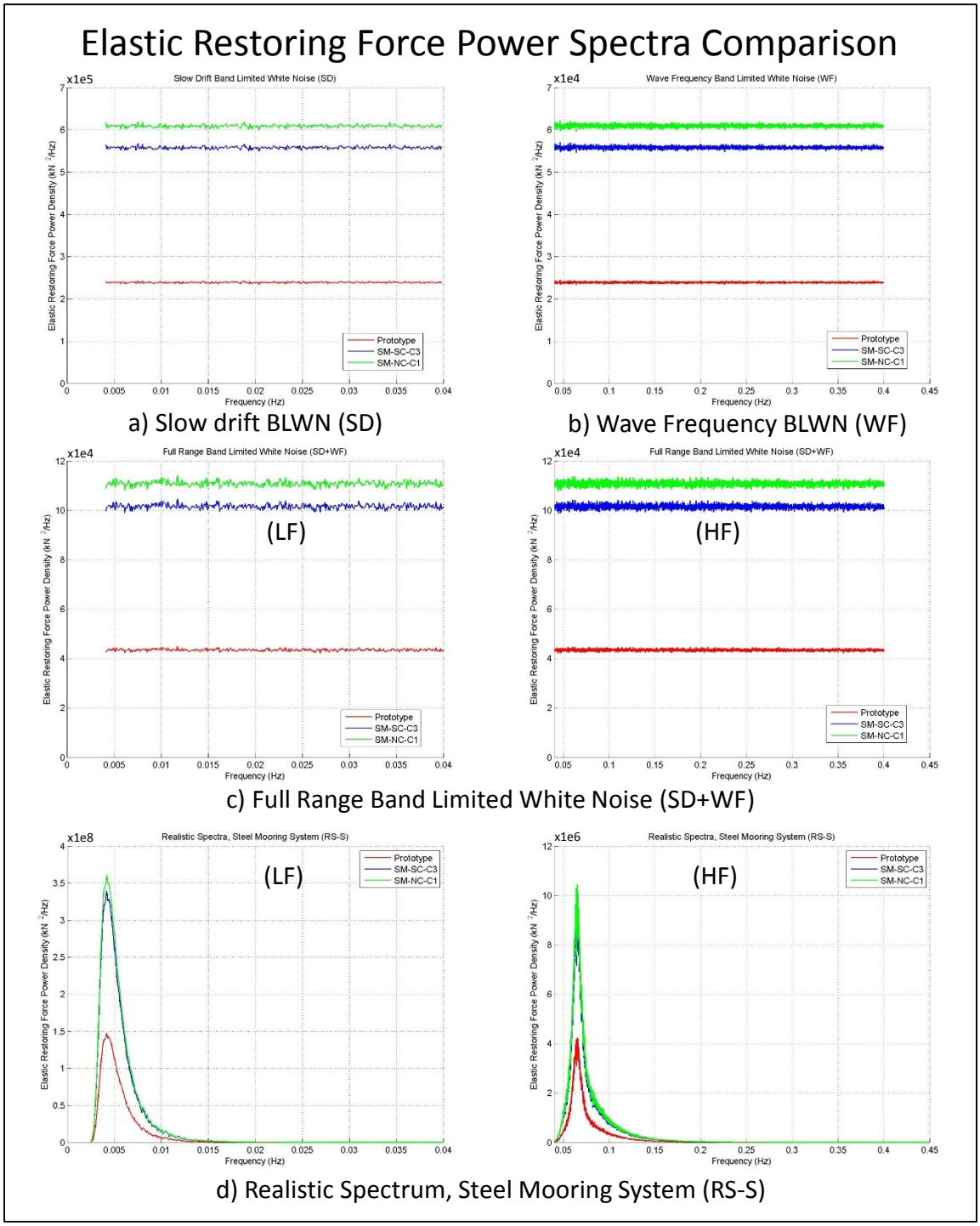

Figure 4.47. Restoring force power spectra comparison, steel wire mooring system.

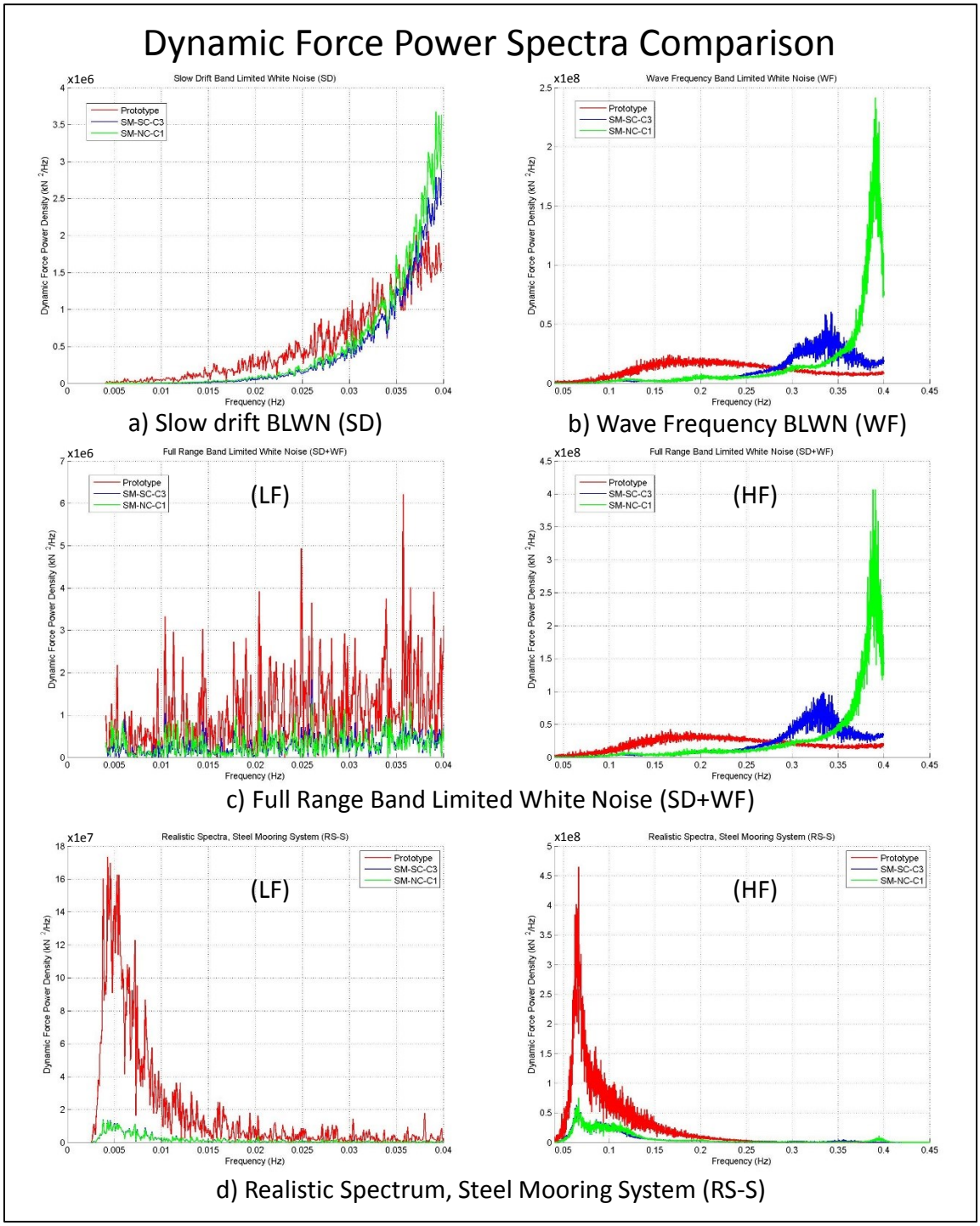

Figure 4.48. Dynamic force power spectra comparison, steel wire mooring system.

Once the dynamic force time series are calculated for each one of the four different simulations considered in this study case, the dynamic force decomposition procedure described previously in this chapter (Section 4.2) is applied. So, the mooring system inertia and damping factors are calculated, and those factors are compared between the equivalent mooring systems and the prototype. As expected from the previous comparisons of the dynamic force time series and the dynamic force power spectra, the inertia (Figure 4.49) and damping (Figure 4.50) factors are different for the entire frequency range considered.

There is an observation that must be highlighted, at least for the equivalent mooring system responses. There is a correlation at high frequencies (higher than 0.1 Hz) between an abrupt change in the inertia factor and a peak in the damping factor and this peak is also correlated with a peak in the dynamic force power spectrum. For example, considering the non-symmetric equivalent mooring system (SM-NC-C1) response, there is an abrupt change in the inertia factor around 0.38 Hz (Figure 4.49) and there is a peak in the damping factor (Figure 4.50) around the same frequency; there is also a peak around this frequency in the dynamic force power spectrum (Figure 4.48). Similarly, the symmetric equivalent mooring SM-SC-C3 has an abrupt change in the inertia factor around 0.35 Hz (Figure 4.49), and a peak in the damping factor (Figure 4.50) and dynamic force power spectrum (Figure 4.48) around the same frequency.

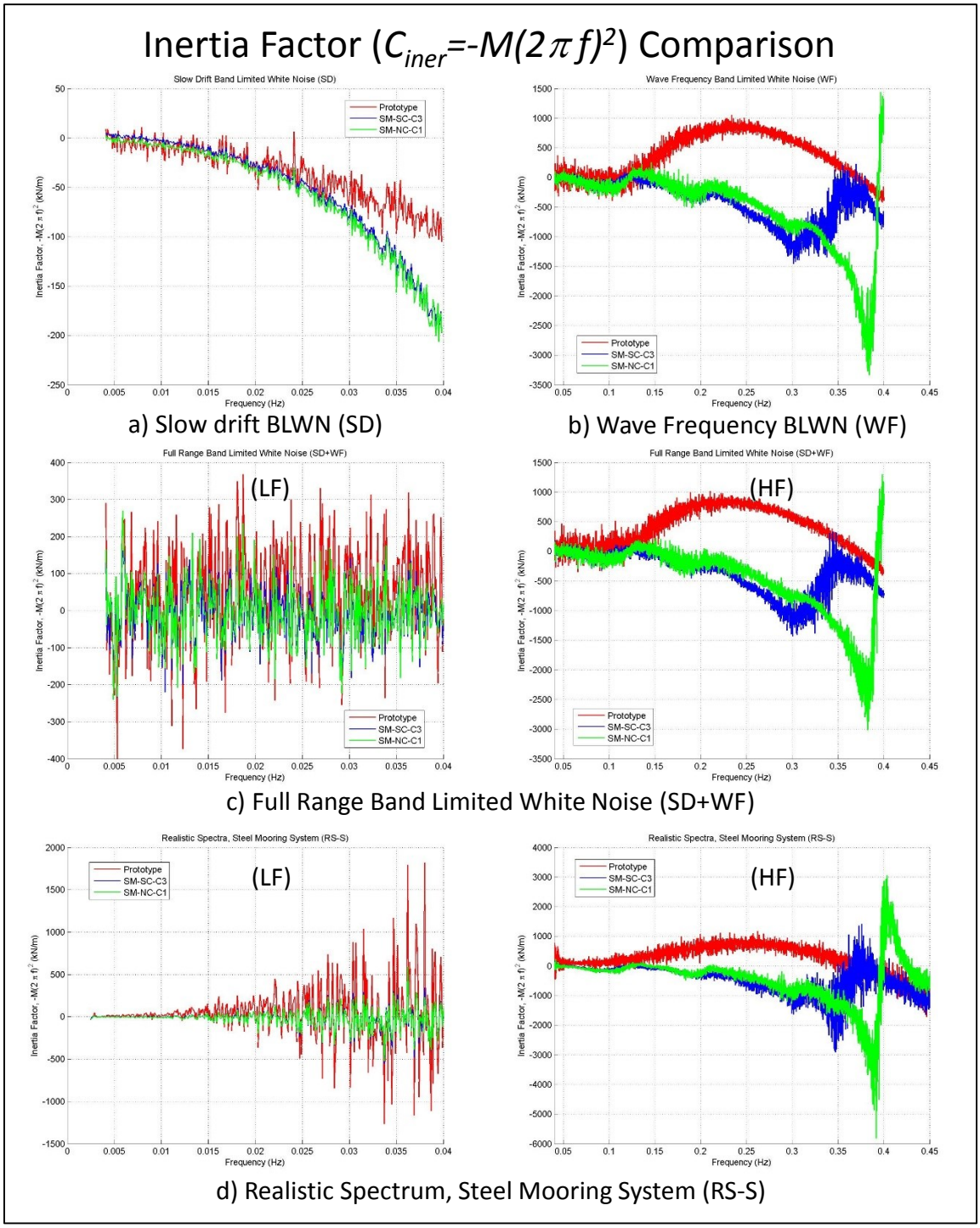

Figure 4.49. Inertia factor (C_{iner}) comparison, steel wire mooring system.

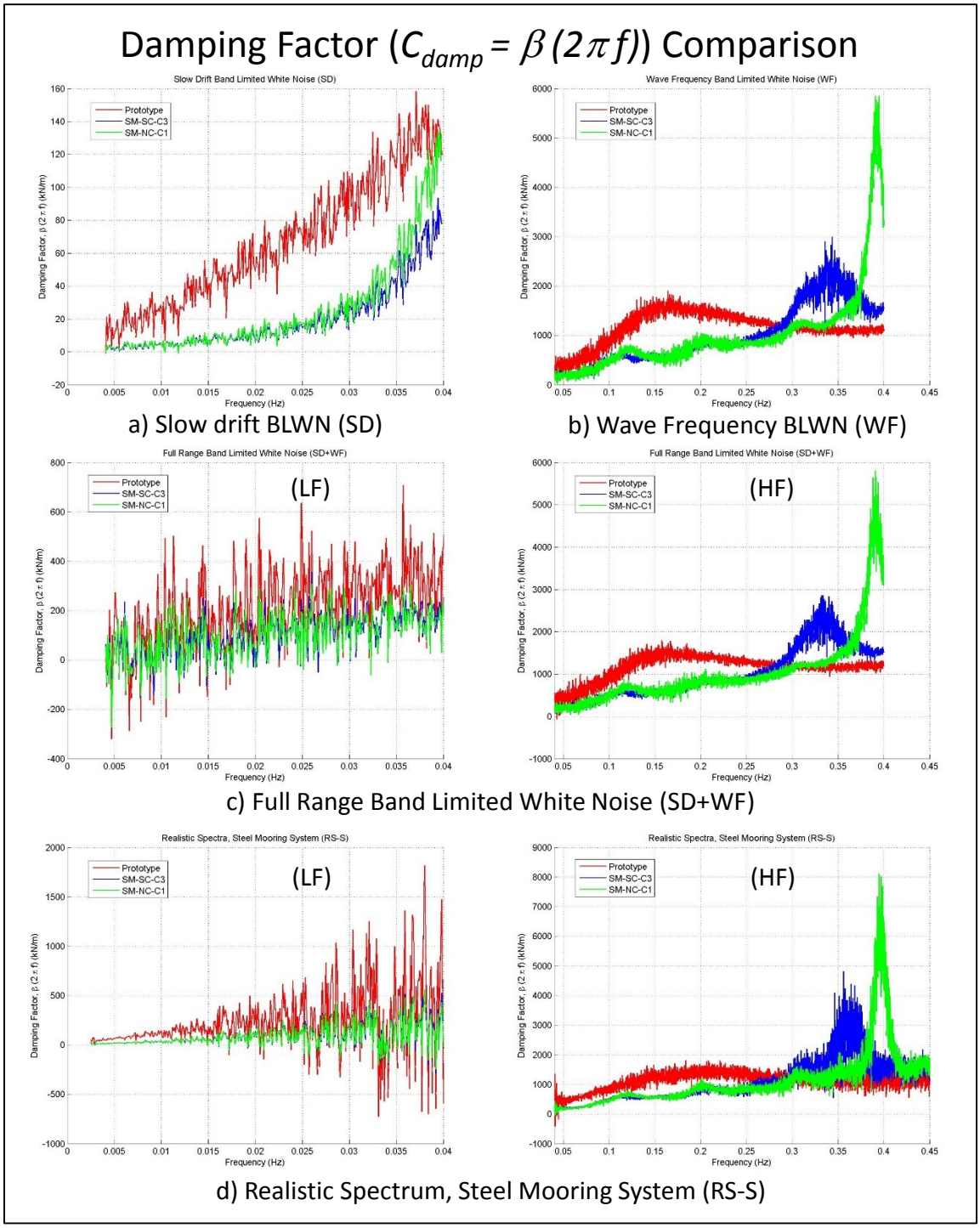

Figure 4.50. Damping factor (C_{damp}) comparison, steel wire mooring system.

The mooring system inertia force and damping force contribution time series are calculated based on the inertia and damping factors shown in Figure 4.49 and Figure 4.50, respectively, and the excitation displacement Fourier coefficients, applying the procedure described previously in Section 4.2.

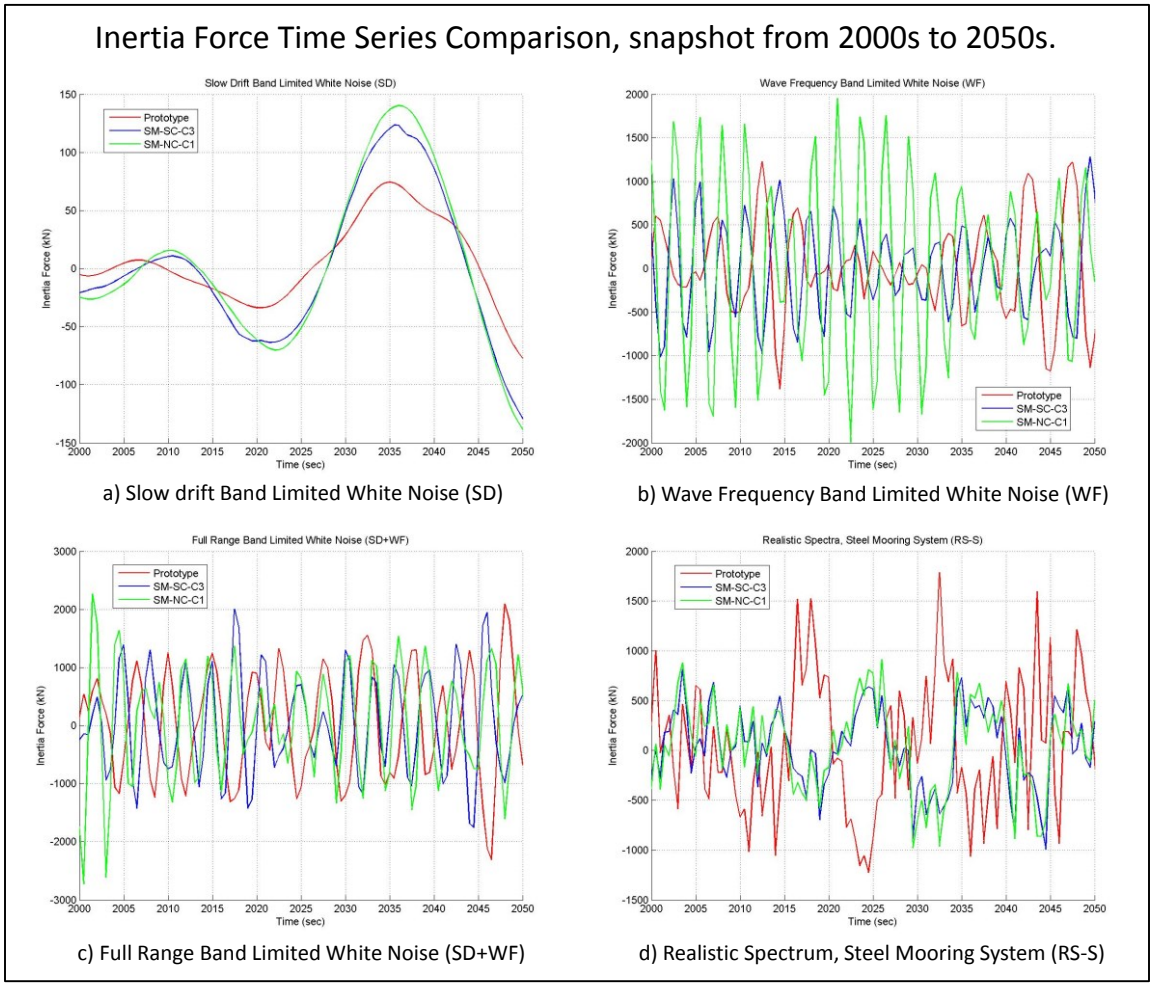

Figure 4.51. Inertial force contribution time series comparison snapshot, steel wire mooring system.

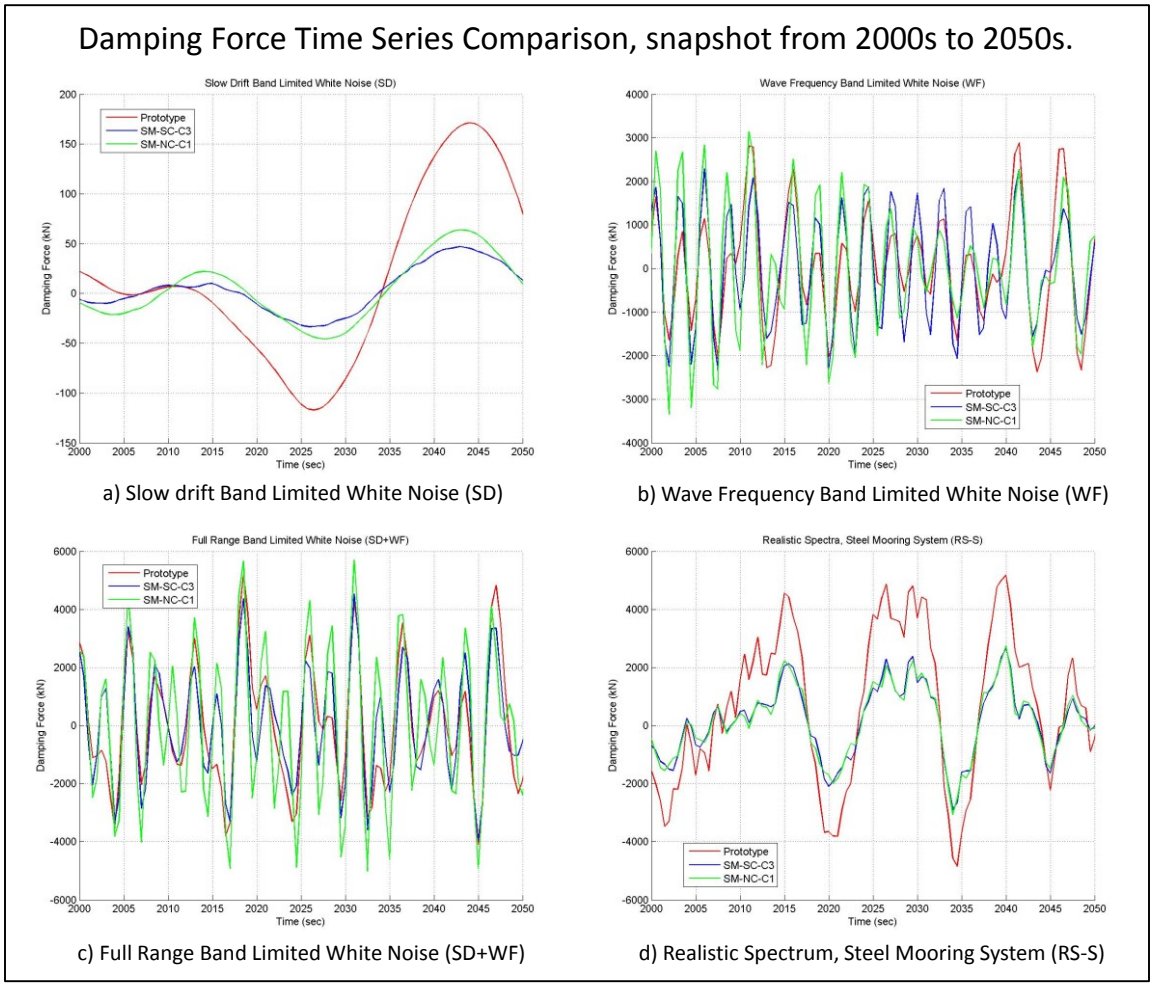

Figure 4.52. Damping force contribution time series comparison snapshot, steel wire mooring system.

The mooring system inertia force and damping force contribution time series are shown in Figure 4.51 and Figure 4.52, respectively. The equivalent mooring system inertia and damping force contributions are quite different than those of the prototype, for each one of the four forced excitations considered.

In Figure 4.53 are shown the mooring system inertia and damping contributions to the dynamic force at low and high frequencies for each one of the three mooring systems considered in this study using the realistic spectrum vessel displacement. The damping force contribution is the main component of the dynamic force at any frequency related with the slow drift motion and in the wave frequency range. The dynamic horizontal force exerted by the mooring systems is clearly damping dominated, with the inertia contribution being noticeably smaller than the damping contribution.

The comparisons of the power spectra for the mooring system inertia and damping force contributions are shown in Figure 4.54 and Figure 4.55, respectively. The power spectra are quite different for the equivalent mooring system response compared with the prototype mooring system response, for almost all the frequency range. Looking at the realistic spectrum vessel displacement, it is evident that the energy levels associated with the prototype mooring system inertia and damping forces are larger than those associated with the equivalent mooring systems, at slow drift frequencies and at wave frequencies.

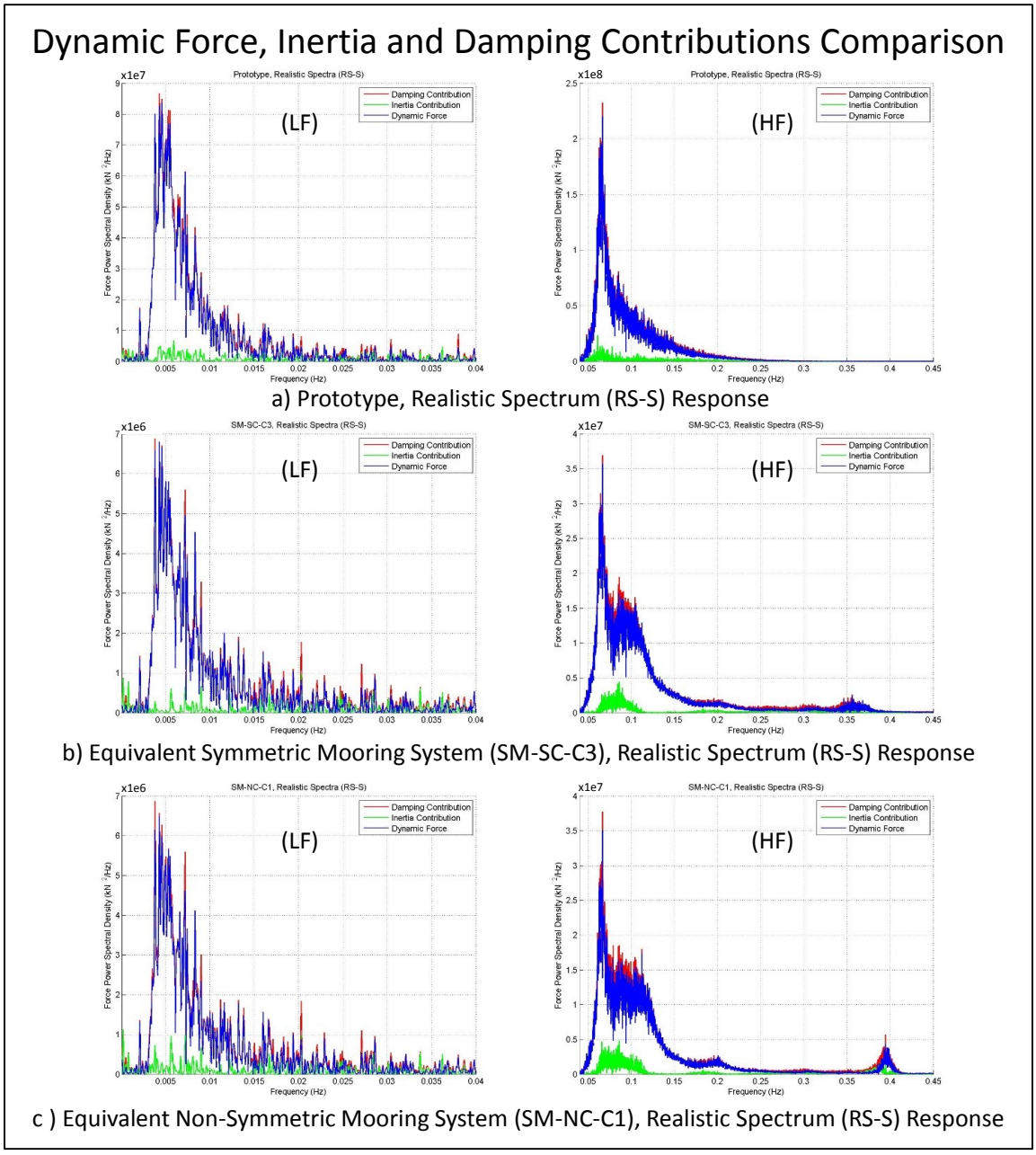

Figure 4.53. Dynamic force component, inertia and damping contributions comparison, steel wire mooring system.

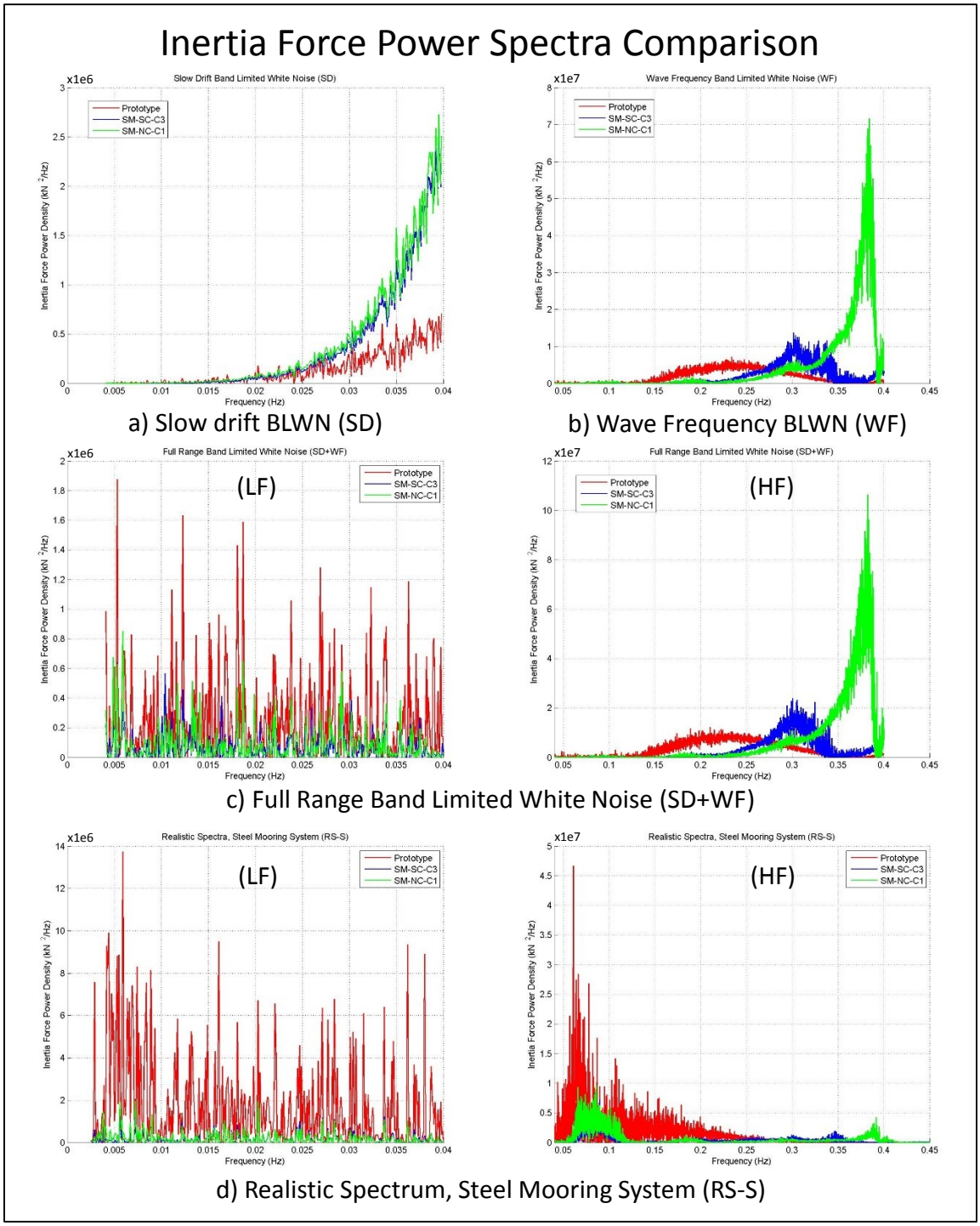

Figure 4.54. Inertia force contribution power spectrum comparison, steel wire mooring system.

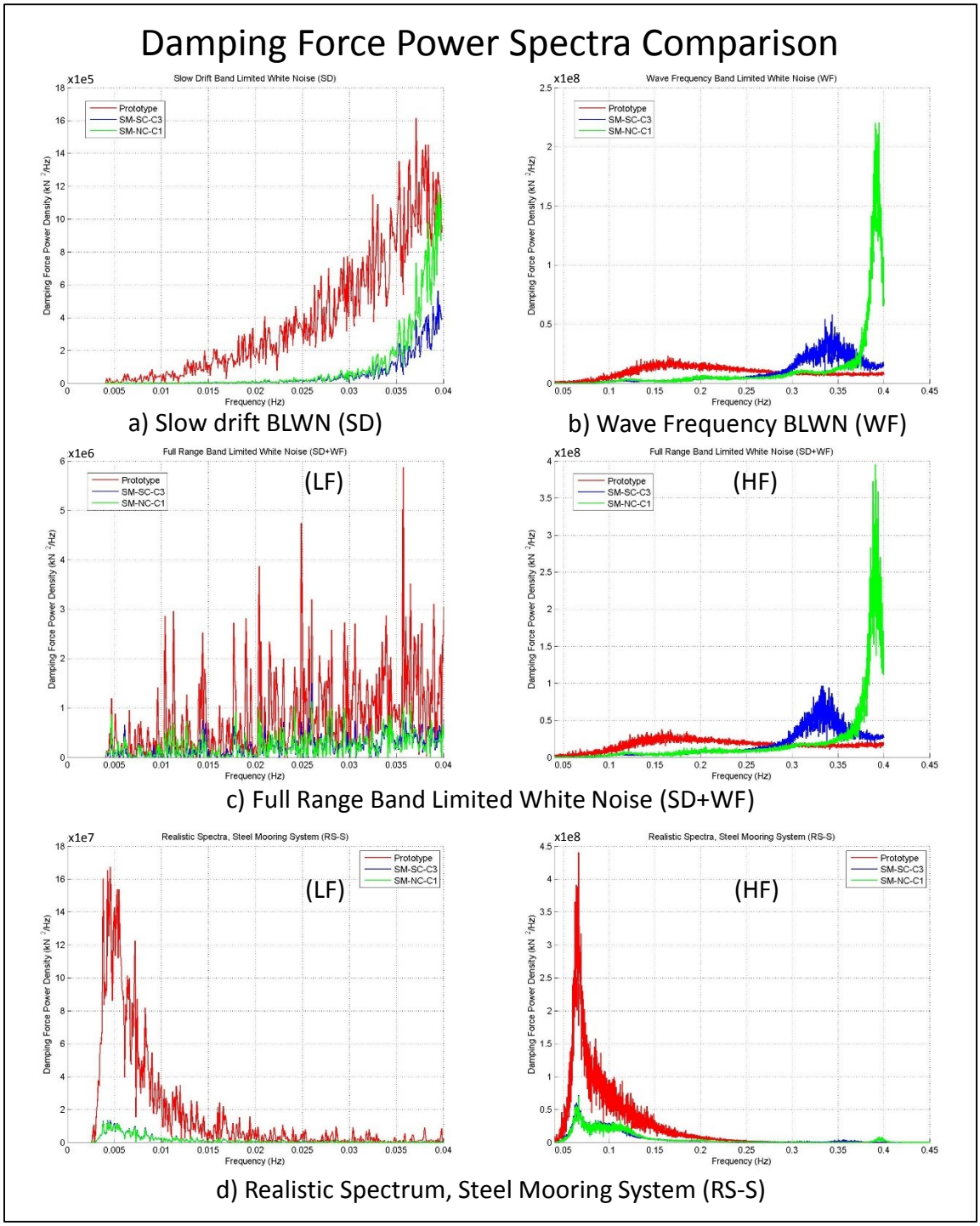

Figure 4.55. Damping force contribution power spectrum comparison, steel wire mooring system.

In the following figures are shown the comparison of the mooring system force contribution Response Amplitude Operators (RAO's) for each one of the mooring systems considered. The response comparison for each one of the mooring system is taking into account the different energy levels for the excitation displacement at each frequency f; those different energy levels for the excitation displacement are: slow drift band limited white noise (SD); wave frequency band limited white noise (WF); full range band limited white noise (SD+WF) and realistic spectrum (RS-S). For the prototype mooring system, Figure 4.56 compares the total force contribution response (a), the elastic restoring force contribution response (b), and the dynamic force contribution response. In the total force and dynamic force contributions there is a noticeable difference in the RAOs at low frequencies up to 0.05Hz, which reflects the non-linear response at those frequencies.

In Figure 4.57 and Figure 4.58 the RAOs for the symmetric and non-symmetric equivalent mooring systems, respectively, are compared. As for the prototype mooring, the total force and dynamic force RAOs present a noticeable difference at low frequencies depending on the type of displacement excitation, indicating a nonlinear relationship between excitation and response. The overlap in the RAOs in the wave frequency range is indicative of a linear relationship between the displacement excitation and the total and dynamic mooring force responses.

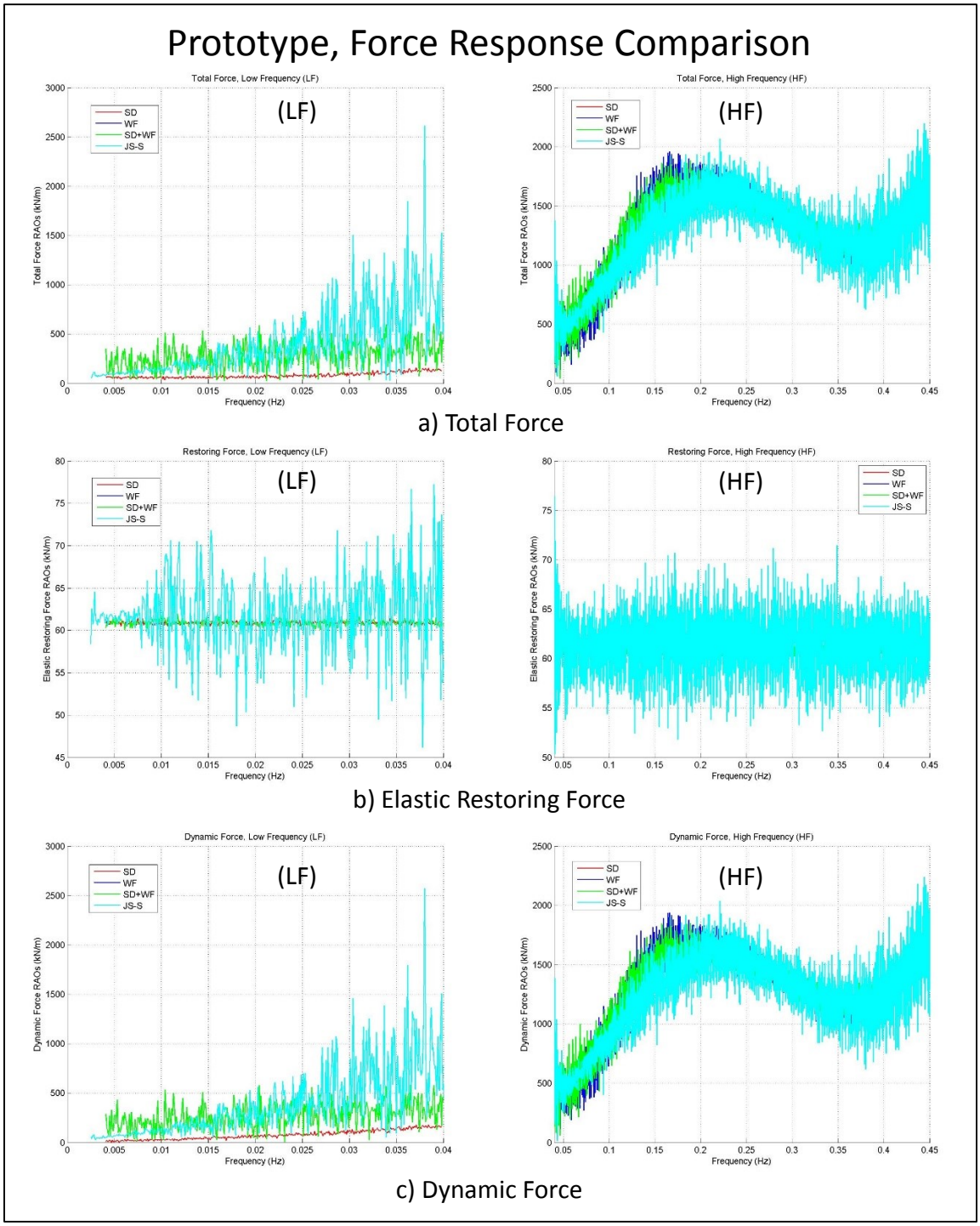

Figure 4.56. Prototype, force response amplitude operator comparison, steel wire mooring system.

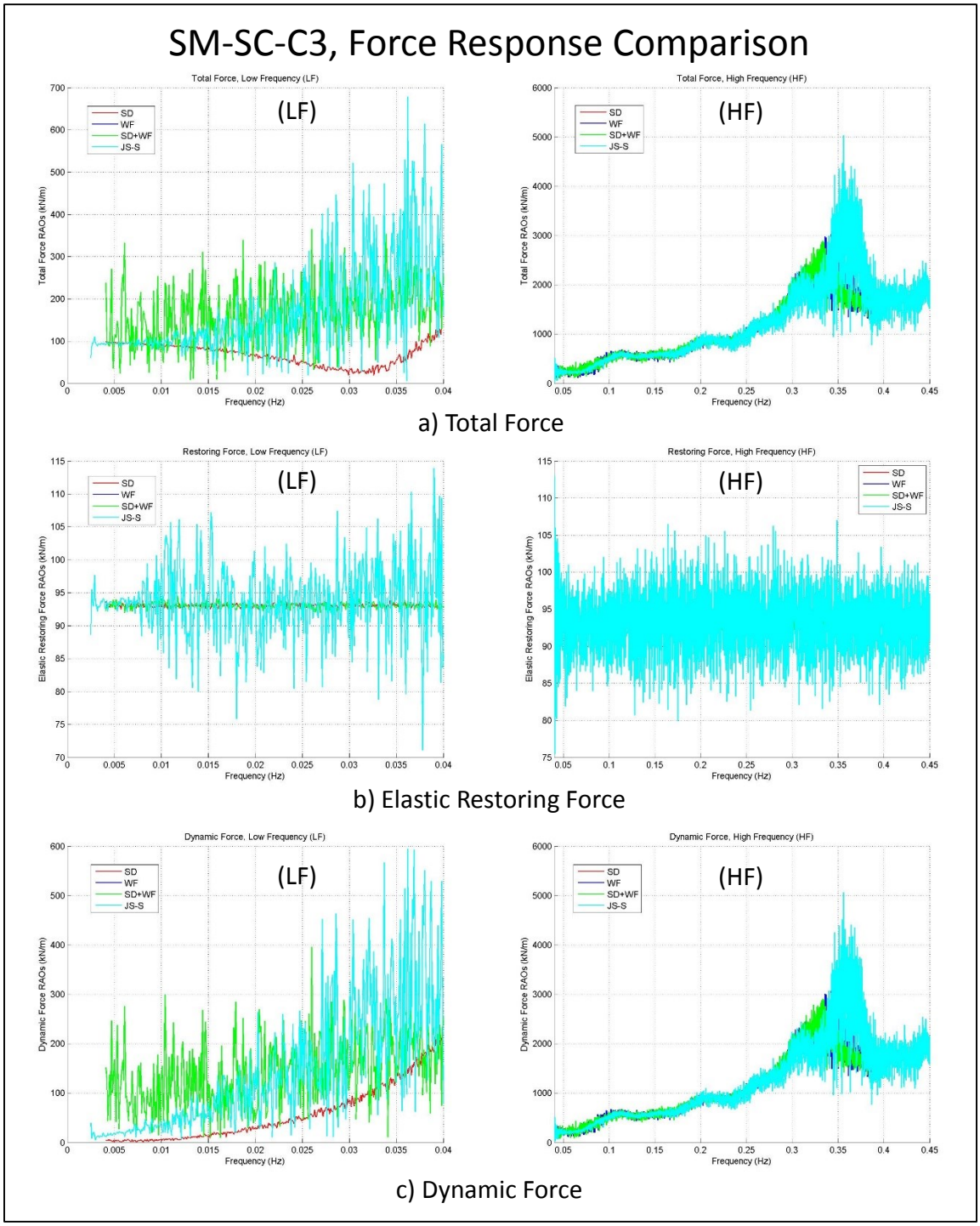

Figure 4.57. Equivalent symmetric truncated mooring system (SM-SC-C3), force response amplitude operator comparison.

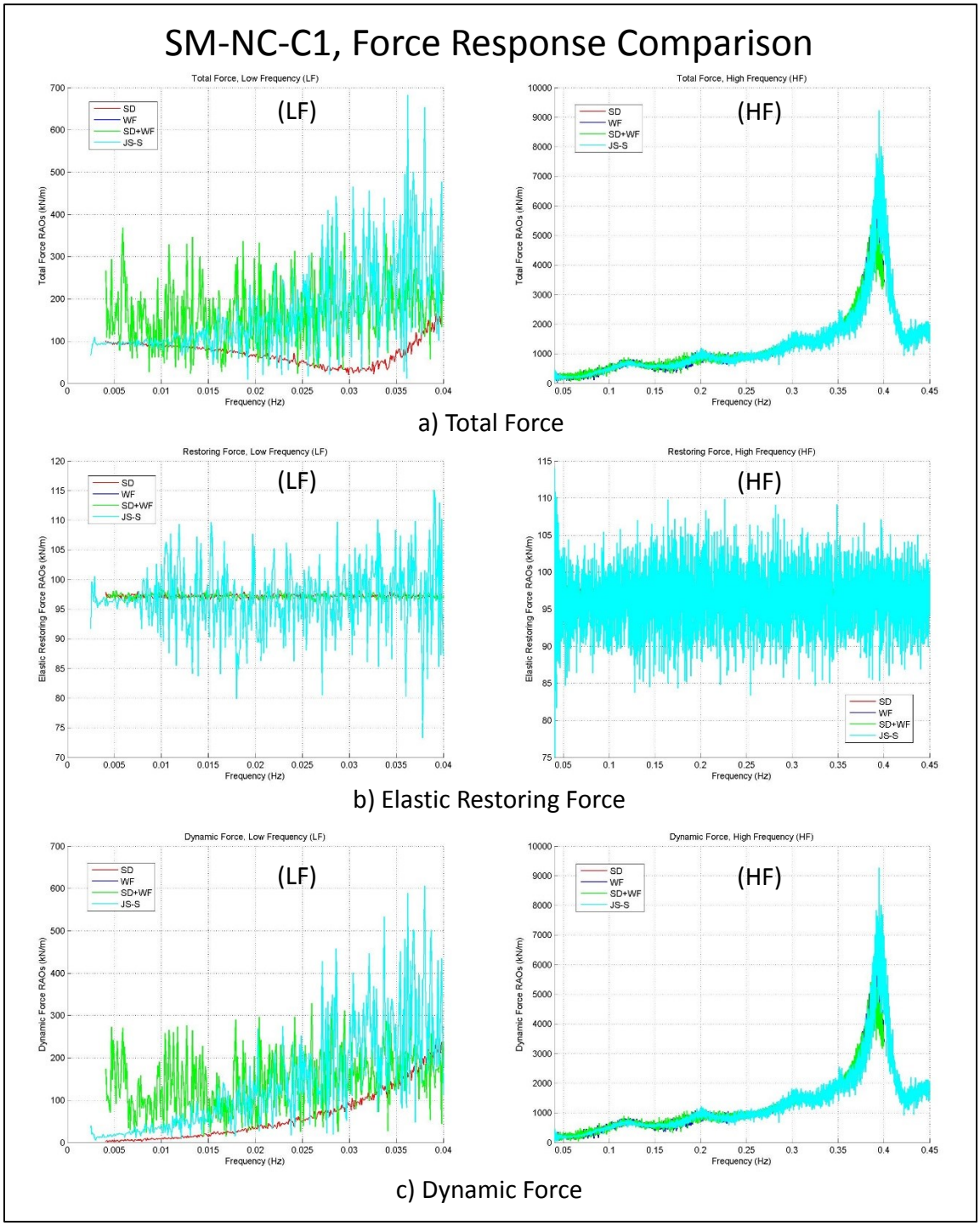

Figure 4.58. Equivalent non-symmetric truncated mooring system (SM-NC-C1), force response amplitude operator comparison.

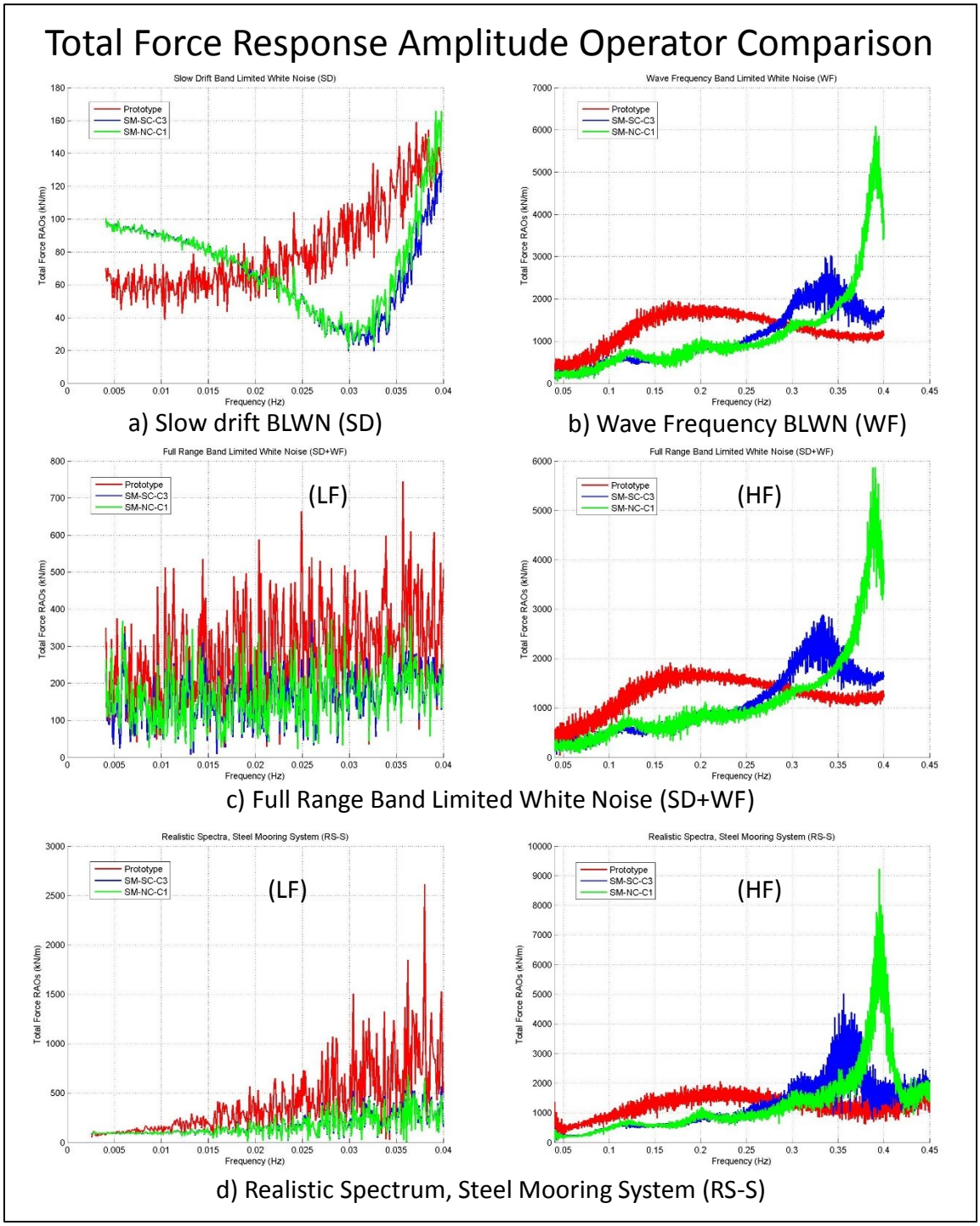

Figure 4.59. Total force response amplitude operators (RAO's) comparison, steel wire mooring system.

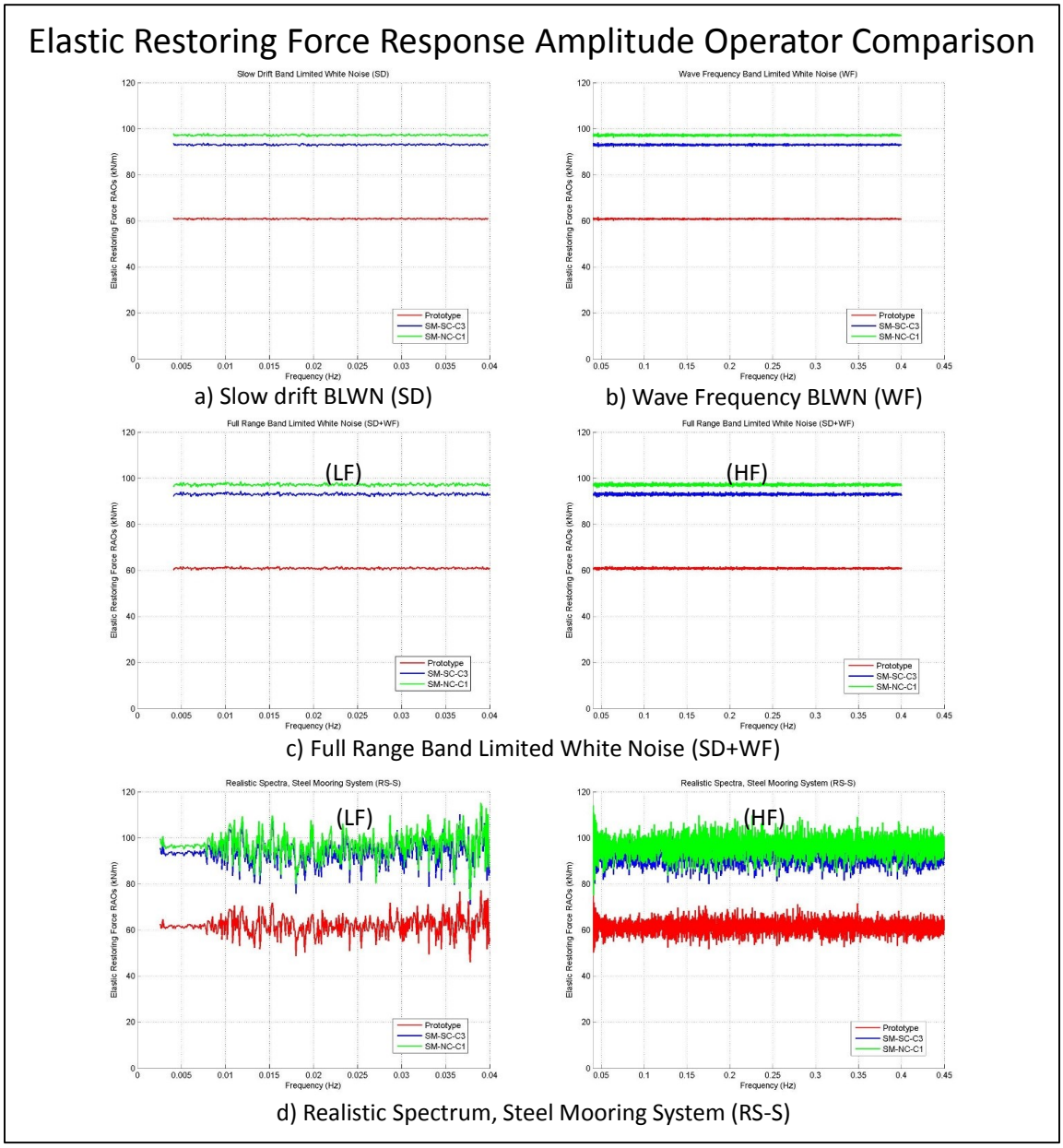

Figure 4.60. Restoring force response amplitude operators (RAO's) comparison, steel wire mooring system.

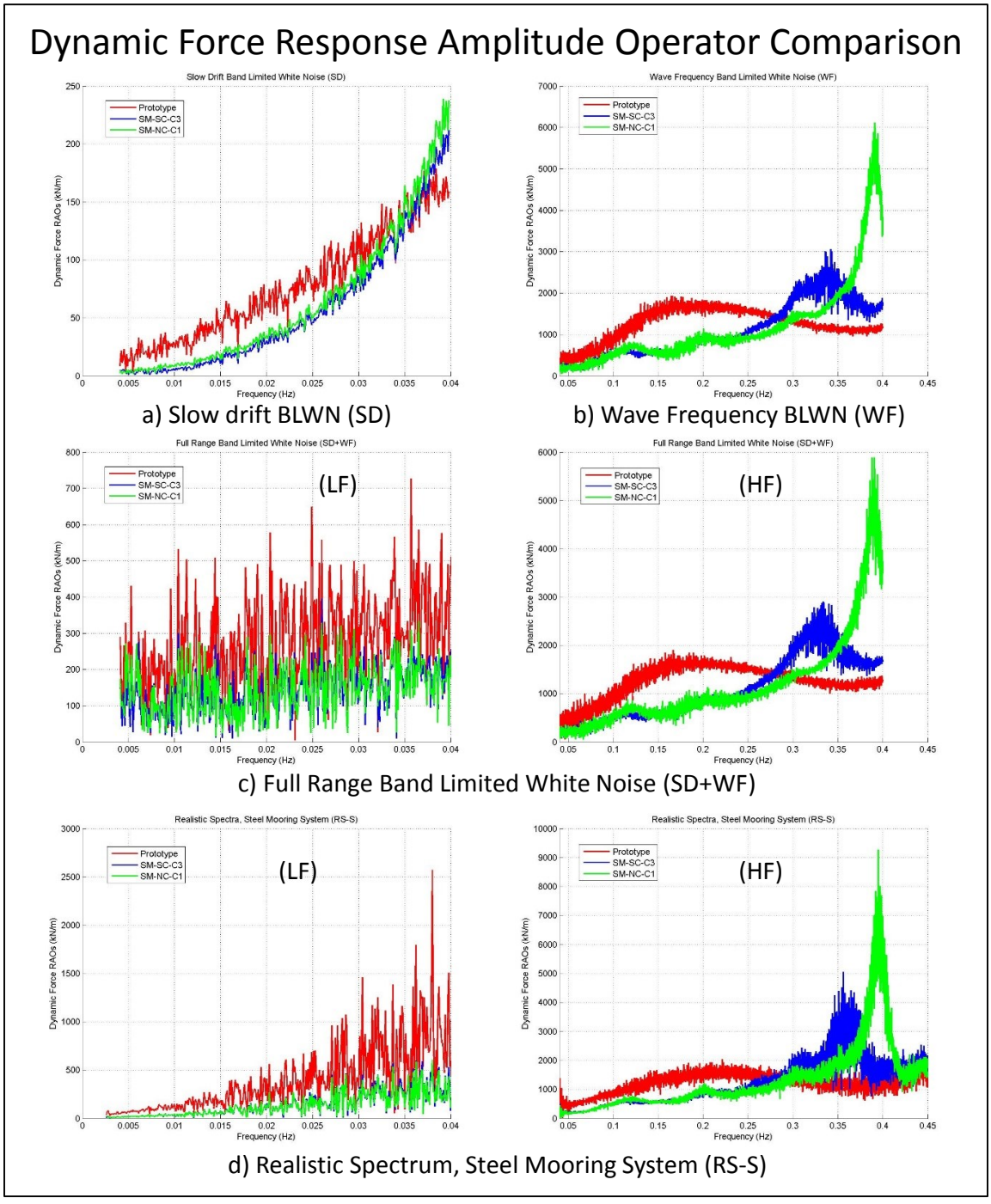

Figure 4.61. Dynamic force response amplitude operators (RAO's) comparison, steel wire mooring system.

The mooring system total force, restoring force and dynamic force contribution Response Amplitude Operators (RAO's) comparison for each one of the forced excitations considered are shown in Figure 4.59, Figure 4.60 and Figure 4.61, respectively. The RAO comparisons show that the responses are completely different between the equivalent mooring systems and the prototype mooring system. The restoring force Response Amplitude Operators indicate the mean value of the horizontal mooring stiffness, and there are large differences related to the design of the equivalent mooring systems and the considerations for the dynamic simulations, as explained previously in this section.

Figure 4.62 shows the phase shift between the mooring system total horizontal force and the forced displacement. At high frequencies (HF) the phase shift between the total force and the displacement excitation are completely different for the equivalent and the prototype mooring system responses. Figure 4.63 shows that the phase shift between the restoring force and the forced displacement for the three mooring systems considered is close to zero, as it should be.

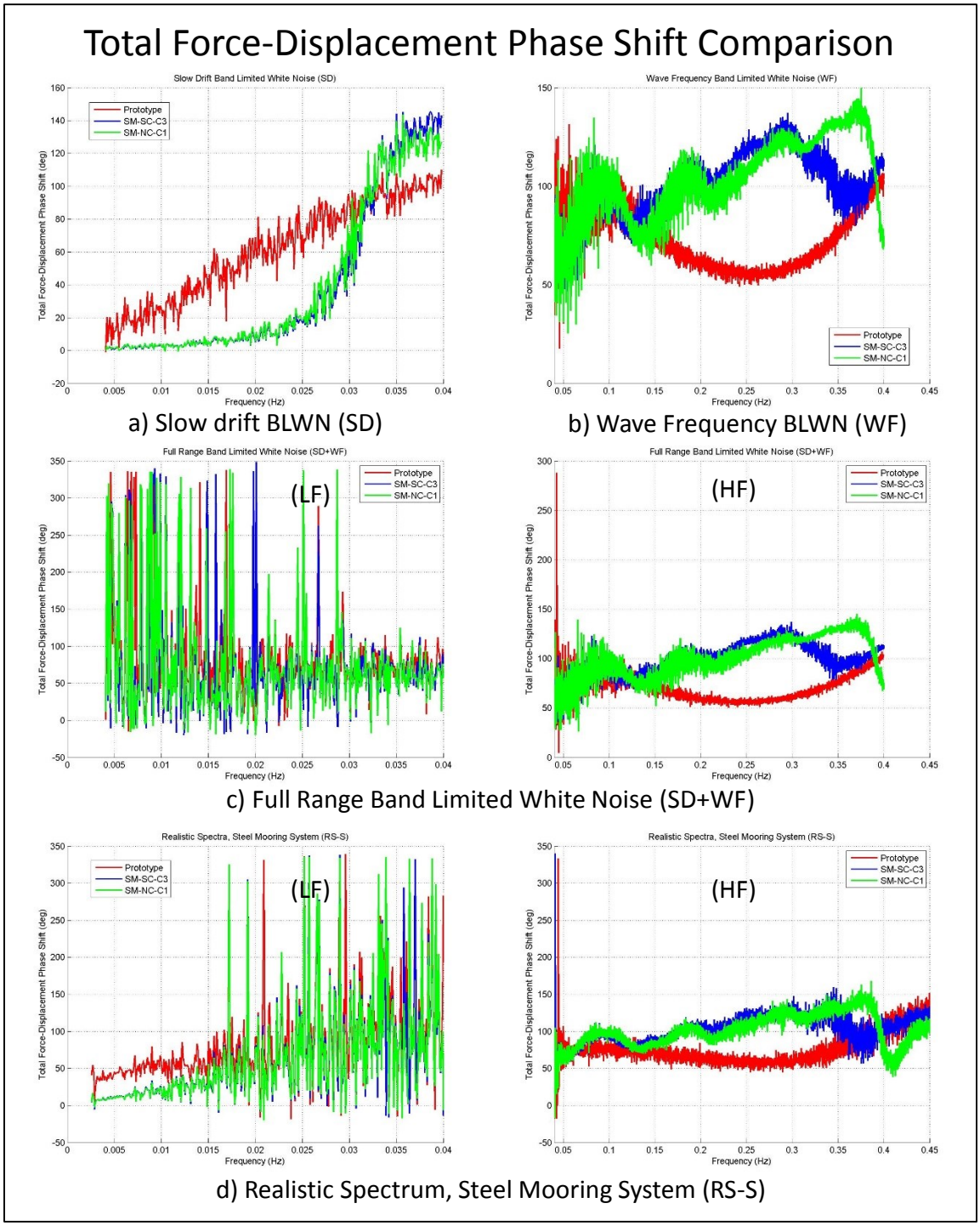

Figure 4.62. Phase shift between total force and displacement comparison, steel wire mooring system.

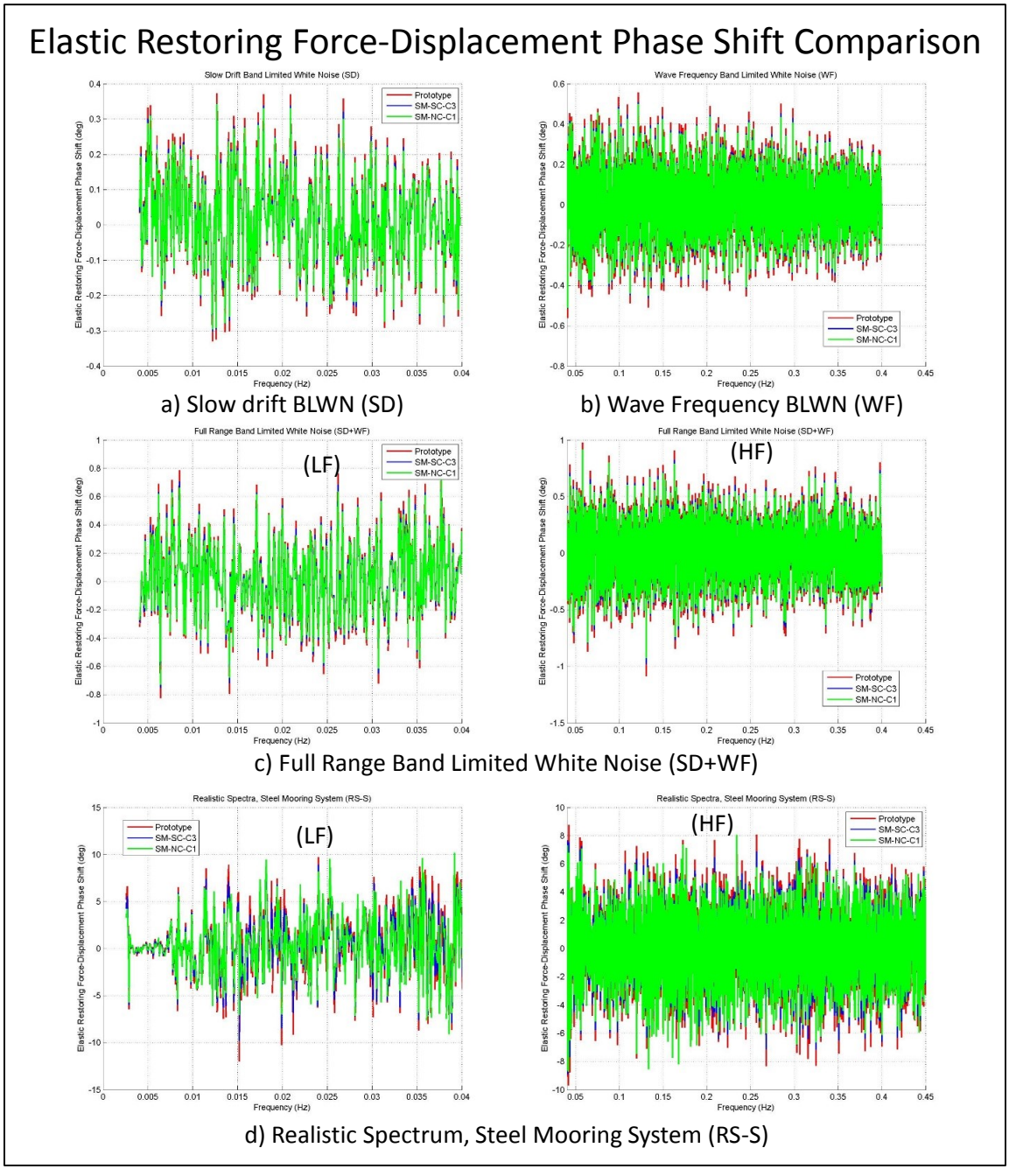

Figure 4.63. Phase shift between restoring force and displacement comparison, steel wire mooring system.

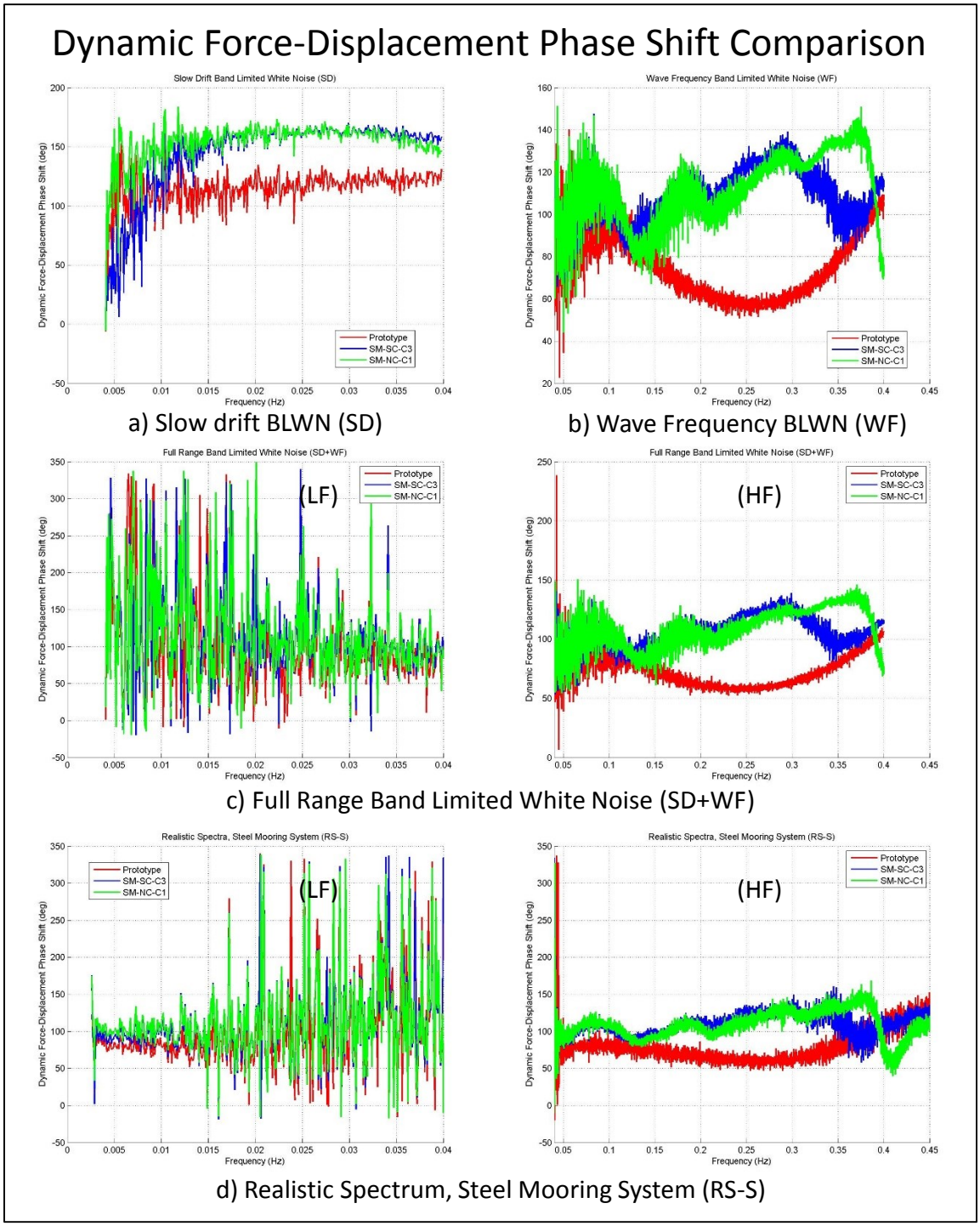

Figure 4.64. Phase shift between dynamic force and displacement comparison, steel wire mooring system.

In Figure 4.64 are shown the phase shift between the mooring system dynamic force contribution and the forced excitation displacement; for those plots a value of 90 degrees means that the inertia force contribution factor ($-M\omega^2$) is equal to zero, so the dynamic force component is just the damping force. For the dynamic force a phase angle less than 90 degrees means that the inertia force contribution is in phase with the displacement, which leads to a negative virtual mass contribution, so this equivalent mass instead of generating a retardation effect to the motion, it is contributing to the motion. For phase shifts greater than 90 degrees the equivalent mass is acting as a retardation effect. At low frequencies this phase shift is close to 90 degrees which means that the dynamic force is dominated by the damping force contribution, as it was expected from a previous observation in this section.

Figure 4.65 shows the coherence between the total force and the displacement excitation for the three mooring systems considered and for each one of the excitations used. For the realistic spectrum displacement excitation the coherence values for the frequency range between 0.015 and 0.045 Hz show a non-linear dependency between the displacement excitation and the mooring system total force response because there is essentially no vessel displacement in this frequency range. The slow drift (SD) and wave frequency (WF) band limited white noise vessel excitation each show a linear dependency between vessel displacement and mooring system total force. On the other hand the full range band limited white noise (SD+WF) shows a non-linear relationship between vessel displacement and mooring system total force for all the low frequency range, presumably because of strong nonlinear interactions in the wave frequency range.

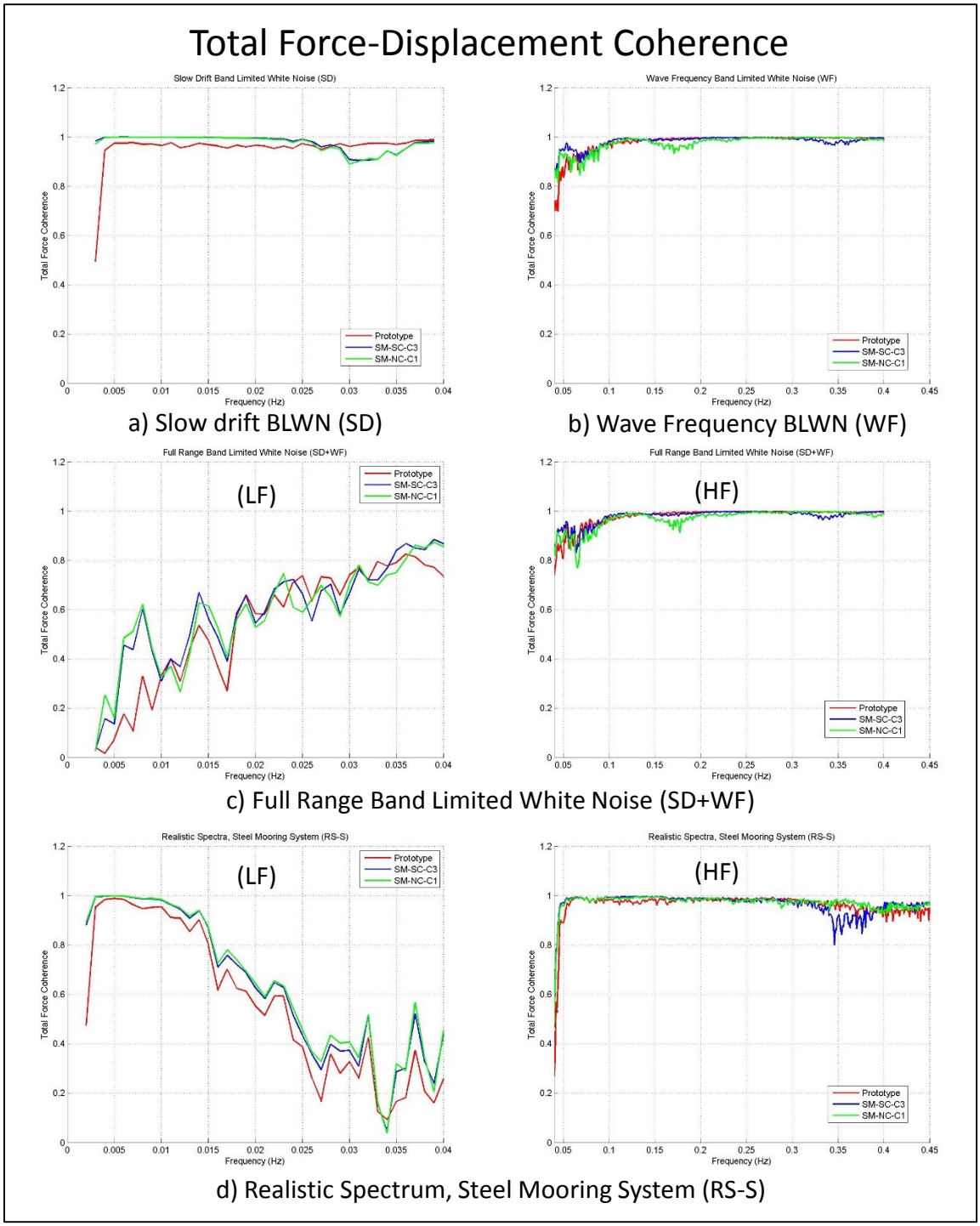

Figure 4.65. Total force and displacement coherence comparison, steel wire mooring system.

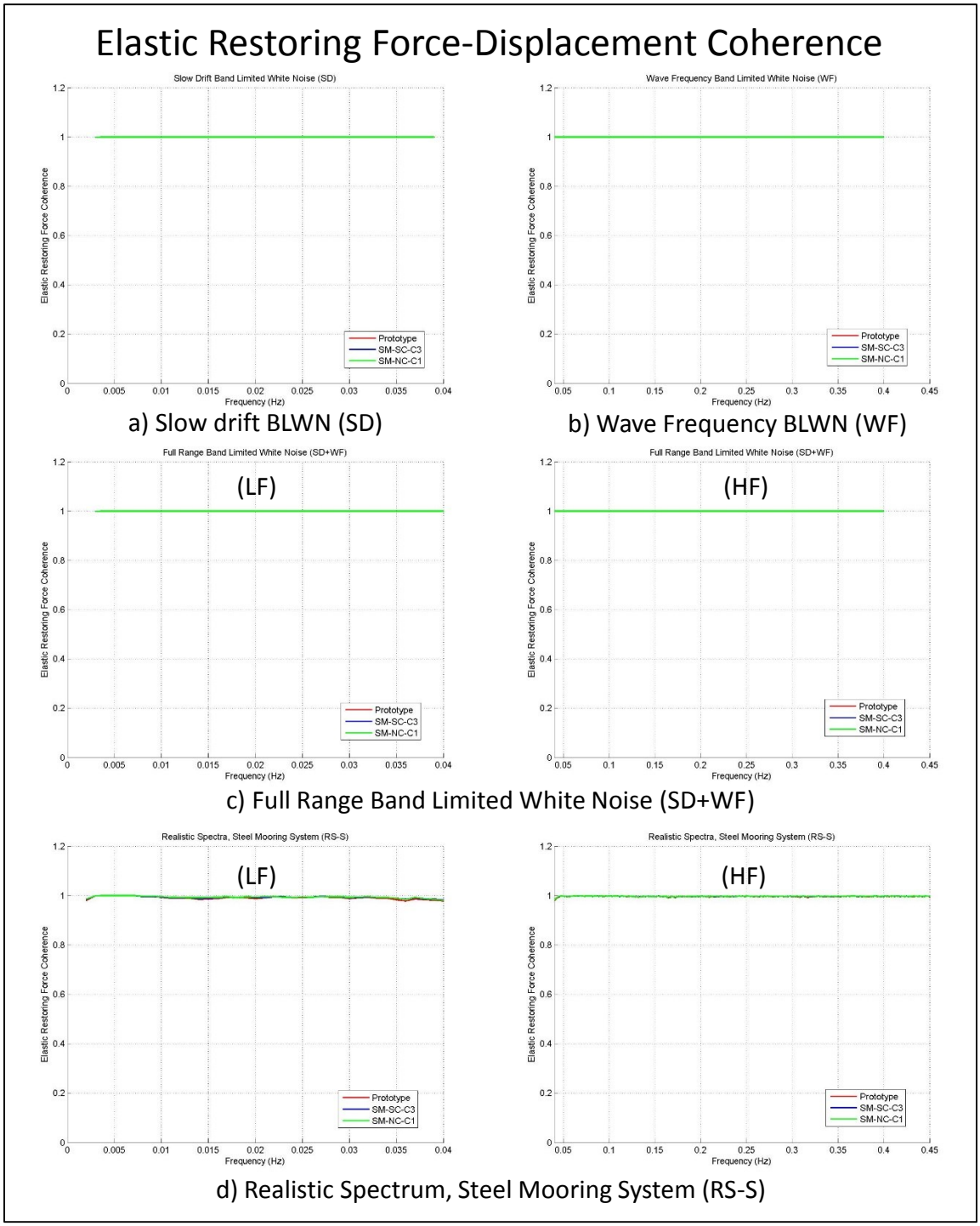

Figure 4.66. Restoring force and displacement coherence comparison, steel wire mooring system.

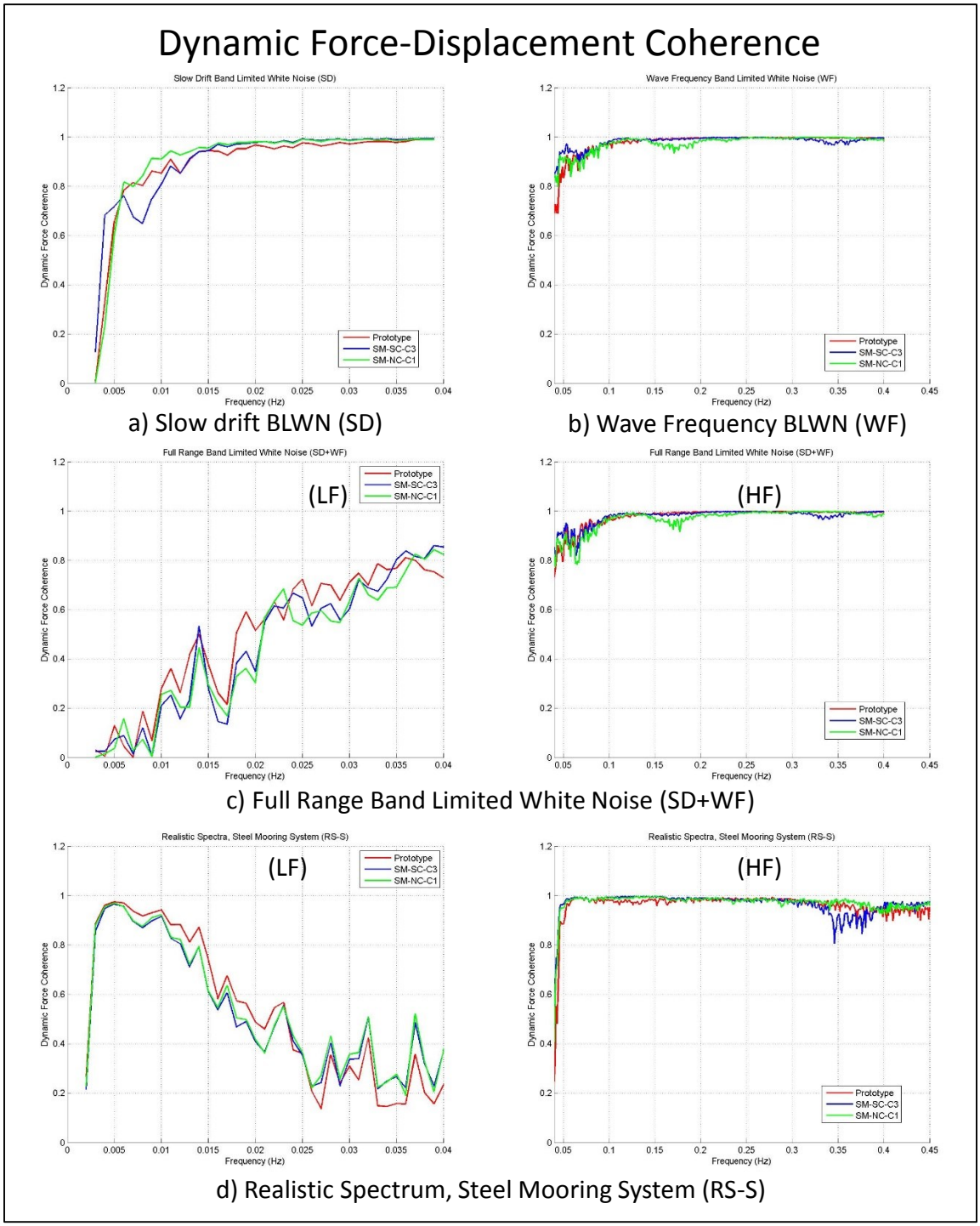

Figure 4.67. Dynamic force and displacement coherence comparison, steel wire mooring system.

In Figure 4.66 are shown the coherence functions between the mooring system restoring force contribution and the displacement excitation. As expected all the comparisons show a linear dependency between the restoring force and the excitation displacement. Therefore, the non-linear behavior is due to the mooring dynamic force contribution, as is shown in Figure 4.67.

As for the polyester mooring, in order to have a perspective on the values associated with the mooring system damping contributions to the floater, the damping factor $C_{damp}=\beta\,(2\pi f)$ is normalized by the critical damping value β_{cr} associated with the slow drift resonance motion, multiplied by the circular frequency ($\omega=2\pi f$), in order to determine an equivalent critical damping ratio contribution from the total horizontal mooring force in the surge direction. The complete system characteristics used to calculate the values for the normalization of the mooring system damping factor are included in Table 4.6.

Table 4.6. Moored floating system dynamic characteristics, steel wire mooring system.

Characteristic	Value
Floater Total Mass at Slow Drift resonance ($M_t=M_f+M_a$)	87,000 ton
Mooring System Horizontal Stiffness (K)	61 kN/m
Natural Angular Frequency (ω_n)	0.026389 rad/sec
Natural Frequency (f_n)	0.0042 Hz
Natural Period (T_n)	238 sec
Critical Damping ($\beta_{cr}=2\,M_t\,\omega_n$)	4,599 kN s/m

The mooring system damping force contribution is plotted as a frequency dependent critical damping ratio in Figure 4.68. There is a large difference in the damping ratio between the equivalent mooring systems and the prototype mooring at low frequencies less than 0.04Hz, where the mean value is around 50% for the prototype and 10% for the equivalent mooring systems. In the wave frequency range, the mooring system critical damping ratio contribution is around 30% for the prototype and 12% for the equivalent mooring systems.

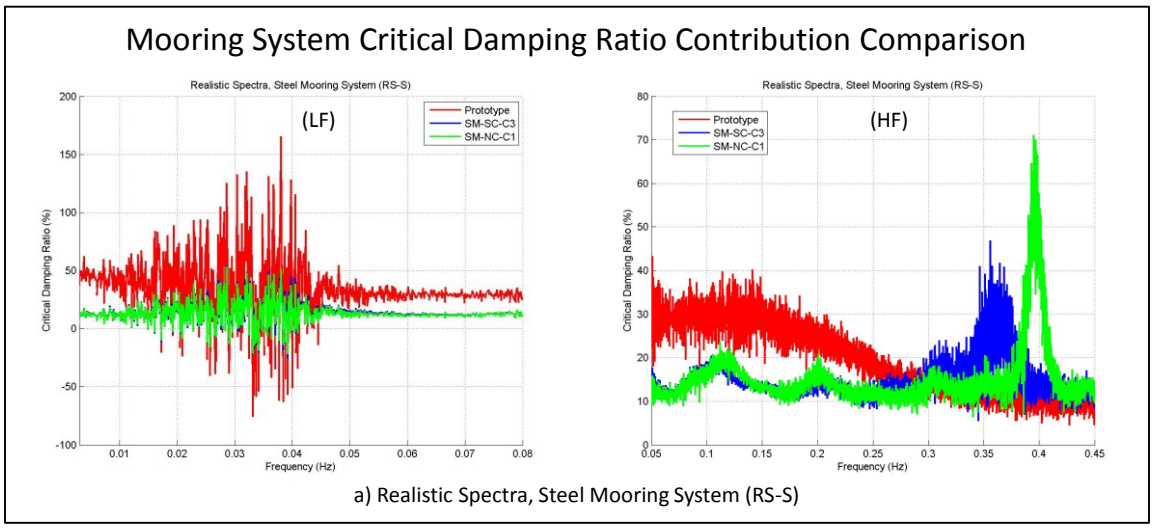

Figure 4.68. Steel wire mooring system critical damping ratio contribution comparison, low frequency (LF) and high frequency (HF) ranges.

In order to quantify the damping level without the nonlinear contributions the mooring forces associated with a single frequency forced vessel displacement were calculated. The single frequency selected corresponds to the slow drift resonance

response, in this case 0.0042 Hz. A displacement amplitude of 30 m is used for this forced oscillation.

As for the previous study case, the floater's hull damping contribution is calculated considering the drag coefficient (*Cd*) at the model scale based on the plot for drag coefficient (*Cd*) vs Reynold's number (*Re*) for various values of Keulegan-Carpenter's number (*KC*) developed by Sarpkaya (1976).

Table 4.7. Damping contribution comparison at slow drift resonance response, steel mooring system.

SYSTEM	Damping Contribution	
	Coefficient (kN s/m)	Critical Damping Ratio (%)
Prototype Mooring System	986.59	21.45
Equivalent Symmetric Truncated Mooring System (SM-SC-C3)	163.24	3.55
Equivalent Non-Symmetric Truncated Mooring System (SM-NC-C1)	154.31	3.36
Floater's Hull	1,691.24	36.77

Table 4.7 summarizes the results for the equivalent and prototype mooring systems and for the hull, for single frequency vessel motion at 0.0042 Hz. The damping contribution of the equivalent mooring systems at this frequency is significantly smaller (critical damping ratio of 3.55% for the symmetric equivalent mooring system and 3.35% for the non-symmetric equivalent mooring system) than the hull damping contribution

(critical damping ratio of 36.77%). The damping contribution for the prototype mooring system (critical damping ratio of 21.45%) is more comparable to the hull contribution at this frequency. So, as for the polyester mooring system, the damping contributed by the equivalent steel mooring systems is much less than that contributed by the prototype mooring system.

4.3.3 Polyester vs Steel Wire Mooring System

There are important differences in the static response between polyester and steel wire mooring systems, mainly related to the mooring line weight contribution to the catenary effect. For polyester mooring systems, the mooring lines are in a taut configuration (Chapter III, Section 3.3.1, Figure 3.21, polyester mooring system, prototype configuration) where the mooring line tension is mainly dominated by the axial stiffness, so the weight effect in the restoring force is smaller than the axial stiffness contribution.

The polyester mooring system static response, for a set of offsets in the surge direction, shows a more linear behavior, as it is shown for the prototype restoring force response in Figure 3.11 (Chapter III, Section 3.3.1). On the other hand, the steel wire mooring systems have a semi-taut configuration where the weight effect in the catenary is more noticeable (Chapter III, Section 3.3.2, Figure 3.36, steel wire mooring system prototype configuration). Because the mooring line weight has a more important role in the mooring system restoring force than the mooring line axial stiffness, the mooring system static restoring force curve has a more significant nonlinear behavior. This

nonlinear behavior is noticeable for the prototype restoring force response in Figure 3.26 (Chapter III, Section 3.3.2).

Based on the differences mentioned above, the statically equivalent mooring systems for the polyester mooring system look completely different than those for the steel wire mooring system. For the study cases considered in this research work, the design for the polyester equivalent mooring systems are a semi-taut configuration where there are not any segments laying on the basin floor at any offset considered, as it is shown in Figure 3.21 (Chapter III, Section 3.3.1, polyester mooring system, equivalent mooring systems configurations at calm water equilibrium position and at maximum offset position). On the other hand, the design of the steel wire equivalent mooring system incorporates long segments of chain laying on the basin floor, so the weight effect in the catenary solution is introduced as there are segments of chain lifted from the floor on the upweather side and lowered to the floor on the downweather side as the floater moves away from the calm water equilibrium position, as it is shown in Figure 3.36 (Chapter III, Section 3.3.2, steel wire mooring system, equivalent mooring systems at calm water equilibrium position and at maximum offset position). Indeed, for the design of the steel wire statically equivalent mooring system, initially in the design phase cable was used for the upper and lower segments in the equivalent mooring line configurations, but it was found to be almost impossible to match the prototype restoring force curve, so the cable segments were replaced by chain segments to introduce more weight in the mooring lines. With the use of heavier chain segments a better match of the equivalent restoring force curves with the prototype restoring force curve was obtained.

In regard to the dynamic behavior comparison between the steel wire and polyester mooring system, Figure 4.69 compares the power spectra for the total force (a), restoring force (b), and dynamic force (c), including the low frequency and high frequency ranges, respectively. We see that at low frequencies, as expected, the polyester mooring system total force contribution is considerably larger than for the steel wire mooring system because the polyester mooring system horizontal stiffness (mean value of 210 kN/m) is around 3.5 times the steel wire mooring system horizontal stiffness (mean value of 61 kN/m). In this frequency range, the total force exerted by the polyester mooring system is completely dominated by the restoring force and the dynamic force contribution is considerably smaller than the restoring force, while for the steel wire mooring system the restoring force is of the same order of magnitude as the dynamic force contribution.

In the wave frequency range, the restoring force is of the same order of magnitude as the dynamic force contribution exerted by the polyester mooring system, but the dynamic contribution is larger than the mooring restoring force, while for the steel wire mooring system the dynamic force contribution is considerably larger than the restoring force. The dynamic force contribution exerted by the steel wire mooring system is quite larger than the dynamic force exerted by the polyester mooring system. So, for those study cases, it can be concluded that the dynamic behavior of the steel wire mooring lines plays a more important role in the total force exerted by the mooring system to the floater than the dynamic behavior of the polyester mooring lines. This dynamic behavior is the reason why at wave frequencies the total force contribution to the floater is larger for the steel wire mooring system than for the polyester mooring system.

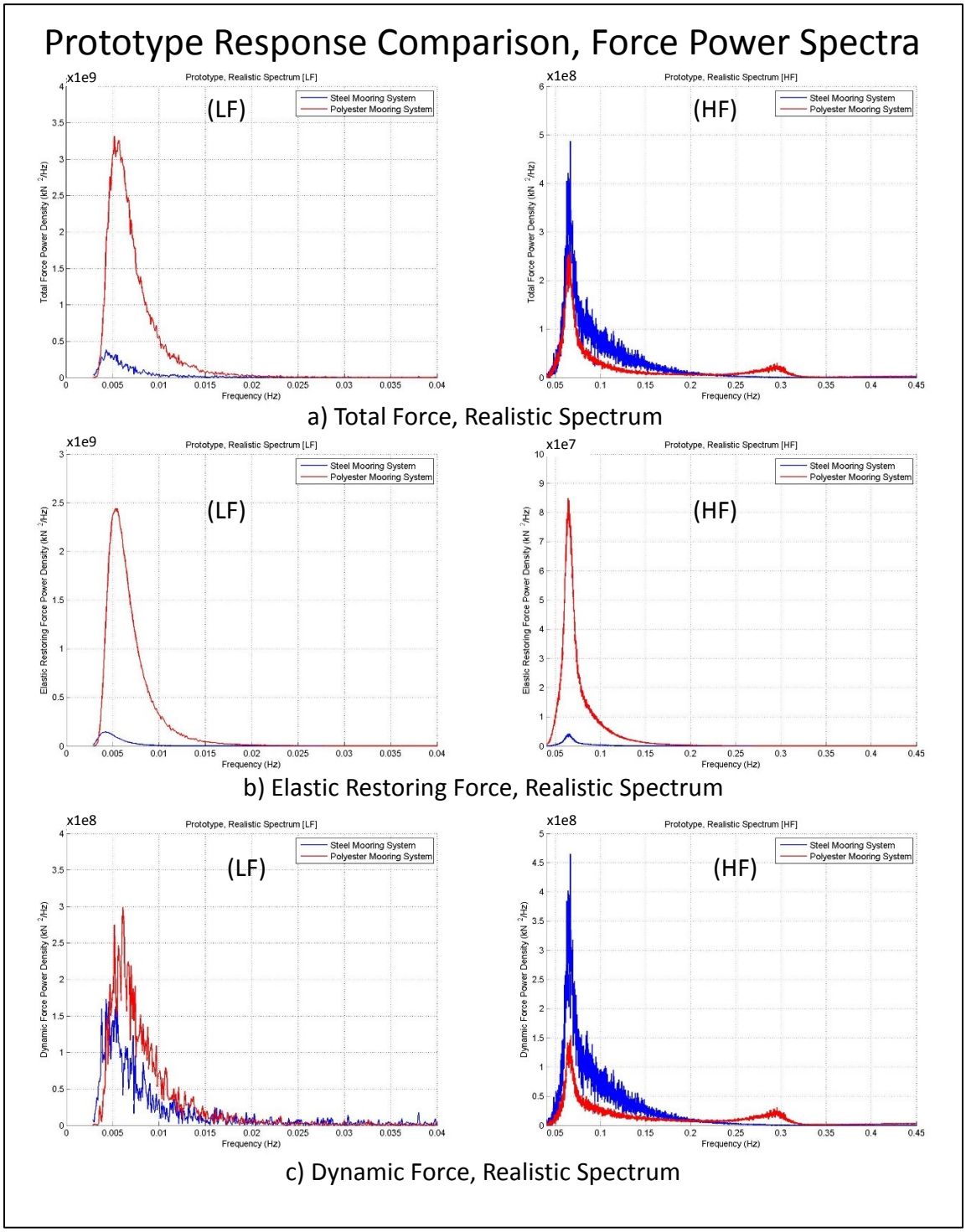

Figure 4.69. Prototype, polyester vs steel wire mooring system, power spectra comparison, low frequency (LF) and high frequency (HF) ranges.

Figure 4.70 compares the inertia factor and the damping factor for the steel wire and polyester mooring systems. At low frequencies (between 0.003 Hz and 0.015 Hz) the inertia factors are larger for the polyester mooring system than for the steel wire mooring system and the damping factors show a similar behavior between those mooring systems. In this frequency range, the inertia factors for both mooring systems lead to a negative virtual mass contribution, although the inertia contributions are smaller than the damping contributions exerted by the mooring systems. The effect of the negative virtual mass is to exert a force acting in favor of the motion instead of acting against the motion. In the wave frequency range, the inertia and damping factors for the steel wire mooring system are larger than for the polyester mooring system.

Figure 4.71 compares the inertia and damping force power spectra for the steel wire and polyester mooring systems. The damping force contribution dominates the dynamic response for both mooring systems, so the damping force contribution is considerably larger than the inertia force contributions, at low and at high frequencies. At low frequencies, the inertia and damping force contributions exerted by the polyester mooring system are larger than for the steel wire mooring system, even though the inertia and damping factors are larger for the steel wire mooring than for the polyester mooring system. This is due to the realistic displacement spectrum used for the forced motion which has resonant peaks at different frequencies: 0.0042 Hz for the steel wire mooring system and 0.0053 Hz for the polyester mooring system. This means that for the same amplitude displacement at those frequencies, there is a difference of around 26% for the velocity (ωX) and around 59% for the acceleration ($\omega^2 X$), which causes larger dynamic forces for

the polyester mooring. In the wave frequency range, the inertia and damping force contributions exerted by the steel wire mooring system are considerably larger than for the polyester mooring system.

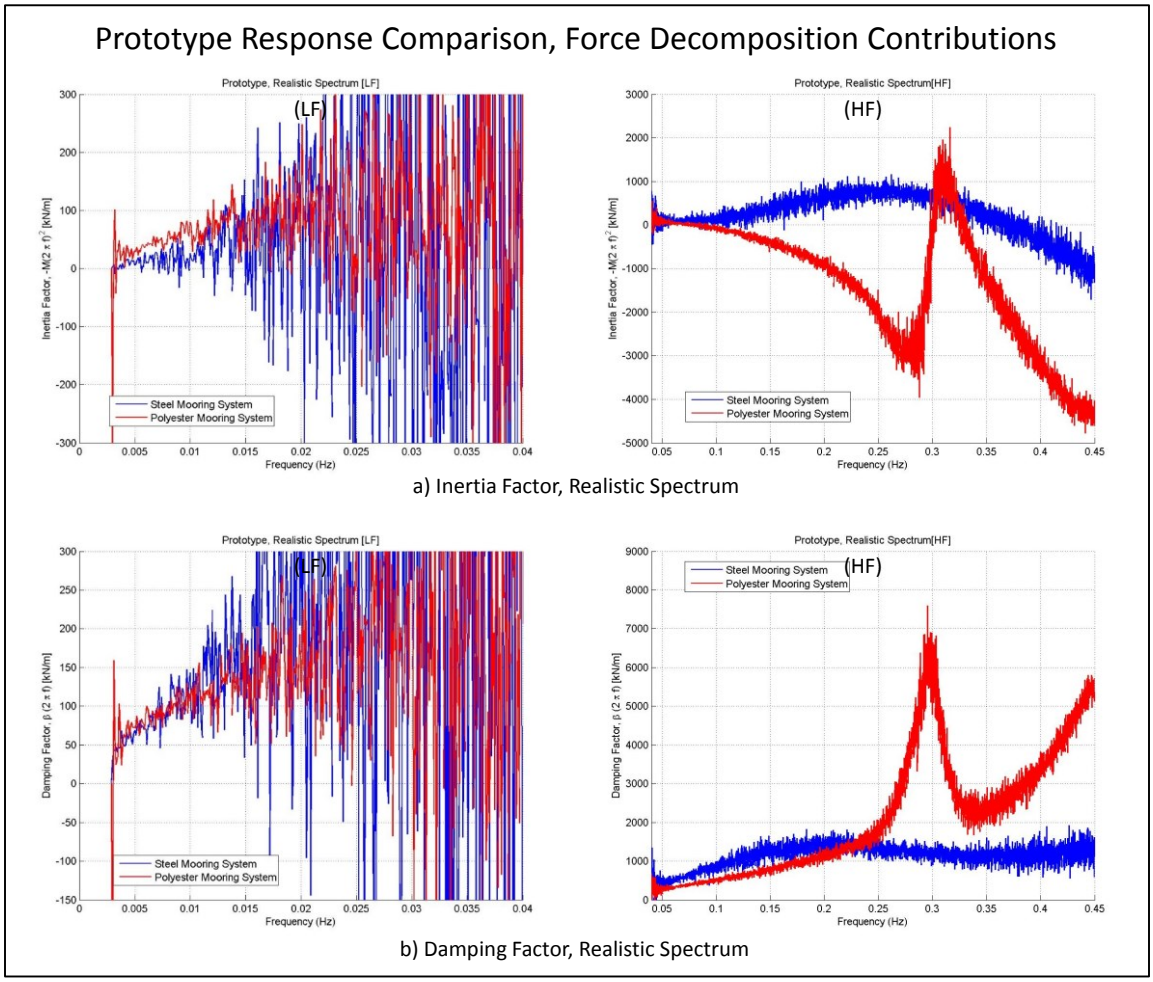

Figure 4.70. Prototype, polyester vs steel wire mooring system, inertia and damping factors comparison, low frequency (LF) and high frequency (HF) ranges.

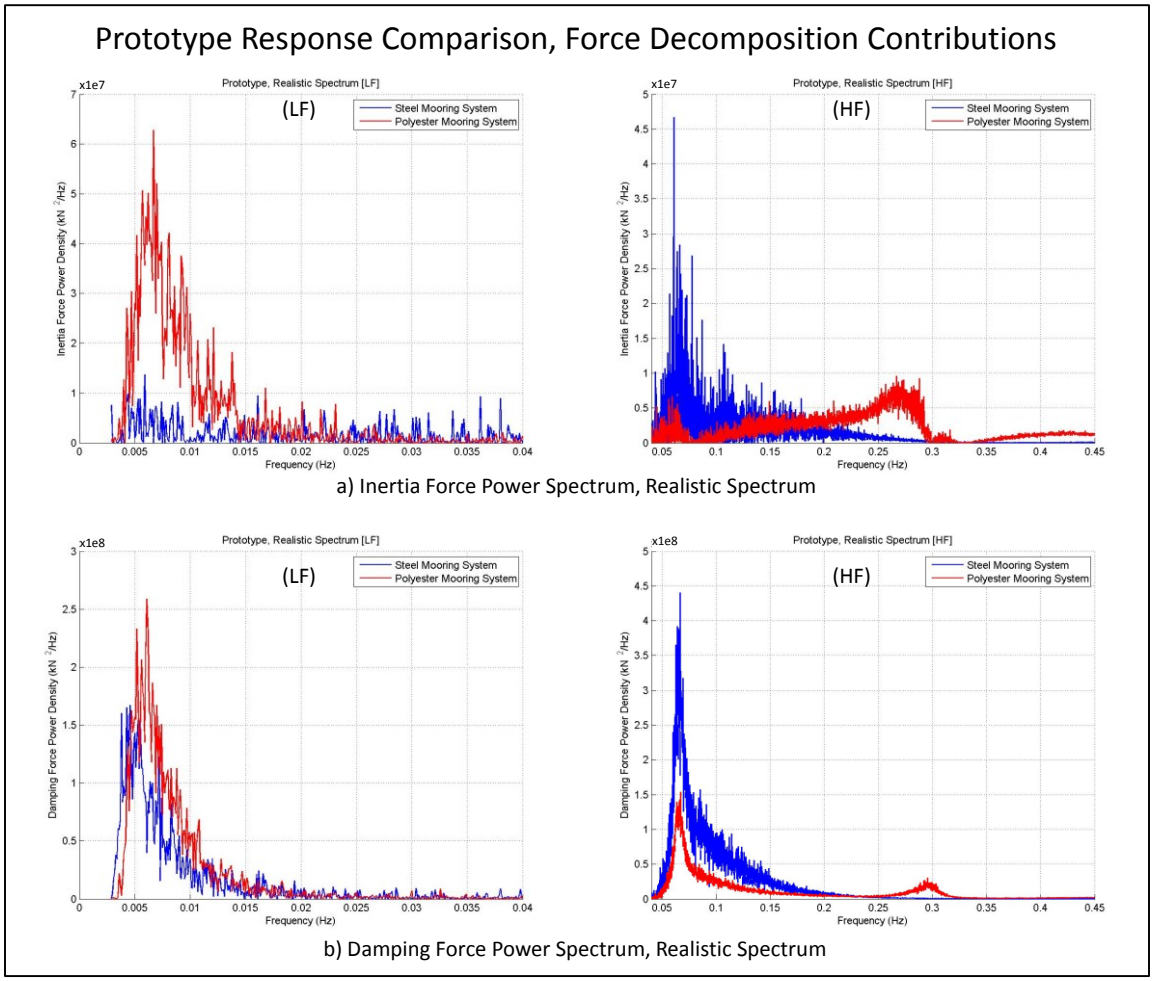

Figure 4.71. Prototype, polyester vs steel wire mooring system, inertia and damping power spectra comparison, low frequency (LF) and high frequency (HF) ranges.

5 SUMMARY, CONCLUSIONS AND FUTURE WORK

Numerical simulations and model testing are used to design a floating system to assess its behavior in operational conditions and in extreme weather conditions, always looking to preserve the safety and functionality of all the components involved. The adequacy of a concept design is verified through model testing of a prototype to evaluate its behavior. Testing the response of a deepwater (> 500 m depth) floating system is a challenge because the basin dimensions required to accommodate the scaled full depth mooring and riser system are beyond the capabilities of available facilities worldwide, both now and for the foreseeable future. Due to basin dimension limitations it is necessary to design and employ an equivalent mooring/riser system so that the net forces and moments imparted by the truncated mooring/riser system to the floater in its 6 rigid body degrees of freedom are as closely reproduced as practically. The level of complexity required to match the static and dynamic responses of the prototype with an equivalent truncated mooring and riser system is currently beyond reach.

It is currently the common practice to focus the design effort entirely on reproducing the net *static* restoring forces and moments that the mooring and risers impart on the floater over some pre-defined range of offsets. The primary contribution of the research documented herein is the development of an automated procedure for optimized design of statically equivalent mooring and riser systems. The design strategy used by the Offshore Technology Research Center has been adopted, which focuses exclusively on reproducing the net six degree of freedom restoring forces and moments exerted on the

floater with a statically equivalent system whose individual lines are not constrained to bear any resemblance to individual lines of the prototype system but rather are as simple as possible so that they can be robustly represented in a numerical model. In order to evaluate and compare the *dynamic* behavior of the forces imparted by the mooring system on the floater, for both the full depth prototype and statically equivalent truncated mooring systems, a procedure to assess the mooring system inertia and damping contributions to the floater was developed.

The automated design optimization procedure that was developed is based on use of a Genetic Algorithm, which is initiated with a large population of randomly generated candidate designs and employs natural selection principles guided by a fitness function to generate offspring (design modifications) that, over the course of generation after generation, evolve to characteristics that better achieve the desired performance. Because of the significant computational burden involved in the evolutionary process, an efficient solver is required to calculate the nonlinear static equilibrium of the floater and its mooring and riser system under an arbitrary applied environmental force. Accordingly a fit-for-purpose program was successfully developed to calculate the three-dimensional static equilibrium of a floating structure with attached mooring and riser systems. The program was validated by comparing the results calculated with the fit-for-purpose program with Orcaflex program results, for both a single mooring line case and a semisubmersible case with a complete mooring system attached. Excellent correlation was demonstrated between the fit-for-purpose program and Orcaflex results.

In the future, specific improvements could be made to the fit-for-purpose program to incorporate non-linear axial stiffness for polyester segments and also to include the friction for any segment laying on the seabed.

The Genetic Algorithm (GA) procedure was developed in Matlab for the design of the statically equivalent truncated mooring and riser systems. The fit-for-purpose program is used to calculate the static force versus offset curves for the six floater degrees of freedom for each one of the individuals in the population, so that the fitness function value for each member can be calculated. For each individual in the population, the fitness function value is calculated using a weighting factor for each floater degree of freedom applied to the root mean square error in the static offset curve for that degree of freedom, as measured relative to the target static offset curves for the prototype. Four different GA solution scenarios were developed successfully:

1. symmetric equivalent mooring system were all lines are identical,
2. non-symmetric equivalent mooring system where the upweather lines are identical but different than the downweather lines (which are also identical),
3. asymmetric equivalent mooring system with each individual line having a unique design based on six design parameters per mooring line, and
4. equivalent catenary riser system with each individual riser having a unique design based on six design parameters per riser plus two design parameters to locate the floater in the X-Y plane over the pit in the basin.

In order to demonstrate the effectiveness and robustness of the GA solution scenarios developed four study cases were considered:

1. a semisubmersible with a symmetric, 16-line polyester mooring system in 2,200 m water depth,
2. a semisubmersible with a symmetric, 16-line steel wire mooring system in 1,900 m water depth,
3. a semisubmersible with a non-symmetric, 12-line polyester mooring system and 3 steel catenary risers in 1,219 m (4,000 ft) water depth, and
4. a spar with a non-symmetric, 9-line polyester mooring system and 2 steel catenary risers in 1,219 m (4,000 ft) water depth.

Based on the results obtained it is considered that the GA solution scenarios were successfully implemented. It is important to highlight that there is an effort required for the user to define the weighting factors to improve the final design of the statically equivalent mooring system, based on his acceptance criteria for each one of the six degrees of freedom static response.

The main differences between the polyester mooring system and steel wire mooring system were discussed, highlighting that the polyester mooring system has a taut configuration and its restoring force is dominated by the mooring line axial stiffness while the steel mooring system has a semi-taut configuration where the mooring line weight plays an important role in the restoring force. Indeed, the equivalent mooring systems looks different; for the polyester equivalent mooring system all the mooring lines are lifted from the seabed at any offset while for the steel wire equivalent mooring system there are

long segments laying on the seabed. Furthermore, for the steel wire equivalent mooring system the cable segments were replaced by chain segments to improve the match with the prototype static response.

The design of the equivalent mooring and riser system is based on reproducing the static response of the vessel with the prototype mooring/riser system attached. To gain insight on the distortion of the dynamic mooring forces exerted on the floater when dynamic effects are ignored in the design, an effort was made to assess the dynamic mooring force contributions of the prototype and statically equivalent mooring systems so that they could be compared. The assessment was made by examining time domain simulations where the floater was forced to oscillate in the surge direction only with motions derived from prescribed spectra. Four different vessel forced oscillation spectra were used in the assessment. The total horizontal component of top tension exerted by the mooring system was decomposed into restoring force and dynamic force components, and the latter were further decomposed into orthogonal components that contribute inertia and damping to the surge motion of the floater. The various corresponding mooring force components for the equivalent and prototype mooring systems were compared in the time and frequency domain using various signal processing tools.

Two study cases were developed to demonstrate the effectiveness of the procedure developed for assessing the inertia and damping contributions exerted by the mooring system. The cases considered were the 16-line polyester mooring system and steel wire mooring system used in the GA study cases.

For both the polyester and steel mooring system study cases it was shown that in a realistic extreme sea state the dynamic mooring force contribution is dominated by the drag coefficient (C_d) of the mooring lines. This means that if we wish to minimize the mooring-induced distortion of the dynamic behavior of the prototype, in the design of the equivalent mooring system we should focus on adjusting the relative-velocity drag force on the mooring lines by changing the line diameter or the drag coefficient.

The relative importance of the restoring force in extreme sea states depends on the situation. For the prototype polyester mooring systems, the restoring force is dominant at low frequencies but at wave frequencies the dynamic force is of comparable magnitude. For the prototype steel mooring system the restoring force is of comparable to the dynamic force at low frequencies but insignificant at wave frequencies. On the other hand, for the equivalent polyester mooring system the restoring force is dominant at low frequencies but smaller than the dynamic force at wave frequencies. For the equivalent steel mooring system the restoring force is dominant at low frequencies an much smaller than the dynamic force at wave frequencies. To the extent that the dynamic force balance on the floater at wave frequencies is dominated by wave radiation and diffraction forces, it would appear at first that the distortion of the mooring forces on the floater is not so important at wave frequencies and is primarily of interest at low frequencies. Indeed, although the restoring force is dominant at the slow drift frequency the phasing of the dynamic mooring force is of considerable importance as it affects the damping of the slow drift motion.

Upon decomposing the dynamic force into inertia and damping force contributions, it is shown that the frequency dependence of these component contributions

is quite different for the prototype and equivalent mooring systems. However in all cases (polyester vs steel, prototype vs equivalent) the damping force contribution dominates over the inertia force contribution in both the low and wave frequency ranges in extreme sea states.

Interestingly, even though the mooring force contribution is dominated by the nonlinear drag force on the mooring lines, the dynamic mooring force exerted on the floater at wave frequencies is shown to be linearly related to the vessel displacement. However, as expected, it is also shown that the wave frequency motion of the floater impacts the low frequency dynamic force exerted by the mooring lines, through the nonlinear relative velocity drag force mechanism. Therefore the damping-dominated dynamic force contribution at wave frequencies is important to preserve if one wants to accurately model the damping of the low frequency motion.

It is shown that the prototype mooring line damping force contribution to the slow drift motion of the floater can be of comparable magnitude as the viscous damping force contributed by the relative velocity drag on the hull. However for the equivalent polyester and steel mooring systems assessed, the mooring line damping force exerted at the slow drift frequency is much smaller than that exerted by the prototype mooring system, indicating that in a model test situation the simulated slow drift motion would be larger than it should be.

Because of the unavoidable distortion of geometric nonlinearities introduced by a truncated mooring system, matching the prototype mooring system damping force contribution at low frequency, which is impacted by the mooring system damping force

at wave frequencies, will not simply be a matter of adjusting the drag force exerted on individual mooring lines. Other innovative control measures will need to be introduced. Furthermore introducing dynamic effects into design optimization using a Genetic Algorithm approach will require an efficient extension of the fit-for-purpose static equilibrium solver developed herein. These will be challenging topics for future research.

REFERENCES

Buchner, B., Wichers, J.E.W. and de Wilde, J.J. (1999). "Features of the State-of the art Deepwater Offshore Basin". Proceedings: Offshore Technology Conference. Houston, Texas. OTC 10841.

Carbono, A.J.J., Menezes, I.F.M., Martha, L.F. (2005). "Mooring Pattern Optimization using Genetic Algorithms". Proceedings: 16th World Congresses of Structural and Multidisciplinary Optimization. Rio de Janeiro, 30 May - 03 June, 2005, Brazil.

Cao, Y. (2013). "An Active Hybrid Decomposes Mooring System (Hydemoor) for Model Testing of Offshore Platform". Marintek Review, No.1, March 2013.

Elgamiel, H., Markov, N. and Grinius, V. (2006). "New Mooring Simulation Approaches in Model Testing". Proceedings of the Sixteenth (2006) International Offshore and Polar Engineering Conference, San Francisco, California, USA, May 28-June 2, 2006. 273-277.

Fan T., Qiao D., Ou J. (2014). "Innovative Approach to Design Truncated Mooring System Based on Static and Damping Equivalent". Ships and Offshore Structures. DOI: 10.1080/17445302.2013.867631.

Fryer, D., Watts, S., Evans, M. (2001). "Experiment Methods for Non-Linear Hydrodynamic Response to Waves". Proceedings: 20th International Conference on Offshore Mechanics and Arctic Engineering. June 3-8, 2001, Rio de Janeiro, Brazil. OFT-1251, 729-738.

Huse, E. and Matsumoto, K. (1988). "Practical Estimation of Mooring Line Damping". Proceedings: 20th Annual Offshore Technology Conference. Houston, Texas. OTC 5676, 543-552.

Huse, E. and Matsumoto, K. (1989). "Mooring Line Damping Due to First- and Second-Order Vessel Motion". Proceedings: 21st Annual Offshore Technology Conference. Houston, Texas. OTC 6137, 135-148.

Irvine, H. Max. (1981). "Cable Structures", pages 16-20. The MIT Press Series in Structural Mechanics, Cambridge, Massachusetts.

ITTC (2002). The Specialist Committee on Waves. Final Report and Recommendations to the 23rd ITTC. Proceedings of the 23rd International Towing Tank Conference. Volume II, page 539.

ITTC (2008). “Recommended Procedures and Guidelines. Testing and Extrapolation Methods Loads and Responses, Ocean Engineering, Truncation of Test Models and Integration with Numerical Simulations”. Ocean Engineering Committee of 25th ITTC. Approved on the 25th International Towing Tank Conference.

Kim, M.H., Koo, B.J., Mercier, R.M., Ward, E.G. (2005). “Vessel/mooring/riser coupled dynamic analysis of a turret-moored FPSO compared with OTRC experiment”. Journal of Ocean Engineering, Vol. 32, 1780-1802.

Manoharan, S., Shanmuganathan S. (1999). “A comparison of search mechanisms for structural optimization”. Journal of Computers and Structures, 363-372.

Mathworks Inc., 2012. MatLab User Manual. Mathworks, Inc., Natick, MA.

Orcina Ltd., 2010. Orcaflex User Manual. Orcina Ltd., Ulverston, Cumbria, UK.

Sarpkaya, T. (1976). “In-line and transverse forces on cylinders in oscillating flow at high Reynold’s number”. Proceedings of the Eighth Offshore Technology Conference, Houston, Texas, OTC 2533, 1976, 95-108.

Sivanandam, S.N., Deepa, S.N. (2008). Book: “Introduction to Genetic Algorithms” Springer-Verlag Berlin Heidelberg.

Stansberg C., Karlsen, S., Ward, E.G., Wichers, J.E.W (2004). “Model Testing for Ultradeep Waters”. Offshore Technology Conference. OTC 16587.

Stansberg, C., Ormberg, H., Oritsland, O. (2002). “Challenges in Deep Water Experiments: Hybrid Approach”. Journal of Offshore Mechanics and Arctic Engineering. Volume 124, 90-96.

Stansberg, C.T., Øritsland, O. and Kleiven, G. (2000) “VERIDEEP: Reliable Methods for Laboratory Verification of Mooring and Stationkeeping in Deep Water”. Proceedings: 2000 Annual Offshore Technology Conference, 1–4 May, Houston, Texas. OTC 12087.

Triantafyllou, M.S. and Yue, D.K.P (1994). “Damping of Moored Floating Structures”. Proceedings: 26th Annual Offshore Technology Conference, 2-5 May, Houston, Texas. OTC 7489, 215-224.

Udoh, I. E. (December 2008). “Development of Design Tool for Statically Equivalent Deepwater Mooring Systems”. Master of Science thesis. College Station, Texas: Texas A&M University.

Vinje, T. (1989). “On the Significance of Negative Added Mass”. Proceedings: 8th International Conference on Offshore Mechanics and Arctic Engineering. March 19-23, 1989, The Hague. 53-61.

Waals, O.J. and Van Dijk, R.R.T. (2004). “Truncation Methods for Deep Water Mooring Systems for a Catenary Moored FPSO and a Semi Taut Moored Semisubmersible”, Proceedings: Deep Offshore Technology Conference, New Orleans, USA.

Wichers, J.E.W. and Huijsmans, R.H.M. (1990). “The Contribution of Hydrodynamic Damping Induced by Mooring Chains on Low-Frequency Vessel Motions”. Proceedings: 22nd Annual Offshore Technology Conference, Houston, Texas, May 7-10. OTC 6218, 171-182.

Zhang, H., Sun, Z., Yang, J. and Gao, M. (2009). “Investigation on optimization design of equivalent water depth truncated mooring system”. Science in China Series G: Physics, Mechanics & Astronomy, 277-292.

Zhang, H., Gao, W., Wang, Q., Jiang, J. and Zhao, Z. (2012). “Investigation on Optimization Design of an Equivalent Water Depth Truncated Mooring System Based on INSGA-II”. Journal of Marine Sciences and Application, 11: 208-215.